

SYNTHESIS AND CHARACTERIZATION OF THIOPHENE BASED CONJUGATED POLYMERS FOR OPTOELECTRONIC APPLICATIONS

Thesis

Submitted in partial fulfillment of the requirements for the degree of

DOCTOR OF PHILOSOPHY

By

MURALI M.G.

(Reg.No. CY08F06)



DEPARTMENT OF CHEMISTRY

NATIONAL INSTITUTE OF TECHNOLOGY KARNATAKA

SURATHKAL, MANGALORE – 575 025

July, 2012

DECLARATION

By the Ph.D. Research Scholar

I hereby declare that the Research Thesis entitled **“Synthesis and characterization of thiophene based conjugated polymers for optoelectronic applications”** which is being submitted to the **National Institute of Technology Karnataka, Surathkal** in partial fulfilment of the requirements for the award of the degree of Doctor of Philosophy in **Chemistry** is a bonafide report of the research work carried out by me. The material contained in this Research Thesis has not been submitted to any University or Institution for the award of any degree.

Murali M.G.

Reg. No. CY08F06

Department of Chemistry

Place: NITK-Surathkal

Date:

CERTIFICATE

This is to certify that the Research Thesis entitled **“Synthesis and characterization of thiophene based conjugated polymers for optoelectronic applications”** submitted by **Murali M.G.** (Register Number: CY08F06) as the record of the research work carried out by him is accepted as the Research Thesis submission in partial fulfilment of the requirements for the award of degree of Doctor of Philosophy.

Research Guide

Dr. Udaya Kumar D.

Date:

Chairman-DRPC

Date:

Dedicated to
My Beloved Father

ACKNOWLEDGEMENT

First and foremost, I would like to thank my research supervisor Dr. Udaya Kumar D. Assistant Professor, Department of Chemistry, National Institute of Technology Karnataka, Surathkal who introduced me to this field of research and supervised my work at all stages. I also thank him for his optimism and belief in me to carry out this work. I am extremely indebted to him for his encouragement, guidance and friendly support during my research.

I would like to express my gratitude to my RPAC members Dr. D. Krishna Bhat, Department of Chemistry and Dr. Anandhan Srinivasan, Metallurgical and Materials Engineering Department, for taking their time to attend my seminars, having fruitful discussions and valuable suggestions.

I would also like to thank Prof. A. V. Adhikari, Prof. A. N. Shetty, Prof. A. C. Hegde, Dr. B. R. Bhat, Dr. A. M. Isloor and Dr. Darshak R. T., Department of Chemistry, NITK, Surathkal for their good wishes and moral support.

I sincerely thank Dr. Reji Phillip, Raman Research Institute, Bangalore, for providing facility for NLO studies and for his valuable suggestions. I also thank Mr. Safakath K. for his assistance in carrying out z-scan studies.

My special thanks to Dr. Ritu Srivastava, National Physical Laboratory, New Delhi for providing facility for PLEDs fabrication of my polymer samples. I also thank Miss. Vandana Yadav for her help during the device fabrication.

I am thankful to Prof. Samson A. Jenekhe and Dr. Hao Xin, University of Washington, Seattle, USA for photovoltaic characterization of my polymer samples.

I would like to express my appreciation to my friends, Mr. Naveen P., Prashanth K. R. and Miss. Nikhila for their help and company. I wish to thank my other friends, Mr. Vishnumurthy K. A., Shridhar, A. M., Mahesh Padaki, Srikanth Jois, Ganesh B. M., Subramanya I Bhat, Madhuprasad, Shrikanth, Ahipa and all other research colleagues in the department who extended me all round support during my research work.

It will not be complete without mentioning my gratitude to the non-teaching staff members of Chemistry Department Mrs. Kasthuri R., Mrs. Sharmila, Miss. Deepa,

Mr. Prashant, Mr. Ashok, Mr. Pradeep and Mr. Harish for their timely help in the department.

I am extremely grateful to NITK Surathkal for offering the research scholarship and to Department of Chemistry for providing the facilities to carry out my research.

My parents has always been supportive throughout my life, and I wouldn't be where I am today without them. I ever remember the good wishes, inspiration, wholehearted support, love and affection in each and every ways received from my mother, father, brother Mr. Mohan and from family members.

Finally, I would like express my sincere gratitude to each and everyone who have helped me in my carrier.

Murali M.G.

ABSTRACT

In the last three decades, a great deal of attention has been focused on the synthesis of conjugated polymers, because of their significant applications in the field of optoelectronic devices. In this context, the present research work is concentrated on design and synthesis of five new series of thiophene based donor-acceptor (D-A) conjugated polymers (**P1–P12**) for optoelectronic applications. The chemical structures of the polymers are designed by the selection of proper electron donor and electron acceptor units and they are synthesized using multistep synthetic routes. The newly synthesized intermediate compounds, monomers and polymers are characterized by ^1H NMR and FTIR spectroscopic methods as well as using elemental analyses. All the polymers are thermally stable up to 300 °C under nitrogen atmosphere. The linear optical properties of the polymers are studied by using UV-Visible absorption and fluorescence emission spectroscopic techniques. The optical band gap of the polymers is in the range of 1.70 – 2.63 eV. The electrochemical redox behavior of the polymers is investigated by cyclic voltammetry. The electrochemical studies reveal that polymers possess low-lying HOMO and low-lying LUMO energy levels. The preliminary studies on the electroluminescent properties show that polymers **P5**, **P9**, **P10** and **P12** emit red, green, green and white light respectively with lower threshold voltages. The photovoltaic properties of the low band gap polymers **P6** and **P7** are evaluated by fabricating bulk heterojunction solar cells using polymer as both electron donor and acceptor material. The devices exhibit satisfactorily good power conversion efficiency with high open circuit voltage. The nonlinear optical properties of the polymers are studied using z-scan technique. They show strong optical limiting/saturable absorption behavior. Polymers **P1** and **P5** are used to prepare polymer/TiO₂ nanocomposite films and their nonlinear optical properties are studied. The incorporation of TiO₂ nanoparticles into the polymer matrix marginally enhances the nonlinear absorption of the polymer.

Keywords: Conjugated polymers; Optical band gap; Cyclic voltammetry; Polymer light emitting diodes; Bulk heterojunction solar cells; Nanocomposite; Z-scan.

CONTENTS

CHAPTER 1		Page No.
INTRODUCTION TO CONJUGATED POLYMERS		
1.1	INTRODUCTION	1
1.2	MECHANISM OF CONDUCTION IN CONJUGATED POLYMERS	2
1.3	SYNTHESIS OF CONJUGATED POLYMERS	5
1.4	DONOR–ACCEPTOR CONJUGATED POLYMERS	5
1.5	LITERATURE REVIEW	8
1.6	AIM, SCOPE AND OBJECTIVES OF THE PRESENT WORK	24
1.6.1	Design of donor-acceptor conjugated polymers P1–P12	27
 CHAPTER 2		
SYNTHESIS AND STRUCTURAL CHARACTERIZATION OF MONOMERS AND POLYMERS		
2.1	INTRODUCTION	35
2.2	MATERIALS AND INSTRUMENTATION	36
2.3	SYNTHESIS AND STRUCTURAL CHARACTERIZATION OF MONOMERS M1–M10	
2.3.1	Synthesis	37
2.3.2	Experimental section	42
2.3.3	Structural characterization of intermediate compounds and monomers	53
2.4	SYNTHESIS AND STRUCTURAL CHARACTERIZATION OF POLYMERS	
2.4.1	3,4-Didodecyloxythiophene based polymers carrying 1,3,4-oxadiazole and phenyl or 3,4-propylenedioxythiophene segments (P1 and P2)	73
2.4.2	3,4-Didodecyloxythiophene based polymers carrying 1,3,4-oxadiazole, phenylenevinylene and thienylenevinylene units (P3 and P4)	80
2.4.3	3,4-Didodecyloxythiophene based polymers carrying cyanovinylene moieties (P5–P8)	84
2.4.4	3,4-Didodecyloxythiophene based polymers carrying 1,3,4-oxadiazole and fluorenevinylene segments (P9 and P10)	91

2.4.5	3,4-Didodecyloxythiophene based polymers carrying 1,3,4-oxadiazole and cyanophenylenevinylene segments (P11 and P12)	94
2.5	CONCLUSIONS	98

CHAPTER 3

STUDY OF LINEAR OPTICAL AND ELECTROCHEMICAL PROPERTIES OF THE POLYMERS

3.1	INTRODUCTION	100
3.2	LINEAR OPTICAL PROPERTIES	104
3.2.1	Materials and instruments	104
3.2.2	Results and discussion	106
3.3	ELECTROCHEMICAL PROPERTIES	118
3.3.1	Materials and instruments	119
3.3.2	Results and discussion	120
3.4	CONCLUSIONS	135

CHAPTER 4

STUDY OF ELECTROLUMINESCENT AND PHOTOVOLTAIC PROPERTIES OF THE POLYMERS

4.1	INTRODUCTION	137
4.2	POLYMER LIGHT EMITTING DIODES	137
4.2.1	Materials and instruments	140
4.2.2	Fabrication of polymer light emitting diodes	140
4.2.3	Electroluminescent properties of polymers P5, P9, P10 and P12	141
4.3	POLYMER SOLAR CELLS	148
4.3.1	Materials and instruments	153
4.3.2	Fabrication of polymer solar cells	154
4.3.3	Photovoltaic properties of polymers P6 and P7	154
4.4	CONCLUSIONS	158

CHAPTER 5
STUDY OF NONLINEAR OPTICAL PROPERTIES OF THE
POLYMERS AND POLYMER/TiO₂ NANOCOMPOSITES

5.1	INTRODUCTION	159
5.2	EXPERIMENTAL SECTION	163
5.2.1	Materials and instrumentation	164
5.2.2	Z-scan measurements	164
5.3	RESULTS AND DISCUSSION	
5.3.1	Nonlinear optical properties of polymers P1–P12	165
5.3.2	Preparation and characterization of polymer/TiO ₂ nanocomposites	172
5.3.3	Nonlinear optical properties of polymers P1 and P5 films and polymer/TiO ₂ nanocomposite films	176
5.4	CONCLUSIONS	179

CHAPTER 6
SUMMARY, CONCLUSIONS AND FUTURE SCOPE

6.1	SUMMARY	181
6.2	CONCLUSIONS	184
6.3	FUTURE SCOPE	186
	APPENDIX I	188
	REFERENCES	192
	LIST OF PUBLICATIONS	211
	CURRICULUM VITAE	214

LIST OF FIGURES, SCHEMES AND TABLES

Figures

- Figure 1.1** Schematic representation of π -conjugation in poly(acetylene)
- Figure 1.2** Some important conjugated polymers
- Figure 1.3** Schematic representation of band formation during the polymerization of a conjugated monomer into a π -conjugated polymer
- Figure 1.4** Structures of polaron and bipolaron in poly(pyrrole)
- Figure 1.5** Molecular orbital interaction between donor (D) and acceptor (A) moieties
- Figure 1.6** Structures of newly designed D-A type conjugated polymers (**P1–P12**)
- Figure 2.1** ^1H NMR spectrum of 3,4-didodecyloxythiophene-2,5-carboxyhydrazide (**M1**)
- Figure 2.2** Enlarged image of the ^1H NMR spectrum of **M1**
- Figure 2.3** FTIR spectrum of 3,4-didodecyloxythiophene-2,5-carboxyhydrazide (**M1**)
- Figure 2.4** ^1H NMR spectrum of N^2, N^5 -di-(4-methylbenzoyl)-3,4-bis(dodecyloxy)thiophene-2,5-dicarbohydrazide (**10**)
- Figure 2.5** FTIR spectrum of N^2, N^5 -di-(4-methylbenzoyl)-3,4-bis(dodecyloxy)thiophene-2,5-dicarbohydrazide (**10**)
- Figure 2.6** ^1H NMR spectrum of 5,5'-(3,4-bis(dodecyloxy)thiophene-2,5-diyl)bis(2-p-tolyl-1,3,4-oxadiazole) (**11**)
- Figure 2.7** FTIR spectrum of 5,5'-(3,4-bis(dodecyloxy)thiophene-2,5-diyl)bis(2-p-tolyl-1,3,4-oxadiazole) (**11**)
- Figure 2.8** ^1H NMR spectrum of 5,5'-(3,4-bis(dodecyloxy)thiophene-2,5-diyl)bis(2-(4-(bromomethyl)phenyl)-1,3,4-oxadiazole) (**12**)
- Figure 2.9** ^1H NMR spectrum of **M4**
- Figure 2.10** FTIR spectrum of (3,4-bis(dodecyloxy)thiophene-2,5-diyl)dimethanol (**13**)
- Figure 2.11** ^1H NMR spectrum of 3,4-bis(dodecyloxy)thiophene-2,5-dicarbaldehyde (**M5**)

- Figure 2.12** FTIR spectrum of 3,4-bis(dodecyloxy)thiophene-2,5-dicarbaldehyde (**M5**)
- Figure 2.13** ^1H NMR spectrum of 3,3'-(3,4-bis(dodecyloxy)thiophene-2,5-diyl)bis(2-(thiophen-2-yl)acrylonitrile) (**M6**)
- Figure 2.14** Enlarged image of ^1H NMR spectrum of **M6**
- Figure 2.15** FTIR spectrum of 3,3'-(3,4-bis(dodecyloxy)thiophene-2,5-diyl)bis(2-(thiophen-2-yl)acrylonitrile) (**M6**)
- Figure 2.16** ^1H NMR spectrum of 3,3'-(3,4-bis(dodecyloxy)thiophene-2,5-diyl)bis(2-(5-formylthiophen-2-yl)acrylonitrile) (**M7**)
- Figure 2.17** Enlarged image of ^1H NMR spectrum of **M7**
- Figure 2.18** FTIR spectrum of 3,3'-(3,4-bis(dodecyloxy)thiophene-2,5-diyl)bis(2-(5-formylthiophen-2-yl)acrylonitrile) (**M7**)
- Figure 2.19** ^1H NMR spectrum of 2,7-bis[(*p*-triphenylphosphonio)methyl]-9,9'-di-*n*-hexylfluorene dibromide (**M8**)
- Figure 2.20** ^1H NMR spectrum of N^2, N^5 -di(thiophene-2-carbonyl)-3,4-bis(dodecyloxy)thiophene-2,5-dicarbohydrazide (**18**)
- Figure 2.21** FTIR spectrum of N^2, N^5 -di(thiophene-2-carbonyl)-3,4-bis(dodecyloxy)thiophene-2,5-dicarbohydrazide (**18**)
- Figure 2.22** ^1H NMR spectrum of 5,5'-(3,4-bis(dodecyloxy)thiophene-2,5-diyl)bis(2-(thiophen-2-yl)-1,3,4-oxadiazole) (**19**)
- Figure 2.23** Enlarged image of ^1H NMR spectrum of **19**
- Figure 2.24** FTIR spectrum of 5,5'-(3,4-bis(dodecyloxy)thiophene-2,5-diyl)bis(2-(thiophen-2-yl)-1,3,4-oxadiazole) (**19**)
- Figure 2.25** ^1H NMR spectrum of 5,5'-(3,4-bis(dodecyloxy)thiophene-2,5-diyl)bis(2-(5-bromothiophen-2-yl)-1,3,4-oxadiazole) (**20**)
- Figure 2.26** Enlarged image of ^1H NMR spectrum of **20**
- Figure 2.27** ^1H NMR spectrum of monomer **M9**
- Figure 2.28** Enlarged image of ^1H NMR spectrum of **M9**
- Figure 2.29** FTIR spectrum of **M9**
- Figure 2.30** ^1H NMR spectrum of N^2, N^5 -di(4-bromobenzoyl)-3,4-bis(dodecyloxy)thiophene-2,5-dicarbohydrazide (**22**)

- Figure 2.31** FTIR spectrum of N^2,N^5 -di(4-bromobenzoyl)-3,4-bis(dodecyloxy)thiophene-2,5-dicarbohydrazide (**22**)
- Figure 2.32** ^1H NMR spectrum of 5,5'-(3,4-bis(dodecyloxy)thiophene-2,5-diyl)bis(2-(4-bromophenyl)-1,3,4-oxadiazole) (**23**)
- Figure 2.33** FTIR spectrum of 5,5'-(3,4-bis(dodecyloxy)thiophene-2,5-diyl)bis(2-(4-bromophenyl)-1,3,4-oxadiazole) (**23**)
- Figure 2.34** ^1H NMR spectrum of 4',4'-(5,5'-(3,4-bis(dodecyloxy)thiophene-2,5-diyl)bis(1,3,4-oxadiazole-5,2-diyl))dibiphenyl-4-carbaldehyde (**M10**)
- Figure 2.35** Enlarged image of ^1H NMR spectrum of **M10**
- Figure 2.36** FTIR spectrum of 4',4'-(5,5'-(3,4-bis(dodecyloxy)thiophene-2,5-diyl)bis(1,3,4-oxadiazole-5,2-diyl))dibiphenyl-4-carbaldehyde (**M10**)
- Figure 2.37** FTIR spectrum of polyhydrazide **Ph-P1**
- Figure 2.38** ^1H NMR spectrum of polyhydrazide **Ph-P1**
- Figure 2.39** FTIR spectrum of polymer **P1**
- Figure 2.40** ^1H NMR spectrum of polymer **P1**
- Figure 2.41** FTIR spectrum of polymer **P2**
- Figure 2.42** Thermogravimetric traces of polymers **P1** and **P2**
- Figure 2.43** ^1H NMR spectrum of polymer **P3**
- Figure 2.44** FTIR spectrum of polymer **P3**
- Figure 2.45** Thermogravimetric traces of polymers **P3** and **P4**
- Figure 2.46** ^1H NMR spectrum of polymer **P5**
- Figure 2.47** ^1H NMR spectrum of polymer **P6**
- Figure 2.48** ^1H NMR spectrum of polymer **P7**
- Figure 2.49** ^1H NMR spectrum of polymer **P8**
- Figure 2.50** FTIR spectrum of polymer **P6**
- Figure 2.51** Thermogravimetric traces of polymers **P5–P8**

- Figure 2.52** ^1H NMR spectrum of polymer **P10**
- Figure 2.53** FTIR spectrum of polymer **P9**
- Figure 2.54** Thermogravimetric traces of polymers **P9** and **P10**
- Figure 2.55** ^1H NMR spectrum of polymer **P12**
- Figure 2.56** FTIR spectrum of polymer **P11**
- Figure 2.57** Thermogravimetric traces of polymers **P11** and **P12**
- Figure 3.1** Schematic representations of the interaction of HOMO and LUMO energy levels in a conjugated system
- Figure 3.2** State energy diagram of some possible photophysical processes in an organic molecule
- Figure 3.3** Structures of newly synthesized polymers (**P1–P12**)
- Figure 3.4** UV-Vis absorption spectra of **P1** and **P2**
- Figure 3.5** Fluorescence emission spectra of **P1** and **P2**
- Figure 3.6** UV-Vis absorption spectra of **P3** and **P4**
- Figure 3.7** Fluorescence emission spectra of **P3** and **P4**
- Figure 3.8** UV-Vis absorption spectra of **P5–P8** in solution
- Figure 3.9** UV-Vis absorption spectra of **P5–P8** in thin film
- Figure 3.10** Fluorescence emission spectra of **P5–P8** in solution
- Figure 3.11** UV-Vis absorption spectra of **P9** and **P10**
- Figure 3.12** Fluorescence emission spectra of **P9** and **P10**
- Figure 3.13** UV-Vis absorption spectra of **P11** and **P12**
- Figure 3.14** Fluorescence emission spectra of **P11** and **P12**
- Figure 3.15** Photographs of polymer solutions (**P1–P12**) under day light
- Figure 3.16** Typical cyclic voltammetric experimental set up

- Figure 3.17** Cyclic voltammetric traces of **P1** and **P2**
- Figure 3.18** Cyclic voltammograms of **P3** and **P4**
- Figure 3.19** Cyclic voltammograms of **P5–P8**
- Figure 3.20** Cyclic voltammetric traces of **P9** and **P10**
- Figure 3.21** Cyclic voltammetric traces of **P11** and **P12**
- Figure 3.22** HOMO and LUMO levels of new polymers **P1–P12**, PPV and PBD
- Figure 4.1** Schematic diagram of working principle of LED
- Figure 4.2** Energy level diagram of polymers **P5**, **P9**, **P10** and **P12** in comparison with the energy levels of PEDOT:PSS, ITO and Al
- Figure 4.3** a) Electroluminescence spectra of the ITO/PEDOT:PSS/**P5**/Al device at varying forward applied voltage and b) Current density-voltage characteristics of the device
- Figure 4.4** a) Electroluminescence spectrum of the ITO/PEDOT:PSS/**P9**/Al device at a forward applied voltage of 5 V and b) Current density-voltage characteristics of the device
- Figure 4.5** Photographs of polymer solutions **P5**, **P9**, **P10** and **P12** under UV light
- Figure 4.6** a) Electroluminescence spectra of the ITO/PEDOT:PSS/**P10**/Al device at varying forward applied voltage and b) Current density-voltage characteristics of the device
- Figure 4.7** a) Electroluminescence spectra of the ITO/PEDOT:PSS/**P12**/Al device at varying forward applied voltages and b) Current density-voltage characteristics of the device
- Figure 4.8** CIE 1931 chromaticity coordinates (x,y) of PLEDs based on polymers **P5**, **P9**, **P10** and **P12**
- Figure 4.9** Schematic illustration of a photoenergy conversion in solar cells (left). Typical device architecture of a bulk heterojunction polymer solar cell (right)
- Figure 4.10** Current-voltage (*J-V*) curves of an organic solar cell in dark and under illumination

- Figure 4.11** Energy level diagram of polymers **P5–P8**, PEDOT:PSS, P3HT and PC₇₁BM
- Figure 4.12** Current density-voltage curves of BHJ solar cells based on a) **P6:PC₇₁BM** and b) **P7:PC₇₁BM** in dark and under 100 mW/cm² AM1.5 solar illumination
- Figure 4.13** Current density-voltage curves of non-fullerene BHJ solar cells based on a) **P3HT:P6** and b) **P3HT:P7** in dark and under 100 mW/cm² AM1.5 solar illumination
- Figure 5.1** Energy level diagram showing 2PA, 3PA, ESA and ISC
- Figure 5.2** The open aperture z-scan setup
- Figure 5.3** Z-scan curves of polymers **P1–P4**
- Figure 5.4** Z-scan curves of polymers **P9–P12**
- Figure 5.5** Z-scan curves of polymers **P5–P8**
- Figure 5.6** FESEM images of a) **P1/TiO₂** nanocomposite and b) **P5/TiO₂** nanocomposite film (inset: magnified image, Mag=100 KX)
- Figure 5.7** FTIR spectra of a) **P1**, pure TiO₂ nanoparticles and **P1/TiO₂** nanocomposite and b) **P5**, pure TiO₂ nanoparticles and **P5/TiO₂** nanocomposite
- Figure 5.8** UV-Vis absorption spectra of **P1** in chloroform solution, **P1** thin film and **P1/TiO₂** nanocomposite thin film
- Figure 5.9** UV-Vis absorption spectra of **P5** in chloroform solution, **P5** thin film and **P5/TiO₂** nanocomposite thin film
- Figure 5.10** TGA curves of **P1** and **P1/TiO₂** nanocomposite
- Figure 5.11** TGA curves of **P5** and **P5/TiO₂** nanocomposite
- Figure 5.12** Z-scan curves of a) **P1** film and b) **P1/TiO₂** nanocomposite film
- Figure 5.13** Z-scan curves of a) **P5** film and b) **P5/TiO₂** nanocomposite film

Schemes

- Scheme 2.1** Synthesis of monomers **M1** and **M2**
- Scheme 2.2** Synthesis of terephthaloyl chloride (**M3**)
- Scheme 2.3** Synthesis of Wittig salt monomer **M4**
- Scheme 2.4** Synthesis of dicarbaldehyde monomer **M5**
- Scheme 2.5** Synthesis of cyanovinylene monomer **M6** and cyano dicarbaldehyde monomer **M7**
- Scheme 2.6** Synthesis of fluorene Wittig salt monomer **M8**
- Scheme 2.7** Synthesis of monomer **M9**
- Scheme 2.8** Synthesis of monomer **M10**
- Scheme 2.9** Synthesis of polymers **P1** and **P2**
- Scheme 2.10** Synthesis of polymers **P3** and **P4**
- Scheme 2.11** Synthesis of polymers **P5–P8**
- Scheme 2.12** Synthesis of polymers **P9** and **P10**
- Scheme 2.13** Synthesis of polymers **P11** and **P12**

Tables

- Table 3.1** UV-Vis absorption and fluorescence emission spectral data of the polymers
- Table 3.2** Electrochemical potentials, HOMO and LUMO levels of the polymers
- Table 3.3** The barrier energies of new polymers for electron/hole injection
- Table 4.1** Photovoltaic properties of the BHJ polymer solar cells
- Table 5.1** Effective TPA coefficient (β) of the polymers

CHAPTER 1

INTRODUCTION TO CONJUGATED POLYMERS

Abstract

This chapter gives a brief introduction to conjugated polymers. It also covers a brief description of the literature review on synthesis, characterization and optoelectronic applications of various donor-acceptor conjugated polymers. Further, the aim, scope and objectives of the present research work are discussed. Also, the structural design criteria of five new series of thiophene based donor-acceptor type conjugated polymers (P1–P12) have been described.

1.1 INTRODUCTION

Conjugated polymers (CPs), which are intrinsic semiconductors due to their delocalized π -electrons, have attracted much research attention in the last three decades. Conjugated polymers are organic materials, which generally are comprised of carbon, hydrogen and simple heteroatoms like nitrogen, oxygen and sulfur. Conductivity in these materials arises uniquely from the π -conjugation. That is to say, extended and delocalized conjugation originating in overlap of π -orbitals. So, the polymer that possesses the electrical, electronic, magnetic and optical properties of a metal while retaining the mechanical properties and processability commonly associated with a conventional polymer, is termed as an ‘intrinsically conducting polymer’, which is more commonly known as a ‘synthetic metal’. Most of the conjugated polymers studied today (Figures 1.1 and 1.2) have a regular alternation of single and double bonds along the polymer chain.

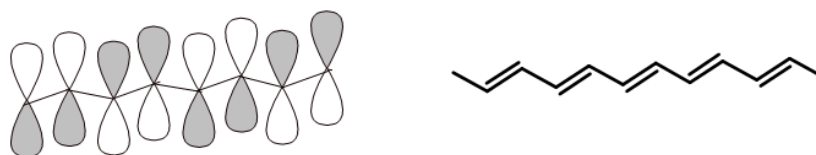


Figure 1.1 Schematic representation of π -conjugation in poly(acetylene)

Extensive research work in the field of CPs has started in late 1970s with the discovery of metallic electrical conductivity in oxidatively doped poly(acetylene) (Chiang et al. 1977). This important discovery led to award of Nobel Prize in Chemistry in the year 2000 to three scientists, Shirakawa, MacDiarmid and Heeger. This pioneering work motivated the researchers to synthesize and to study the

properties of other new classes of π -conjugated polymers based on aromatic precursors such as p-phenylenevinylene, thiophene, pyrrole, carbazole, fluorene and their derivatives (Roncali 1992, McCullough 1998, Skotheim and Reynolds 2007, Sahin et al. 2011 and Junkers et al. 2012). Early work in this field held the hope that these types of polymer systems would serve as replacements for highly conductive metals, such as copper and aluminum for electrical transport or battery electrodes. However, due to the instability of these systems when highly doped, other more practical uses have been realized such as polymer light emitting diodes (PLEDs) (Kraft et al. 1998), photovoltaics (Brabec et al. 2001), thin film transistors (Halls et al. 1995), sensors (McQuade et al. 2000), nonlinear optical materials (Prasad and Williams 1991) and electrochromic devices (Invernale et al. 2009). Moreover, in order to tune the specific properties desired for end user applications, a proper modification of the monomer structure is essential that manipulate both the electronic and optical properties of these polymer systems.

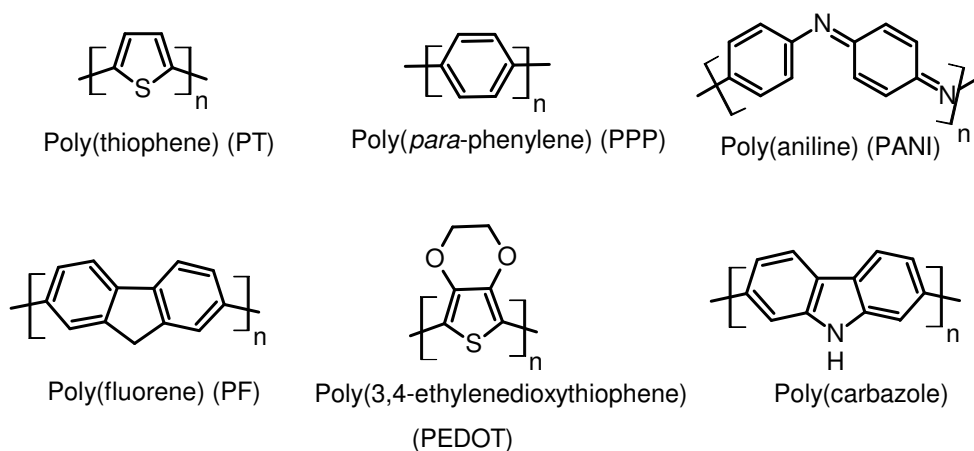


Figure 1.2 Some important conjugated polymers

1.2 MECHANISM OF CONDUCTION IN CONJUGATED POLYMERS

In conjugated polymers, analogous to inorganic semiconductors, the highest occupied band (which originates from the highest occupied molecular orbital, HOMO, of a single monomer unit) is called the valence band, while the lowest unoccupied band (originating from the lowest unoccupied molecular orbital, LUMO, of a single monomer unit) is called the conduction band. The difference in energy between these

levels is called the band gap (E_g). The band structure of a conjugated polymer originates from the interaction of the π -orbitals of the repeating units (monomers) throughout the chain. During the conversion of monomers to polymer in the polymerization reaction, the HOMO and LUMO levels of the repeating unit disperse into the valence and conduction bands. The schematic representation of the band structure of a conjugated polymer is illustrated in Figure 1.3.

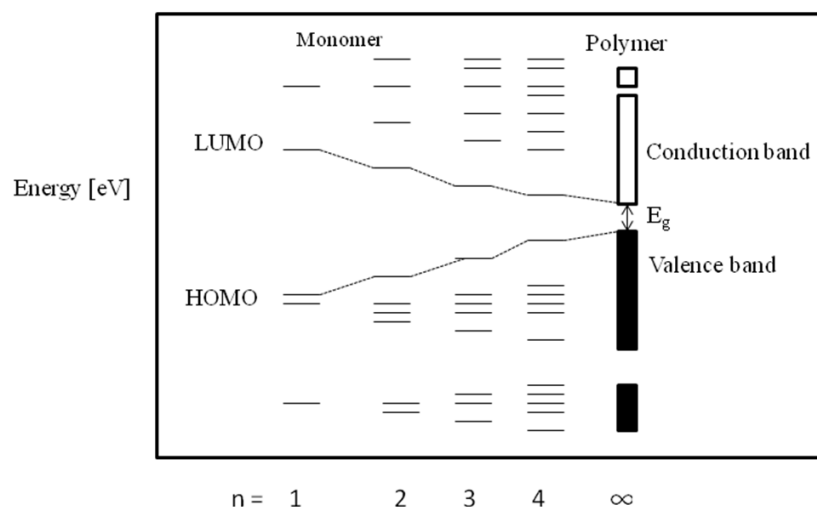


Figure 1.3 Schematic representation of band formation during the polymerization of a conjugated monomer into a π -conjugated polymer

Band theory explains the mechanism of conduction in conducting polymers. According to this theory, conductivity arises due to the formation of a half filled valence band from a continuous delocalized π -system. The conductivity of CPs could be enhanced by the doping process, which involves either oxidation or reduction of the polymer chain. In an oxidation process it could either lose an electron from one of the bands or it could localize the charge over a small section of the chain. Localizing the charge causes a local distortion due to a change in geometry, which costs the polymer some energy. However, the generation of this local geometry decreases the ionization energy of the polymer chain and increases its electron affinity making it more able to accommodate the newly formed charges. This method increases the energy of the polymer less than it would if the charge was delocalized and hence takes

place in preference of charge delocalization. A similar scenario occurs for a reductive process.

The main criteria of doping in conjugated polymer is the ability to oxidize or reduce the polymer without lowering its stability or whether or not they are capable of initiating side reactions that inhibit the polymers ability to conduct electricity. An example is that, doping of a conjugated polymer with bromine. Bromine is too powerful oxidant and adds across the double bonds to form sp^3 carbons. The doping process and generation of charge carriers in poly(pyrrole) proceeds in the following way. In the oxidation doping of poly(pyrrole) an electron is removed from the polymer backbone producing a free radical and a spinless positive charge. The radical and the cation are coupled to each other via local resonance of the charge and the radical. This combination of a charge site and a radical is called a polaron. Upon further oxidation, the free radical of the polaron is removed, creating a new spinless defect called a bipolaron. This is of lower energy than the creation of two distinct polarons. At higher doping levels it becomes possible that two polarons combine to form a bipolaron. Thus at higher doping levels polarons are replaced with bipolarons. Figure 1.4 represents the structures of polaron and bipolaron in poly(pyrrole).

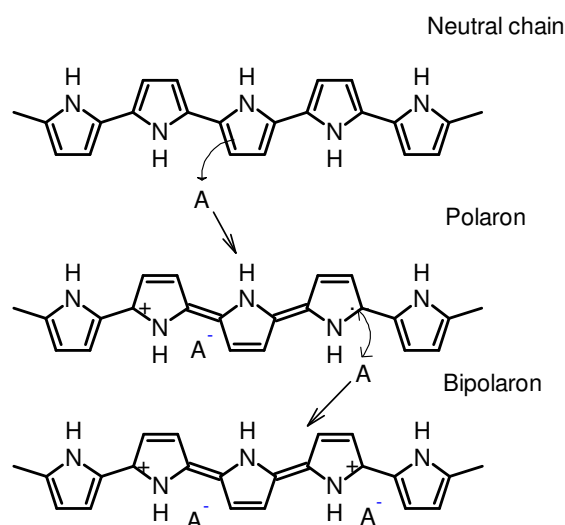


Figure 1.4 Structures of polaron and bipolaron in poly(pyrrole)

1.3 SYNTHESIS OF CONJUGATED POLYMERS

Synthetic methods of conjugated polymers can be classified into two types.

- a) Electrochemical synthesis
- b) Chemical synthesis

Most of the electrochemical syntheses are addition polymerizations and many chemical syntheses are condensation polymerizations. In an electrochemical polymerization, a potential is applied across a solution containing monomer and an electrolyte, producing a conductive polymer film on the anode. Electrochemical polymerization is convenient, since the polymer does not need to be isolated and purified, but it produces structures with varying degrees of structural irregularities. Condensation polymerization generally involves loss or elimination of a chemical species resulting from the reaction of end groups on monomer chains. Chemical synthesis offers two advantages compared with electrochemical synthesis of conjugated polymers: i) a greater selection of monomers and ii) using proper catalysts the ability to synthesize perfectly regio-regular substituted conjugated polymers.

1.4 DONOR–ACCEPTOR CONJUGATED POLYMERS

Conjugated polymers with carbon and heteroatom frameworks have attracted considerable attention due to their structural diversity and fascinating optoelectronic properties. However, design and synthesis of π -conjugated polymers with low oxidation potential, broad absorption spectrum, low band gap, efficient photoinduced charge transfer and separation and ambipolar charge transport with high mobilities are crucial for the fabrication of the devices (Nielsen et al. 2013). In particular, tuning of the HOMO–LUMO energy levels and hence the band gap energy is of great importance for directing material properties towards the desired applications.

In this direction, the donor-acceptor (D–A) approach, introduced by Havinga et al. (1993) in macromolecular systems via alternating electron rich (D) and electron deficient (A) substituents along the conjugated backbone, has attracted a good deal of attention in recent years. The D–A conjugated polymers absorb light at longer wavelengths than the wide band gap conjugated polymers made of all donor units. Judiciously chosen D and A groups are particularly desirable for low band gap polymers due to the significant enhancement of intramolecular charge transfer (ICT)

interaction and conjugation length, which lead to extended absorption and a higher absorption coefficient. Also, an extended rigid π -conjugation with quinonoid character in the polymer backbone facilitates intermolecular interactions between the polymer chains and increases the charge mobility of the polymer (Xiao et al. 2010). Hence, a conjugated polymer with an alternating sequence of appropriate donor and acceptor units in the main chain can induce a reduction in its band gap energy. Further, molecular orbital calculations have shown that the hybridization of the energy levels of the donor and the acceptor moieties result in D–A systems with unusually low HOMO–LUMO separation (Brocks and Tol 1996). If the HOMO levels of the donor and the LUMO levels of the acceptor moiety are close in energy, the resulting band structure will show a low energy gap (Zotti et al. 1999 and Balan et al. 2008). In such systems, the HOMO energy level is raised and the LUMO energy level is lowered by the interaction of D and A molecular orbitals as shown in Figure 1.5.

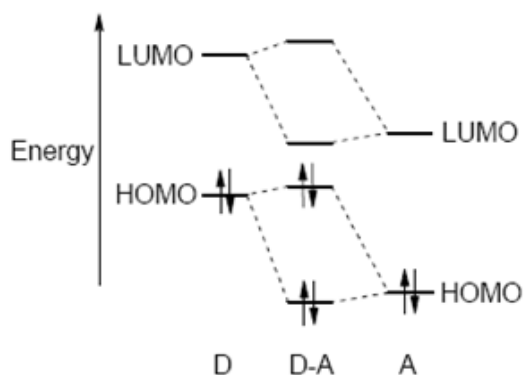


Figure 1.5 Molecular orbital interactions between donor (D) and acceptor (A) moieties (van Mullekom 2000)

In D–A systems, the introduction of electron withdrawing groups reduces E_g by lowering the LUMO levels whereas, the introduction of electron donating groups reduces E_g by raising the HOMO levels (Ajayaghosh 2003). Therefore, introduction of strong electron donors and acceptors in the conjugated polymer backbone is one of the design criteria to obtain extremely low band gap polymers. Also, the electron or hole affinity can be enhanced simultaneously or controlled independently in D–A

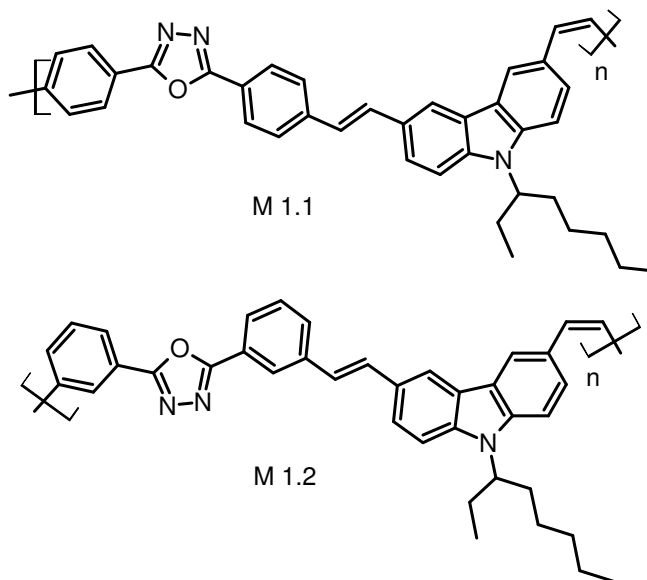
system by modifying the chemical structure of the electron rich or the electron deficient substituents. In other words conjugated polymers with desired HOMO and LUMO energy levels could be obtained by the proper selection of donor and acceptor units. Because of this reason, D–A conjugated polymers are emerging as promising materials for polymer light emitting diodes and polymer solar cells (PSCs). In addition, the increase in effective π -electron delocalization in D–A polymers results in large third-order nonlinear optical susceptibilities, and hence these polymers are considered also as potential candidates in the area of nonlinear optics (Albota et al. 1998 and Huang et al. 2012).

In this context, various D–A conjugated polymers have been designed and synthesized by a number of research groups for optoelectronic applications. Commonly used electron donating moieties in D–A conjugated polymers are thiophene, fluorene, carbazole and pyrrole with various substitution patterns. The substituent groups play an important role in controlling the polymer properties such as chemical, thermal and electronic properties. The most widely used electron withdrawing groups are cyanovinylene, 1,3,4-oxadiazole, 2,1,3-benzothiadiazole, perylene diimides, 2,6-dimethyl-4H-pyran-4-ylidene)propanedinitrile etc. The D–A conjugated polymers can be synthesized by reacting two monomeric units containing proper reactive functionalities, using various reaction methodologies such as condensation reaction, coupling reaction etc. Alternatively, suitable D–A type monomers could be synthesized first which then undergo facile chemical or electrochemical polymerization leading to the formation of D–A polymers.

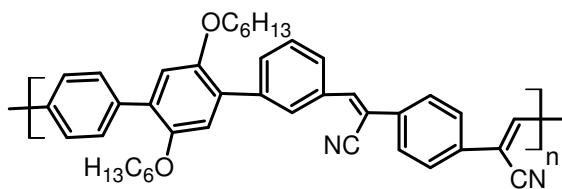
In the following section, a brief account on the literature reports on important D–A type conjugated polymers carrying different types of donor and acceptor moieties has been presented. Further, their synthetic methodologies and the effect of various D/A units on optical and electrochemical properties of the polymers have been highlighted.

1.5 LITERATURE REVIEW

Two new conjugated polymers M 1.1 and M 1.2 carrying carbazole and 1,3,4-oxadiazole units were synthesized via Wittig polycondensation methodology by Song et al. (1999). The turn-on voltages of M 1.1 and M 1.2 were 7.5 and 10.5 V respectively, when single layer light emitting diodes of the structure ITO glass/polymer/Al were fabricated. In particular, single layer device based on M 1.1 showed maximum brightness of 500 cd/m² at 20 V.

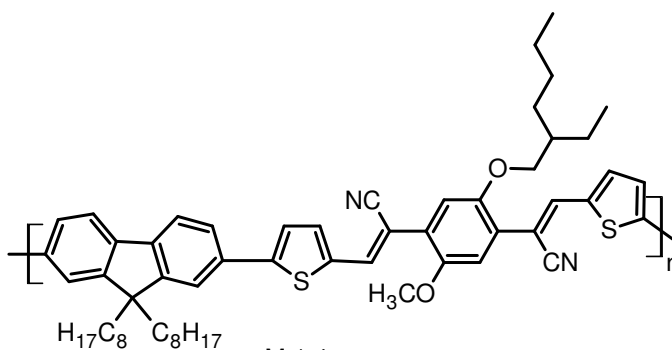


Wu et al. (2001) synthesized a new luminescent conjugated polymer M 1.3 containing cyanovinylene groups as electron acceptor units via Suzuki coupling reaction. The resulting polymer showed high thermal stability, high electron affinity, good solubility and thin film forming properties. The electron affinity (-3.13 eV) of the polymer is higher than that of poly(p-phenylenevinylene) (PPV), owing to the introduction of electron withdrawing cyanovinylene groups. The observed electron affinity would greatly facilitate the electron injection from the cathode of the PLED and hence high work function Ag was used as the cathode in the fabrication of PLEDs. The double layer PLEDs based on the structure of ITO/CuPc/M1.3/Ca/Ag showed high electron transporting ability and good electroluminescence performance with the emission of bright orange light.



M 1.3

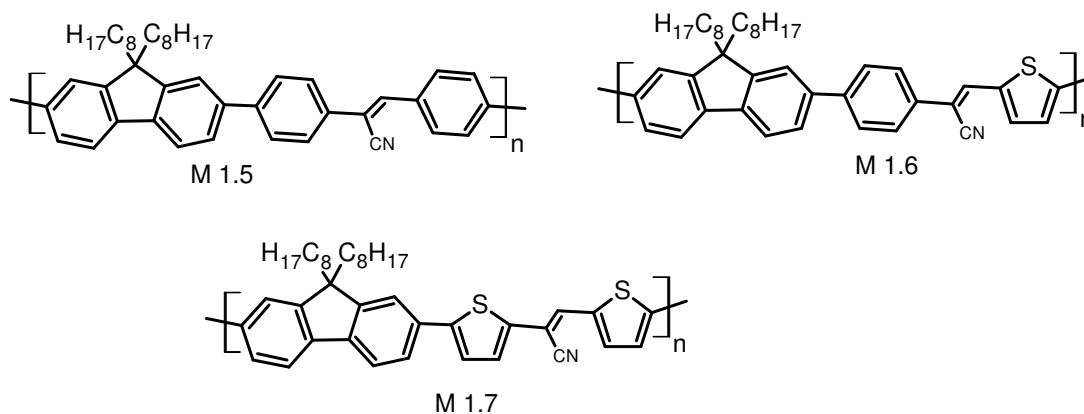
Cho et al. (2004) reported the synthesis, characterization and electroluminescence properties of fluorene based alternating polymers containing different comonomers. It was observed that incorporation of electron rich thiophene and electron deficient cyano moieties in the polymer backbone leads to higher HOMO and lower LUMO levels in all the polymers. In particular, the HOMO and LUMO energy levels of polymer M 1.4 are -5.59 and -3.69 eV respectively. Further, single layer LED devices fabricated from the polymers emitted bluish green to pure red light. The device based on M 1.4 exhibited pure red emission with CIE coordinate values (0.63, 0.38) with low turn-on voltage of 2.4 V. The maximum luminance and external quantum efficiency were approximately 3100 cd/m² and 0.46 % respectively.



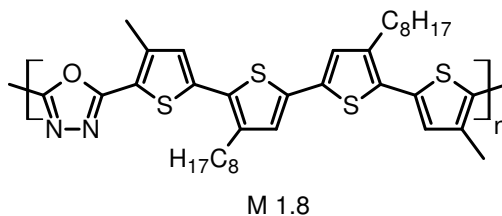
M 1.4

Lee et al. (2005) synthesized fluorene based alternating polymers M 1.5–M 1.7 via Pd-catalyzed Suzuki polymerization with the aim of achieving pure red emission. The photoluminescence and electroluminescence maxima of the polymers were red shifted with respect to those of the homopolymer, poly(9,9'-dioctylfluorene-2,7-diyl), upon introduction of cyanovinylene and aromatic groups. In particular, the absorption and emission maxima of polymers M 1.6 and M 1.7 containing thiophene units were red shifted to a greater extent than those of the polymer containing a phenylene unit (M 1.5). Among these polymers, M 1.7 showed narrow band gap with high-lying

HOMO (-5.52 eV) and low-lying LUMO levels (-3.38 eV) due to the presence of strong electron donating thiophene and electron withdrawing cyanovinylene units in the polymer backbone. Further, the PLED based on M 1.7 exhibited pure red emission with a low turn-on voltage of 3V.

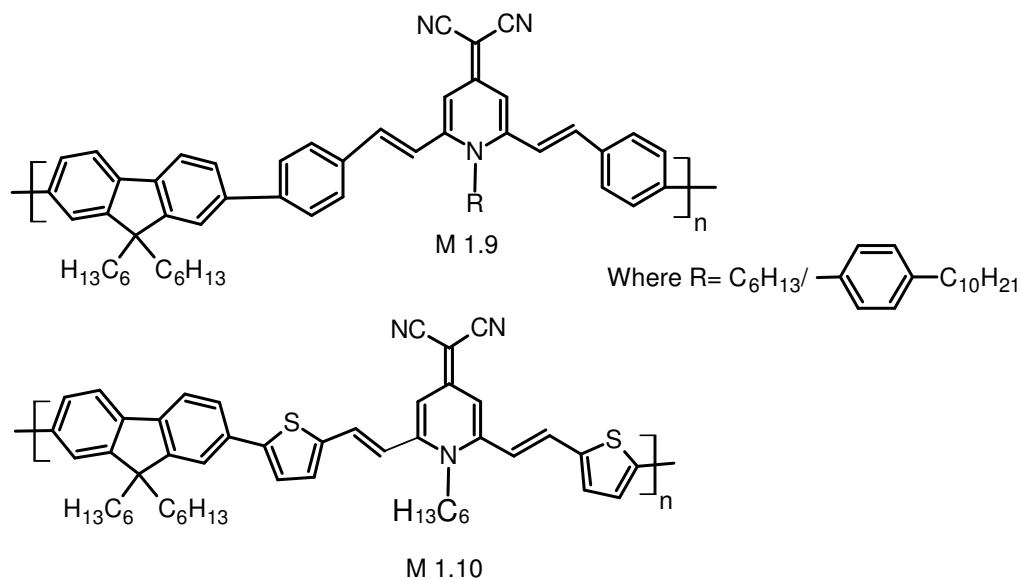


Levi et al. (2006) synthesized a D–A conjugated polymer, M 1.8, carrying alkyl substituted thiophene and 1,3,4-oxadiazole segments via electrochemical polymerization. It was demonstrated that the incorporation of π -conjugated electron accepting oxadiazole units into the polythiophene backbone lead to a significant improvement in the n-doping/undoping redox stability of the resulting polymer.

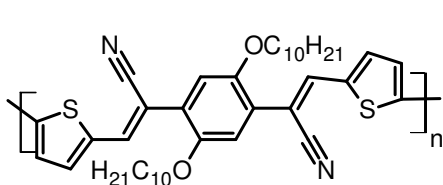


Two new light emitting conjugated polymers M 1.9 and M 1.10 based on fluorene unit were synthesized via Pd-catalyzed Suzuki coupling reaction by Peng et al. (2006). The polymers possess low-lying LUMO energy levels ranging from -3.14 to -3.28 eV and high-lying HOMO energy levels ranging from -5.43 to -5.64 eV with improved redox stability. Further, single layer LEDs fabricated from these polymers exhibited orange to red emission with external quantum efficiencies in the range 0.43 – 1.06 %. The authors concluded that incorporation of electron acceptor 2-[2,6-bis(2-

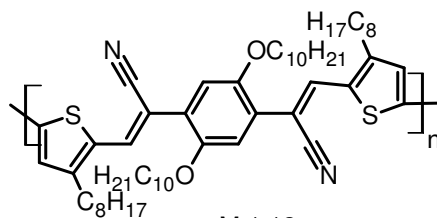
arylvinyl)pyridine-4-ylidene]malononitrile (BPM) unit to form D–A architecture in the polymer chain not only increased the electron affinities, but also improved the hole injection and transport properties of the polymers.



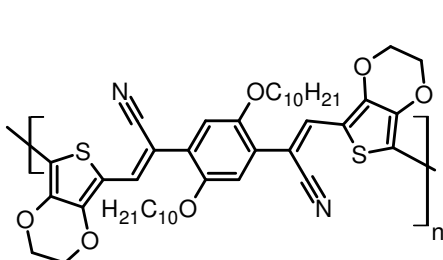
Low band gap donor-acceptor conjugated polymers M 1.11–M 1.14 were synthesized by Colladet et al. (2007) for organic solar cell applications. The polymers consist of bis(1-cyano-2-thienylvinylene)phenylene base structure with long alkoxy and alkyl side chains to increase solubility of the polymers. Polymer M 1.13 showed the lowest band gap among these polymers. It was observed that the reduction potentials of the polymers are hardly affected by the incorporation of the ethylenedioxy groups. These results suggest that the reduction process is mainly dominated by the presence of the cyanovinylene linkages. But there was a variation in HOMO energy levels of the polymers. These results indicate that changing the substituents on the thiophene unit allows the modulation of the HOMO level/ionization potential of the polymer. Bulk heterojunction solar cells made by the blend of low band gap polymers with [6,6]-phenyl-C₆₁-butyric acid methyl ester (PC₆₁BM) displayed maximum power conversion efficiency (PCE) of around 0.19 %.



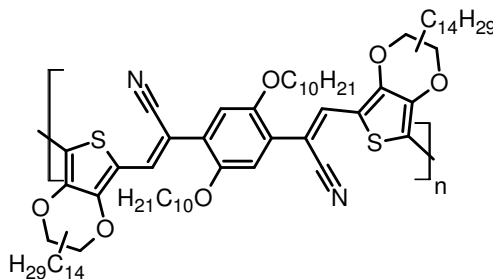
M 1.11



M 1.12

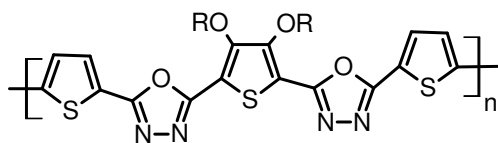


M 1.13



M 1.14

Hegde et al. (2010) reported the synthesis, optical, electrochemical and nonlinear optical properties (NLO) of a series of D–A conjugated polymers M 1.15 consisting of alternate hole transporting thiophene and electron transporting 1,3,4-oxadiazole units. The increase in the length of the alkoxy side chain of the thiophene ring does not show any significant change in the optical and electrochemical properties of the polymers. The NLO properties of the polymers were investigated at 532 nm using single beam z-scan and degenerate four wave mixing (DFWM) techniques with nanosecond laser pulses. The polymers exhibited strong optical limiting behavior due to ‘effective’ three-photon absorption process.

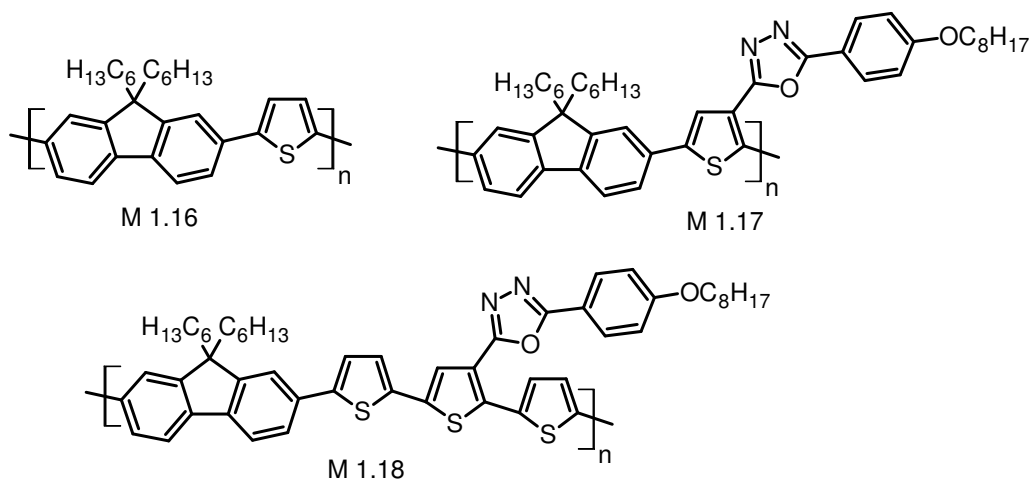


M 1.15

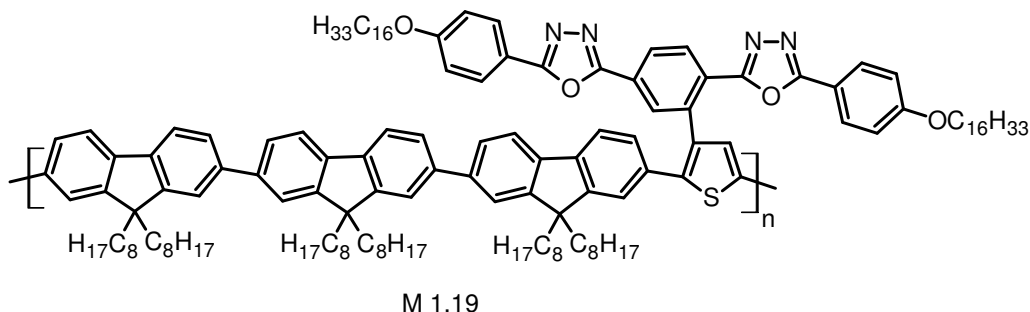
R = -C₄H₉, C₁₀H₂₁, C₁₄H₂₉

Zhao et al. (2009) synthesized three alternating fluorene and thiophene based polymers, M 1.16–M 1.18 via Pd-catalyzed Suzuki coupling reaction. The incorporation of oxadiazole bulky side chains affects greatly on thermal, optical, electrochemical and photovoltaic properties of the polymers. The LUMO energy levels of -2.60 and -2.78 eV respectively for polymers M 1.17 and M 1.18 are lower than that of M 1.16. These results suggest that the electron injection and transporting

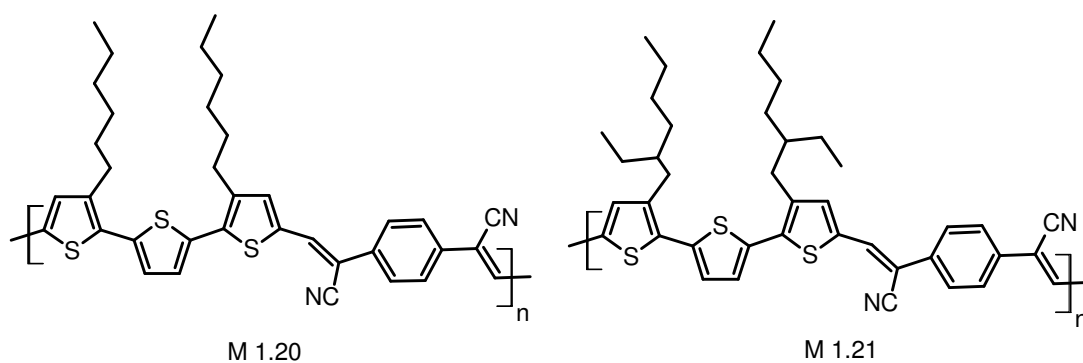
properties of the polymers are improved by the introduction of strong electron deficient oxadiazole side chains. The PSC based on M 1.18 showed maximum PCE of 1.49 %.



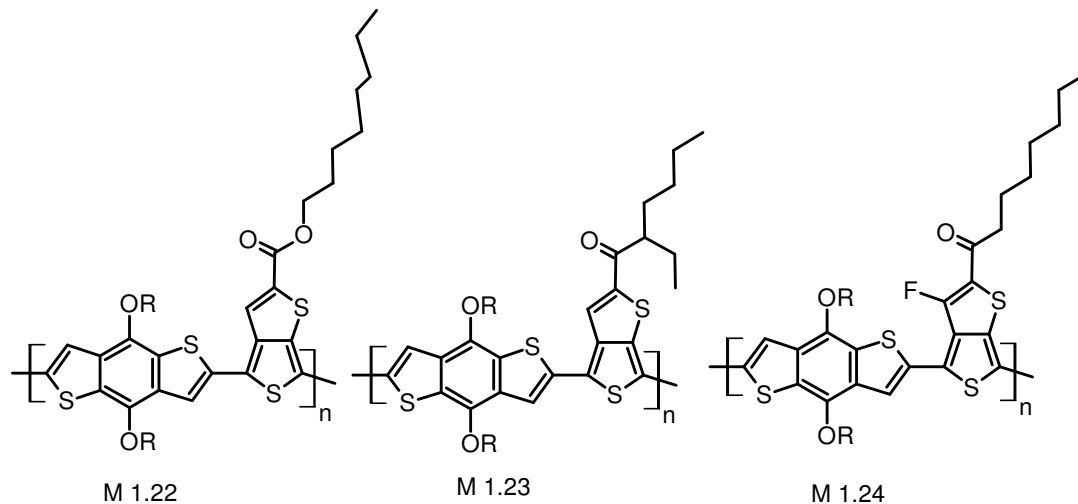
Synthesis and characterization of new conjugated polymers composed of 9,9'-dioctylfluorene and thiophene based monomer containing oxadiazole unit was discussed by Yang et al. (2009). The polymers exhibited lower HOMO and LUMO energy levels as compared to poly(fluorene) (PF) which resulted in better electron injection and transport properties. Light emitting devices were fabricated with a configuration of ITO/PEDOT:PSS/polymer/Ca/Al for all polymers. Among them, device based on M 1.19 attained brightness of 5558 cd/m^2 with current efficiency of 0.39 cd/A .



Bricaud et al. (2009) reported the synthesis of conjugated polymers M 1.20 and M 1.21 containing cyanovinylene linkages. UV-Vis absorption and cyclic voltammetric data showed that these polymers exhibit lower band gap, improved light harvesting properties and low-lying HOMO level. Bilayer heterojunction solar cells were fabricated using polymer as donor material and thermally evaporated films of fullerene C₆₀ as acceptor material. The best device showed a maximum external quantum efficiency of ~20 % and a PCE of 0.4 % under simulated AM 1.5 solar illumination.

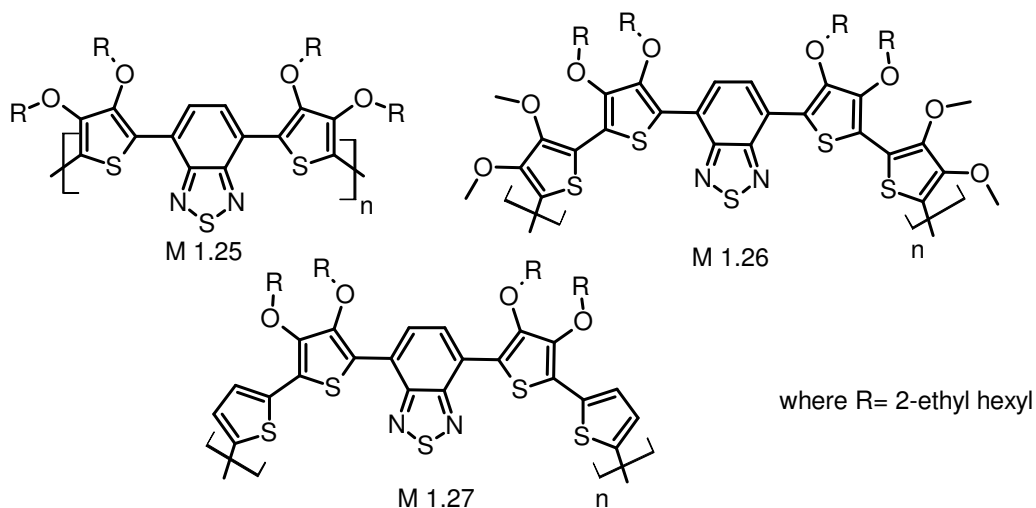


Chen et al. (2009) studied the relation between energy levels of the donor/acceptor materials and the open-circuit voltage (V_{oc}) in bulk heterojunction (BHJ) polymer solar cells. It was demonstrated that the V_{oc} of polymer solar cells constructed based on a low band gap polymer, M 1.22, can be tuned, step by step, using different functional groups, to achieve values as high as 0.76 V. This increased open-circuit voltage combined with a high short-circuit current density (J_{sc}) resulted in a polymer solar cells with a PCE as high as 6.77 %. The authors concluded that introducing stronger electron withdrawing groups to the backbone of the polymers found to be effective in lowering the HOMO of polymers, which directly affects the V_{oc} of PSCs.

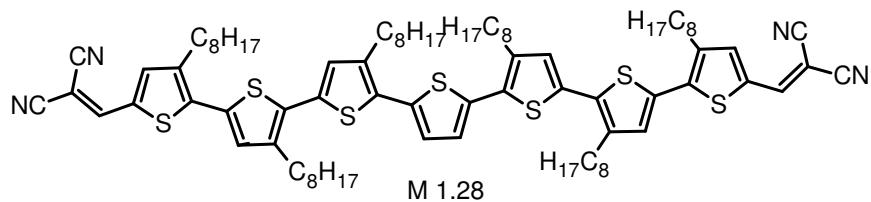


R=2-ethyl hexyl

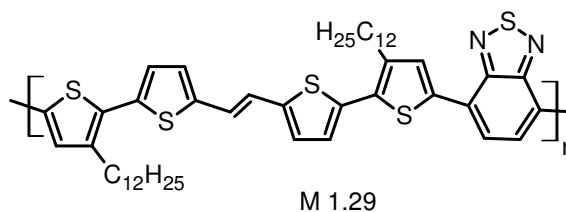
Structure-property relationships and performance in photovoltaic devices of a series of green colored D–A conjugated polymers, M 1.25–M 1.27 comprised of electron rich 3,4-dioxythiophenes and electron deficient 2,1,3-benzothiadiazole unit were examined by Beaujuge et al. (2010). The photovoltaic properties of the polymers were investigated in BHJ solar cells with PC₆₀BM as the acceptor. Polymers M 1.25 and M 1.26 afforded green colored devices with PCE up to 1.9 % under AM 1.5 G solar illumination. To enhance efficiency of the device, PEDOT:PSS was replaced by MoO₃ and [6,6]-phenyl-C₇₀-butyric acid methyl ester (PC₇₀BM) was used instead of PC₆₀BM in the device structure based on M 1.27. This device showed a PCE of 2.71 % in absence of any tedious solvent or thermal annealing treatment. Finally, the authors highlighted the importance of adjusting the device configuration as a function of the intrinsic properties such as band structure, mobility of the charge carriers of the semiconducting polymers.



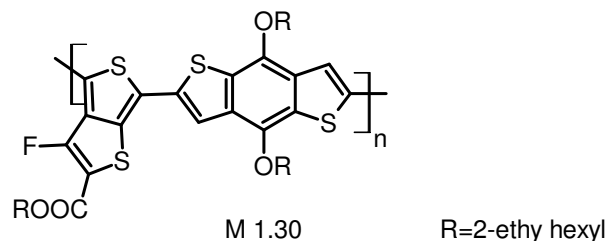
A solution processable low band gap cyanovinyl-substituted oligothiophene, M 1.28, was used as the electron donor in BHJ solar cells by Liu et al. (2010). The molecule showed electrochemical band gap of 1.71 eV and the optical band gap of 1.68 eV. BHJ solar cell with the structure, ITO/PEDOT:PSS/M 1.28:PC₆₁BM/LiF/Al showed a PCE of 2.45 %.



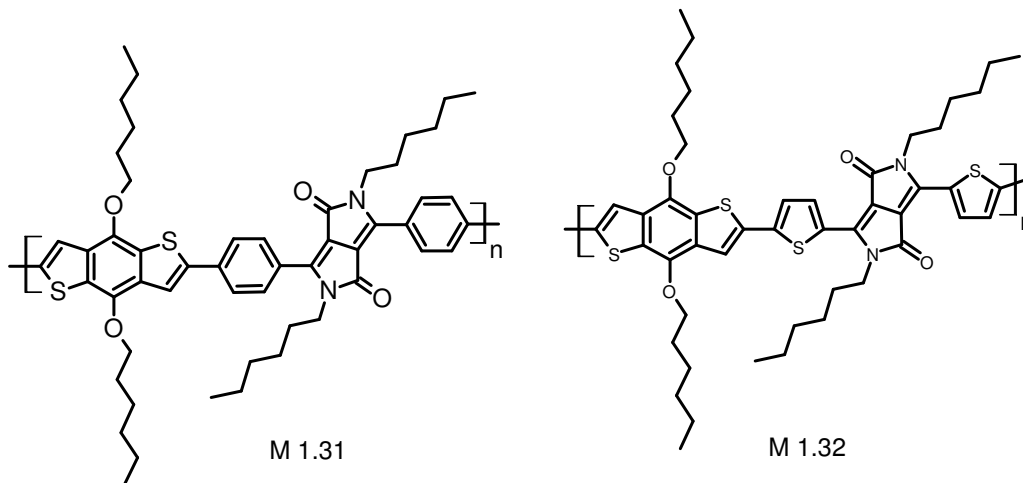
A conjugated polymer, M 1.29 comprised of electron rich thienylenevinylene and electron deficient 2,1,3-benzothiadiazole was synthesized by Lim et al. (2010). The polymer showed broad absorption over the entire visible region with a low band gap of 1.57 eV. The photovoltaic properties of the polymer were investigated in a BHJ solar cell using PC₇₁BM as the electron acceptor and a PCE of 1 % was achieved. The Authors concluded that though the polymer showed low band gap, low HOMO energy level and high hole mobility, the photovoltaic efficiency was relatively low because of the change in the electronic properties of the polymer after blending with PC₇₁BM.



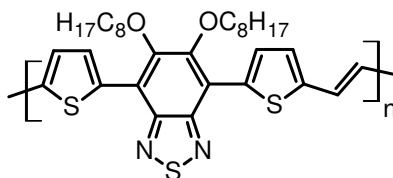
Liang et al. (2010) developed a new semiconducting polymer, M 1.30 for BHJ solar cells. The authors stated that introduction of fluorine into the thieno[3,4-b]thiophene unit provides a polymer with relatively low-lying HOMO energy level and hence higher value of V_{oc} . The BHJ solar cells based on the blend films of polymer with PC₇₁BM exhibited PCE of 7.4 %. Both external quantum efficiency (EQE) and internal quantum efficiency (IQE) values were high, implying that the solar energy harvesting is very efficient in the device. The Authors concluded that thieno[3,4-b]thiophene-benzodithiophene based polymers are a promising class of materials for developing high performance polymer solar cells.



Kanimozhi et al. (2010) synthesized two diketopyrrolopyrrole based copolymers M 1.31 and M 1.32, containing donor-acceptor structural units, via Stille coupling reaction. The polymers showed absorption in the longer wavelength region and exhibited promising photovoltaic performance in bulk heterojunction devices. The solar cell based on polymer M 1.32 showed a maximum PCE of 2.78 % after annealing the device at 100 °C. The Authors concluded that structural manipulation of active material influences the efficiency of organic solar cells.

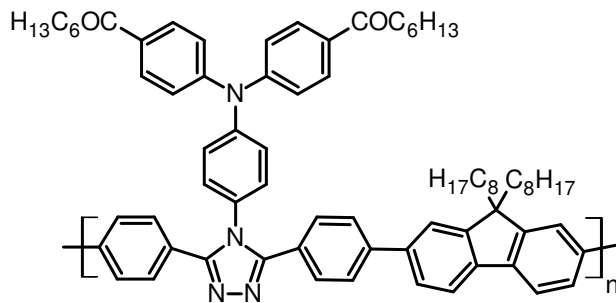


A planar poly(thienylenevinylene) derivative, M 1.33, was synthesized by Qing et al. (2011) via Stille coupling reaction. The polymer exhibited good solubility, good thermal stability, broad absorption in the visible region and narrow band gap of 1.65 eV. The HOMO and LUMO energy levels of the polymer are -4.97 and -2.99 eV respectively. The PCE of the PSC based on M 1.33/PC₇₀BM reached 1.53 %. The results revealed that planar poly(thienylenevinylene) derivatives containing an electron withdrawing 2,1,3-benzothiadiazole unit could be promising candidates for photovoltaic applications.

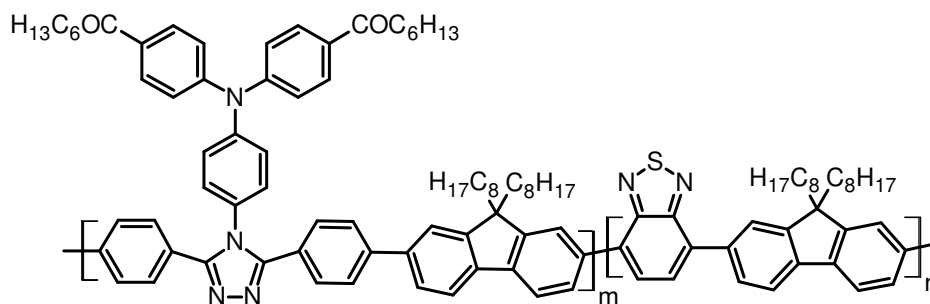


M 1.33

Wang et al. (2011) synthesized two conjugated polymers M 1.34 and M 1.35 containing electron deficient 1,2,4-triazole unit in the main chain with electron rich triphenylamine pendant groups via the Suzuki coupling reaction. The incorporation of 2,1,3-benzothiadiazole structure in M 1.35 reduced the coplanarity of the conjugated polymer, which prohibited the polymer from aggregation. Further, the polymer (M 1.35) showed lower HOMO (-5.78 eV) and LUMO (-3.40 eV) levels than those of polymer M 1.34 which does not contain 2,1,3-benzothiadiazole unit. The PLED based on polymer M 1.35 exhibited maximum electroluminescence efficiency of 2.60 cd/A.

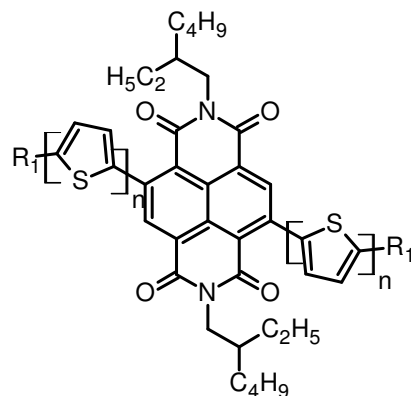


M 1.34



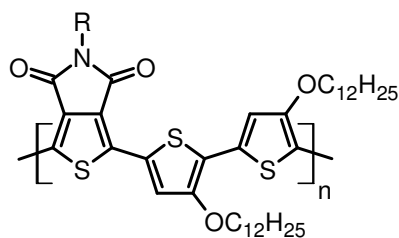
M 1.35

A series of novel oligothiophene and naphthalene diimide based oligomers with D–A architecture were synthesized and used for the design of non-fullerene electron acceptor materials for organic solar cells (Ahemed et al. 2011). The oligomers showed broad absorption bands with optical band gaps in the range of 1.4 – 2.1 eV. The LUMO energy level of the oligomers was relatively constant at -4.0 to -4.1 eV, whereas the HOMO energy level was in the range of -5.5 to -6.1 eV. The BHJ solar cells incorporating one of the n-type oligomer semiconductors (M 1.36 with $n = 3$ and $R_1 = C_6H_{13}$) as the electron acceptor and poly(3-hexylthiophene) (P3HT) as the electron donor showed a PCE of 1.5 % with a V_{oc} of 0.82 V.

Where $n = 1, 2, 3, 4$ $R_1 = H, C_6H_{13}$

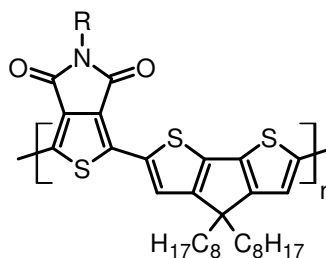
M 1.36

Guo et al. (2011) reported the synthesis of three new D–A conjugated polymers M 1.37–M1.39 incorporating thieno[3,4-*c*]pyrrole-4,6-dione acceptor and dialkoxy bithiophene or cyclopentadithiophene units as donor units. The BHJ solar cells using polymers M 1.37 or M 1.38 as the electron donor and PC₇₁BM as the electron acceptor exhibit low open-circuit voltage in the range 0.40 – 0.60 V and power conversion efficiencies below 1.5 %. However, polymer M 1.39 containing cyclopentadithiophene donor units exhibit relatively a deeper HOMO level of -5.26 eV. Hence a high V_{oc} of ~0.8 V with a PCE of 3 % was achieved in the BHJ solar cell based on polymer M 1.39.



M 1.37: R=n - dodecyl

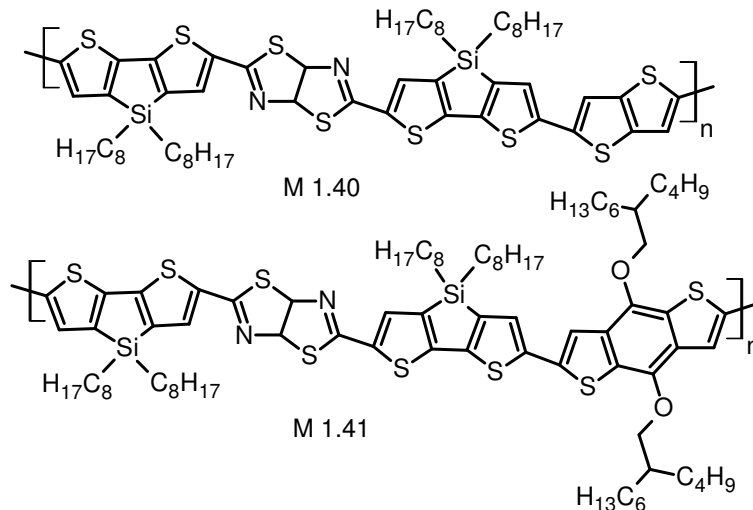
M 1.38: R=2-butyloctyl



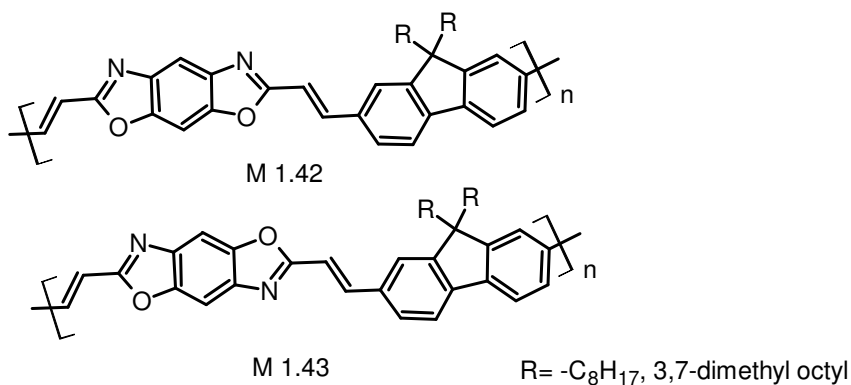
M 1.39: R=n - dodecyl

New thiazolothiazole and dithienosilole based D–A polymeric semiconductors, M 1.40 and M 1.41 were synthesized by Subramaniyan et al. (2011) via Stille coupling reaction. The polymers showed low band gaps (1.73 – 1.77 eV), broad absorption band, high carrier mobility and oxidative stability with excellent film forming properties. The PC₇₁BM based BHJ solar cells utilizing M 1.41 were found to have a

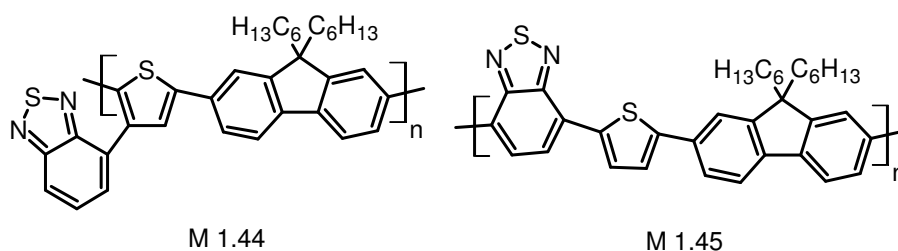
highest power conversion efficiency of 5.3 % under 100 mW/cm² AM 1.5G irradiation in air.



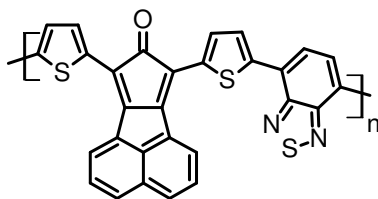
New fluorescent poly(arylenevinylene)s M 1.42 and M 1.43 containing benzobisoxazole and fluorene moieties were synthesized via Horner-Wadsworth-Emmons coupling reaction (Intemann et al. 2011). The flexible side chains on the fluorene ring led to good solubility while maintaining good thermal stability whereas the incorporation of the electron accepting benzobisoxazole moiety into the polymer chain led to high electron affinity. Preliminary studies on the electroluminescence properties showed that these polymers exhibit promising brightness in guest-host OLEDs. The solution processed light emitting diodes using dilute blends of the polymer in a poly(N-vinyl carbazole) matrix gave blue emission with luminous efficiencies of up to 1 cd/A at ~470 nm.



Two model polymers, M 1.44 and M 1.45, containing fluorene as electron donating and 2,1,3-benzothiadiazole as electron accepting moiety were synthesized by Chang et al. (2012) via Suzuki coupling reaction. Polymer solar cells with ITO/PEDOT:PSS/M 1.44 or M 1.45:PC₇₁BM(1:4)/Al structure were constructed and demonstrated to show a power conversion efficiency of 0.82 and 1.24 % for M 1.44 and M 1.45, respectively. The observed superior device performance for M 1.45 was attributed to the efficient solar light harvesting and charge transport due to the lower band gap and close molecular packing in the polymer.



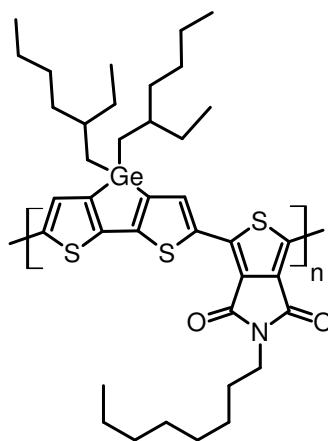
Alternating copolymer M1.46 based on 7,9-di(thiophen-2-yl)-8H-cyclopenta[a]acenaphthylen-8-one-co-benzothiadiazole (DTCPA) and 2,1,3-benzothiadiazole unit was synthesized by Ranjith et al. 2012 via Stille coupling reaction. The resulting polymer showed a broad absorption in the range 300 – 800 nm with a band gap of about 1.51 eV. Photovoltaic properties of the copolymer were studied by fabricating polymer solar cell using the blend of copolymer and PC₆₁BM as the active material. The experimental results suggested that optimization of the device fabrication will improve the performance of the device.



M 1.46

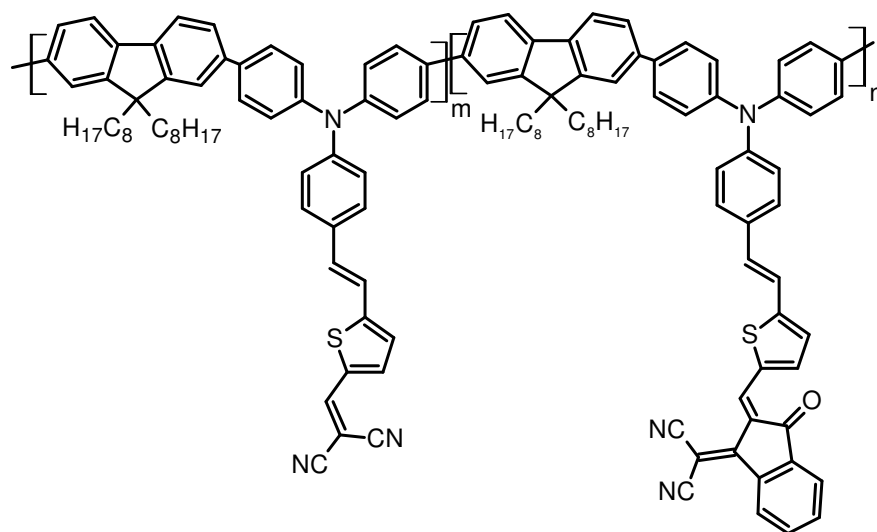
Small et al. (2012) demonstrated the inverted polymer solar cells based on a low band gap polymer, M 1.47 with an alternating dithienogermole–thienopyrrolodione repeating units. The inverted solar cell was constructed with a structure of substrate (rigid or flexible)/ITO/electron transporting layer/photoactive layer/hole transporting

layer/top anode. Enhanced charge collection in inverted polymer solar cells was demonstrated using surface modified ZnO/polymer nanocomposite as electron transporting layer. The PCE of the device was found to be 7.4 %, which is the highest efficiency reported to date for polymer solar cells.



M 1.47

Duan et al. (2012) designed a new series of narrow band gap conjugated polymers for light absorption in the entire visible region. The polymers were synthesized by attaching two different acceptor groups, malononitrile and 2-(1,2-dihydro-1-oxoindene-3-ylidene)malononitrile, into the same polymer main chain via Knoevenagel condensation. The absorption spectra of the polymers were greatly extended in the visible region by simultaneously using acceptors of different electron withdrawing ability. The polymers exhibited deep HOMO energy levels whereas the LUMO energy levels of the polymers were controlled by attaching strongest acceptor units to the side chain of the polymers. The polymers exhibited promising photovoltaic properties and the maximum PCE of 2.83 % was achieved for the device based on M 1.48 when blended with PC₇₁BM.



M 1.48

Owing to the importance and established properties of the various donor-acceptor type conjugated polymers, in the present study it has been planned to design and synthesize new D-A type conjugated polymers carrying electron releasing 3,4-disubstituted thiophene, 9,9'-dialkylfluorene units and electron accepting 1,3,4-oxadiazole, cyanovinylene and cyanophenylenevinylene units in the polymer main chain.

1.6 AIM, SCOPE AND OBJECTIVES OF THE PRESENT WORK

In the last three decades, conjugated polymers have attracted much attention as active materials for optoelectronic applications, such as PLEDs, field-effect transistors, photovoltaic cells, optical switching devices, data storage devices etc. In particular, an electroluminescent conjugated polymer as the active material in the field of PLEDs has attracted considerable research interest because these materials are potential candidates in flat-panel display and lighting applications. In this regard, conjugated polymers have drawn great interest mainly because of easy processing, low operating voltages, faster response times and facile color tuning over the full visible range, which makes them suitable for large area flat panel displays. Among these factors, the main advantage of the conjugated polymers is the color tunability as obtained by changing the molecular structure of the emitting polymers by introducing suitable substituents into the polymer backbone. Further, it is necessary to develop

conjugated polymers of pure blue, green and red emission colors for full color LED devices. Due to this reason, the design and synthesis of new conjugated polymers of varied optoelectronic properties play a vital role in the area of display technology.

However, in most of the electroluminescent conjugated polymers such as poly[2-methoxy-5-(2'-ethylhexyloxy)-p-phenylenevinylene] (MEH-PPV), hole injection and transport are more favorable than electron injection and transport due to its high LUMO energy level, which results an imbalance in the rates of electron and hole injection and thus lowering the device efficiency (Braun and Heeger 1991 and Kraft et al. 1993). The high device efficiency can be achieved by balancing the electron and hole injection rates.

The PSCs based on conjugated polymer as electron donors with fullerene derivatives as electron acceptor have received tremendous attention for their unique advantages over traditional silicon based solar cells and dye sensitized solar cells (DSSCs), which includes low cost solution fabrication processing, light weight, large area and flexible panels as well as potential to clean and renewable energy (Poortmans and Arkhipov 2006). The main concern of the studies of PSCs is to increase the PCE of the devices. In this regard, narrow band gap polymers are considered to be promising candidates for improved light harvesting in high-performance PSCs (Wang et al. 2013).

Recently, conjugated polymers are gaining considerable interest as a promising class of NLO materials as well, because of their large third-order nonlinear optical response, chemical stability and processability (Ji et al. 2003 and Hua et al. 2004). In this direction, a deeper understanding of structure-property relationship would help in designing new organic conjugated molecules by the judicious choice of functional substituents, and thus to tune their optical properties for applications in optoelectronic devices. Therefore various structural design criteria have been used to obtain efficient conjugated polymers for device applications.

Among them, the donor-acceptor type architecture in the macromolecular systems via alternating electron rich and electron deficient substituents along a polymer backbone is the well known approach to obtain efficient polymers. In this system, the interaction between a strong electron donor (D) and strong electron acceptor (A) units

in the main chains gives rise to an increased double bond character between them. Hence, a conjugated polymer with an alternating sequence of appropriate donor and acceptor units in the main chain may show a low band gap. Moreover, incorporation of both electron donor and acceptor segments into the polymer backbone is the most promising approach of adjusting the HOMO and LUMO levels of the conjugated polymers. Furthermore, the presence of strong electron donor and electron acceptor units in the polymer increases the effective π -electron delocalization. The strong delocalization of π -electrons in the polymeric backbone determines a very high molecular polarizability and thus results in remarkable third-order optical nonlinearities. Thus D–A type polymers are being considered as promising class of nonlinear materials. Other important class of materials being considered as promising for photonic applications is metal and semiconductor nanoparticles. Research has shown that it is advantageous to embed metal/semiconductor nanoparticles in thin polymer films for application purposes because the polymer matrix serves as a medium to assemble the nanoparticles and stabilize them against aggregation. Furthermore, the nanocomposite structures are known to substantially enhance the optical nonlinearities (Chen et al. 2008).

In this view, the present work is aimed to develop suitable donor-acceptor conjugated polymers for optoelectronic applications. The chemical structures of D–A conjugated polymers are designed by the selection of proper electron donor and acceptor units and the polymers are synthesized using multistep synthetic routes. 3,4-Dialkoxythiophene and 9,9'-dialkylfluorene units are used as the electron donor moieties in the polymeric structures. The electron withdrawing units like 1,3,4-oxadiazole, cyanovinylene and cyanophenylenevinylene are used as electron acceptor segments. In this context, the following main objectives have been proposed in the present research work.

1. To design and synthesize five series of new donor-acceptor type conjugated polymers containing 3,4-didodecyloxythiophene/9,9'-dialkylfluorene units as electron donor and 1,3,4-oxadiazole/cyanovinylene/cyanophenylenevinylene units as electron acceptor along with some conjugative spacers.

2. To confirm the chemical structure of all intermediates and the monomers using FTIR spectroscopy, ^1H NMR spectroscopy and elemental analyses.
3. To characterize the polymers using FTIR and ^1H NMR spectroscopic methods, elemental analyses, gel permeation chromatography (GPC) and thermogravimetric analysis (TGA).
4. To evaluate linear optical and electrochemical properties of the synthesized D–A conjugated polymers.
5. To discuss the structure-property relationship by correlating the results obtained in the optical and electrochemical studies of the polymers with their chemical structure.
6. To investigate the electroluminescent behavior of the polymers by fabricating PLEDs using polymers as emissive layer.
7. To carryout preliminary studies on photovoltaic properties of the narrow band gap polymers by fabricating BHJ solar cells using polymer as donor materials and by fabricating non-fullerene BHJ solar cells using polymer as acceptor materials.
8. To prepare and to characterize conjugated polymer/ TiO_2 nanocomposites.
9. To evaluate NLO properties of the conjugated polymers and their nanocomposites using z-scan technique.

1.6.1 Design of donor-acceptor conjugated polymers P1–P12

As described in literature, the D–A conjugated polymers are promising candidates for optoelectronic applications due to their good charge carrying and optical properties. In order to achieve desired properties in such polymers, following important factors should be considered during the molecular design of these polymers.

(i) Presence of extended conjugation length (ii) change in the identity of the conjugation bridge (iii) increase in the π -donor and π -acceptor strength (iv) incorporation of more polarisable double bonds (v) increase in the planarity of the polymer backbone and (vi) good solution processability of the polymers. On the basis of these factors, five new series of thiophene based D–A type conjugated polymers (**P1–P12**) are designed and synthesized in the present study. The core structure of all

the polymers consists of electron donating 3,4-didodecyloxythiophene unit and it is attached to different electron accepting units along the polymer backbone. It is known that thiophene derivatives are good candidates as electroactive materials because of their versatility in the structural modification and good semiconducting property. The presence of long alkoxy pendants at 3- and 4- positions of the thiophene ring is to improve the solvent processability of the corresponding polymer. Further, different conjugated spacer units have also been incorporated in between donor and acceptor segments so as to extend the conjugation in the repeating unit. Based on the chemical structure of the polymer chains, which consists of donor and acceptor (push-pull structure) π -conjugated units along the polymer backbone, these D–A conjugated polymers are expected to show low band gaps due to the intramolecular charge transfer interactions between the donor and the acceptor units. Furthermore, the synthesized polymers are expected to show good redox, optical and thermal properties. The design criteria and the structural features of these polymers (**P1–P12**) are discussed in the following sections. The chemical structures of the target polymers are given in Figure 1.6.

1.6.1.1 3,4-Didodecyloxythiophene based polymers carrying 1,3,4-oxadiazole and phenyl or 3,4-propylenedioxythiophene (PDOT) segments (P1 and P2)

It is known that the most prominent features of thiophene derivatives are their good thermal stability both in the neutral and doped states and wide electronic and optical tunability. Further, they possess lower delocalization energy and the addition of thiophene ring to the backbone of conjugated polymeric materials narrows the HOMO and LUMO band gaps. Since 3,4-didodecyloxythiophene derivatives are both electron rich and hole transporting, it is necessary to introduce electron withdrawing units to the main chains or side chains of the polymer to attain large electron affinities. The strong electron withdrawing 1,3,4-oxadiazole unit is widely used in electron injection and hole blocking materials because of its high electron affinity, good thermal and chemical stability. Hence 1,3,4-oxadiazole unit is introduced as electron acceptor unit in the main chain of polymers **P1** and **P2**. The polymer chain in **P1** contains 3,4-didodecyloxythiophene, 1,3,4-oxadiazole and phenyl units whereas in

case of **P2**, the phenyl ring is replaced by a 3,4-propylenedioxythiophene (PDOT) unit. Though the pendant alkoxy groups on thiophene ring facilitates solvent processability of the polymer, the steric interaction of alkoxy groups of adjacent thiophene rings reduces the coplanarity of the rings and hence decreases the effective conjugation length of the polymer. Such a steric effect is very prominent in case of poly(3,4-dialkoxythiophene)s and related polymers when two 3,4-dialkoxythiophene rings are placed adjacent or nearby through a conjugated linker. Hence, in the present study, it has been planned to keep apart two 3,4-dialkoxythiophene rings along the polymer chain by introducing a suitable conjugated spacer unit. The (1,3,4-oxadiazolyl)benzene unit in **P1** and (1,3,4-oxadiazolyl)-3,4-propylenedioxythiophene unit in **P2** are incorporated between two alkoxy substituted thiophene rings, so as to minimize steric interactions between the alkoxy groups. Further, incorporation of these conjugative spacer units also ensures the D–A structure in the polymers.

1.6.1.2 3,4-Didodecyloxythiophene based polymers carrying 1,3,4-oxadiazole, phenylenevinylene and thienylenevinylene units (P3 and P4)

In this series, two new D–A conjugated polymers **P3** and **P4** are designed and synthesized. Similar to **P1** and **P2**, these polymers also contain 3,4-didodecyloxy thiophene moiety as the electron donor unit and 1,3,4-oxadiazole moiety as the electron acceptor unit, along with additional aromatic and vinylic linkages along the polymer chain. In case of **P3**, 3,4-dialkoxythiophene rings are separated by a spacer, 2-(ethynylphenyl)-1,3,4-oxadiazole moiety, which not only serve to planarize the polymer backbone by overcoming torsional interactions between the rings, thus extending effective conjugation length, but also to increase the π -electron delocalization along the polymer backbone. The chemical structure of the repeating unit in **P4** is almost similar to that in **P3**, except that one of the 3,4-dialkoxythiophene ring in **P3** is replaced by an unsubstituted thiophene ring in **P4**. Such a simple structural modification in the polymer chain allows studying the effect of alkoxy pendant groups on optical and electrochemical properties of the conjugated polymers.

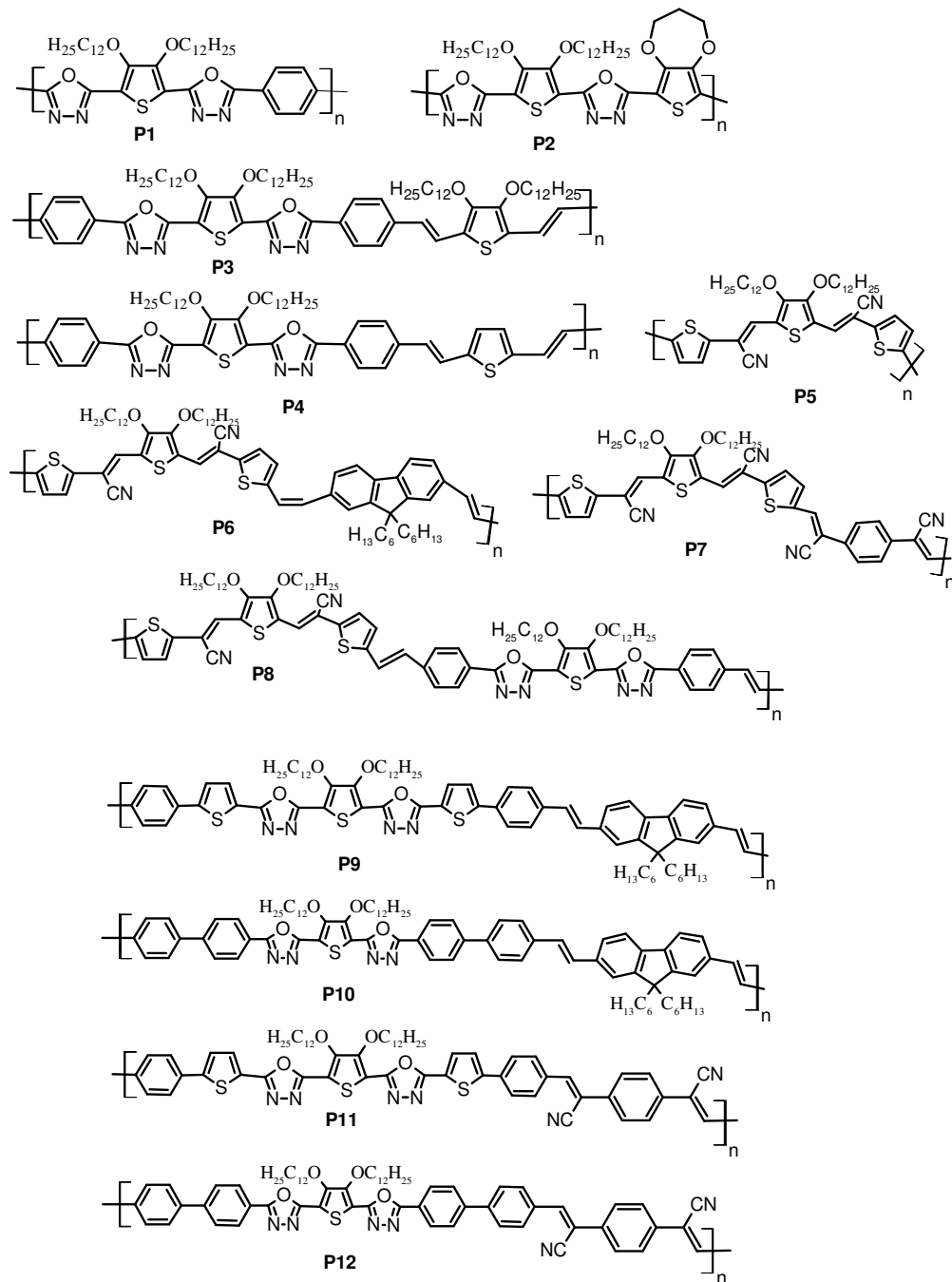


Figure 1.6 Structures of newly designed D–A type conjugated polymers (P1–P12)

1.6.1.3 3,4-Didodecyloxythiophene based polymers carrying cyanovinylene moieties (P5–P8)

The core structure of polymers **P5–P8** consists of electron donating 3,4-didodecyloxythiophene and electron accepting cyanovinylene units. The repeating unit in polymer **P5** consists of a core 3,4-didodecyloxythiophene unit which is connected to two thiophene ring through a cyanovinylene linker. The two unsubstituted thiophene rings on either sides of the monomer unit not only keep apart any two dialkoxy substituted thiophene rings along the polymer chain and thus avoids the appearance of steric interactions between the alkoxy groups, but also result in an alternating D–A arrangement along the polymer chain due to electron rich nature of the thiophene ring. Other three polymers **P6–P8** also contain the same molecular structure in their repeating units, along with additional conjugated units. The conjugation length of repeating unit in **P6–P8** is extended as compared to that in **P5**, by introducing an electron donating dialkylfluorene unit in **P6** and an electron withdrawing cyanophenylenevinylene unit in **P7** and a donor-acceptor conjugated system in **P8**. It is expected that, incorporation of these units along the polymer chain would affect optical and electrochemical properties of the polymers.

In the present study, it has been intended to study the effect of incorporation of electron donating or electron withdrawing units to the monomeric unit which already has a D–A structure. That is to say, incorporation of additional conjugated segments in **P6**, **P7** and **P8** not only extend the conjugation length but also affect the alternating D–A arrangement along the polymer chain. For instance in **P6**, dialkylfluorene unit being electron rich in nature do not extend the alternating D–A structure whereas in **P7**, incorporation of electron withdrawing cyanophenylenevinylene unit extends the alternating D–A structure throughout the monomer chain. In other words, the extent of alternating D–A arrangement is larger in case **P7** than that in **P6**. This factor would also influence the polymer properties in addition to the nature (electron donating or electron withdrawing) of the additional conjugated units. So, the chemical structures of **P6–P8** are designed in such a way that, a comparative study on the influence of extent of D–A structure on optical and electrochemical properties of these polymers is

possible. Other design criteria are as follows. Fluorene unit is selected as electron donor unit in **P6**, because fluorene derivatives show high solution and solid-state fluorescence quantum yields (60–80 %), good film forming and hole transporting properties. Further, they exhibit unique chemical and physical properties because they contain a rigid planar biphenyl unit and the fluorene rings are easily substituted with alkyl groups at the remote C-9 position, which improves the solubility and processability of the polymer without significantly increasing the steric interactions in the polymer backbone. As a result, polyfluorene derivatives are promising electron donors in D–A conjugated systems. In addition, the presence of vinylene linkages in polymers **P5–P8** facilitates to planarize the polymer structure. Furthermore, due to the presence of strong electron acceptor cyanovinylene moiety in the polymer backbone, the newly designed polymers are expected to show narrow band gaps with broader absorption in the visible range. Hence the newly designed polymers are expected to show improved photovoltaic properties.

1.6.1.4 3,4-Didodecyloxythiophene based polymers carrying 1,3,4-oxadiazole and fluorenevinylene segments (P9 and P10)

It has been planned to synthesis two new D–A conjugated polymers **P9** and **P10** based on 3,4-didodecyloxythiophene carrying dialkylfluorene units as electron donor segment in their backbone. The polymeric structure also includes high electron affinity 1,3,4-oxadiazole ring. As compared to **P6–P8**, the number of vinylic linkages in the polymer chains of **P9** and **P10** is reduced so as to obtain chemically stable polymers. The vinylic (–C=C–) linkages generally tend to undergo photo-oxidation reactions during the working of polymer device leading to a shorter life time and lower performance of the device. Hence from the application point of view, it is desirable to have a polymer with less number of vinylic units in the polymer chain. The role of thiophene ring attached to 1,3,4-oxadiazole ring in **P9** is two-fold. Being an electron donating unit it extends the alternate D–A arrangement along the chain. It also serves to reduce steric interactions in the polymer and hence to planarize the polymer chain. In **P10**, conjugative spacer thiophene ring is replaced by a phenyl ring. As a result, the polymer chain in **P10** contains a biphenyl unit. The major concern

with this structural change (**P9** to **P10**) is that the two phenyl rings of the biphenyl unit being nonplanar may strongly influence the electronic structure of the polymer. Thus it would be interesting to study and compare the optical and electrochemical properties of these two polymers and hence to explore effect of the structural modification on polymer properties. Further **P9** and **P10** are expected to show good thermal stability as their chains are made up of rigid aromatic units.

1.6.1.5 3,4-Didodecyloxythiophene based polymers carrying 1,3,4-oxadiazole and cyanophenylenevinylene units (P11 and P12)

The chain structure of polymers **P11** and **P12** are comparable with those of **P9** and **P10** respectively. The electron rich dialkylfluorene rings in **P9** and **P10** are replaced with a strong electron withdrawing cyanophenylenevinylene unit in the backbone of **P11** and **P12**. This structural modification is expected to enhance electron transporting and hole blocking properties of the polymers. It would further help in understanding the structure-property relationship in D–A conjugated polymers. So it is worth while exercise to synthesize these polymers and to study and compare their optical and electrochemical properties.

The present work describes the synthesis and characterization of five series of thiophene based D–A polymers (**P1–P12**). The thesis is divided into six chapters. **Chapter 2** describes the synthesis and structural characterization of various intermediate compounds and the monomers. Also, the synthetic procedures followed for the synthesis of five series of D–A conjugated polymers (**P1–P12**) are described. Further, the spectral characterization details of these polymers are presented in this chapter.

In **Chapter 3**, the linear optical and electrochemical properties of the polymers have been discussed. The linear optical properties of the polymers are studied using UV-Visible absorption and fluorescence emission spectroscopic methods. Whereas, the cyclic voltammetry (CV) is used to investigate the electrochemical redox behavior of the polymers and the HOMO and the LUMO energy levels of the polymers are estimated. The structure-property relationship has been discussed by correlating the

chemical structure of the polymers with the results obtained in optical and electrochemical studies.

The electroluminescent and photovoltaic properties of the conjugated polymers are presented in **Chapter 4**. The preliminary studies on the electroluminescent properties of the polymers are carried out by fabricating light emitting devices of the structure ITO/PEDOT:PSS/polymer/Al, using polymers P5, P9, P10 and P12 as the emissive layer. The photovoltaic properties of the low band gap polymers P5–P8 are investigated by fabricating bulk heterojunction solar cells using polymer as donor materials and PC₇₁BM as acceptor material. Also, non-fullerene BHJ solar cells are fabricated using polymers as acceptor material and poly(3-hexylthiophene) as the donor material.

The NLO properties of the polymers (**P1–P12**) are investigated by using z-scan technique. The experimental details and the results obtained in the z-scan study are discussed in **Chapter 5**. It also covers the discussion on preparation and characterization of P1/TiO₂ and P5/TiO₂ nanocomposites. The NLO properties of the nanocomposites are also studied and compared with those of the polymers.

Finally, summary and conclusions of the present research work are given in **Chapter 6** along with an account on scope for the future work.

CHAPTER 2

SYNTHESIS AND STRUCTURAL CHARACTERIZATION OF MONOMERS AND POLYMERS

Abstract

This chapter presents the details of synthesis and characterization of various intermediate compounds and the monomers. The chapter also describes the synthesis of five series of newly designed thiophene based donor-acceptor conjugated polymers (P1–P12). The chemical structures of all the intermediate compounds, the monomers and the polymers are confirmed by ¹H NMR and FTIR spectroscopic methods as well as by elemental analyses. The average molecular weight data of the polymers and the results obtained in the thermogravimetric analysis of the polymers are also presented in the chapter.

2.1 INTRODUCTION

The newly designed five series of thiophene based D–A conjugated polymers (**P1–P12**) were synthesized from the corresponding monomers using a proper reaction methodology viz polycondensation, coupling reaction and oxidative polymerization reaction. The required monomers for the polymerization reactions were synthesized using multistep synthetic routes. The monomers (**M1–M10**) used for the synthesis of five series of newly designed thiophene based D–A polymers are summarized as below.

Monomers used for the synthesis of polymers **P1** and **P2** (Scheme 2.9) are:

- (1) 3,4-Didodecyloxythiophene-2,5-carboxyhydrazide (**M1**) (Scheme 2.1)
- (2) 3,4-Propylenedioxythiophene-2,5-dicarboxylic acid chloride (**M2**)
- (3) Terephthalic acid chloride (**M3**) (Scheme 2.2)

Monomers used for the synthesis of polymers **P3** and **P4** (Scheme 2.10) are:

- (1) (4,4'-(5,5'-(3,4-bis(dodecyloxy)thiophene-2,5-diyl)bis(1,3,4-oxadiazole-5,2-diyl))bis(4,1-phenylene))bis(methylene)bis(triphenylphosphonium) bromide (**M4**) (Scheme 2.3)
- (2) 3,4-Bis(dodecyloxy)thiophene-2,5-dicarbaldehyde (**M5**) (Scheme 2.4)
- (3) Thiophene-2,5-dicarbaldehyde

Monomers used for the synthesis of polymers **P5–P8** (Scheme 2.11) are:

- (1) 3,3'-(3,4-Bis(dodecyloxy)thiophene-2,5-diyl)bis(2-(thiophen-2-yl)acrylonitrile) (**M6**) (Scheme 2.5)

- (2) 3,3'-(3,4-Bis(dodecyloxy)thiophene-2,5-diyl)bis(2-(5-formylthiophen-2-yl)acrylonitrile) (**M7**)
- (3) 2,7-Bis[(p-triphenylphosphonio)methyl]-9,9'-di-*n*-hexylfluorene dibromide (**M8**) (Scheme 2.6)
- (4) 1,4-Phenylenediacetonitrile
- (5) Wittig salt monomer (**M4**)

Monomers used for the synthesis of polymers **P9** and **P10** (Scheme 2.12) are:

- (1) 4,4'-(5,5'-(5,5'-(3,4-Bis(dodecyloxy)thiophene-2,5-diyl)bis(1,3,4-oxadiazole-5,2-diyl))bis(thiophene-5,2-diyl))dibenzaldehyde (**M9**) (Scheme 2.7)
- (2) 4',4''-(5,5'-(3,4-Bis(dodecyloxy)thiophene-2,5-diyl)bis(1,3,4-oxadiazole-5,2-diyl))dibiphenyl-4-carbaldehyde (**M10**) (Scheme 2.8)
- (3) Fluorene Wittig salt monomer (**M8**)

Monomers used for the synthesis of polymers **P11** and **P12** (Scheme 2.13) are:

- (1) Dicarbaldehyde monomer (**M9**)
- (2) Dicarbaldehyde monomer (**M10**)
- (3) 1,4-Phenylenediacetonitrile

The experimental protocol used for the synthesis of all intermediate compounds, monomers and the target polymers and their structural characterization details are discussed in the subsequent sections of this chapter.

2.2 MATERIALS AND INSTRUMENTATION

Thiodiglycolic acid, diethyl oxalate and *n*-bromoalkanes were purchased from Lancaster Company (UK) and were used as received. Terephthalic acid, 4-methyl benzoyl chloride, thiophene-2,5-dicarbaldehyde, thiophene-2-carbonyl chloride, thiophene-2-acetonitrile, 4-bromobenzoyl chloride, 4-formylphenylboronic acid, tetrakis(triphenylphosphine)palladium(0) [Pd (PPh₃)₄], 1,4-phenylenediacetonitrile, lithium aluminum hydride (LiAlH₄) and 2,3-dichloro-5,6-dicyanobenzoquinone (DDQ) were purchased from Sigma Aldrich Chemical Co. and were used as received. All solvents and other reagents were of analytical grade. They were purchased commercially and used without further purification.

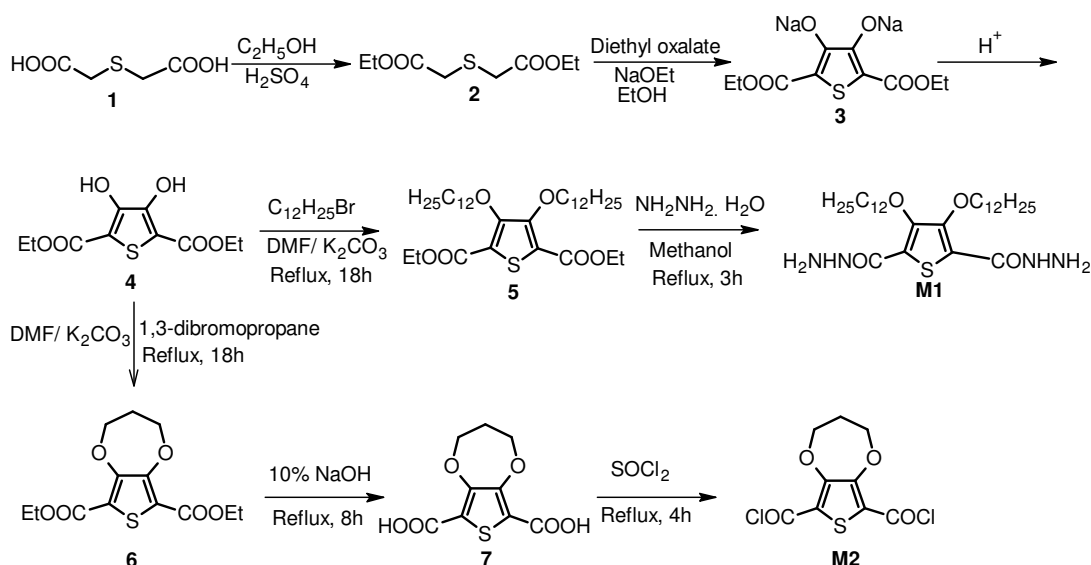
The progress of the reactions was monitored by thin layer chromatography (TLC), performed on a silica gel 60-F₂₅₄ coated aluminum sheet. Melting point was

determined on open capillaries using a Stuart SMP3 (BIBBY STERLIN Ltd. UK) melting point apparatus. ^1H NMR spectra were recorded with a BRUKER 400 MHz NMR spectrometer using trimethyl silane (TMS) as internal reference. Infrared spectra of all the compounds and the polymers were recorded on a NICOLET AVATAR 330 FTIR spectrometer (Thermo Electron Corporation). Elemental analyses were performed on a Flash EA 1112 CHNS analyzer (Thermo Electron Corporation). Molecular weights of the polymers were determined on WATERS make gel permeation chromatography system with reference to polystyrene standards using tetrahydrofuran (THF) as solvent. Thermogravimetric analysis of the polymers was carried out using an EXSTAR TG/DTA 7000 (SII Nanotechnology Inc.) thermal analyzer under nitrogen atmosphere at a heating rate of $5\text{ }^\circ\text{C}/\text{min}$.

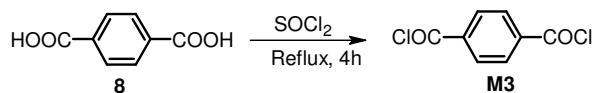
2.3 SYNTHESIS AND STRUCTURAL CHARACTERIZATION OF MONOMERS M1–M10

2.3.1 Synthesis

The synthetic routes for all the intermediate compounds and the monomers (**M1–M10**) are given in Schemes 2.1–2.8.

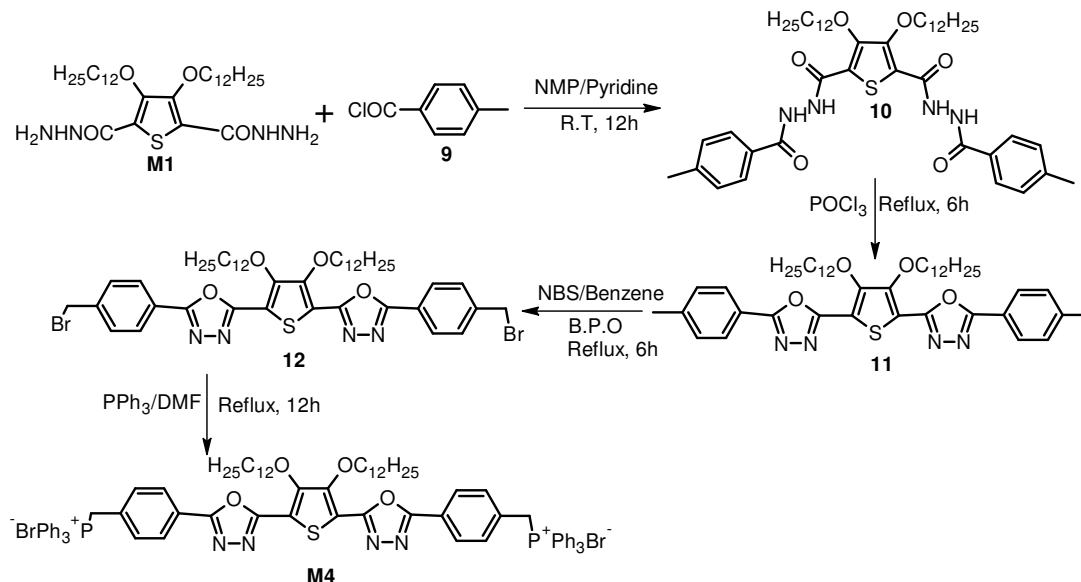


Monomer **M1** was synthesized from 3,4-didodecyloxythiophene-2,5-dicarboxylate (**5**). Compounds **5** and **6** were prepared by a multistep synthetic route starting from thiodiglycolic acid according to the previously reported methods (Overberger et al. 1951, Daoust and Leclerc 1991, Zhang et al. 1998 and Dietrich et al. 1994). All the reactions were performed under inert atmosphere. Compound **5** was treated with hydrazine hydrate in methanol under reflux condition for 3 h to afford the dihydrazide monomer **M1** (Scheme 2.1). Etherification reaction of compound **4** with 1,3-dibromopropane in N,N-dimethylformamide (DMF) in the presence of potassium carbonate (K_2CO_3) as base under reflux condition for 18 h afforded the compound 3,4-propylenedioxythiophene-2,5-dicarboxylate (**6**) in good yield. Compound **6** was then hydrolyzed with 10 % NaOH solution under reflux condition for 8 h to obtain 3,4-propylenedioxythiophene-2,5-dicarboxylic acid (**7**). The conversion of dicarboxylic acid **7** to its acid chloride **M2** was achieved by treating it with thionyl chloride ($SOCl_2$) under reflux condition for 4 h (Scheme 2.1). The obtained product **M2** was taken as such for the next step without any further purification. Similarly, terephthaloyl chloride (**M3**) was synthesized by treating terephthalic acid (**8**) with thionyl chloride (Scheme 2.2).



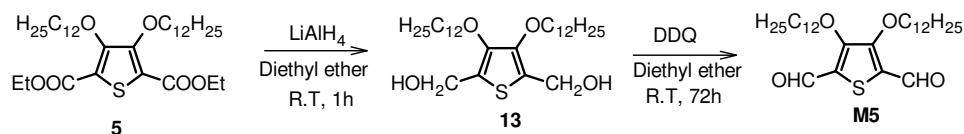
Scheme 2.2 Synthesis of terephthaloyl chloride (**M3**)

To prepare Wittig salt monomer **M4**, initially the dihydrazide **M1** was treated with 4-methylbenzoyl chloride (**9**) in N-methylpyrrolidinone (NMP) in the presence of pyridine to get dicarbohydrazide **10** in good yield. Cyclization of dicarbohydrazide **10** to bisoxadiazole **11** was achieved by the cyclodehydration of the hydrazide group into 1,3,4-oxadiazole ring using phosphorus oxychloride ($POCl_3$), which function both as solvent and dehydrating agent. The bromination of bisoxadiazole **11** to dibromo compound **12** was carried out by using N-bromosuccinimide (NBS) in benzene under reflux condition. Finally, the dibromo compound **12** was converted into Wittig salt monomer **M4** using triphenylphosphine (PPh_3) in DMF under reflux condition (Scheme 2.3).



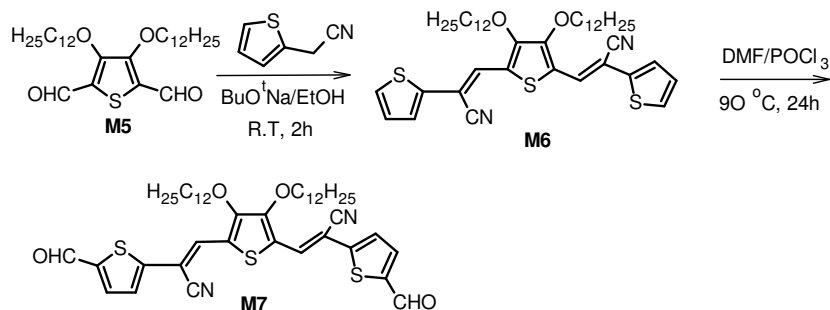
Scheme 2.3 Synthesis of Wittig salt monomer **M4**

The dicarbaldehyde monomer **M5** was synthesized starting from compound **5** (Scheme 2.4). In the first step, diester compound **5** was reduced using lithium aluminum hydride in diethyl ether solvent at room temperature to obtain (3,4-bis(dodecyloxy)thiophene-2,5-diyl)dimethanol (**13**). The bisalcohol **13** was then oxidized to dicarbaldehyde monomer **M5**, using 2,3-dichloro-5,6-dicyano-1,4-benzoquinone as the oxidizing agent.



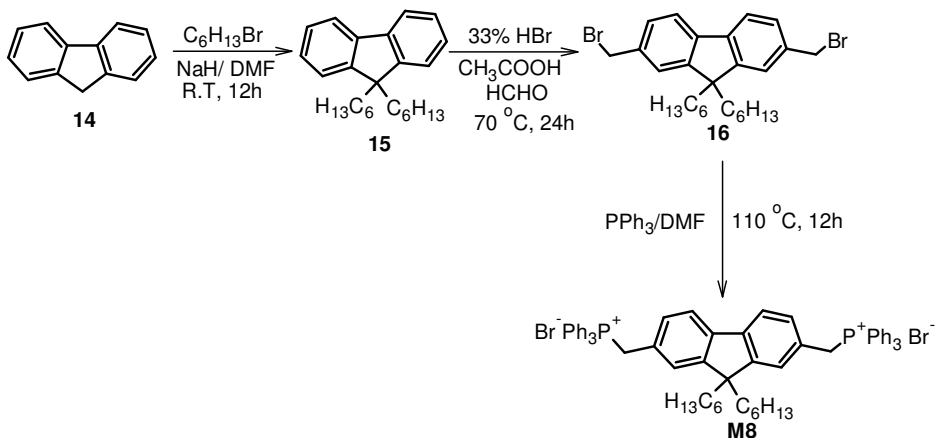
Scheme 2.4 Synthesis of dicarbaldehyde monomer **M5**

The thiophene based monomer containing cyanovinylene groups **M6**, was synthesized using Knoevenagel reaction methodology. The dicarbaldehyde **M5** was treated with thiophene-2-acetonitrile in the presence of sodium tert-butoxide (BuO^tNa) in ethanol at room temperature to obtain monomer **M6**. Further, the formylation of monomer **M6** via Vilsmeier-Haack reaction was carried out using POCl_3 and DMF to afford the cyano dicarbaldehyde **M7** in reasonably good yield (Scheme 2.5).

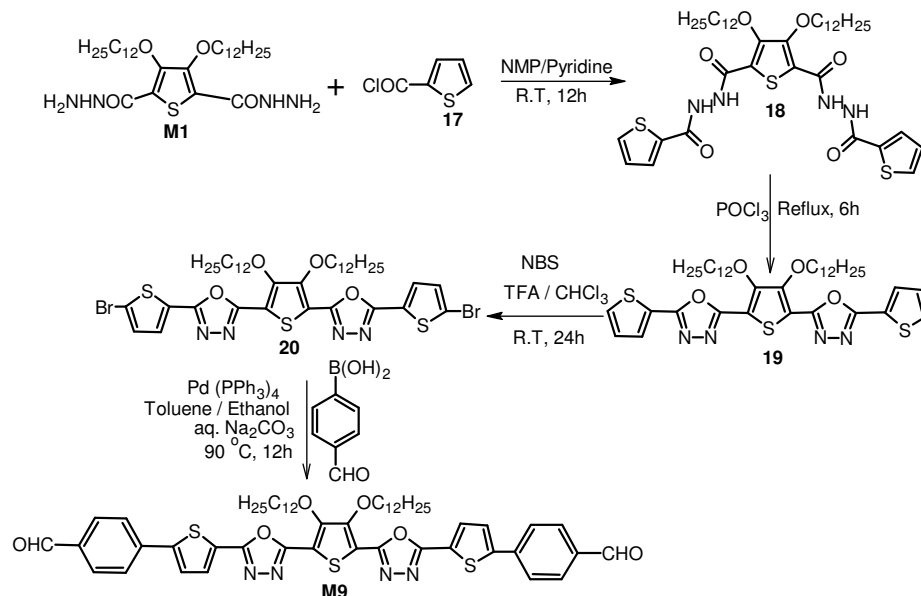


Scheme 2.5 Synthesis of cyanovinylene monomer **M6** and cyano dicarbaldehyde monomer **M7**

The fluorene based Wittig salt monomer **M8** was prepared starting from fluorene (**14**). Alkylation of fluorene was carried out with *n*-hexyl bromide in the presence of sodium hydride (NaH) in DMF at room temperature to afford 9,9'-di-*n*-hexylfluorene (**15**). The alkylated compound **15** was then treated with 33 % HBr solution in acetic acid and paraformaldehyde at 70 °C to give 2,7-bis(bromomethyl)-9,9'-di-*n*-hexyl fluorene (**16**). Finally, compound **16** was treated with triphenylphosphine in DMF under reflux condition to get the fluorene Wittig salt **M8** (Scheme 2.6). The synthesis of the dibromo compound **16** and the fluorene Wittig salt **M8** were carried out according to the literature procedure described by Zheng et al. (2002).

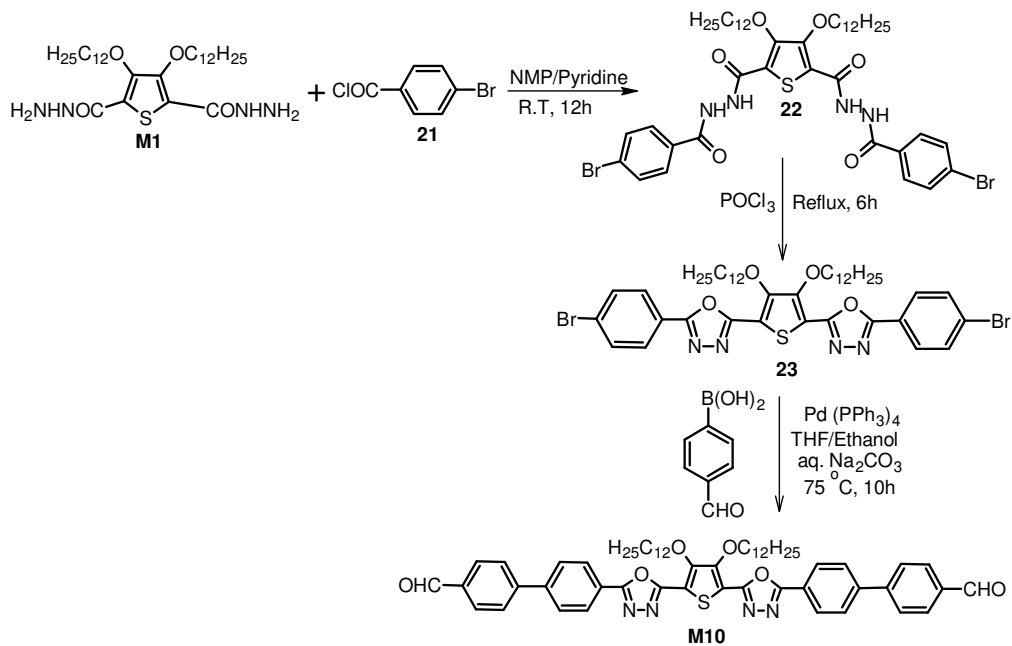


Scheme 2.6 Synthesis of fluorene Wittig salt monomer **M8**



Scheme 2.7 Synthesis of monomer **M9**

The synthesis of monomer **M9** involves a multistep route starting from dihydrazide monomer **M1** (Scheme 2.7). Initially, the dihydrazide **M1** was treated with thiophene-2-carbonyl chloride (**17**) in NMP in the presence of pyridine at room temperature to obtain intermediate compound **18**. Cyclization of compound **18** to bisoxadiazole **19** was achieved by using POCl_3 under reflux condition for 6 h. The monomer **M9** was synthesized from bisoxadiazole **19** by a two step route. The first step of the synthesis involved bromination of the bisoxadiazole. The reaction of bromine (Br_2) in chloroform (CHCl_3) with compound **19** did not give the required brominated product **20**. *N*-Bromosuccinimide bromination method using different solvents like DMF, carbon tetrachloride (CCl_4) or benzene were also unsuccessful. The failure of these methods could be due to the deactivation of thiophene rings in **19** towards bromination by the presence of electron deficient 1,3,4-oxadiazole units attached to the thiophene rings. However bromination reaction was successful when compound **19** was treated with NBS in trifluoroacetic acid/chloroform (3:1) solvent mixture, yielding the dibromo compound **20** in reasonable yield. The monomer **M9** was then obtained by a Suzuki coupling reaction between dibromo compound **20** and 4-formylphenylboronic acid using $\text{Pd}(\text{PPh}_3)_4$ as the catalyst in toluene/ethanol (1:1) solvent mixture.



Scheme 2.8 Synthesis of monomer **M10**

Similarly, the monomer **M10** was prepared starting from the dihydrazide monomer **M1**. The dihydrazide **M1** was reacted with 4-bromobenzoyl chloride (**21**) in NMP at room temperature to give the intermediate compound **22**, which was then converted to the bisoxadiazole **23** using POCl₃ under reflux condition. Finally, monomer **M10** was prepared by Suzuki coupling reaction between the dibromo compound **23** and 4-formylphenylboronic acid.

2.3.2 Experimental section

The experimental protocols used for the synthesis of all the intermediate compounds and the monomers are given below.

Synthesis of 3,4-didodecyloxythiophene-2,5-carboxydihydrazide (**M1**)

To a solution of diethyl 3,4-didodecyloxythiophene-2,5-dicarboxylate **5** (1 g) in 20 ml of methanol, 5 ml hydrazine hydrate was added. The reaction mixture was refluxed for 3 h. Upon cooling the solution to room temperature a white precipitate was obtained. The precipitate was filtered, washed with petroleum ether and dried under vacuum to get the product as white solid. The crude product was recrystallized from ethanol to get the pure product as white fluffy solid in 80 % yield.

M.P: 112 °C. ¹H NMR (400MHz, DMSO-*d*₆, δ): 8.8 (s, 2H, -CONH), 4.5 (s, 4H, -NH₂), 4.1 (t, 4H, -OCH₂-), 1.7 – 1.1 (m, 40H, (-CH₂)₁₀-), 0.84 (t, 6H, -CH₃).

FTIR (cm⁻¹): 3410, 3333 and 3191 (>N-H), 2916 and 2849 (-C-H), 1648 (>C=O), 1501, 1465, 1418, 1370, 1299, 1125, 1043, 951. Element. anal. calcd. for C₃₀H₅₆N₄O₄S (%): C 63.34, H 9.92, N 9.85, S 5.64. Found (%): C 63.32, H 9.96, N 9.80, S 5.60.

Synthesis of 3,4-propylenedioxythiophene-2,5-dicarboxylate (6)

To a solution of diethyl 3,4-dihydroxythiophene-2,5-dicarboxylate **4** (1 g, 3.84 mmol) in 15 ml of dry DMF, 2 g potassium carbonate was added at room temperature. The reaction mixture was stirred at room temperature for 30 minutes and then 1,3-dibromopropane (0.43 ml, 4.23 mmol) was added drop wise over a period of 10 minutes. The resulting mixture was refluxed for 18 h. The reaction mixture was cooled to room temperature and it was poured into crushed ice water. The precipitate was filtered, washed with water and dried in vacuum to get the product as white powder in 85 % yield.

M.P: 85 °C. ¹H NMR (400MHz, DMSO-*d*₆, δ): 4.28 (q, 4H), 3.82 (t, 4H, -OCH₂-), 2.25 (m, 2H), 1.29 (t, 6H). FTIR (cm⁻¹): 2978 and 2923 (-C-H), 1685 (>C=O), 1563, 1489, 1430, 1373, 1290, 1246, 1150, 1096, 905, 853. Element. anal. calcd. for C₁₂H₁₄O₆S (%): C 50.34, H 4.93, S 11.18. Found (%): C 50.32, H 4.91, S 11.14.

Synthesis of 3,4-propylenedioxythiophene-2,5-dicarboxylic acid (7)

A mixture of 3,4-propylenedioxythiophene-2,5-dicarboxylate **6** (0.5 g, 1.66 mmol) and 20 ml sodium hydroxide (10 %) was refluxed for 8 h. The solution was then cooled to room temperature and was acidified with concentrated hydrochloric acid to get a white precipitate. The precipitate was filtered off, washed with water and dried to get the product as white solid in 75 % yield.

M.P: 140 °C. ¹H NMR (400MHz, DMSO-*d*₆, δ): 13 (s, broad, -COOH), 3.81 (t, 4H, -OCH₂-), 2.28 (m, 2H). FTIR (cm⁻¹): 3300 – 2889, 2545, 1669, 1450, 1369, 1298, 1178, 1099, 924. Element. anal. calcd. for C₈H₆O₆S (%): C 41.74, H 2.63, S 13.19. Found (%): C 41.70, H 2.60, S 13.22.

Synthesis of 3,4-propylenedioxythiophene-2,5-dicarboxylic acid chloride (M2)

To a mixture of 3,4-propylenedioxythiophene-2,5-dicarboxylic acid **7** (0.5 g, 2 mmol) and 1 ml DMF, 5 ml of thionyl chloride was added. The reaction mixture was refluxed for 4 h. The completion of the reaction was confirmed by thin layer chromatography (TLC). The excess SOCl₂ was removed by distillation and the product was isolated as light yellow needles. The crude product was taken as such for the next step without further purification.

Synthesis of terephthalic acid chloride (M3)

A mixture of terephthalic acid **8** (0.5 g, 3 mmol) in 5ml of SOCl₂ and 0.5 ml of DMF was refluxed for 4 h. After completion of the reaction, the excess of SOCl₂ was distilled off to get the product as yellow needles.

Synthesis of N²,N⁵-di-(4-methylbenzoyl)-3,4-bis(dodecyloxy)thiophene-2,5-dicarbo hydrazide (10)

To a mixture of dihydrazide monomer **M1** (1 g, 1.75 mmol) and pyridine (0.1 ml) in NMP (10 ml), 4-methylbenzoyl chloride **9** (0.596 g, 3.86 mmol) was added slowly at room temperature. The reaction mixture was stirred at room temperature for 12 h. After completion of the reaction (progress of the reaction was monitored by TLC), the reaction mixture was poured into excess of ice water to get a precipitate. The precipitate obtained was collected by filtration, washed with water and dried in oven. The crude product was recrystallized from ethanol/chloroform mixture to get the pure product as white solid in 80 % yield.

M.P: 99 °C. ¹H NMR (400MHz, CDCl₃, δ): 10.23 (s, 2H, >NH), 9.19 (s, 2H, >NH), 7.75 (d, 4H, Ar), 7.27 (d, 4H, Ar), 4.30 (t, 4H, -OCH₂-), 2.42 (s, 6H, Ar-CH₃), 1.99 – 1.25 (m, 40H, -(CH₂)₁₀-), 0.87 (t, 6H, -CH₃). FTIR (cm⁻¹): 3380 and 3279 (>N-H), 2924 and 2853 (-C-H), 1597 (>C=O), 1449, 1368, 1282, 1070, 734. Element. anal. calcd. for C₄₆H₆₈N₄O₆S (%): Calcd. C 68.62, H 8.52, N 6.96, S 3.97. Found (%): C 68.60, H 8.54, N 6.90, S 4.01.

Synthesis of 5,5'-(3,4-bis(dodecyloxy)thiophene-2,5-diyl)bis(2-p-tolyl-1,3,4-oxadiazole) (11)

A mixture of compound **10** (1 g) and POCl₃ (10 ml) was refluxed under nitrogen atmosphere for 6 h. The reaction mixture was then cooled to room temperature and poured into excess of ice cold water. The resulting precipitate was collected by filtration and was washed with water and dried in oven. The crude product was further purified by recrystallization from ethanol/chloroform mixture to get the pure product as white solid in 85 % yield.

M.P: 98–100 °C. ¹H NMR (400MHz, CDCl₃, δ): 8.01 (d, 4H, Ar), 7.34 (d, 4H, Ar), 4.31 (t, 4H, -OCH₂), 2.45 (s, 6H, Ar-CH₃), 1.9 – 1.25 (m, 40H, -(CH₂)₁₀-), 0.87 (t, 6H, -CH₃). FTIR (cm⁻¹): 2914 and 2848 (-C-H), 1556 (-C=N-), 1481, 1464 (-C=C-), 1350, 1051 (=C-O-C=), 958. Element. anal. calcd. for C₄₆H₆₄N₄O₄S (%): Calcd. C 71.83, H 8.39, N 7.29, S 4.16. Found (%): C 71.80, H 8.42, N 7.33, S 4.18.

Synthesis of 5,5'-(3,4-bis(dodecyloxy)thiophene-2,5-diyl)bis(2-(4-(bromomethyl)phenyl)-1,3,4-oxadiazole) (12)

A mixture of compound **11** (0.5 g, 0.65 mmol), N-bromosuccinimide (0.25 g, 1.43 mmol) and 5 mg of benzoyl peroxide in 5 ml of benzene was refluxed for 6 h. After completion of the reaction (progress of the reaction was monitored by TLC), solvent was evaporated, the reaction mixture was added with 20 ml of water and stirred for 2 h. The resulting solid was filtered off. The crude product was recrystallized from ethyl acetate/chloroform mixture to get the pure product as yellowish solid in 60 % yield.

M.P: 124 – 126 °C. ¹H NMR (400MHz, CDCl₃, δ): 8.12 (d, 4H, Ar), 7.57 (d, 4H, Ar), 4.54 (s, 4H, Ar-CH₂Br), 4.32 (t, 4H, -OCH₂-), 1.90 – 1.25 (m, 40H, -(CH₂)₁₀-), 0.87 (t, 6H, -CH₃). FTIR (cm⁻¹): 2918 and 2850 (-C-H), 1583, 1550 (-C=N-), 1461, 1360, 1271, 1221, 1048, 956, 813, 725. Element. anal. calcd. for C₄₆H₆₂ Br₂N₄O₄S (%): Calcd. C 59.59, H 6.75, N 6.05, S 3.45. Found (%): C 59.56, H 6.72, N 6.08, S 3.41.

Synthesis of (4,4'-(5,5'-(3,4-bis(dodecyloxy)thiophene-2,5-diyl)bis(1,3,4-oxadiazole-5,2-diyl))bis(4,1-phenylene)bis(methylene)bis(triphenylphosphonium) bromide (M4)

A mixture of compound **12** (0.5 g, 0.53 mmol) and triphenylphosphine (0.31 g, 1.18 mmol) in 5 ml DMF was refluxed for 12 h. The reaction mixture was cooled to room temperature and poured in to 25 ml of ethyl acetate. The resulting precipitate was filtered off, washed with ethyl acetate and dried to get the product as buff solid in 90 % yield.

M.P: 178 – 180 °C. ¹H NMR (400MHz, CDCl₃, δ): 7.89 – 7.24 (m, 38H, Ar), 6.10 (d, 4H, Ar-CH₂-), 4.30 (t, 4H, -OCH₂-), 1.89 – 1.25 (m, 40H, -(CH₂)₁₀-), 0.86 (t, 6H, -CH₃). FTIR (cm⁻¹): 2918 and 2850 (-C-H), 1581, 1489, 1431, 1371, 1106, 1048, 848, 717. Element. anal. calcd. for C₈₂H₉₂Br₂N₄O₄P₂S (%): Calcd. C 67.84, H 6.39, N 3.86, S 2.20. Found (%): C 67.80, H 6.43, N 3.63, S 2.24.

Synthesis of (3,4-bis(dodecyloxy)thiophene-2,5-diyl)dimethanol (13)

To a solution of diethyl 3,4-didodecyloxythiophene-2,5-dicarboxylate **5** (1 g, 1.67 mmol) in 10 ml diethyl ether, lithium aluminum hydride (0.15 g, 4.18 mmol) was added at 0 °C. The reaction mixture was stirred at room temperature for 1 h. After completion of reaction (monitored by TLC), the resulting mixture was quenched with saturated ammonium chloride solution. The residue obtained was filtered through celite and then washed with dichloromethane. The filtrate was washed with water, dried with MgSO₄ and concentrated to get the product as white solid in 80 % yield.

M.P: 73 °C. ¹H NMR (400MHz, CDCl₃, δ): 7.11 (br, 2H, -OH), 4.72 (s, 4H, -CH₂OH), 4.02 (t, 4H, -OCH₂-), 1.80 – 1.26 (m, 40H, -(CH₂)₁₀-), 0.88 (t, 6H, -CH₃). FTIR (cm⁻¹): 3311 (-OH), 2915 and 2848 (-C-H), 1500, 1462, 1427, 1364, 1240, 1086, 992. Element. anal. calcd. for C₃₀H₅₆O₄S (%): C 70.26, H 11.01, S 6.24. Found (%): C 70.24, H 10.98, S 6.20.

Synthesis of 3,4-bis(dodecyloxy)thiophene-2,5-dicarbaldehyde (M5)

To a solution of compound **13** (0.5 g, 0.97 mmol) in 5 ml diethyl ether, 2,3-dichloro-5,6-dicyanobenzoquinone (0.66 g, 2.29 mmol) was added portion wise at room temperature. The reaction mixture was stirred at room temperature for 72 h.

After completion of the reaction (monitored by TLC), the solvent was evaporated. The solid residue obtained was redissolved in 50 ml n-hexane and filtered off. The organic layer was washed with water several times, dried with MgSO₄ and concentrated. The obtained crude solid product was recrystallized from ethanol to get the pure product as white crystals in 60 % yield.

M.P: 53 °C. ¹H NMR (400MHz, CDCl₃, δ): 10.09 (s, 2H, -CHO), 4.26 (t, 4H, -OCH₂-), 1.83 – 1.26 (m, 40H, -(CH₂)₁₀-), 0.88 (t, 6H, -CH₃). FTIR (cm⁻¹): 2914 and 2848 (-C-H), 1656 (>C=O), 1480, 1430, 1366, 1263, 1186, 1037, 798. Element. anal. calcd. for C₃₀H₅₂O₄S (%): C 70.82, H 10.31, S 6.29. Found (%): C 70.80, H 10.28, S 6.26.

Synthesis of 3,3'-(3,4-bis(dodecyloxy)thiophene-2,5-diyl)bis(2-(thiophen-2-yl)acrylonitrile) (M6)

To a stirred solution of monomer **M5** (1 g, 1.96 mmol) and thiophene-2-acetonitrile (0.5 g, 4.12 mmol) in 10 ml absolute ethanol under argon atmosphere, a solution of 0.56 g of sodium tert-butoxide (5.89 mmol) in 5 ml of absolute ethanol was added through a syringe. The mixture was stirred at room temperature for 2 h. The precipitated solid was filtered off to give dark red shiny solid in 70 % yield.

M.P: 89 °C. ¹H NMR (400MHz, CDCl₃, δ): 7.57 (s, 2H, -olephinic proton-), 7.37 – 7.35 (dd, J₁=1.2Hz, J₂=3.6Hz, 2H, Ar), 7.30 – 7.28 (dd, J₁=1.2Hz, J₂=5.2Hz, 2H, Ar), 7.07 – 7.05 (dd, J₁=4Hz, J₂=5.2Hz, 2H, Ar), 4.11 (t, J=6.4Hz, 4H, -OCH₂-), 1.80 – 1.26 (m, 40H, -(CH₂)₁₀-), 0.88 (t, J=6.8Hz, 6H, -CH₃). FTIR (cm⁻¹): 2913 and 2845 (-C-H), 2206 (-CN), 1568, 1454, 1377, 1282, 1159, 1013, 946. Element. anal. calcd. for C₄₂H₅₈N₂O₂S₃ (%): C 70.16, H 8.14, N 3.90, S 13.35. Found (%): C 70.12, H 8.12, N 3.86, S 13.32.

Synthesis of 3,3'-(3,4-bis(dodecyloxy)thiophene-2,5-diyl)bis(2-(5-formylthiophen-2-yl)acrylonitrile) (M7)

To a stirred solution of anhydrous DMF (0.5 ml, 6.67 mmol), freshly distilled POCl₃ (0.6 ml, 6.67 mmol) was added drop wise at 0 °C over a period of 30 min. The reaction mixture was stirred at room temperature for 30 min. To this solution, cyanovinylene monomer **M6** (0.4 g, 0.55 mmol) in 10 ml of 1,2-dichloroethane was

added drop wise. Then the reaction mixture was stirred at 90 °C for 24 h. After completion of reaction (progress of the reaction was monitored by TLC), it was poured into ice water, and neutralized to pH 6-7 by the drop wise addition of saturated sodium hydroxide solution. The mixture was extracted with ethyl acetate. The organic layer was dried with MgSO₄ and concentrated. Finally, the crude product was purified by silica gel column using a mixture of hexane and ethyl acetate (10/3) as an eluent, to get the required cyano dicarbaldehyde as dark red solid in 65 % yield.

M.P: 157 °C. ¹H NMR (400MHz, CDCl₃, δ): 9.89 (s, 2H, -CHO), 7.77 (s, 2H, -olephinic proton-), 7.71 (d, J=4Hz, 2H, Ar), 7.46 (d, J=4Hz, 2H, Ar), 4.15 (t, 4H, -OCH₂-), 1.80 – 1.25 (m, 40H, -(CH₂)₁₀-), 0.87 (t, 6H, -CH₃). FTIR (cm⁻¹): 2917 and 2848 (-C-H), 2207 (-CN), 1662 (-C=O), 1566, 1513, 1438, 1376, 1314, 1276, 1209, 1022, 806. Element. anal. calcd. for C₄₄H₅₈N₂O₄S₃ (%): C 68.19, H 7.55, N 3.62, S 12.39. Found (%): C 68.22, H 7.51, N 3.66, S 12.42.

Synthesis of 9,9'-di-*n*-hexylfluorene (15)

To a solution of fluorene **14** (1 g, 6 mmol) in DMF (10 ml), sodium hydride (0.43 g, 18 mmol) was added portion wise under nitrogen at 0 °C. To this solution, *n*-hexyl bromide (2.19 g, 13.2 mmol) was added drop wise. The solution was warmed to room temperature and stirred for 12 h. After completion of the reaction (monitored by TLC), the resulting mixture was poured into ice cold water. The aqueous solution was extracted with dichloromethane. The organic layer was separated, dried with MgSO₄ and concentrated. The crude product obtained was purified by recrystallization from hexane in yield 70 %.

M.P: 37 °C. ¹H NMR (400MHz, CDCl₃, δ): 7.70 (d, 2H), 7.34 – 7.28 (m, 6H), 1.95 (t, 4H), 1.12 – 1.06 (m, 12H), 0.88 – 0.83 (m, 4H), 0.75 (t, 6H). FTIR (cm⁻¹): 2914, 2854, 1451, 731. Element. anal. calcd. for C₂₅H₃₄ (%): C 89.75, H 10.25. Found (%): C 89.71, H 10.22.

Synthesis of 2,7-bis(bromomethy)-9,9'-di-*n*-hexylfluorene (16)

A mixture of 9,9'-di-*n*-hexylfluorene **15** (2 g, 5.98 mmol), paraformaldehyde (1.85 g, 50.98 mmol) and 18 g of 33 % HBr solution in acetic acid was stirred for 24 h at 70 °C. The reaction mixture was cooled to room temperature and poured into 100 ml of

ice cold water. The mixture was extracted with dichloromethane and the extracted solution was washed with water, saturated NaHCO₃ and NaCl solutions. The organic layer was separated, dried with MgSO₄ and concentrated to get a pale yellow liquid. The crude liquid was purified by silica gel column using a mixture of hexane and ethyl acetate (10/1) as an eluent, giving a colorless liquid in 78 % yield.

¹H NMR (400MHz, CDCl₃, δ): 7.39 – 7.25 (m, 6H), 4.59 (s, 4H, Ar-CH₂Br), 1.97 – 1.93 (m, 4H), 1.13 – 1.03 (m, 12H), 0.89 – 0.82 (m, 4H), 0.77 – 0.73 (m, 6H). FTIR (cm⁻¹): 2920, 2853, 1455, 1210, 818. Element. anal. calcd. for C₂₇H₃₆Br₂ (%): C 62.30, H 6.98. Found (%): C 62.12, H 6.68.

Synthesis of 2,7-bis[(p-triphenylphosphonio)methyl]-9,9'-di-*n*-hexylfluorene dibromide (M8)

A mixture of 2,7-bis(bromomethyl)-9,9'-di-*n*-hexylfluorene **16** (1 g, 2.02 mmol) and triphenylphosphine (1.32 g, 5.06 mmol) in DMF (10 ml) was heated for 12 h at 110 °C under nitrogen atmosphere. The reaction mixture was cooled to room temperature and 100 ml of diethyl ether was added slowly into the solution with stirring. The white solid separated was filtered, washed with ether and dried in a vacuum oven at 40 °C to get the product in 90 % yield.

M.P: >200 °C. ¹H NMR (400MHz, CDCl₃, δ): 8.02 – 7.82 (m, 30H), 7.58 – 7.17 (m, 6H), 5.6 – 5.56 (d, 4H, Ar-CH₂-), 1.54 – 1.50 (m, 4H), 1.16 – 0.78 (m, 16H), 0.2 (br, 6H). FTIR (cm⁻¹): 3407, 3340, 2921, 2852, 1434, 1109, 744. Element. anal. calcd. for C₆₃H₆₆Br₂P₂ (%): C 72.40, H 6.37. Found (%): C 72.36, H 6.42.

Synthesis of N²,N⁵-di(thiophene-2-carbonyl)-3,4-bis(dodecyloxy)thiophene-2,5-dicarbohydrazide (18)

To a mixture of dihydrazide monomer **M1** (1 g, 1.75 mmol) and pyridine (0.1 ml) in NMP (10 ml), thiophene-2-carbonyl chloride **17** (0.56 g, 3.87 mmol) was added slowly at room temperature. The reaction mixture was stirred at room temperature for 12 h. After completion of the reaction (progress of the reaction was monitored by TLC), it was poured into excess of ice water to get a precipitate. The precipitate obtained was collected by filtration, washed with water and dried in oven. The crude

product was recrystallized from ethanol/chloroform mixture to get the pure product as white solid in 85 % yield.

M.P: 93 °C. ¹H NMR (400MHz, CDCl₃, δ): 10.00 (s, 2H, >NH), 9.39 (s, 2H, >NH), 7.69 – 7.68 (dd, J₁=1.2Hz, J₂=3.6Hz, 2H, Ar), 7.54 – 7.52 (dd, J₁=0.8Hz, J₂=4.8Hz, 2H, Ar), 7.10 – 7.08 (dd, J₁=4Hz, J₂=4.8Hz, 2H, Ar), 4.29 (t, J=6.8Hz, 4H, –OCH₂–), 1.96 – 1.24 (m, 40H, –(CH₂)₁₀–), 0.87 (t, J=6.8Hz, 6H, –CH₃). FTIR (cm⁻¹): 3233 and 3088 (>N-H), 2917 and 2850 (–C-H), 1677 (>C=O), 1612, 1539, 1459, 1412, 1365, 1274, 1088, 847. Element. anal. calcd. for C₄₀H₆₀N₄O₆S₃ (%): C 60.89, H 7.67, N 7.10, S 12.17. Found (%): C 60.92, H 7.63, N 7.12, S 12.13.

Synthesis of 5,5'-(3,4-bis(dodecyloxy)thiophene-2,5-diyl)bis(2-(thiophen-2-yl)-1,3,4-oxadiazole) (19)

A mixture of dicarbohydrazide **18** (1.5 g 1.90 mmol) and 15 ml POCl₃ was refluxed under nitrogen atmosphere for 6 h. The reaction mixture was then cooled to room temperature and poured in to excess of ice cold water. The resulting precipitate was collected by filtration and was washed with water and dried in oven. The crude product was further purified by recrystallization from ethanol to get the pure product as yellow solid in 80 % yield.

M.P: 111 °C. ¹H NMR (400MHz, CDCl₃, δ): 7.84 – 7.83 (dd, J₁=1.2Hz, J₂=3.6Hz, 2H, Ar), 7.60 – 7.59 (dd, J₁=1.2Hz, J₂=4.8Hz, 2H, Ar), 7.22 – 7.19 (dd, J₁=3.6Hz, J₂=4.8Hz, 2H, Ar), 4.29 (t, J=6.4Hz, 4H, –OCH₂–), 1.90 – 1.25 (m, 40H, –(CH₂)₁₀–), 0.87 (t, J=6.8Hz, 6H, –CH₃). FTIR (cm⁻¹): 2915 and 2847 (–C-H), 1568 (–C=N–), 1514, 1467, 1422, 1374, 1032 (=C–O–C=). Element. anal. calcd. for C₄₀H₅₆N₄O₄S₃ (%): C 63.80, H 7.50, N 7.45, S 12.75. Found (%): C 63.78, H 7.46, N 7.42, S 12.78.

Synthesis of 5,5'-(3,4-bis(dodecyloxy)thiophene-2,5-diyl)bis(2-(5-bromothiophen-2-yl)-1,3,4-oxadiazole) (20)

To a stirred solution of bis(oxadiazole) **19** (1 g, 1.32 mmol) and N-bromosuccinimide (0.51 g, 2.96 mmol) in 2 ml chloroform, trifluoroacetic acid (6 ml) was added at room temperature. The reaction mixture was stirred at room temperature under dark for 24 h. After completion of the reaction (progress of the reaction was monitored by TLC), it was poured into water to get a precipitate. The precipitate

obtained was collected by filtration, washed with water and dried in oven. The crude product was purified by repeated recrystallization from absolute ethanol to get the desired dibromo derivative as pale yellow solid in 65 % yield.

M.P: 82 °C. ¹H NMR (400MHz, CDCl₃, δ): 7.56 (d, J=4Hz, 2H, Ar), 7.16 (d, J=4Hz, 2H, Ar), 4.29 (t, J=6.4Hz, 4H, -OCH₂-), 1.89 – 1.25 (m, 40H, -(CH₂)₁₀-), 0.88 (t, J=6.4Hz, 6H, -CH₃). FTIR (cm⁻¹): 2916 and 2851, 1563, 1510, 1474, 1422, 1382, 1023. Element. anal. calcd. for C₄₀H₅₄Br₂N₄O₄S₃ (%): C 52.74, H 5.98, N 6.15, S 10.54. Found (%): C 52.72, H 5.90, N 6.20, S 10.58.

Synthesis of 4,4'-(5,5'-(5,5'-(3,4-bis(dodecyloxy)thiophene-2,5-diyl)bis(1,3,4-oxadiazole-5,2-diyl))bis(thiophene-5,2-diyl))dibenzaldehyde (M9)

To a mixture of dibromo compound **20** (0.5 g, 0.548 mmol) and 4-formylphenylboronic acid (0.172 g, 1.2 mmol) in 10 ml of a solvent mixture of toluene and ethanol (1:1 volume ratio) under argon atmosphere, 2 M aqueous Na₂CO₃ (0.19 g) solution was added. After 30 min of degassing with argon, 3 mol % (0.019 g, 0.0164 mmol) of Pd (PPh₃)₄ was added. The reaction mixture was stirred at 90 °C for 12 h under argon atmosphere. After completion of the reaction (progress of the reaction was monitored by TLC), the reaction mixture was poured into distilled water and extracted with chloroform. The organic layer was dried with MgSO₄ and concentrated. The crude product was purified by silica gel column using a mixture of hexane and ethyl acetate (10/2) as an eluent, giving a yellow fluorescent solid in 70 % yield.

M.P: 208 °C. ¹H NMR (400MHz, CDCl₃, δ): 10.05 (s, 2H, -CHO), 7.96 (d, J=8.4 Hz, 4H, Ar), 7.84 – 7.82 (t, 6H, Ar), 7.52 (d, J=4 Hz, 2H, Ar), 4.33 (t, J=6.8Hz, 4H, -OCH₂-), 1.92 – 1.24 (m, 40H, -(CH₂)₁₀-), 0.86 (t, J=6.4Hz, 6H, -CH₃).

FTIR (cm⁻¹): 2917 and 2849 (-C-H), 1690 (>C=O), 1570(-C=N-), 1513, 1457, 1379, 1288, 1210 1020. Element. anal. calcd. for C₅₄H₆₄N₄O₆S₃ (%): C 67.47, H 6.72, N 5.83, S 9.99. Found (%): C 67.42, H 6.70, N 5.80, S 10.04.

Synthesis of N²,N⁵-di(4-bromobenzoyl)-3,4-bis(dodecyloxy)thiophene-2,5-dicarbohydrazide (22)

To a mixture of dihydrazide monomer **M1** (1 g, 1.75 mmol) and pyridine (0.1 ml) in NMP (10 ml), 4-bromobenzoyl chloride **21** (0.85 g, 3.87 mmol) was added slowly at room temperature. The reaction mixture was stirred at room temperature for 12 h. After completion of the reaction (progress of the reaction was monitored by TLC), it was poured into excess of ice water to get a precipitate. The precipitate obtained was collected by filtration, washed with water and dried in oven. The crude product was recrystallized from ethanol/chloroform mixture to get the pure product as white solid in 80 % yield. M.P: 192–193 °C. ¹H NMR (400MHz, CDCl₃, δ): 10.22 (s, 2H, >NH), 9.39 (s, 2H, >NH), 7.77 – 7.74 (m, 4H, Ar), 7.66 – 7.63 (m, 4H, Ar), 4.33 (t, 4H, –OCH₂–), 2.03 – 1.27 (m, 40H, –(CH₂)₁₀–), 0.9 (t, 6H, –CH₃). FTIR (cm⁻¹): 3288 (>N-H), 2918 and 2850 (-C-H), 1641 (>C=O), 1595, 1461, 1412, 1283, 1068. Element. anal. calcd. for C₄₄H₆₂Br₂N₄O₆S (%): C 56.52, H 6.69, N 6.0, S 3.42. Found (%): C 56.50, H 6.64, N 6.04, S 3.46.

Synthesis of 5,5'-(3,4-bis(dodecyloxy)thiophene-2,5-diyl)bis(2-(4-bromophenyl)-1,3,4-oxadiazole) (23)

A solution of dicarbohydrazide **22** (1 g 1.06 mmol) in 10 ml POCl₃ was refluxed under nitrogen atmosphere for 6 h. The reaction mixture was then cooled to room temperature and poured in to excess of ice cold water. The resulting precipitate was collected by filtration and was washed with water and dried in oven. The crude product was further purified by recrystallization from ethanol to get the pure product as pale yellow solid in 70 % yield.

M.P: 114–116 °C. ¹H NMR (400MHz, CDCl₃, δ): 8.04 – 8.00 (m, 4H, Ar), 7.74 – 7.70 (m, 4H, Ar), 4.35 (t, 4H, –OCH₂–), 1.92 – 1.28 (m, 40H, –(CH₂)₁₀–), 0.9 (t, 6H, –CH₃). FTIR (cm⁻¹): 2916 and 2850 (-C-H), 1592 (-C=N-), 1516, 1469, 1388, 1275, 1064 (=C–O–C=). Element. anal. calcd. for C₄₄H₅₈Br₂N₄O₄S (%): C 58.78, H 6.51, N 6.24, S 3.56. Found (%): C 58.74, H 6.28, N 6.22, S, 3.58.

Synthesis of 4',4''-(5,5'-(3,4-bis(dodecyloxy)thiophene-2,5-diyl)bis(1,3,4-oxadiazole-5,2-diyl))dibiphenyl-4-carbaldehyde (M10)

Under argon atmosphere, to a mixture of dibromo compound **23** (0.5 g, 0.556 mmol) and 4-formylphenylboronic acid (0.18 g, 1.22 mmol) in 10 ml THF and ethanol mixture (1:1 volume ratio), 2 M aqueous Na₂CO₃ solution (0.18 g) was added. After 30 min of degassing with argon, 3 mol % (0.019 g, 0.0166 mmol) of Pd (PPh₃)₄ was added. The reaction mixture was stirred at 75 °C for 10 h under argon atmosphere. After completion of reaction (progress of the reaction was monitored by TLC), the reaction mixture was poured into distilled water and extracted with chloroform. The organic layer was dried with MgSO₄ and concentrated. The crude product was purified by silica gel column using a mixture of hexane and ethyl acetate (8/2) as an eluent, giving a brown solid in 65 % yield.

M.P: 198 °C. ¹H NMR (400MHz, CDCl₃, δ): 10.13 (s, 2H, -CHO), 8.27 (d, J=8.4 Hz, 4H, Ar), 8.04 (d, J=8.4 Hz, 8H, Ar), 7.85 (d, J=7.2 Hz, 4H, Ar), 4.38 (t, 4H, -OCH₂-), 1.98 – 1.26 (m, 40H, -(CH₂)₁₀-), 0.89 (t, 6H, -CH₃). FTIR (cm⁻¹): 2919 and 2850 (-C-H), 1697 (-C=O), 1591 (-C=N-), 1485, 1375, 1213, 1043 (=C-O-C=). Element. anal. calcd. for C₅₈H₆₈N₄O₆S (%): C 73.38, H 7.23, N 5.91, S 3.37. Found (%): C 73.42, H 7.26, N 5.95, S 3.30.

2.3.3 Structural characterization of intermediate compounds and monomers

The chemical structures of all intermediate compounds and the monomers were confirmed by ¹H NMR spectroscopy, FTIR spectroscopy and elemental analyses. The elemental analysis data of all intermediate compounds and the monomers are given in the experimental part. The results obtained in the ¹H NMR and FTIR spectral studies are presented in this section. The ¹H NMR spectrum of monomer **M1** is as shown in Figure 2.1, which showed singlet peaks at δ 8.8 and at δ 4.5 due to -CONH and -NH₂ protons respectively. Further, a triplet peak at δ 4.1 is due to the -OCH₂- protons and the multiple peaks in the range of δ 1.7 – 1.1 are due to the -(CH₂)₁₀- protons of the dodecyloxy chains of the thiophene ring. The methyl protons were resonated at δ 0.84 as a triplet for six protons. The enlarged ¹H NMR spectrum of **M1** in the range δ 0.5 – 4.5 is given in Figure 2.2. The FTIR spectrum of **M1** (Figure 2.3) showed peaks in the range 3410 – 3191 cm⁻¹ and at 1648 cm⁻¹ indicating the presence -NHNH₂ and >C=O

groups respectively. The elemental analysis data of monomer **M1** was in well agreement with its molecular formula.

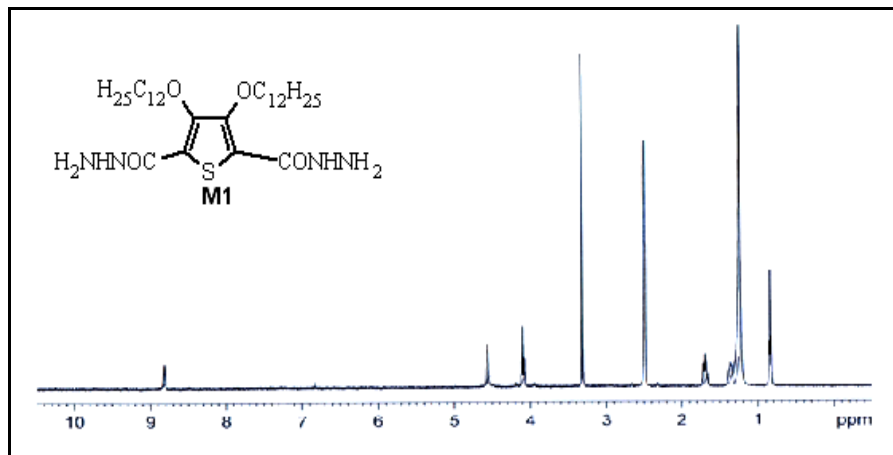


Figure 2.1 ^1H NMR spectrum of 3,4-didodecyloxythiophene-2,5-carboxyhydrazide (**M1**)

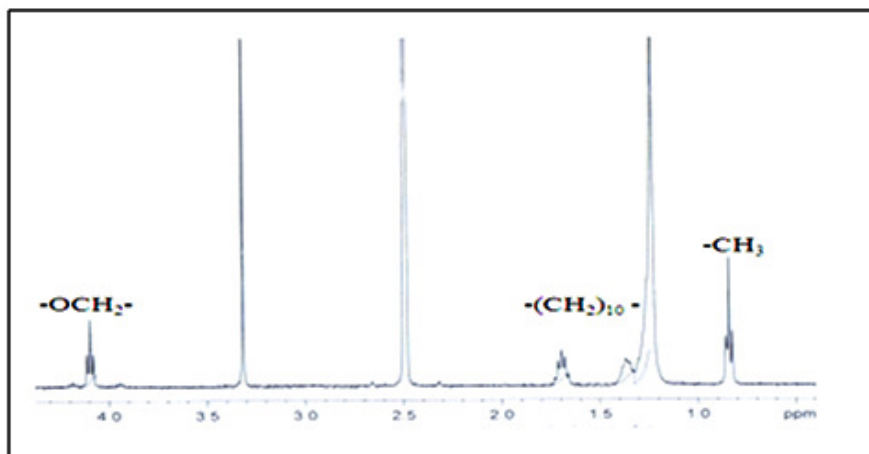


Figure 2.2 Enlarged image of the ^1H NMR spectrum of **M1**

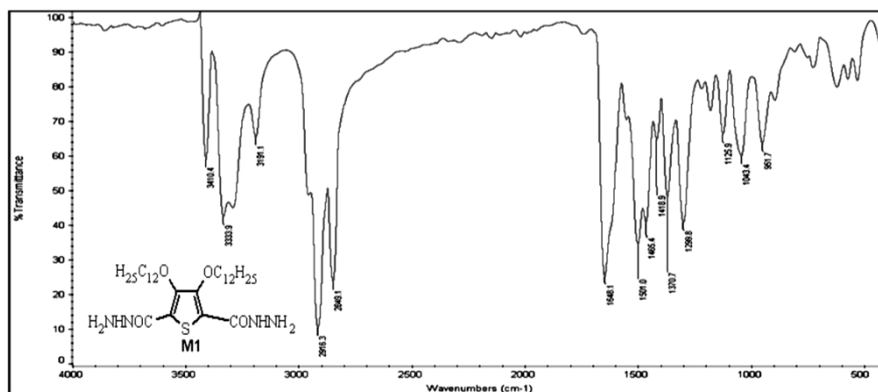


Figure 2.3 FTIR spectrum of 3,4-didodecyloxythiophene-2,5-carboxyhydrazide (M1)

The formation of 3,4-propylenedioxythiophene-2,5-dicarboxylate (**6**) and the hydrolysis of compound **6** to 3,4-propylenedioxythiophene-2,5-dicarboxylic acid (**7**) were evidenced by ^1H NMR and FTIR spectroscopic studies as well as by elemental analysis data. The ^1H NMR spectrum of compound **6** showed a triplet peak at δ 3.82 and a multiplet peak at δ 2.25 due to $-\text{OCH}_2-$ and $-\text{CH}_2-$ protons of the propylenedioxy ring respectively. Further, appearance of a quartet peak at δ 4.28 and a triplet peak at δ 1.29 are due to $-\text{CH}_2$ and $-\text{CH}_3$ protons of the ester groups respectively. The FTIR spectrum (Figure A1) exhibited peaks at 2978 and 2923 cm^{-1} due to $-\text{C-H}$ stretching vibrations and a sharp peak at 1685 cm^{-1} indicates the presence of $>\text{C=O}$ group. In the ^1H NMR spectrum of compound **7**, the $-\text{COOH}$ protons resonated as a singlet at δ 13.0. Further, its FTIR spectrum (Figure A2) displayed peaks around 3300 cm^{-1} and at 1669 cm^{-1} , which confirms the formation of $-\text{COOH}$ group. In addition, the elemental analysis data of compounds **6** and **7** showed the percentage elements corresponding to their actual molecular formulae.

The ^1H NMR spectrum of N^2, N^5 -di-(4-methylbenzoyl)-3,4-bis(dodecyloxy)thiophene-2,5-dicarbohydrazide (**10**) is as shown in Figure 2.4, which showed $-\text{NH}$ protons as two singlets at δ 10.23 and δ 9.19 corresponding to $-\text{CONH}$ group of phenyl and 3,4-didodecyloxythiophene rings respectively. The aromatic protons resonated as two doublets at δ 7.75 and 7.27 (Figure A3). Also, tolyl methyl protons were observed at δ 2.42. The FTIR spectrum (Figure 2.5) displayed sharp peaks at 3380 and 1597 cm^{-1} indicating the presence of $>\text{NH}$ and $>\text{C=O}$ groups respectively.

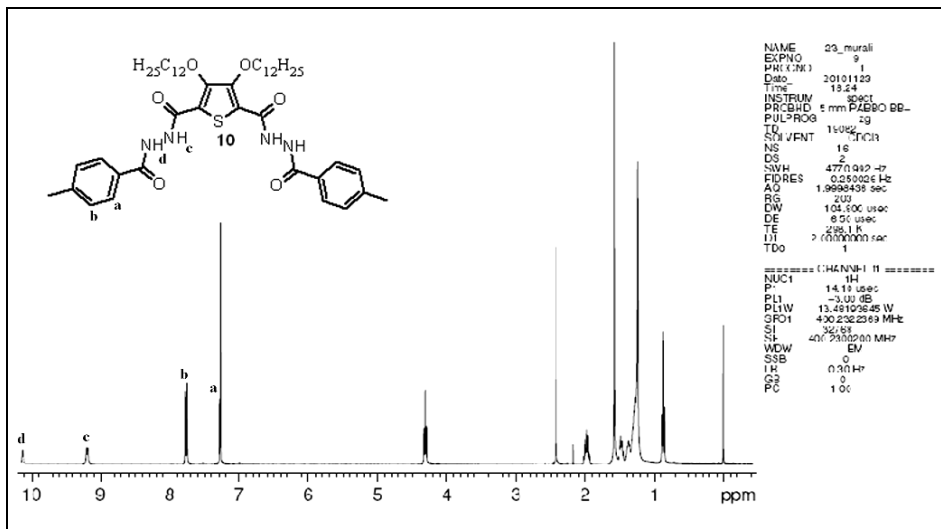


Figure 2.4 ^1H NMR spectrum of N^2,N^5 -di-(4-methylbenzoyl)-3,4-bis(dodecyloxy) thiophene-2,5-dicarbohydrazide (**10**)

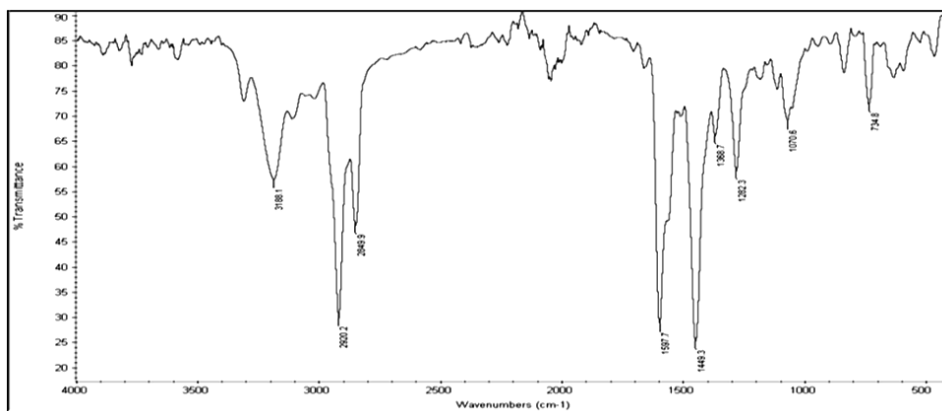


Figure 2.5 FTIR spectrum of N^2,N^5 -di-(4-methylbenzoyl)-3,4-bis(dodecyloxy) thiophene-2,5-dicarbohydrazide (**10**)

The successful completion of the cyclodehydration reaction involved in the conversion of dicarbohydrazide **10** to bisoxadiazole **11** was confirmed by the spectral studies. In the ^1H NMR spectrum of bisoxadiazole **11** (Figure 2.6), the disappearance of two singlet peaks due to $>\text{NH}$ protons confirms the cyclization of dicarbohydrazide **10**. Further, the FTIR spectrum of bisoxadiazole **11** (Figure 2.7) did not show any absorption peaks corresponding to $>\text{NH}$ and $>\text{C}=\text{O}$ groups whereas new absorption peaks appeared at 1556 and 1051 cm^{-1} due to $-\text{C}=\text{N}-$ and $=\text{C}-\text{O}-\text{C}=\text{C}$ stretching vibrations respectively indicating formation of the 1,3,4-oxadiazole ring.

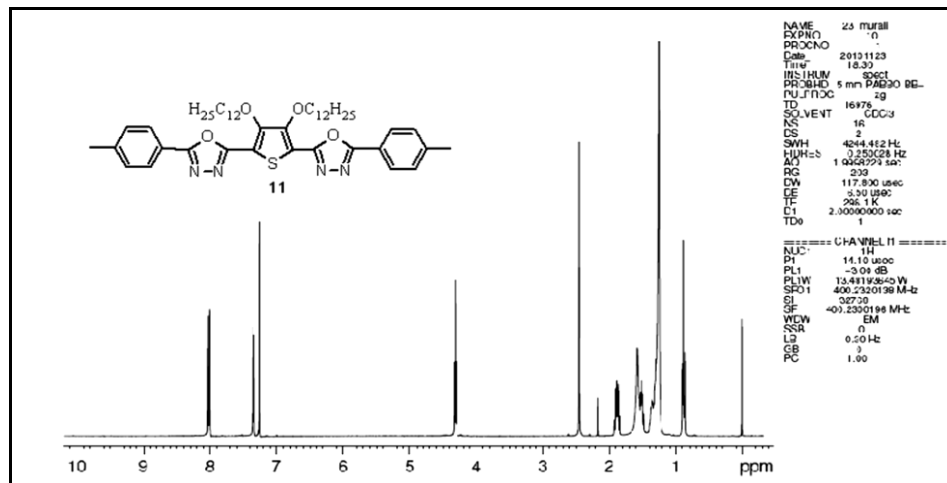


Figure 2.6 ^1H NMR spectrum of 5,5'-(3,4-bis(dodecyloxy)thiophene-2,5-diyl)bis(2-p-tolyl-1,3,4-oxadiazole) (**11**)

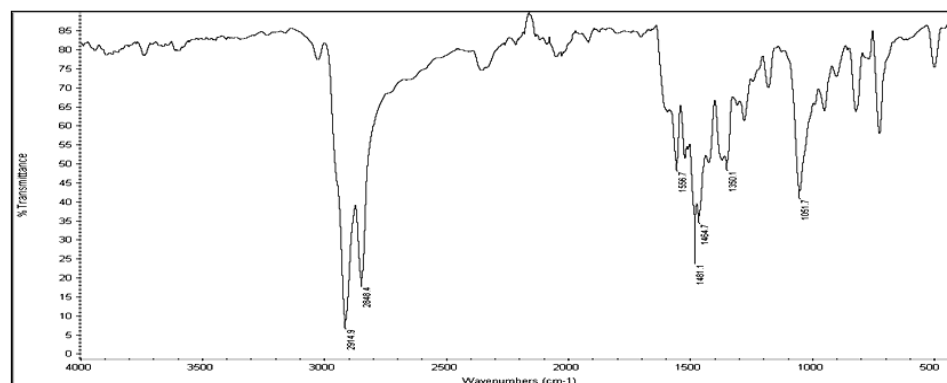


Figure 2.7 FTIR spectrum of 5,5'-(3,4-bis(dodecyloxy)thiophene-2,5-diyl)bis(2-p-tolyl-1,3,4-oxadiazole) (**11**)

The ^1H NMR spectrum of 5,5'-(3,4-bis(dodecyloxy)thiophene-2,5-diyl)bis(2-(4-(bromomethyl)phenyl)-1,3,4-oxadiazole) (**12**) is as shown in Figure 2.8. The peak corresponding to the tolyl methyl protons at δ 2.45 disappeared in the spectrum whereas a new singlet peak is appeared at δ 4.54 due to the bromomethyl ($-\text{CH}_2\text{Br}$) protons, thus confirming the bromination of the tolyl methyl groups. The spectrum also displayed other characteristic peaks corresponding to the aromatic and the alkoxy protons present in the molecule. The dibromo compound **12** was then converted into its Wittig salt monomer **M4**.

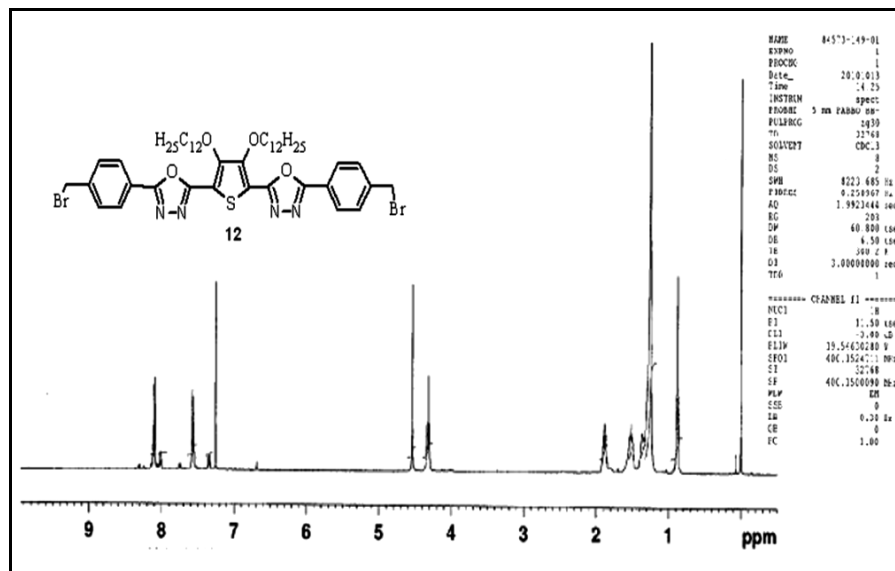


Figure 2.8 ^1H NMR spectrum of 5,5'-(3,4-bis(dodecyloxy)thiophene-2,5-diyl)bis(2-(4-(bromomethyl)phenyl)-1,3,4-oxadiazole) (**12**)

The ^1H NMR spectrum (Figure 2.9) of monomer **M4** displayed a singlet peak at δ 6.10 with the disappearance of the peak corresponding to bromomethyl ($-\text{CH}_2\text{Br}$) protons at δ 4.54, indicating the successful conversion of compound **12** to monomer **M4**. In addition, the spectrum displayed complex multiple peaks in the range δ 7.89 – 7.24, corresponding to the triphenylphosphine and phenyl protons, which further confirms the formation of the Wittig salt monomer. The elemental analysis data of compounds **10**, **11**, **12** and monomer **M4** further confirmed their actual molecular formulae.

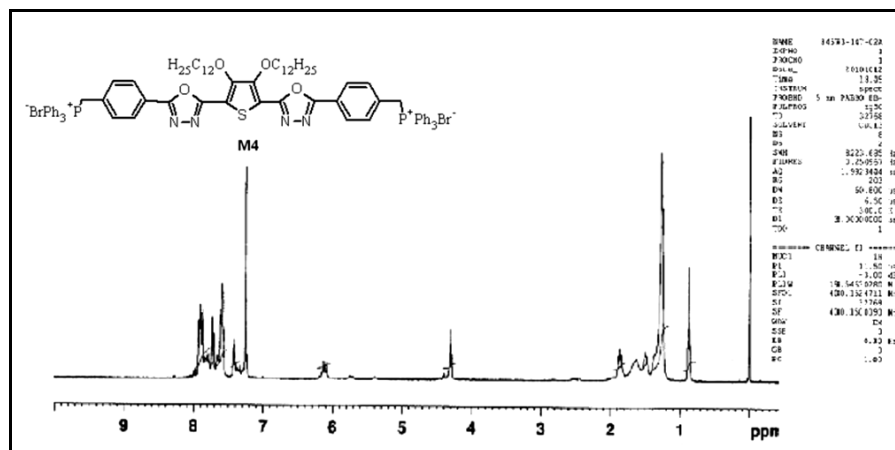


Figure 2.9 ^1H NMR spectrum of **M4**

The reduction of the ester groups ($-\text{CO}_2\text{Et}$) in compound **5** to hydroxymethyl groups ($-\text{CH}_2\text{OH}$) was evident from the ^1H NMR spectrum (Figure A4). A broad peak at δ 7.11 due to $-\text{OH}$ proton and a singlet peak at δ 4.72 due to $-\text{CH}_2\text{OH}$ protons along with other characteristic peaks were observed for compound **13**. Further, its FTIR spectrum (Figure 2.10) displayed a sharp peak at 3311 cm^{-1} indicating the presence of $-\text{OH}$ groups. Finally, compound **13** was converted to the dicarbaldehyde monomer **M5**. The formation of monomer **M5** was evidenced by ^1H NMR spectrum (Figure 2.11), in which the aldehyde protons resonated as a singlet peak at δ 10.09. Whereas its FTIR spectrum (Figure 2.12) exhibited a sharp peak at 1656 cm^{-1} due to $>\text{C}=\text{O}$ groups. Elemental analysis data of compound **13** and monomer **M5** were in agreement with their molecular formulae.

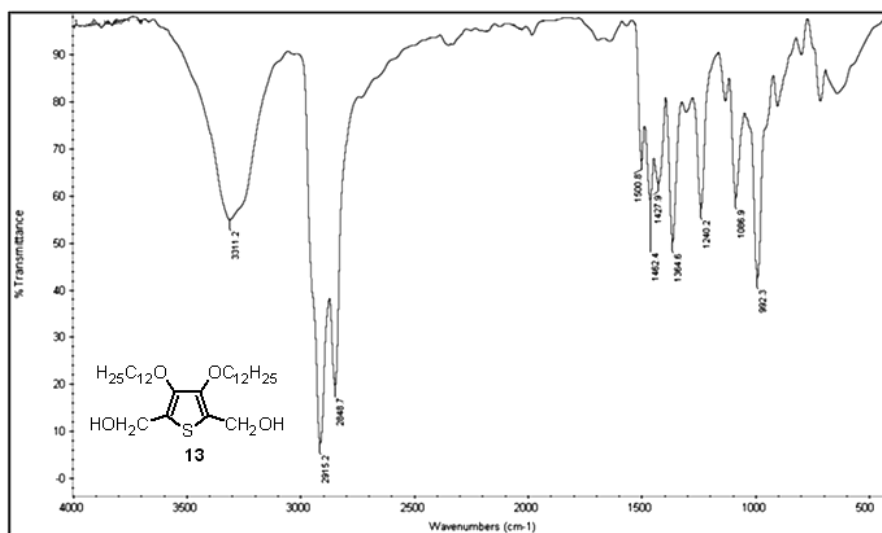


Figure 2.10 FTIR spectrum of (3,4-bis(dodecyloxy)thiophene-2,5-diyl)dimethanol (**13**)

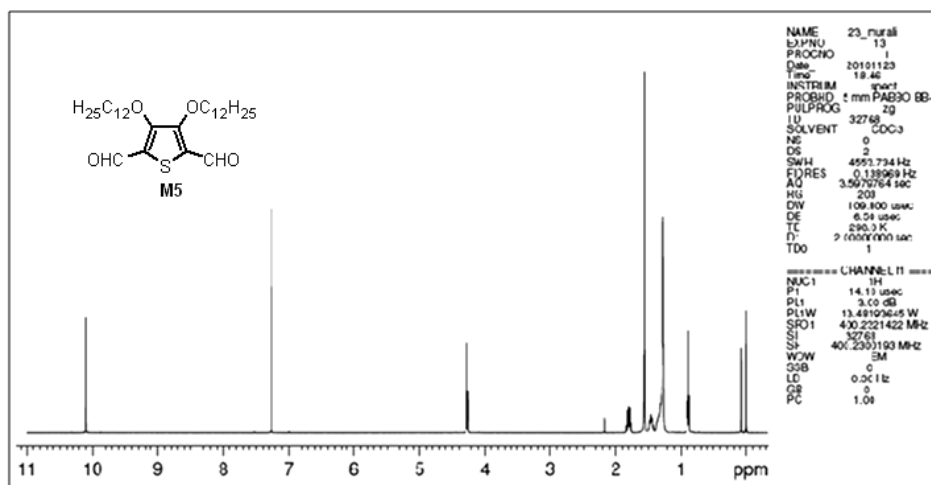


Figure 2.11 ^1H NMR spectrum of 3,4-bis(dodecyloxy)thiophene-2,5-dicarbaldehyde (**M5**)

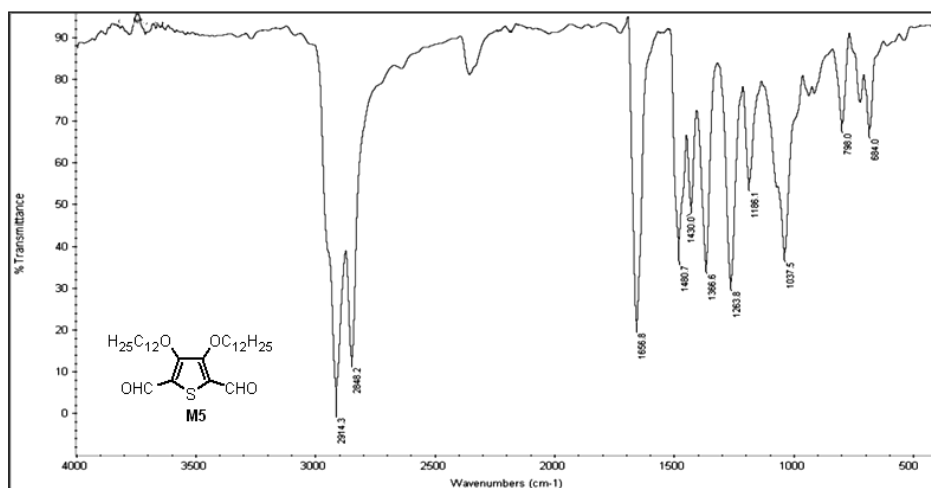


Figure 2.12 FTIR spectrum of 3,4-bis(dodecyloxy)thiophene-2,5-dicarbaldehyde (**M5**)

The chemical structures of cyanovinylene monomer **M6** and cyano dicarbaldehyde monomer **M7** were confirmed by ^1H NMR and FTIR spectral studies. The ^1H NMR spectrum of **M6** is as shown in the Figure 2.13. The spectrum displayed a singlet peak at δ 7.57 due to olefinic protons. The three double doublet peaks in the range of δ 7.37 – 7.35, 7.07 – 7.05 and 7.30 – 7.28 were assigned to thiophene ring protons at positions 2 (the free α -position of the thiophene rings), 3 and 4 respectively. In addition, the triplet peak at δ 4.11 is due to the $-\text{OCH}_2-$ protons of the

alkoxy chains of the thiophene ring and the multiple peaks in the range δ 1.80 – 1.26 are due to the $-(\text{CH}_2)_{10}-$ protons of the alkyl chains.

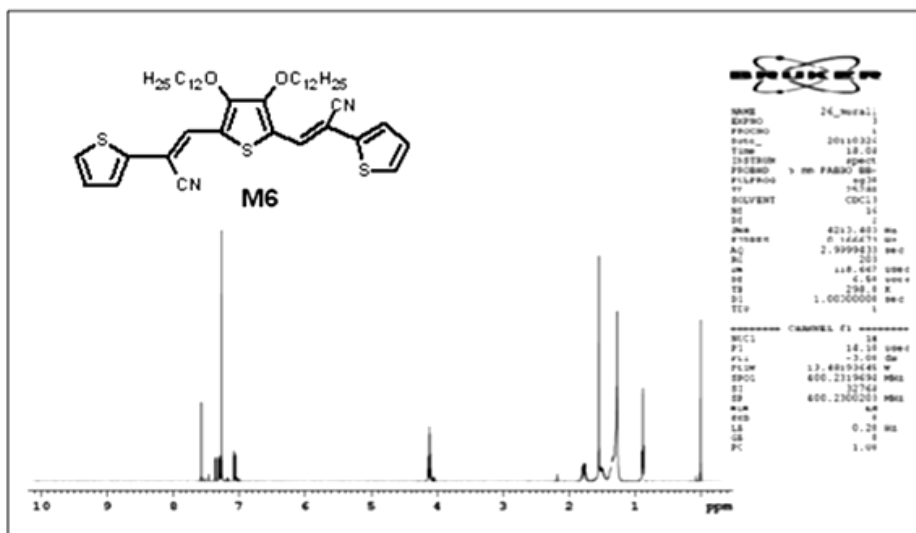


Figure 2.13 ^1H NMR spectrum of 3,3'-(3,4-bis(dodecyloxy)thiophene-2,5-diyl)bis(2-(thiophen-2-yl)acrylonitrile) (**M6**)

The enlarged image of ^1H NMR spectrum of **M6** in the region δ 7.0 – 7.6 is as shown in Figure 2.14, which clearly shows three double doublet peaks due to the thiophene ring protons. The FTIR spectrum (Figure 2.15) of **M6** showed a sharp peak at 2206 cm^{-1} indicating the presence $-\text{CN}$ groups. In the ^1H NMR spectrum (Figure 2.16) of cyano dicarbaldehyde monomer **M7**, the aldehyde ($-\text{CHO}$) protons were observed as a singlet peak at δ 9.89. The formylation at position 2 of the thiophene rings was evident by its enlarged ^1H NMR spectrum (Figure 2.17). The spectrum did not show the double doublet peak corresponding to the proton on α -carbon of the thiophene ring. Further, only doublet peaks were obtained for protons at positions 3 and 4, instead of double doublets. Also, the peaks corresponding to the protons at 3- and 4-position of the thiophene ring are shifted to downfield region due to the formylation of the ring. The FTIR spectrum (Figure 2.18) of **M7** exhibited sharp peaks at 2207 and 1662 cm^{-1} indicating the presence of $-\text{CN}$ and $-\text{CHO}$ groups respectively. The elemental analysis data of monomers **M6** and **M7** matched with their molecular formulae.

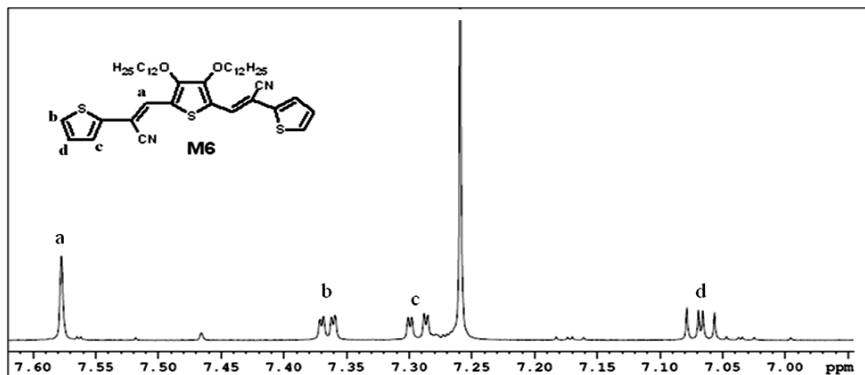


Figure 2.14 Enlarged image of ^1H NMR spectrum of M6

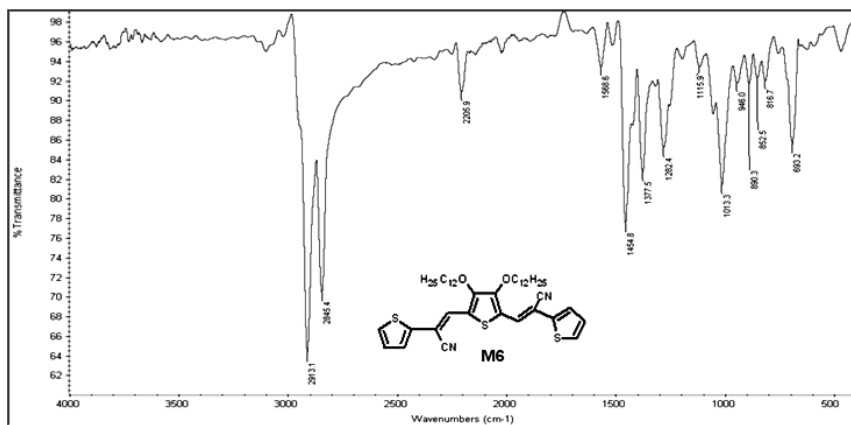


Figure 2.15 FTIR spectrum of 3,3'-(3,4-bis(dodecyloxy)thiophene-2,5-diyl)bis(2-(thiophen-2-yl)acrylonitrile) (M6)

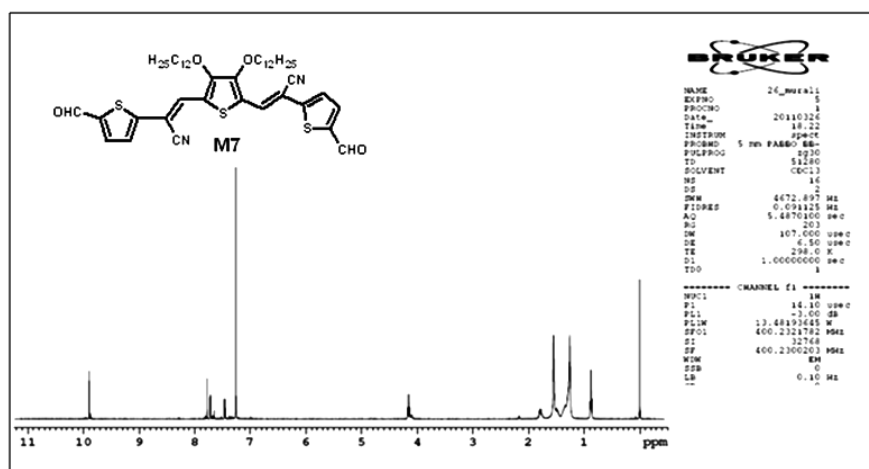


Figure 2.16 ^1H NMR spectrum of 3,3'-(3,4-bis(dodecyloxy)thiophene-2,5-diyl)bis(2-(5-formylthiophen-2-yl)acrylonitrile) (M7)

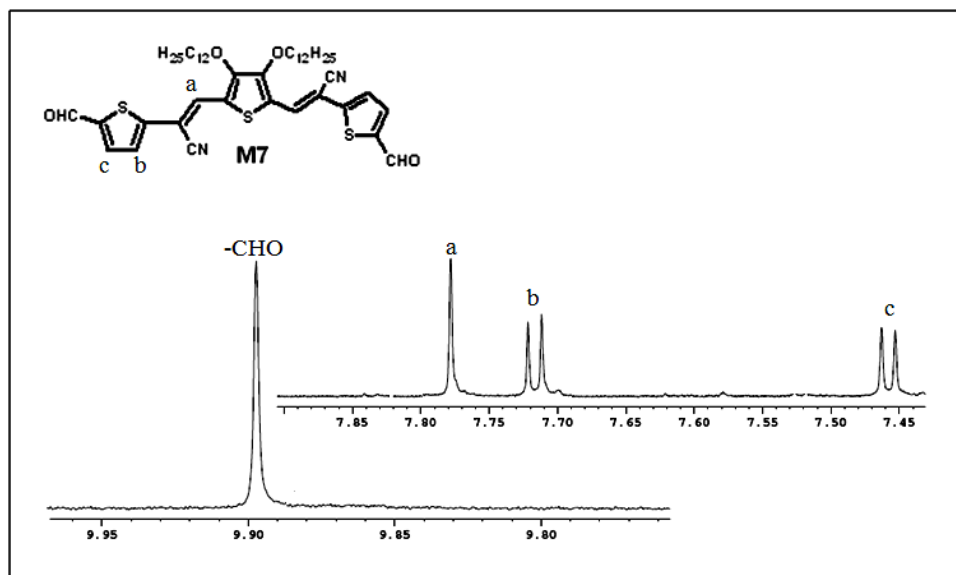


Figure 2.17 Enlarged image of ^1H NMR spectrum of **M7**

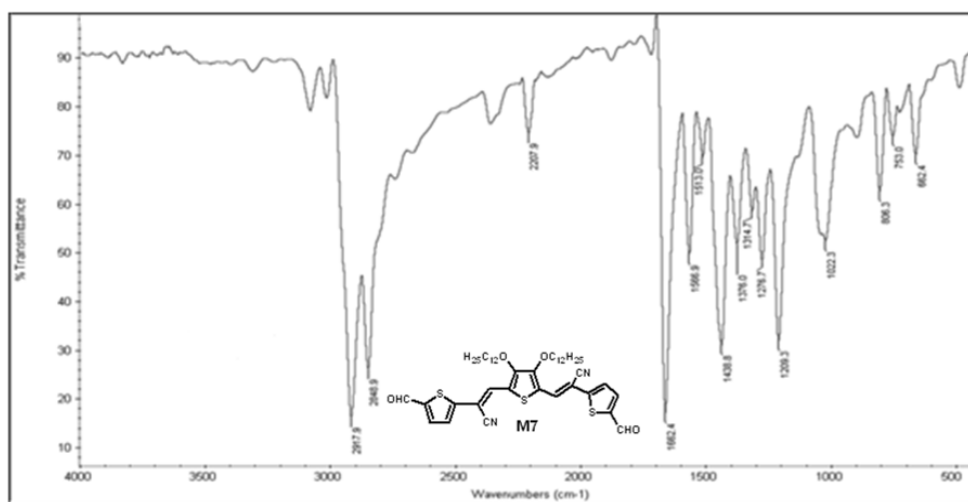


Figure 2.18 FTIR spectrum of 3,3'-(3,4-bis(dodecyloxy)thiophene-2,5-diyl)bis(2-(5-formylthiophen-2-yl)acrylonitrile) (**M7**)

The presence of characteristic peaks in the ^1H NMR spectrum of dihexyl fluorene (**15**) confirms the successful alkylation of the fluorene ring (Figure A5). The protons of the hexyl groups attached at position 9 of the fluorene ring were resonated as multiplet peaks in the range δ 1.95 – 0.83. In addition, multiplet peaks were observed in the range δ 7.77 – 7.28 due to the aromatic protons of the fluorene ring. Bromomethylation of compound **15** gives the dibromo compound **16**, which was then

converted to fluorene Wittig salt monomer **M8**. In the ^1H NMR spectral study, compound **16** showed a singlet peak at δ 4.59 indicating the presence of bromomethyl ($-\text{CH}_2\text{Br}$) protons attached at 2 and 7 positions of the fluorene ring (Figure A6). Whereas the ^1H NMR spectrum (Figure 2.19) of **M8** did not show a peak at δ 4.59, instead a doublet peak was observed at δ 5.6 – 5.56 due to methylene protons attached to the triphenylphosphine group ($-\text{CH}_2\text{PPh}_3$). Further, the elemental analysis data of the compounds **15**, **16** and monomer **M8** showed the percentage elements corresponding to their actual molecular formulae.

The ^1H NMR spectrum of dicarbohydrazide **18** is shown in Figure 2.20. The spectrum showed $>\text{NH}$ protons as two singlets at δ 10 and 9.39 corresponding to $-\text{CONH}$ group of thiophene and 3,4-didodecyloxythiophene rings respectively. The three doublet peaks in the range δ 7.69 – 7.68, 7.10 – 7.08 and 7.54 – 7.52 are assigned to thiophene ring protons at positions 2, 3 and 4 respectively. The $-\text{OCH}_2-$ protons of the alkoxy chains of the thiophene ring resonated as a triplet peak at δ 4.29 and $-(\text{CH}_2)_{10}-$ protons of the alkyl chains appeared as multiple peaks in the range δ 1.96 – 1.24. The FTIR spectrum (Figure 2.21) exhibited sharp peaks at 3233 and 1677 cm^{-1} indicating the presence of $>\text{NH}$ and $>\text{C}=\text{O}$ groups respectively.

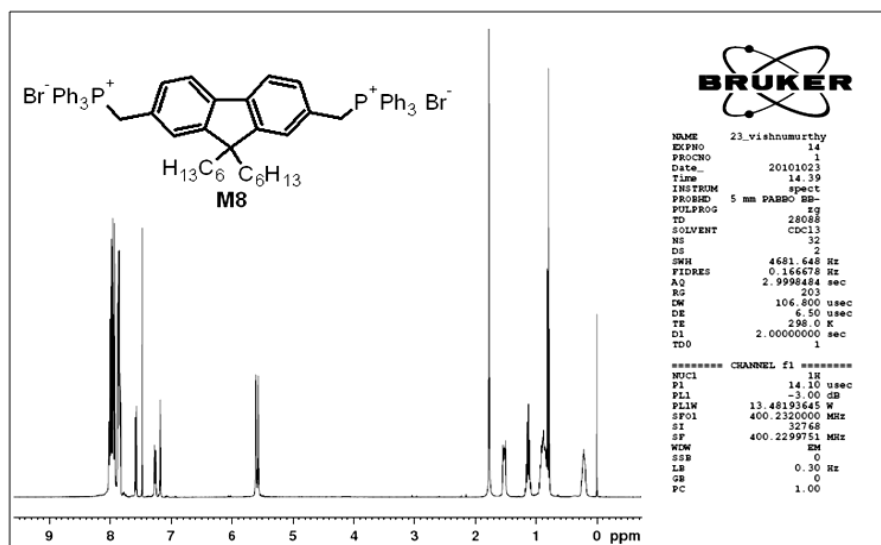


Figure 2.19 ^1H NMR spectrum of 2,7-bis[(p-triphenylphosphonio)methyl]-9,9'-di-n-hexylfluorene dibromide (**M8**)

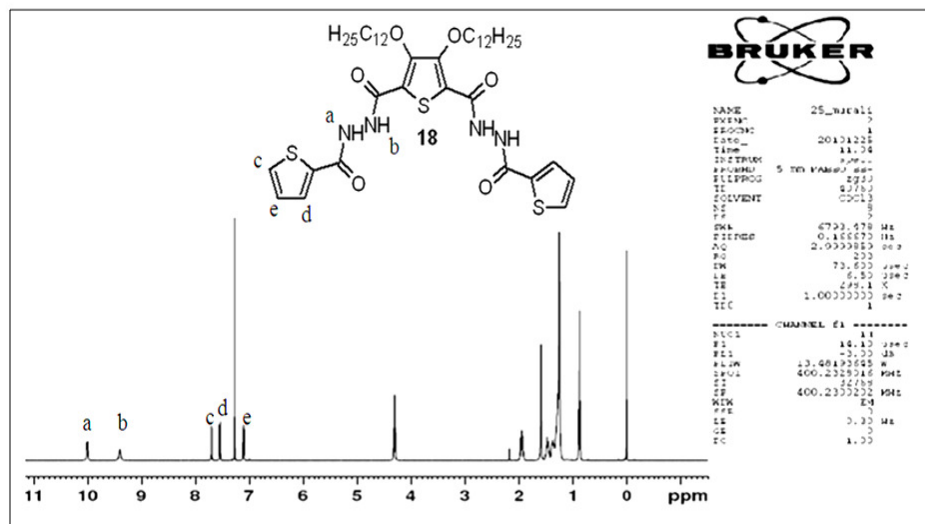


Figure 2.20 ^1H NMR spectrum of N^2,N^5 -di(thiophene-2-carbonyl)-3,4-bis(dodecyloxy)thiophene-2,5-dicarbohydrazide (**18**)

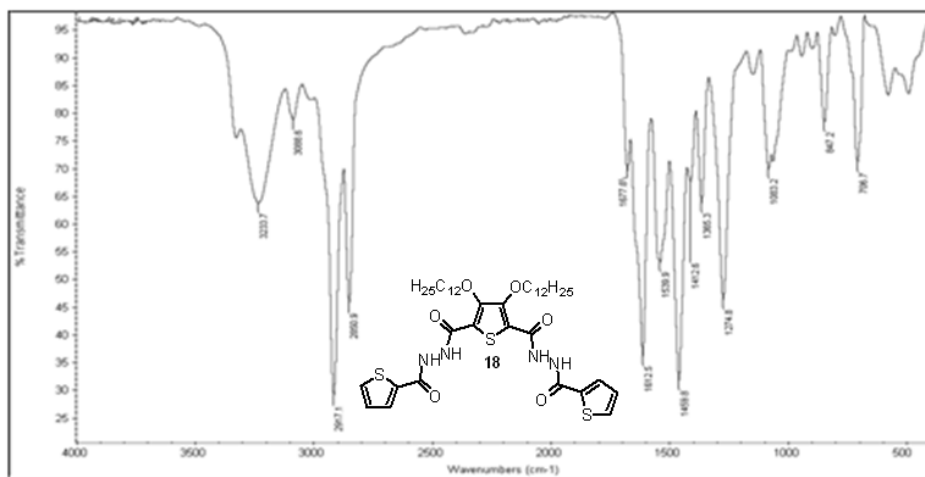


Figure 2.21 FTIR spectrum of N^2,N^5 -di(thiophene-2-carbonyl)-3,4-bis(dodecyloxy)thiophene-2,5-dicarbohydrazide (**18**)

In the ^1H NMR spectrum of bisoxadiazole **19** (Figure 2.22), the disappearance of two singlet peaks due to $>\text{NH}$ protons confirms the formation of required compound in the cyclodehydration reaction. The enlarged image of ^1H NMR spectrum (aromatic region) of **19** is given in Figure 2.23. Further, the FTIR spectrum (Figure 2.24) of bisoxadiazole **19** did not show any absorption peaks corresponding to $>\text{NH}$ and $>\text{C}=\text{O}$ groups. In addition, absorption peaks corresponding to $-\text{C}=\text{N}-$ and $=\text{C}-\text{O}-\text{C}=\text{C}$ groups

of the oxadiazole ring were appeared at 1568 and 1032 cm^{-1} respectively, which further confirmed formation of the 1,3,4-oxadiazole ring.

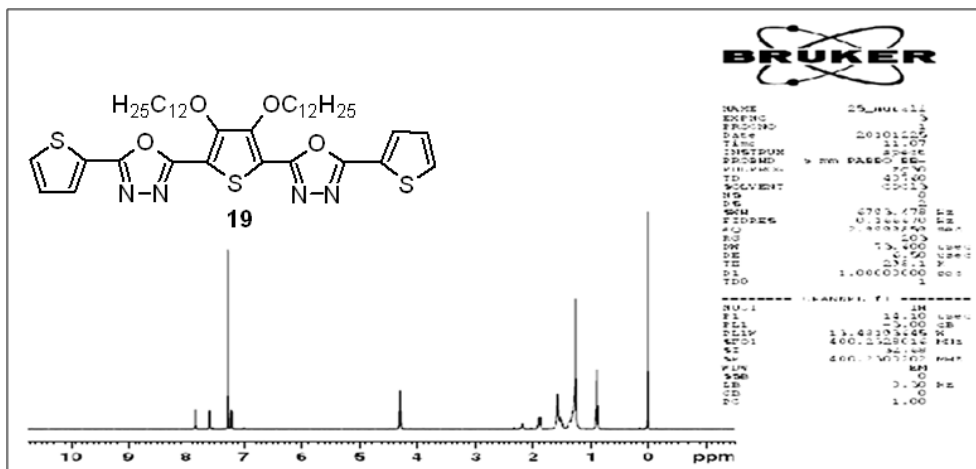


Figure 2.22 ^1H NMR spectrum of 5,5'-(3,4-bis(dodecyloxy)thiophene-2,5-diyl)bis(2-(thiophen-2-yl)-1,3,4-oxadiazole) (**19**)

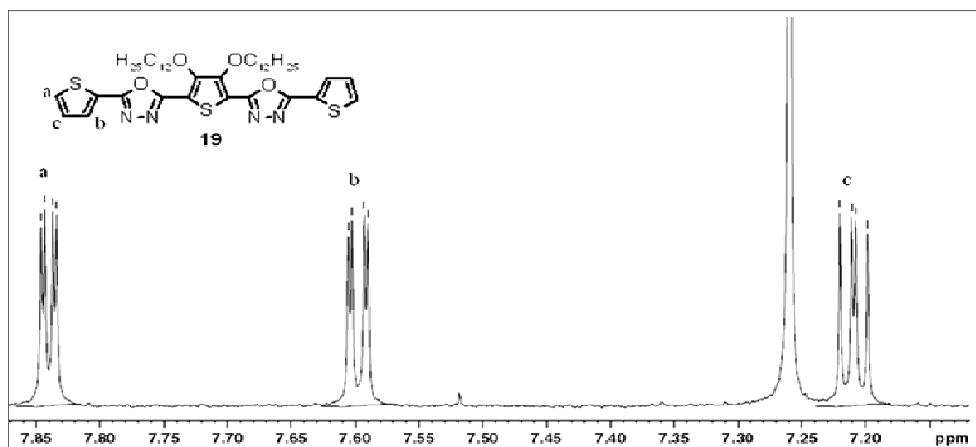


Figure 2.23 Enlarged image of ^1H NMR spectrum of **19**

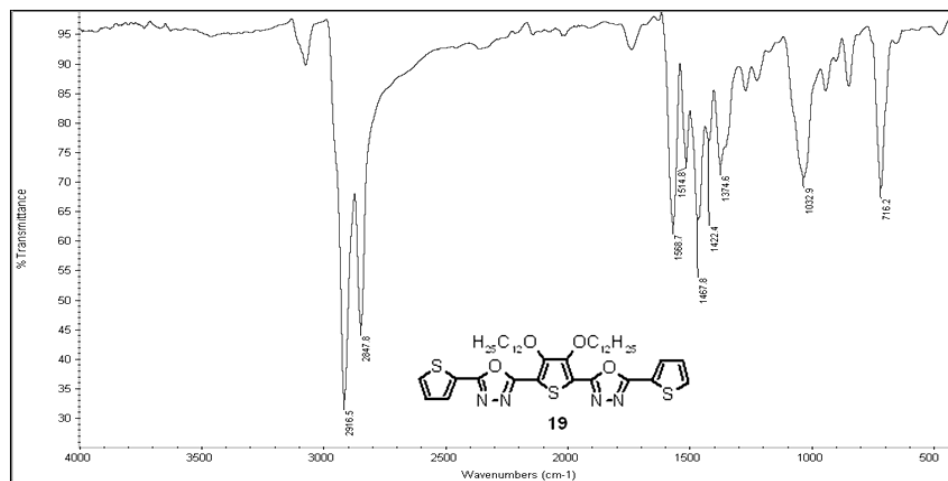


Figure 2.24 FTIR spectrum of 5,5'-(3,4-bis(dodecyloxy)thiophene-2,5-diyl)bis(2-(thiophene-2-yl)-1,3,4-oxadiazole) (**19**)

The presence of characteristic peaks in the ^1H NMR spectrum (Figure 2.25) confirms the chemical structure of dibromo compound **20**. In the spectrum, the double doublet peak corresponding to the proton at position 2 of the thiophene ring was disappeared. The enlarged ^1H NMR spectrum of compound **20** is shown in Figure 2.26. In the spectrum, only doublet peaks were observed for the protons at position 3 and 4 of the thiophene rings due to the bromination of thiophene rings at position 2.

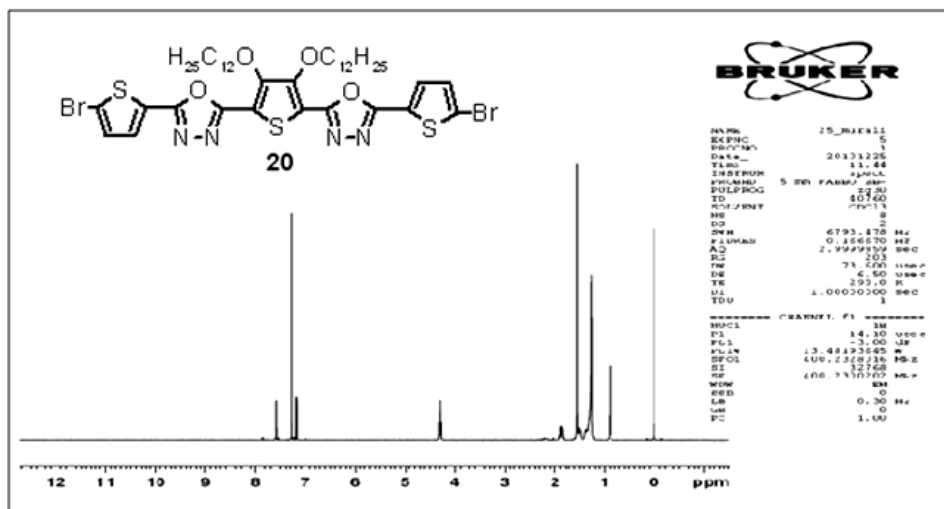


Figure 2.25 ^1H NMR spectrum of 5,5'-(3,4-bis(dodecyloxy)thiophene-2,5-diyl)bis(2-(5-bromothiophen-2-yl)-1,3,4-oxadiazole) (**20**)

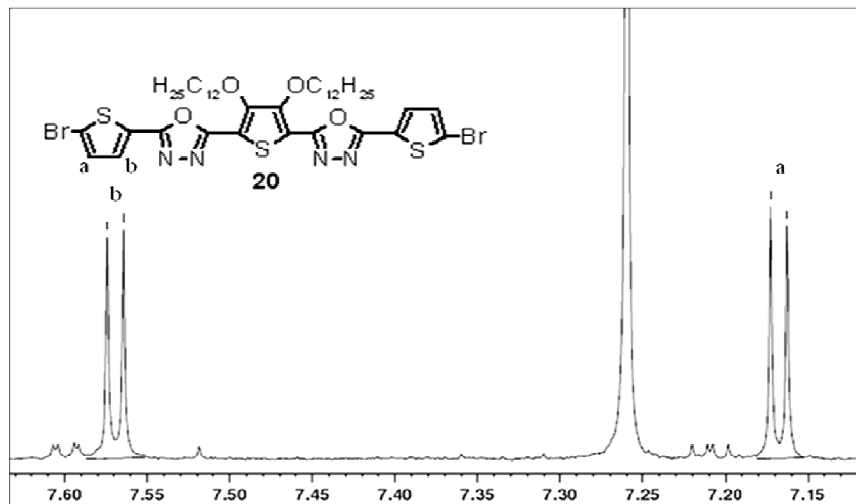


Figure 2.26 Enlarged image of ^1H NMR spectrum of **20**

The successful coupling between dibromo compound **20** and 4-formylphenylboronic acid through Suzuki coupling reaction to obtain monomer **M9** was evidenced by its ^1H NMR spectrum and the spectrum is as shown in Figure 2.27. The two aldehyde (-CHO) protons resonated as a singlet at δ 10.05. In addition, the spectrum (Figure 2.28) showed characteristic peaks corresponding to the protons of aromatic rings and alkoxy chains. Its FTIR spectrum (Figure 2.29) exhibited a sharp peak at 1690 cm^{-1} indicating the presence of $>\text{C}=\text{O}$ groups. The elemental analysis data of compounds **18**, **19**, **20** and monomer **M9** matched well with their molecular formulae.

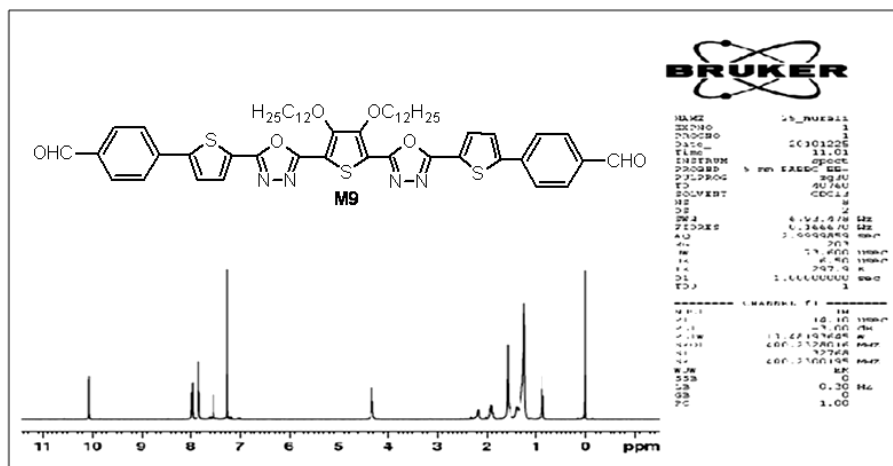


Figure 2.27 ^1H NMR spectrum of monomer **M9**

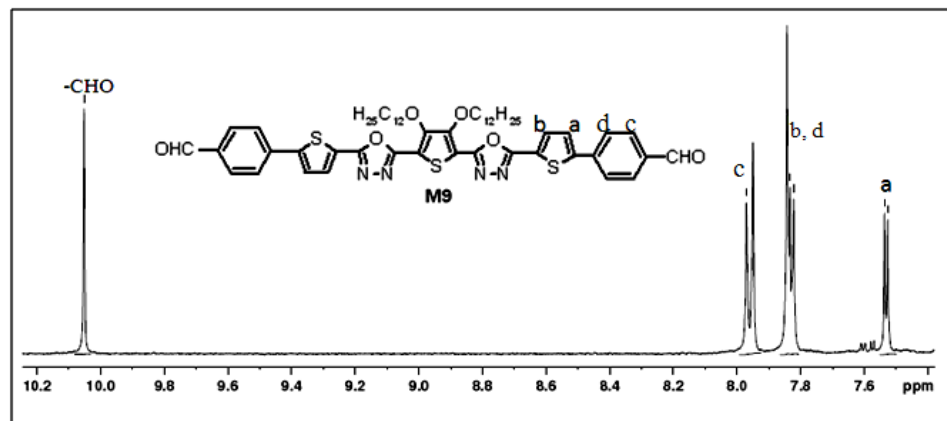


Figure 2.28 Enlarged image of ^1H NMR spectrum of **M9**

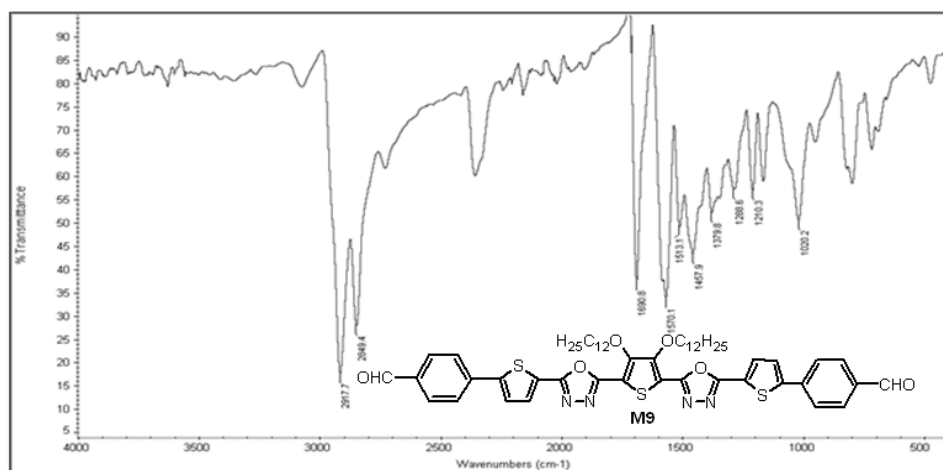


Figure 2.29 FTIR spectrum of **M9**

The ^1H NMR spectrum of N^2, N^5 -di(4-bromobenzoyl)-3,4-bis(dodecyloxy)-thiophene-2,5-dicarbohydrazide **22** is as shown in Figure 2.30. The spectrum exhibited $>\text{NH}$ protons as two singlets at δ 10.22 and 9.39 corresponding to $-\text{CONH}$ groups of phenyl and 3,4-didodecyloxythiophene rings respectively. The multiplet peaks in the range of δ 7.77 – 7.74 and 7.66 – 7.63 are assigned to the aromatic protons. Further, the FTIR spectrum (Figure 2.31) showed sharp peaks at 3288 and 1641 cm^{-1} indicating the presence of $>\text{NH}$ and $>\text{C}=\text{O}$ groups respectively, which confirms the formation of compound **22**.

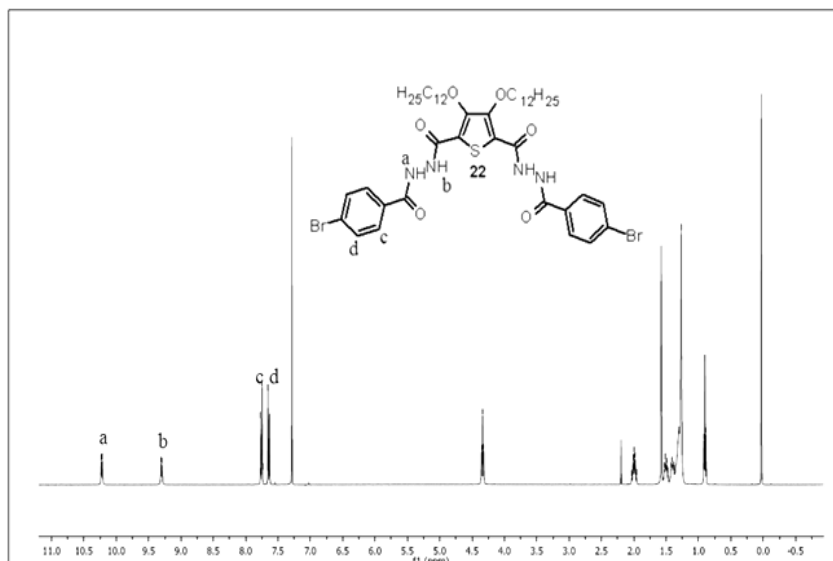


Figure 2.30 ^1H NMR spectrum of N^2, N^5 -di(4-bromobenzoyl)-3,4-bis(dodecyloxy)-thiophene-2,5-dicarbohydrazide (**22**)

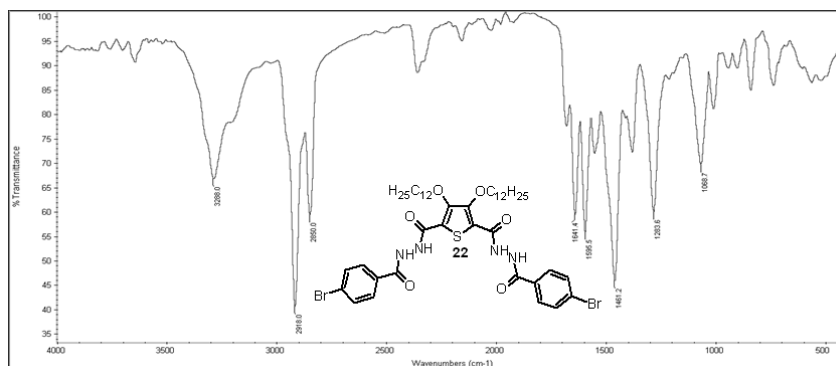


Figure 2.31 FTIR spectrum of N^2, N^5 -di(4-bromobenzoyl)-3,4-bis(dodecyloxy)-thiophene-2,5-dicarbohydrazide (**22**)

A cyclodehydration reaction was carried out for the conversion of compound **22** to bisoxadiazole **23**. The ^1H NMR spectrum (Figure 2.32) of bisoxadiazole **23** is in well agreement with its chemical structure. The absence of two singlet peaks due to $>\text{NH}$ protons confirms the cyclodehydration of the dicarbohydrazide group. Further, the FTIR spectrum of bisoxadiazole **23** (Figure 2.33) showed no absorption peaks corresponding to $>\text{NH}$ and $>\text{C}=\text{O}$ groups whereas it showed new peaks at 1592 and 1064 cm^{-1} for $-\text{C}=\text{N}-$ and $=\text{C}-\text{O}-\text{C}=\text{O}$ groups respectively, indicating formation of the 1,3,4-oxadiazole ring.

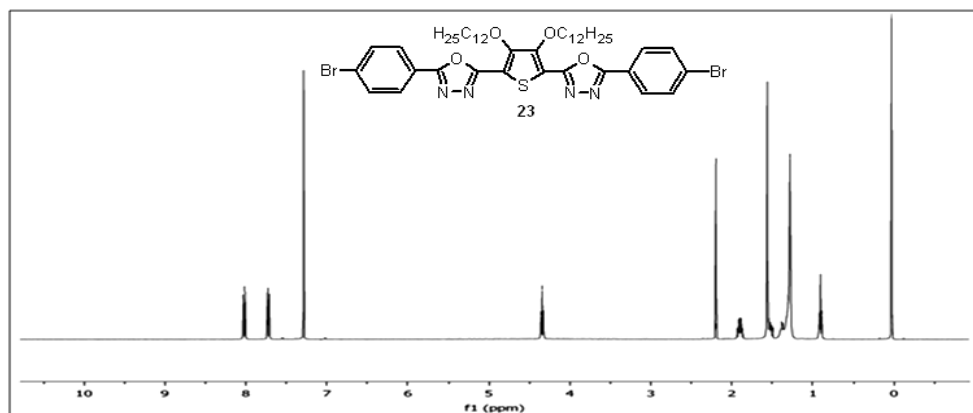


Figure 2.32 ¹H NMR spectrum of 5,5'-(3,4-bis(dodecyloxy)thiophene-2,5-diyl)bis(2-(4-bromophenyl)-1,3,4-oxadiazole) (**23**)

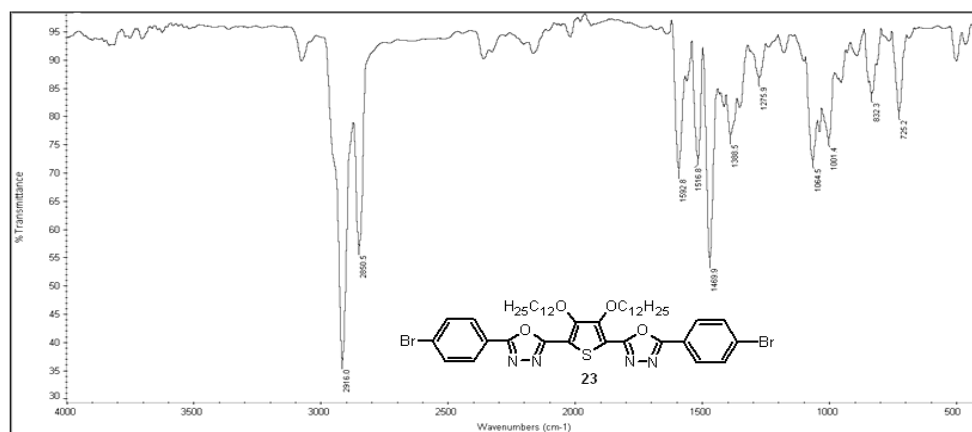


Figure 2.33 FTIR spectrum of 5,5'-(3,4-bis(dodecyloxy)thiophene-2,5-diyl)bis(2-(4-bromophenyl)-1,3,4-oxadiazole) (**23**)

The successful Suzuki coupling between bisoxadiazole **23** and 4-formylphenyl boronic acid leading to the formation of required dialdehyde monomer **M10** was established by recording the ¹H NMR spectrum of **M10** (Figure 2.34). In the spectrum, a singlet peak at δ 10.13 was observed indicating the presence of aldehyde (–CHO) protons. The spectrum also showed characteristic peaks due to phenyl and alkoxy protons. The enlarged image of ¹H NMR spectrum of **M10** in the aromatic region is shown in Figure 2.35. Its FTIR spectrum (Figure 2.36) exhibited a sharp peak at 1697 cm⁻¹ indicating the presence of >C=O groups, which further confirms the chemical structure of the required monomer **M10**. In addition, the elemental analysis

data of monomer **M10** and its intermediates were in good agreement with their molecular formulae.

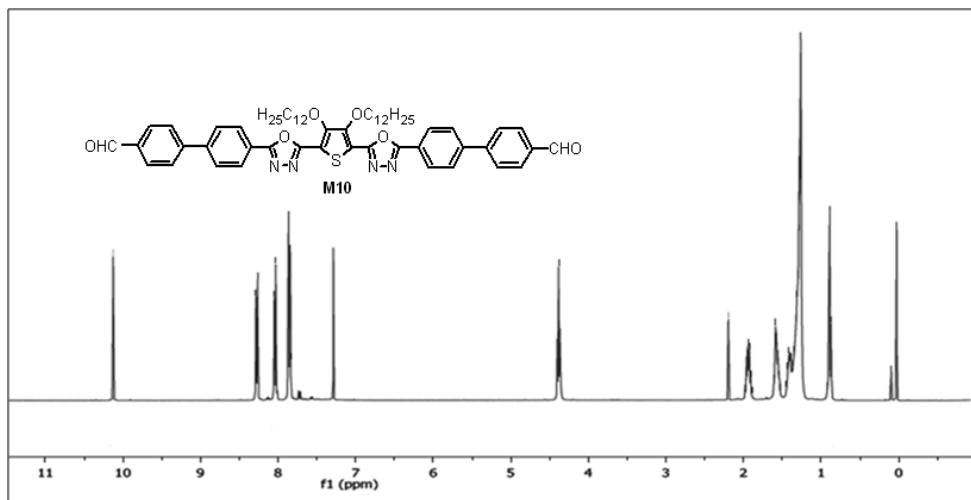


Figure 2.34 ^1H NMR spectrum of 4',4'-(5,5'-(3,4-bis(dodecyloxy)thiophene-2,5-diyl)bis(1,3,4-oxadiazole-5,2-diyl))dibiphenyl-4-carbaldehyde (**M10**)

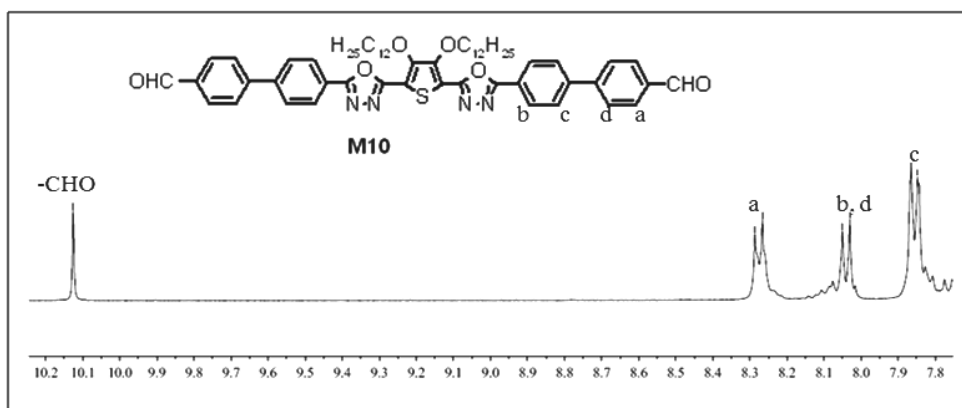


Figure 2.35 Enlarged image of ^1H NMR spectrum of **M10**

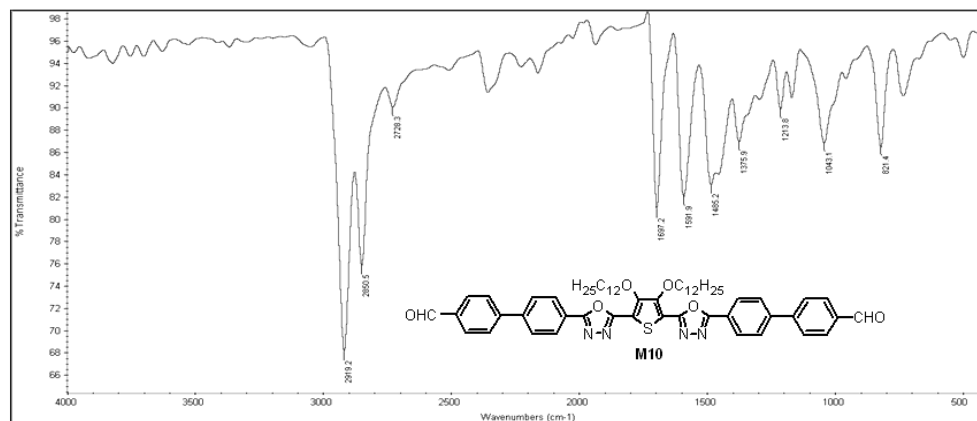


Figure 2.36 FTIR spectrum of 4',4'-(5,5'-(3,4-bis(dodecyloxy)thiophene-2,5-diyl)bis(1,3,4-oxadiazole-5,2-diyl)dibiphenyl-4-carbaldehyde (**M10**)

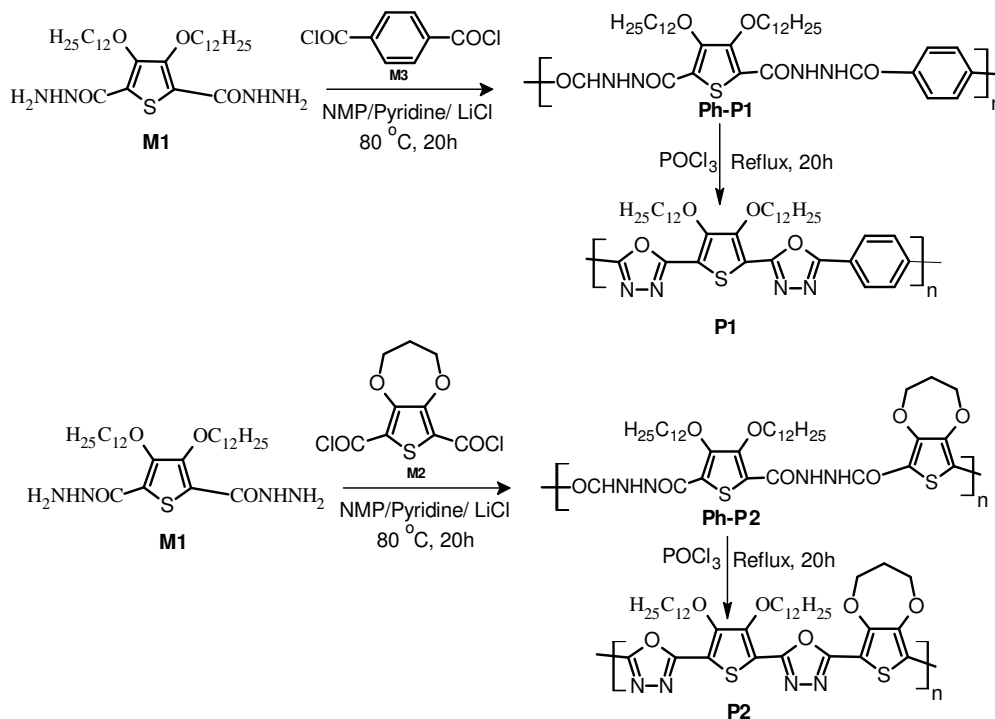
2.4 SYNTHESIS AND STRUCTURAL CHARACTERIZATION OF POLYMERS P1–P12

In this section, the synthesis and characterization of five new series of thiophene based D–A conjugated polymers are described. All the polymers contain electron donating 3,4-didodecyloxythiophene unit as the core moiety in their main chain with other aromatic units. The other structural features of the polymers include phenyl/3,4-propylenedioxythiophene and 1,3,4-oxadiazole units (**P1** and **P2**), thienylenevinylene segments (**P3** and **P4**), cyanovinylene moieties (**P5–P8**), fluorenevinylene units (**P9** and **P10**) and cyanophenylenevinylene segments (**P11** and **P12**).

2.4.1 3,4-Didodecyloxythiophene based polymers carrying 1,3,4-oxadiazole and phenyl or 3,4-propylenedioxythiophene segments (**P1** and **P2**)

The polymers **P1** and **P2** were synthesized according to Scheme 2.9. The chemical structure of polymer chains in **P1** and **P2** are quite similar. The polymer chain in **P1** contains 3,4-didodecyloxythiophene, 1,3,4-oxadiazole and phenyl units whereas in case of **P2**, the phenyl ring is replaced by a 3,4-propylenedioxythiophene (PDOT) unit.

2.4.1.1 Synthesis

Scheme 2.9 Synthesis of polymers **P1** and **P2**

As shown in Scheme 2.9, the polycondensation reaction methodology was used for the synthesis of **P1** and **P2**, wherein the dihydrazide monomer **M1** was reacted with the corresponding diacid chloride (**M2** or **M3**) in NMP in the presence of anhydrous lithium chloride (LiCl) and trace amount of pyridine. The reaction afforded the precursor polyhydrazides **Ph-P1** and **Ph-P2** in good yields. The target polymers, polyoxadiazoles **P1** and **P2**, were obtained via a cyclodehydration reaction of the corresponding polyhydrazide using POCl₃, which act both as solvent and dehydrating agent.

2.4.1.2 Experimental section

Experimental protocols followed for the synthesis of precursor polyhydrazides **Ph-P1** and **Ph-P2** and polymers **P1** and **P2** are given in the following section.

General procedure for the synthesis of precursor polyhydrazides (Ph-P1 and Ph-P2)

To a mixture of dihydrazide **M1** (1 g, 1.71 mmol), anhydrous lithium chloride (0.15 g, 3.42 mmol) and 0.1 ml of pyridine in 10 ml of NMP, the corresponding acid chloride [Terephthaloyl chloride **M3** (0.36 g, 1.71 mmol) for **Ph-P1** and 3,4-propylenedioxythiophene-2,5-dicarboxylic acid chloride **M2** (0.48 g, 1.71 mmol) for **Ph-P2**] was added slowly at room temperature. The reaction mixture was then stirred at room temperature under nitrogen atmosphere for 5 h. The resulting yellow solution was then heated at 80 °C with stirring for 20 h. After cooling to room temperature the reaction mixture was poured into ice cold water to get a precipitate. The precipitate was collected by filtration and was washed with water followed by acetone and finally dried in vacuum at 40 °C to get the corresponding polyhydrazides in 80–85 % yield. The structural characterization data of the polyhydrazides **Ph-P1** and **Ph-P2** are given below.

Ph-P1: Yield: 85 %. ¹H NMR (400MHz, DMSO-*d*₆, δ): 10.9 (s, 2H, –NH), 9.8 (s, 2H, –NH), 8.0 (m, 4H, aromatic), 4.2 (t, 4H, –OCH₂–), 1.8 – 1.1 (m, 40H, –(CH₂)₁₀–), 0.84 (t, 6H, –CH₃). FTIR (cm⁻¹): 3283 (–N-H), 2922 and 2854 (–C-H), 1629 (>C=O), 1452, 1375, 1279. Element. anal. calcd. for C₃₈H₅₈N₄O₆S (%): C 65.29, H 8.37, N 8.02, S 4.58. Found (%): C 65.38, H 8.22, N 8.08, S 4.62.

Ph-P2: Yield: 80 %. ¹H NMR (400MHz, DMSO-*d*₆, δ): 10.8 (s, 2H, –NH), 9.9 (s, 2H, –NH), 4.3 – 3.8 (m, 8H, –OCH₂–), 2.26 (m, 2H, PDOT protons), 1.9 – 1.1 (m, 40H, –(CH₂)₁₀–), 0.8 (t, 6H, –CH₃). FTIR (cm⁻¹): 3347 (–N-H), 2920 and 2852 (–C-H), 1629 (>C=O), 1433, 1372, 1278, 1082. Element. anal. calcd. for C₃₉H₆₀N₄O₈S₂(%): C 60.28, H 7.79, N 7.21, S 8.24. Found (%): C 60.36, H 7.71, N 7.28, S 8.32.

General procedure for the synthesis of polymers P1 and P2

A mixture of the appropriate precursor polyhydrazide (1 g) and 10 ml of POCl₃ was heated at 80 °C under nitrogen atmosphere for 20 h. The reaction mixture was then cooled to room temperature and poured in to excess of ice cold water. The resulting precipitate was collected by filtration and was washed with water and dried in vacuum oven 45 °C to get the corresponding polymers as greenish powder in

70–80 % yield. The analytical characterization data of polymers **P1** and **P2** along with their number average molecular weight (M_n) and polydispersity (PD) are summarized below.

Poly[2-(3,4-bis(dodecyloxy)-5-(1,3,4-oxadiazol-2-yl)thiophen-2-yl)-5-phenyl-1,3,4-oxadiazole] (P1)

Yield: 80 %. $^1\text{H NMR}$ (400MHz, CDCl_3 , δ): 8.32 – 7.94 (m, 4H, aromatic), 4.2 (t, 4H, $-\text{OCH}_2-$), 1.9 – 1.1 (m, 40H, $-(\text{CH}_2)_{10}-$), 0.86 (t, 6H, $-\text{CH}_3$). FTIR (cm^{-1}): 2919 and 2851 ($-\text{C}-\text{H}$), 1572 ($>\text{C}=\text{N}-$), 1454, 1368, 1275, 1043 ($=\text{C}-\text{O}-\text{C}=\text{O}$). Element. anal. calcd. for $\text{C}_{38}\text{H}_{54}\text{N}_4\text{O}_6\text{S}_2$ (%): C 62.78, H 7.49, N 7.71, S 8.8. Found (%): C 62.32, H 7.18, N 7.98, S 8.68. $M_n = 16290$, PD = 1.9.

Poly{2-(3,4-bis(dodecyloxy)-5-(1,3,4-oxadiazol-2-yl)thiophen-2-yl)-5-(3,4-dihydro-2H-thieno[3,4-b][1,4]dioxepin-6-yl)-1,3,4-oxadiazole} (P2)

Yield: 70 %. $^1\text{H NMR}$ (400MHz, CDCl_3 , δ): 4.56 – 3.7 (m, 8H, $-\text{OCH}_2-$), 2.4 (m, 2H, PDOT protons), 1.9 – 1.28 (m, 40H, $-(\text{CH}_2)_{10}-$), 0.8 (t, 6H, $-\text{CH}_3$). FTIR (cm^{-1}): 2918 and 2850 ($-\text{C}-\text{H}$), 1575 ($>\text{C}=\text{N}-$), 1462, 1369, 1029. Element. anal. calcd. for $\text{C}_{39}\text{H}_{56}\text{N}_4\text{O}_6\text{S}_2$ (%): C 63.21, H 7.62, N 7.57, S 8.64. Found (%): C 63.56, H 7.38, N 7.24, S 8.36. $M_n = 15200$, PD = 1.7.

2.4.1.3 Structural characterization of P1 and P2

The chemical structures of the polymers, **P1** and **P2**, were confirmed by FTIR and $^1\text{H NMR}$ spectral studies as well as by elemental analyses. The FTIR spectrum of polyhydrazide **Ph-P1** is as shown in Figure 2.37. The spectrum showed absorption peaks at 3283 and 1629 cm^{-1} indicating the presence of $-\text{N}-\text{H}$ and $>\text{C}=\text{O}$ groups respectively. Further, the $-\text{C}-\text{H}$ absorption bands were observed at 2922 and 2854 cm^{-1} . In addition, the $^1\text{H NMR}$ spectrum confirmed the formation of required polyhydrazide **Ph-P1** and the spectrum is given in Figure 2.38. The four protons of $-\text{CONH}$ group appeared as two singlets. The $-\text{CONH}$ protons attached to phenyl and 3,4-dodecyloxythiophene rings resonated at δ 10.9 and 9.8 respectively. A multiplet peak at δ 8.0 is due to the presence of four aromatic (phenyl) protons. Further, four protons of the alkoxy ($-\text{OCH}_2-$) groups at 3- and 4-positions of the thiophene ring appeared at δ 4.2 as a triplet. A set of multiplet peaks which corresponds to alkyl

chain $(-\text{CH}_2)_{10}-$ appeared in the region δ 1.8 – 1.1. The terminal six methyl protons of the alkoxy chain were resonated at δ 0.84 as a triplet. The FTIR and ^1H NMR spectra of polyhydrazide **Ph-P2** displayed a similar spectral characteristic peaks confirming the formation of the required product.

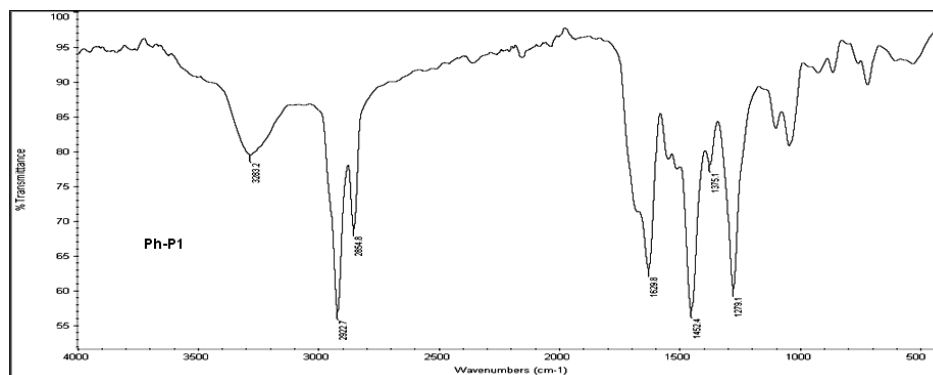


Figure 2.37 FTIR spectrum of polyhydrazide **Ph-P1**

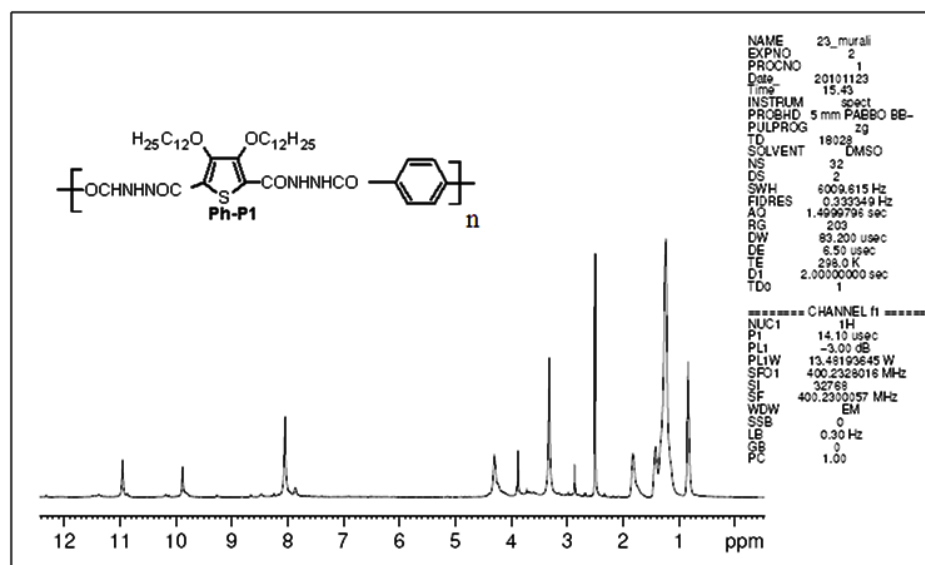


Figure 2.38 ^1H NMR spectrum of polyhydrazide **Ph-P1**

The successful completion of the cyclodehydration reaction of polyhydrazide **Ph-P1** to give polyoxadiazole **P1** was confirmed by FTIR spectroscopy. In the FTIR spectrum of polyoxadiazole **P1** (Figure 2.39), the stretching bands of $>\text{C}=\text{O}$ and $-\text{N}-\text{H}$ groups were absent, whereas new absorption bands corresponding to imine ($-\text{C}=\text{N}-$) group of 1,3,4-oxadiazole ring was observed at 1572 cm^{-1} . In addition, broad peak at 1043 cm^{-1} accounts for $=\text{C}-\text{O}-\text{C}=\text{O}$ stretching of 1,3,4-oxadiazole ring.

In the ^1H NMR spectrum (Figure 2.40), the disappearance of two singlet peaks due to $-\text{NH}$ protons further confirms the cyclization of polyoxadiazole **Ph-P1** to polyoxadiazole **P1**. The spectrum also displayed other characteristic peaks. The four aromatic protons resonated as multiplet in the range δ 8.32 – 7.94. The triplet peak appeared at δ 4.2 is due to alkoxy ($-\text{OCH}_2-$) groups and a set of multiple peaks in range δ 1.9 – 1.1 corresponds to alkyl chain protons ($-(\text{CH}_2)_{10}-$) of the thiophene ring. The terminal methyl protons resonated as a triplet at δ 0.86.

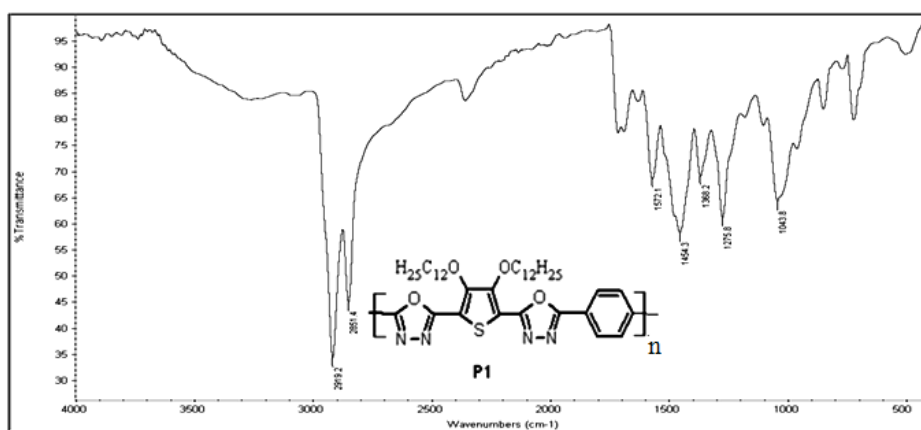


Figure 2.39 FTIR spectrum of polymer **P1**

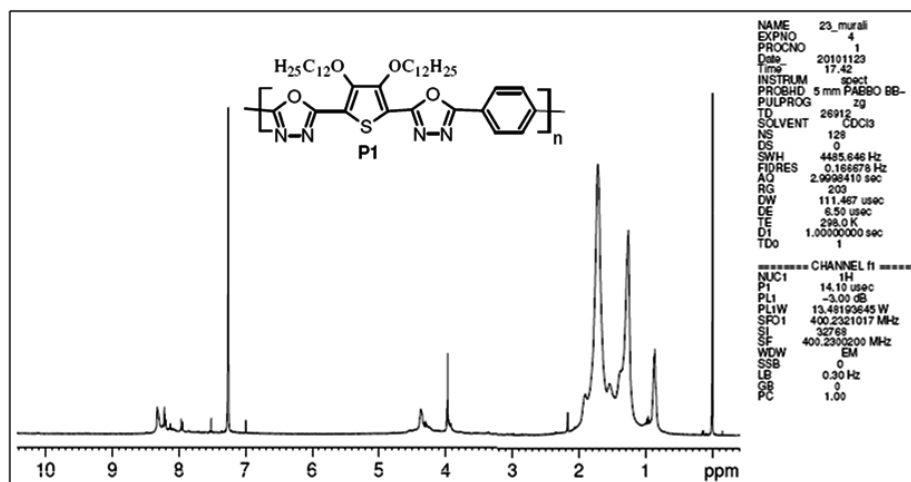


Figure 2.40 ^1H NMR spectrum of polymer **P1**

The FTIR and ^1H NMR spectra of **P2** showed similar spectral characteristic peaks confirming the chemical structure of the polymer. Figure 2.41 shows the FTIR

spectrum of polymer **P2**. The synthesized oxadiazole polymers **P1** and **P2** were greenish in color and were soluble in common organic solvents like CHCl_3 , THF, DMF, DMSO, chlorobenzene etc. Further the elemental analysis data of all the polymers matched with their expected empirical formulae.

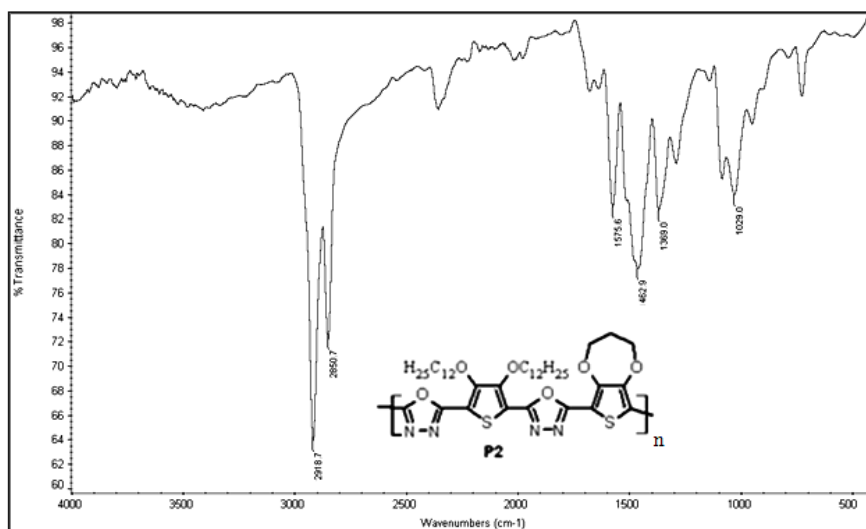


Figure 2.41 FTIR spectrum of polymer **P2**

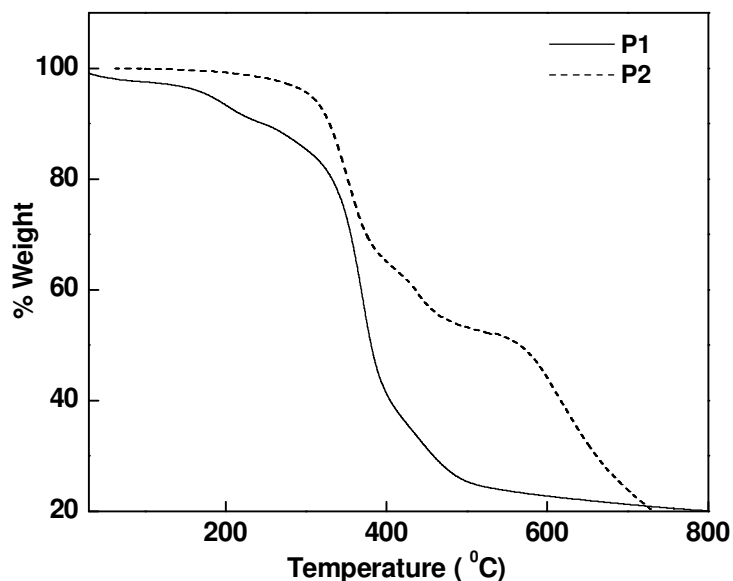


Figure 2.42 Thermogravimetric traces of polymers **P1** and **P2**

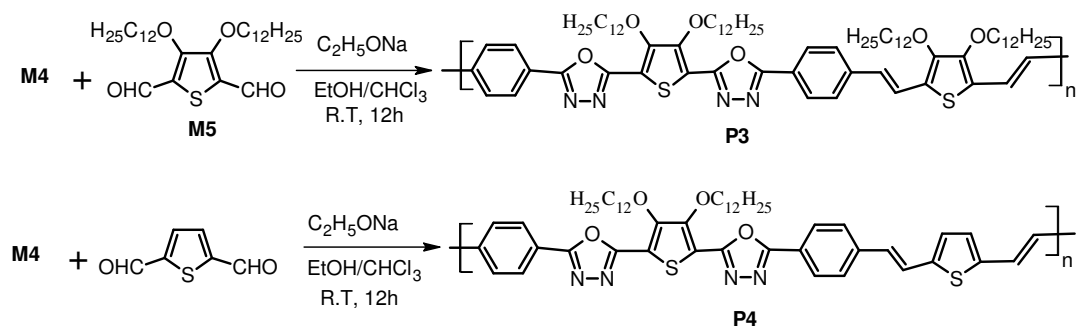
The thermal property of polymers **P1** and **P2** was investigated by thermogravimetric analysis and was carried out under nitrogen atmosphere at a

heating rate of 5 °C/min. The TGA revealed that, the polymers possess good thermal stability. As shown in Figure 2.42, polymer **P1** showed the onset decomposition at 180 °C with a weight loss of around 5 %, whereas polymer **P2** is thermally stable up to a temperature of 310 °C. Above 310 °C, a sharp weight loss was observed, indicating the leaving of alkoxy or alkyl chains along with the decomposition of the polymer backbone. It is evident that polymer **P2** is more thermally stable than polymer **P1**. This could be due to the incorporation of rigid PDOT ring in **P2** which enhances the thermal stability of the polymer.

2.4.2. 3,4-Didodecyloxythiophene based polymers carrying 1,3,4-oxadiazole, phenylenevinylene and thienylenevinylene units (**P3** and **P4**)

Two new D–A type 3,4-didodecyloxythiophene based conjugated polymers **P3** and **P4** containing 1,3,4-oxadiazole units along with phenylenevinylene and thienylenevinylene linkages in their backbone were synthesized according to Scheme 2.10. The details of the synthetic procedure followed and the structural characterization of the polymers are discussed in subsequent sections.

2.4.2.1 Synthesis



Scheme 2.10 Synthesis of polymers **P3** and **P4**

To synthesize polymers **P3** and **P4**, the well known Wittig reaction methodology was employed. In the typical polymerization reaction, the Wittig salt monomer **M4** was treated with the appropriate thiophene dicarbaldehyde (dicarbaldehyde monomer **M5** for **P3** and thiophene-2,5-dicarbaldehyde for **P4**). The polymerization reaction was performed under inert atmosphere at room temperature in ethanol/chloroform

solvent in the presence of sodium ethoxide. The polymers were obtained in reasonably good yield.

2.4.2.2 Experimental section

The detailed synthetic procedure of **P3** and **P4** is given in the following section.

General procedure for the synthesis of polymers **P3** and **P4**

A solution of sodium (23 mg, 1.03 mmol) in 3 ml of anhydrous ethanol was added drop wise at ambient temperature under argon atmosphere to a mixture of thiophene dialdehyde monomer **M5** (107 mg, 0.20 mmol) and Wittig salt monomer **M4** (0.3 g, 0.20 mmol) in chloroform (6 ml). The reaction mixture was stirred at room temperature for 12 h and then it was slowly poured into 100 ml of methanol. The precipitated polymer was filtered off. The crude polymer was redissolved in chloroform and precipitated in methanol several times. After filtration, the sample was vacuum dried to get the polymer **P3** as yellow powder in 65 % yield. Polymer **P4** was synthesized following a similar procedure by treating Wittig salt monomer **M4** (0.3 g, 0.20 mmol) with thiophene-2,5-dicarbaldehyde (30 mg, 0.20 mmol).

Poly[2-(3,4-bis(dodecyloxy)-5-(5-phenyl-1,3,4-oxadiazol-2-yl)thiophen-2-yl)-5-(4-(2-(3,4-bis(dodecyloxy)thiophen-2-yl)vinyl)phenyl)-1,3,4-oxadiazole] (P3)

Yield: 65 %. ¹H NMR (400MHz, CDCl₃, δ): 8.13 – 6.71 (m, 12H, Ar and –CH=CH–), 4.33 (t, 8H, –OCH₂–), 1.90 – 1.27 (m, 80H, –(CH₂)₁₀–), 0.88 (t, 12H, –CH₃). FTIR (cm⁻¹): 2918 and 2851 (–C–H), 1547 (–C=N–), 1460 (–C=C–), 1041 (=C–O–C=). Element. anal. calcd. for C₇₆H₁₁₂N₄O₆S₂ (%): C 73.50, H 9.10, N 4.51, S 5.15. Found (%): C 73.62, H 9.16, N 4.42, S 5.10. M_n = 16100, PD = 2.

Poly[2-(3,4-bis(dodecyloxy)-5-(5-(4-(2-(thiophen-2-yl)vinyl)phenyl)-1,3,4-oxadiazol-2-yl)thiophen-2-yl)-5-phenyl-1,3,4-oxadiazole] (P4)

Yield: 60 %. ¹H NMR (400MHz, CDCl₃, δ): 8.14 – 6.52 (m, 14H, Ar and –CH=CH–), 4.34 (t, 4H, –OCH₂–), 1.90 – 1.35 (m, 40H, –(CH₂)₁₀–), 0.88 (t, 6H, –CH₃). FTIR (cm⁻¹): 2918 and 2849 (–C–H), 1551 (–C=N–), 1485 (–C=C–), 1044 (=C–O–C=). Element. anal. calcd. for C₅₂H₆₆N₄O₄S₂ (%): C 71.36, H 7.61, N 6.41, S 7.31. Found (%): 71.44, H 7.54, N 6.32, S 7.34. M_n = 18200, PD = 1.4.

2.4.2.3 Structural characterization of polymers P3 and P4

The formation of target polymers **P3** and **P4** were evidenced by analytical instrumental methods such as ^1H NMR spectroscopy, FTIR spectroscopy, GPC and elemental analyses. In the ^1H NMR spectra of the polymers, the resonance for the proton corresponding to the aldehyde group was not observed, indicating that the polymers are free from monomeric residues. The ^1H NMR spectrum (Figure 2.43) of **P3** displayed complex multiple peaks in the range δ 8.13 – 6.71 corresponding to the aromatic and vinylic protons. The $-\text{OCH}_2-$ protons (alkoxy chain) of the thiophene ring appeared as a triplet at δ 4.33. In addition, the set of multiple peaks in the range δ 1.90 – 1.27 indicates the presence of $-(\text{CH}_2)_{10}-$ protons of the alkoxy chains. The terminal methyl protons resonated as a triplet at δ 0.88. As shown in Figure 2.44, FTIR spectrum of polymer **P3** did not show any peak corresponding to $>\text{C}=\text{O}$ group, which clearly confirmed the complete conversion of the corresponding dicarbaldhyde monomer in the polymerization reaction. The ^1H NMR and FTIR spectra of **P4** displayed a similar spectral pattern. Both the polymers were yellowish in color and were readily soluble in common organic solvents such as chloroform, THF, chlorobenzene etc.

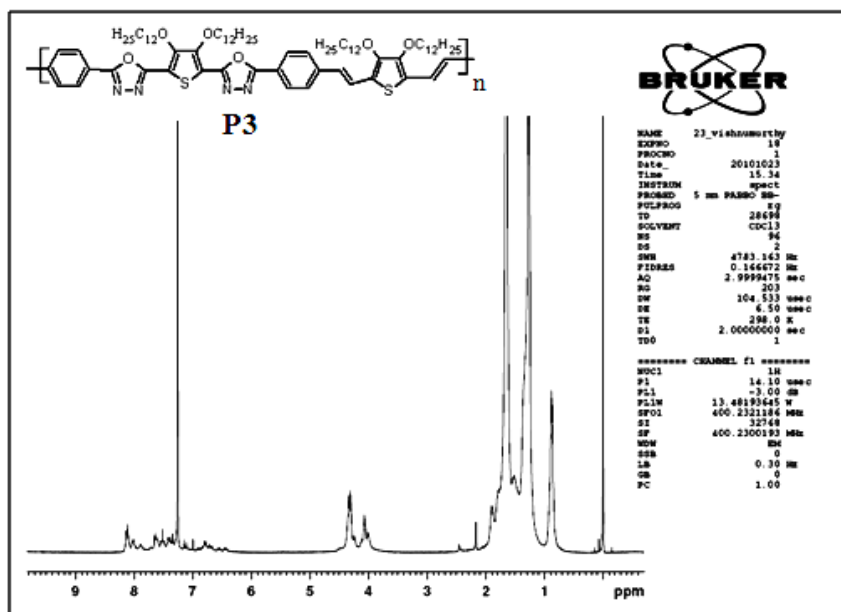


Figure 2.43 ^1H NMR spectrum of polymer P3

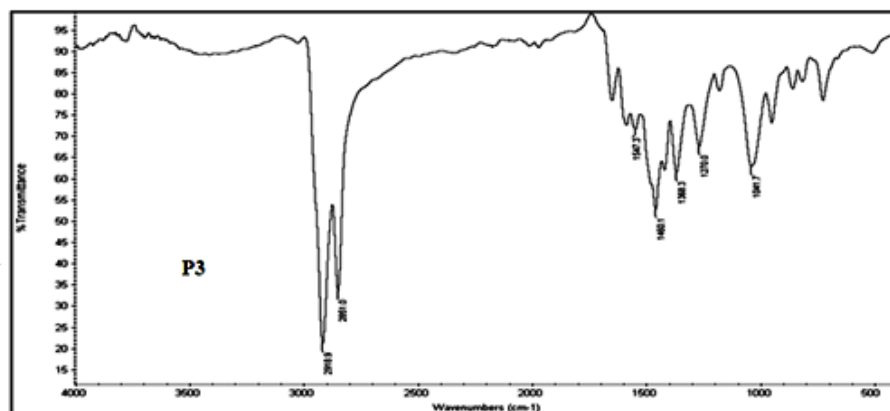


Figure 2.44 FTIR spectrum of polymer **P3**

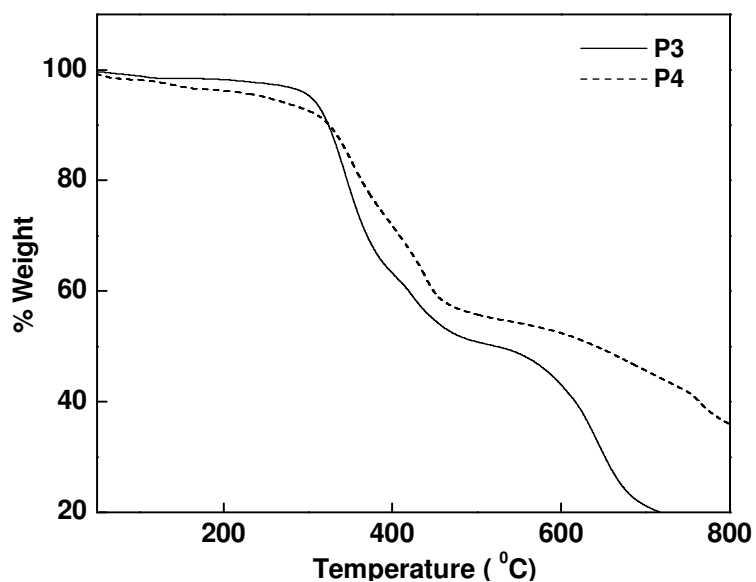


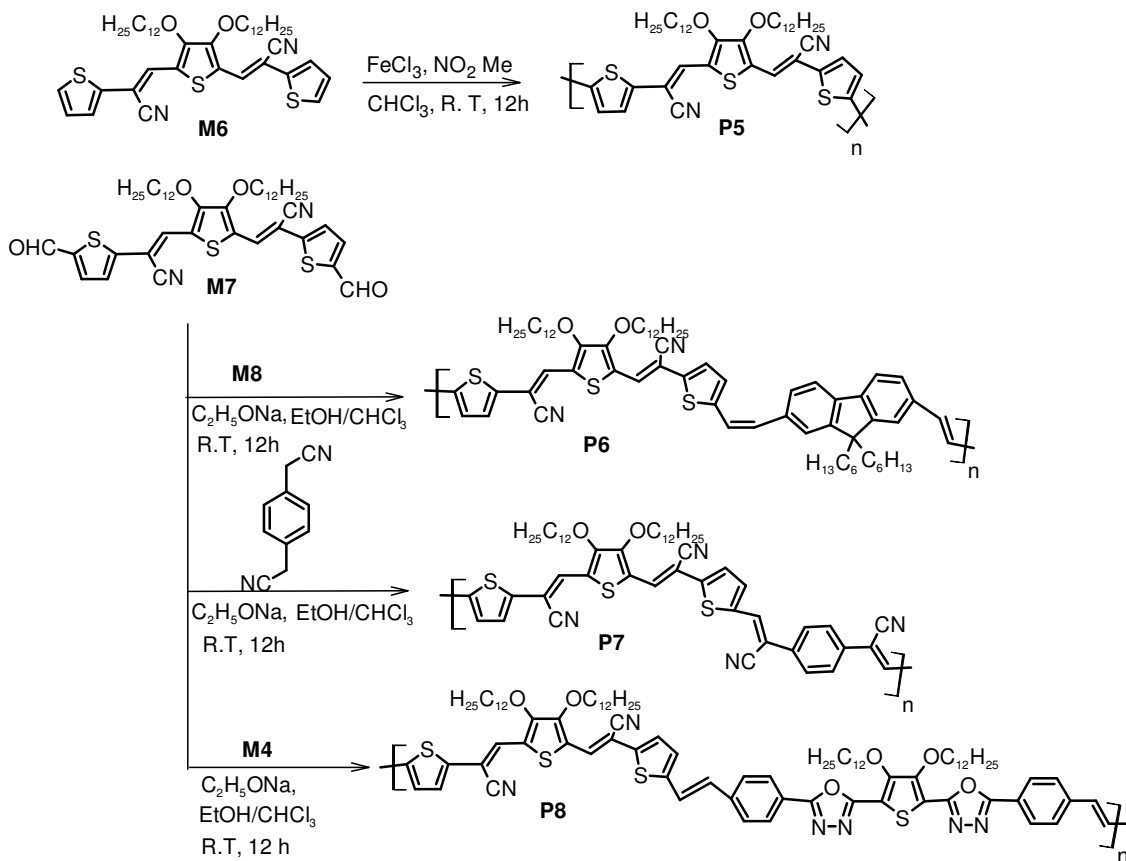
Figure 2.45 Thermogravimetric traces of polymers **P3** and **P4**

Thermogravimetric analysis data reveal that, both the polymers, **P3** and **P4**, possess good thermal stability. As shown in Figure 2.45, no significant weight loss was observed up to a temperature of ~320 °C and beyond this temperature a rapid weight loss was occurred which indicates the decomposition of the polymers backbone.

2.4.3 3,4-Didodecyloxythiophene based polymers carrying cyanovinylene moieties (P5–P8)

The synthetic routes of polymers **P5–P8** are shown in Scheme 2.11. The chain structure in polymer **P5** is made up of 3,4-didodecyloxythiophene and cyanovinylene units, whereas in **P6**, **P7** and **P8**, the conjugation length of the repeating units is extended by incorporating additional arylvinylene units, viz fluorenevinylene in **P6**, cyano phenylenevinylene unit in **P7** and a conjugated system containing phenylenevinylene, dialkoxythiophene and 1,3,4-oxadiazole units in **P8**.

2.4.3.1 Synthesis



Scheme 2.11 Synthesis of polymers **P5–P8**

The chemical polymerization reaction was performed to synthesize polymer **P5** from its monomer **M6**, using FeCl_3 as the oxidizing agent. This method is very useful to prepare poly(thiophene)s due to its simplicity and the high molecular weights achieved. After the polymerization reaction, the residual iron (III) salts present in the

mixture were reduced in concentration with rigorous purification. The crude polymer obtained was precipitated with methanol several times in order to remove residual FeCl_3 . The oxidative polymerization reaction gives the polymer in the oxidized (doped) form. The reduction (dedoping) of the polymer was achieved using hydrazine to get the polymer in the neutral form. Further the polymer was stirred with acetone so as to remove any traces of unreacted monomer. The polymers **P6** and **P8** were obtained through Wittig reaction methodology, by reacting cyanodialdehyde monomer **M7** with the corresponding Wittig salt monomer. Polymer **P7** was prepared by using Knoevenagel condensation reaction between monomer **M7** and 1,4-phenyldiacetonitrile in presence of sodium ethoxide. All the polymerization reactions were carried out under inert atmosphere condition using anhydrous solvent system at room temperature.

2.4.3.2 Experimental section

The synthetic procedure of polymers **P5–P8** and their spectral data are given in the following section.

Synthesis of Poly[3,3'-(3,4-bis(dodecyloxy)thiophene-2,5-diyl)bis(2-(thiophen-2-yl)acrylonitrile)] (P5)

To a stirred solution of monomer **M6** (500 mg, 0.695 mmol) in 50 ml of chloroform, anhydrous FeCl_3 (0.56 g, 3.47 mmol) in nitromethane was added drop wise over a period of 45 minutes at room temperature under argon atmosphere. The light red monomer solution turned progressively dark violet with the addition of the oxidizing agent. The mixture was stirred for 12 h and then added into 200 ml of methanol. The precipitate was filtered, dissolved in CHCl_3 , and extracted with water. Solvent was removed and the residue was redissolved in chloroform (50 ml) and hydrazine monohydrate (25 ml). To reduce the polymer to neutral form, the mixture was stirred for 12 h. After evaporation of CHCl_3 , the residue was again precipitated in methanol (200 ml) several times and the precipitate was collected by filtration. The collected product was then stirred in acetone to remove unreacted monomers. The pure polymer was filtered and dried under vacuum to give polymer **P5** as violet solid.

Yield: 68 %. ^1H NMR (400MHz, CDCl_3 , δ): 7.57 (s, 2H, –olephinic proton–), 7.35 (d, $J=3.6\text{Hz}$, 2H, Ar), 7.14 (d, $J=4\text{Hz}$, 2H, Ar), 4.13 (t, 4H, $-\text{OCH}_2-$), 1.83 – 1.23 (m, 40H, $-\text{CH}_2)_{10-}$), 0.87 (t, 6H, $-\text{CH}_3$). FTIR (cm^{-1}): 2912 and 2846 ($-\text{C-H}$), 2206 ($-\text{CN}$), 1562, 1451, 1368, 1260, 1024, 785, 684. Element. anal. calcd. for $\text{C}_{42}\text{H}_{56}\text{N}_2\text{O}_2\text{S}_3$ (%): C 70.36, H 7.88, N 3.91, S 13.39. Found (%): C 70.28, H 7.76, N 3.84, S 13.52. $M_n=15800$, PD = 2.1.

General procedure for the synthesis of polymers P6–P8

0.5 g (0.64 mmol) of monomer **M7** and 0.14 g (0.64 mmol) of fluorene Wittig salt **M8** were dissolved in 6 ml of chloroform, and a solution of 45 mg sodium (1.93 mmol) in 3 ml of anhydrous ethanol was added drop wise through a syringe at ambient temperature under argon atmosphere. The reaction mixture was stirred at room temperature for 12 h. Then it was slowly poured into 100 ml of methanol. The precipitated dark red solid was washed with methanol. The obtained crude polymer was redissolved in chloroform and precipitated in methanol several times and filtered off. The obtained dark red powder was dried under vacuum at 45 °C to get the polymer **P6**. The similar procedure was followed by treating monomer **M7** (0.5 g, 0.64 mmol) with 1,4-phenylenediacetonitrile (0.1 g, 0.64 mmol) to get polymer **P7**, whereas polymer **P8** was synthesized by treating monomer **M7** (0.5 g, 0.64 mmol) with monomer **M4** (0.93 g, 0.64 mmol).

Poly[3-(5-(2-cyano-2-(5-(2-(9,9-dihexyl-9*n*-fluoren-2-yl)vinyl)thiophen-2-yl)vinyl)-3,4-bis(dodecyloxy)thiophen-2-yl)-2-(thiophen-2-yl)acrylonitrile] (P6)

Yield: 70 %. ^1H NMR (400MHz, $\text{DMSO}-d_6$, δ): 7.67 – 6.74 (m, 16H, Ar and $-\text{CH}=\text{CH}-$), 4.15 (t, 4H, $-\text{OCH}_2-$), 1.96 – 0.85 (m, 66H, alkyl protons), 0.72 (t, 6H, $-\text{CH}_3$). FTIR (cm^{-1}): 2918 and 2849 ($-\text{C-H}$), 2206 ($-\text{CN}$), 1449, 1369, 1281, 1028, 949. Element. anal. calcd. for $\text{C}_{71}\text{H}_{92}\text{N}_2\text{O}_2\text{S}_3$ (%): C 77.41, H 8.42, N 2.54, S 8.71. Found (%): C 77.38, H 8.40, N 2.48, S 8.66. $M_n = 18930$, PD = 2.5.

Poly[2-(5-(2-cyano-2-(4-(1-cyanoethyl)phenyl)vinyl)thiophen-2-yl)-3-(5-(2-cyano-2-(thiophen-2-yl)vinyl)-3,4-bis(dodecyloxy)thiophen-2-yl)acrylonitrile] (P7)

Yield: 65 %. ^1H NMR (400MHz, $\text{DMSO}-d_6$, δ): 8.1 – 7.0 (m, 12H, Ar and $-\text{CH}=\text{C}-$), 4.13 (t, 4H, $-\text{OCH}_2-$), 1.8 – 1.01 (m, 40H, alkyl protons), 0.87 (t, 6H, $-\text{CH}_3$).

FTIR (cm^{-1}): 2916 and 2847 ($-\text{C}-\text{H}$), 2201 ($-\text{CN}$), 1568, 1446, 1365, 1276, 1039, 797. Anal. Calcd. For $\text{C}_{54}\text{H}_{62}\text{N}_4\text{O}_2\text{S}_3$ (%): C 72.45, H 6.99, N 6.26, S 10.72. Found (%): C 72.36, H 6.92, N 6.22, S 10.70. $M_n = 14720$, PD = 2.1.

Poly[2-(5-(4-(5-(3,4-bis(dodecyloxy)-5-(5-(4-ethylphenyl)-1,3,4-oxadiazol-2-yl)thiophen-2-yl)-1,3,4-oxadiazol-2-yl)styryl)thiophen-2-yl)-3-(5-(2-cyano-2-thiophen-2-yl)vinyl)-3,4-bis(dodecyloxy)thiophen-2-yl)acrylonitrile] (P8)

Yield: 60 %. ^1H NMR (400MHz, $\text{DMSO}-d_6$, δ): 8.11 – 6.67 (m, 18H, Ar and $-\text{CH}=\text{CH}-$), 4.38 – 4.0 (m, 8H, Ar), 1.89 – 1.1 (m, 80H, alkyl protons), 0.97 – 0.86 (br, 12H, $-\text{CH}_3$). FTIR (cm^{-1}): 2918 and 2850 ($-\text{C}-\text{H}$), 2207 ($-\text{CN}$), 1572 ($-\text{C}=\text{N}-$), 1450, 1370, 1281, 1029 ($=\text{C}-\text{O}-\text{C}=\text{O}$), 942. Element. anal. calcd. for $\text{C}_{90}\text{H}_{118}\text{N}_6\text{O}_6\text{S}_4$ (%): C 71.58, H 8.02, N 5.57, S 8.48. Found (%): C 71.48, H 7.94, N 5.48, S 8.54.

$M_n = 14100$, PD = 2.2.

2.4.3.3 Structural characterization of polymers P5–P8

The ^1H NMR spectrum of polymer **P5** is as shown in Figure 2.46. In the spectrum, the disappearance of double doublet peak of thiophene ring proton at position 2 and conversion of double doublet peaks into doublet peaks give a clear evidence of successful polymerization of the monomer **M6** to polymer **P5**. The ^1H NMR spectrum exhibited a singlet peak at δ 7.57 due to olefinic protons. The thiophene ring protons at position 3 and 4 resonated as two doublet peaks at δ 7.35 and 7.14 respectively. A triplet peak at δ 4.13 is due to the $-\text{OCH}_2-$ protons and the multiple peaks in the range δ 1.83 – 1.23 are due to the $-(\text{CH}_2)_{10}-$ protons of the alkyl chains of the thiophene ring. The FTIR spectrum of polymer **P5** is as shown in Figure A7 (Appendix).

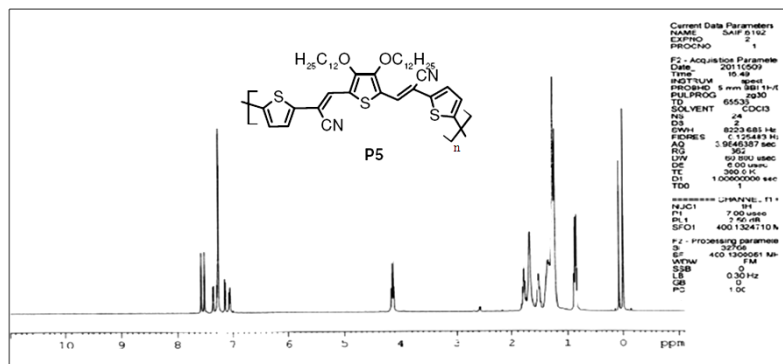


Figure 2.46 ^1H NMR spectrum of polymer **P5**

The ^1H NMR spectra of polymers **P6**, **P7** and **P8** are as shown in Figures 2.47, 2.48 and 2.49 respectively. The successful Wittig reaction between monomers **M7** and **M8** to give the required polymer **P6** was supported by following spectral observations. The resonance peak due to the aldehyde proton of **M7** was absent in the ^1H NMR spectrum of **P6** whereas its FTIR spectrum showed no absorption peak corresponding to $>\text{C}=\text{O}$ stretching vibrations (Figure 2.50). Its ^1H NMR spectrum showed aromatic and vinylic protons as set of multiple peaks in the range δ 7.67 – 6.74. A triplet peak was observed at δ 4.15 which corresponds to $-\text{OCH}_2-$ protons (alkoxy chain) of the thiophene ring. The alkyl protons attached to thiophene [$-(\text{CH}_2)_{10}-$] and fluorene ring [$-\text{C}_6\text{H}_{13}$] are resonated as set of multiple peaks in the range δ 1.96 – 0.85. Similarly, polymers **P7** and **P8** displayed characteristic peaks in their ^1H NMR and FTIR spectra. Polymer **P5** was violet in color whereas polymers **P6–P8** were red in color. Polymers **P5**, **P6** and **P8** were completely soluble in common organic solvents such as chloroform, THF, chlorobenzene etc. However, polymer **P7** is only partially soluble in common organic solvents. This may be due to the presence of less number of solubilising groups in **P7** compared to those in **P6** and **P8**. Polymer **P7** contains only one thiophene ring with alkoxy substitution making it comparatively less soluble in common organic solvents. Whereas in **P6**, there are long alkoxy groups on thiophene ring as well as alkyl groups on fluorene ring and whereas in **P8**, there are two thiophene rings carrying long alkoxy groups thus facilitating the solubility of these polymers.

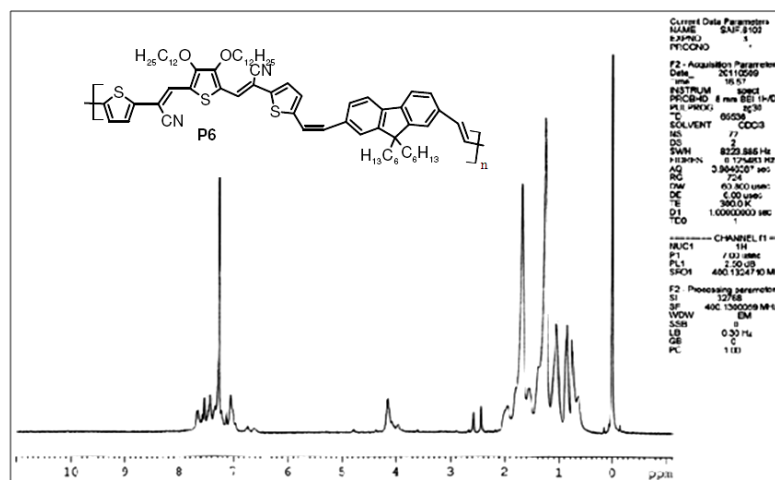
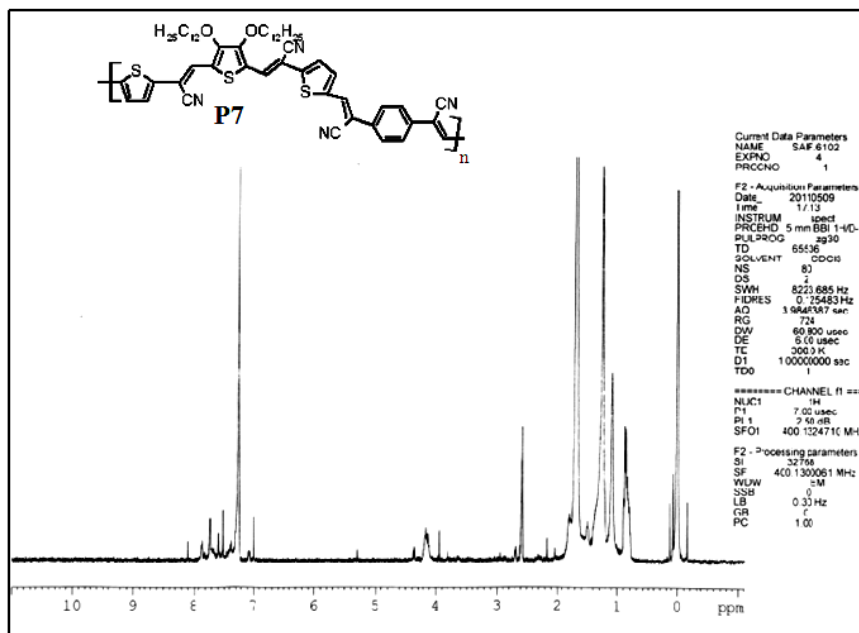
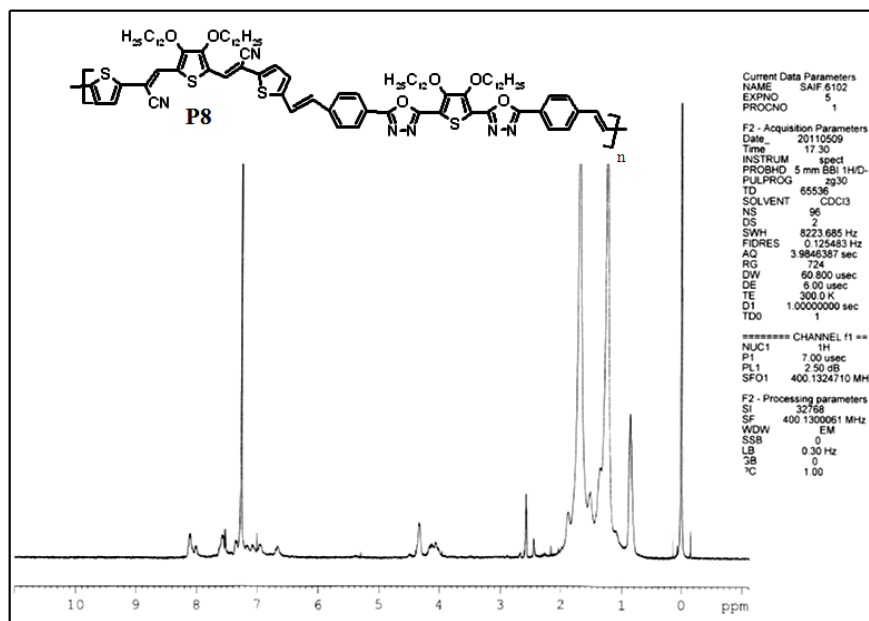


Figure 2.47 ^1H NMR spectrum of polymer **P6**

Figure 2.48 ^1H NMR spectrum of polymer P7Figure 2.49 ^1H NMR spectrum of polymer P8

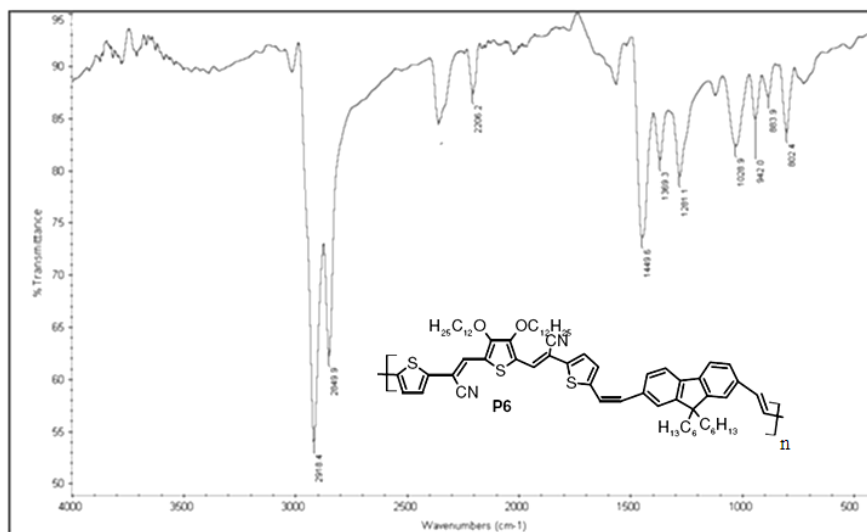


Figure 2.50 FTIR spectrum of polymer **P6**

The TGA reveals that, all the polymers are thermally stable upto a temperature of ~ 320 °C. As shown in Figure 2.51 the onset decomposition temperature of the polymers is in the range of 300 – 320 °C. However, an abrupt weight loss was observed as the temperature was increased to above 320 °C, indicating the decomposition of the polymers backbone.

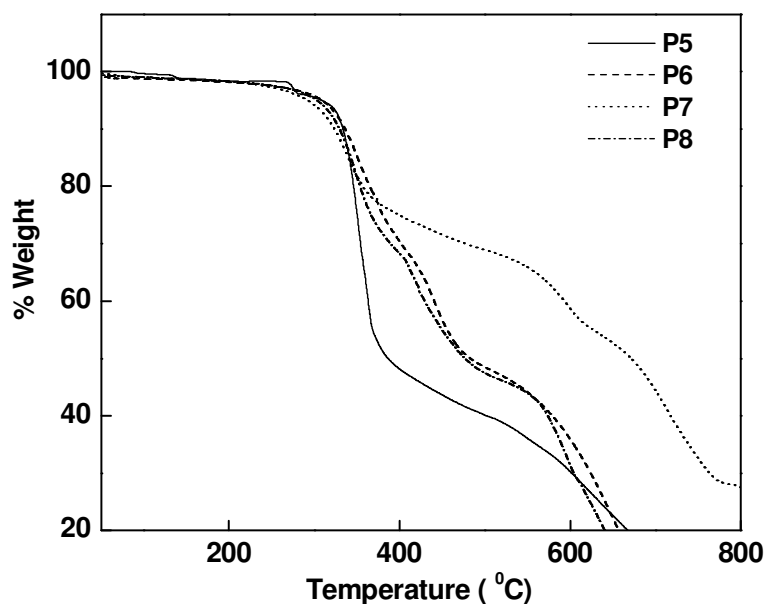


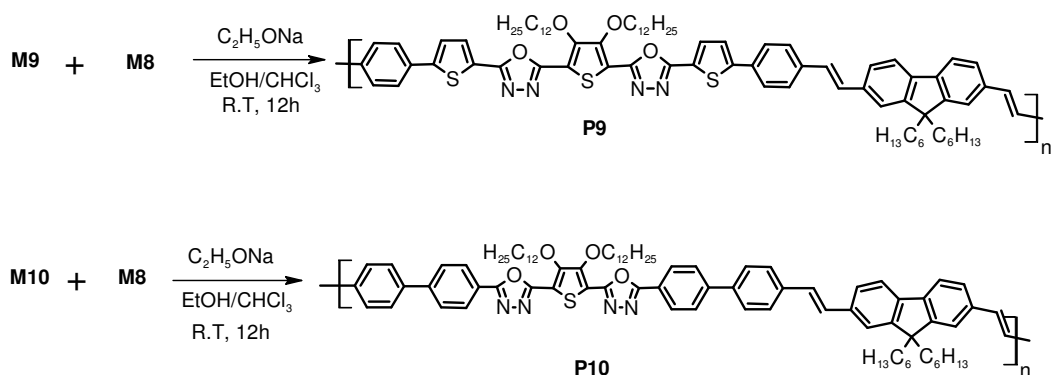
Figure 2.51 Thermogravimetric traces of polymers **P5–P8**

2.4.4 3,4-Didodecyloxythiophene based polymers carrying 1,3,4-oxadiazole and fluorenevinylene segments (**P9** and **P10**)

Two new D–A conjugated polymers **P9** and **P10** based on 3,4-didodecyloxythiophene carrying fluorenevinylene units were synthesized through Wittig reaction methodology according to synthetic route shown in Scheme 2.12.

The synthetic protocol and spectral characterization data of the polymers are presented in the following sections.

2.4.4.1 Synthesis



Scheme 2.12 Synthesis of polymers **P9** and **P10**

The Wittig reaction methodology was employed to synthesize new donor–acceptor conjugated polymers **P9** and **P10**. The polymer structure consists of 3,4-didodecyloxythiophene and 9,9'-*n*-dialkylfluorene moieties as electron donor units and 1,3,4-oxadiazole moiety as the electron acceptor unit along with vinylene linkages. However, in polymer **P9** the electron donating nature is enhanced by linking strong electron donating thiophene unit to 1,3,4-oxadiazole ring, in comparison with polymer **P10**. The polymerization reaction was performed at room temperature, by reacting fluorene Wittig salt **M8** with the corresponding dicarbaldehyde monomer (**M9** for **P9** and **M10** for **P10**) in presence of sodium ethoxide in ethanol/chloroform solvent system.

2.4.4.2 Experimental section

Experimental protocols for the synthesis of polymers **P9** and **P10** and their structural characterization data are given below.

General procedure for the synthesis of polymers **P9** and **P10**

To a mixture of monomer **M9** (0.3 g, 0.312 mmol) and fluorene Wittig salt **M8** (0.35 g, 0.312 mmol) in 6 ml of dry chloroform under argon atmosphere, a solution of sodium (20 mg, 0.936 mmol) in 2 ml of anhydrous ethanol was added drop wise at ambient temperature. The reaction mixture was stirred at room temperature for 12 h. The polymerization reaction mixture was slowly quenched into 100 ml of methanol. The resulting precipitated material was filtered off. The crude polymer was dissolved in chloroform and added drop wise to methanol at room temperature with stirring to precipitate the polymer. Reprecipitation was performed several times to remove oligomers and a yellow powder was obtained as pure polymer **P9** after drying under vacuum. The similar procedure was used for the synthesis of **P10** by treating monomer **M10** (0.3 g, 0.316 mmol) with **M8** (0.35 g, 0.316 mmol).

Poly[2-(3,4-bis(dodecyloxy)-5-(5-(5-phenylthiophen-2-yl)-1,3,4-oxadiazol-2-yl)thiophen-2-yl)-5-(5-(4-(2-(9,9-dihexyl-9n-fluoren-2-yl)vinyl)phenyl)thiophen-2-yl)-1,3,4-oxadiazole] (P9)

Yield: 65 %. ¹H NMR (400MHz, CDCl₃, δ): 7.97 – 6.54 (m, 22H, Ar and –CH=CH–), 4.32 (t, 4H, –OCH₂–), 1.91 – 0.86 (m, 66H, alkyl protons), 0.76 (t, 6H, –CH₃). FTIR (cm⁻¹): 2917 and 2848 (–C–H), 1573 (–C=N–), 1482, 1452, 1368, 1027 (=C–O–C=). Element. anal. calcd. for C₈₁H₉₈N₄O₄S₃ (%): C 75.54, H 7.68, N 4.35, S 7.45. Found (%): C 75.32, H 7.54, N 4.22, S 7.52. M_n = 12200, PD = 7.

Poly{2-(biphenyl-4-yl)-5-(5-(5-(4'-(2-(9,9-dihexyl-9n-fluoren-2-yl)vinyl)biphenyl-4-yl)-1,3,4-oxadiazol-2-yl)-3,4-bis(dodecyloxy)thiophen-2-yl)-1,3,4-oxadiazole} (P10)

Yield: 60 %. ¹H NMR (400MHz, CDCl₃, δ): 8.25 – 6.52 (m, 26H, Ar and –CH=CH–), 4.36 (t, 4H, –OCH₂–), 1.97 – 0.80 (m, 66H, alkyl protons), 0.77 (t, 6H, –CH₃). FTIR (cm⁻¹): 2919 and 2850 (–C–H), 1585 (–C=N–), 1475, 1368, 1279, 1045 (=C–O–C=).

Element. anal. calcd. for $C_{85}H_{102}N_4O_4S$ (%): C 80.02, H 8.06, N 4.39 S 2.51. Found (%): C 80.28, H 8.12, N 4.48, S 2.48. $M_n = 17800$, PD = 2.6.

2.4.4.3 Structural characterization of polymers P9 and P10

The chemical structure of the polymers was confirmed by the spectral analysis. For instance, the 1H NMR spectrum (Figure 2.52) of polymer **P10** displayed complex multiple peaks in the range δ 8.25 – 6.52 corresponding to the aromatic and vinylic protons. A triplet peak at δ 4.36 is due to $-OCH_2-$ protons of the alkoxy chains of the thiophene ring. The multiple peaks in the range 1.97 – 0.80 are due to the protons of alkyl groups present in the polymer structure. The 1H NMR spectrum of polymer **P9** showed a similar spectral trend as that of **P10**. Further, no $>C=O$ absorption peaks were observed in the FTIR spectra of polymers which confirms the successful Wittig reaction between the monomeric units. The FTIR spectrum of polymer **P9** is as shown in Figure 2.53. Both polymers were yellow in color and were soluble in common organic solvents, such as $CHCl_3$, THF, chlorobenzene etc.

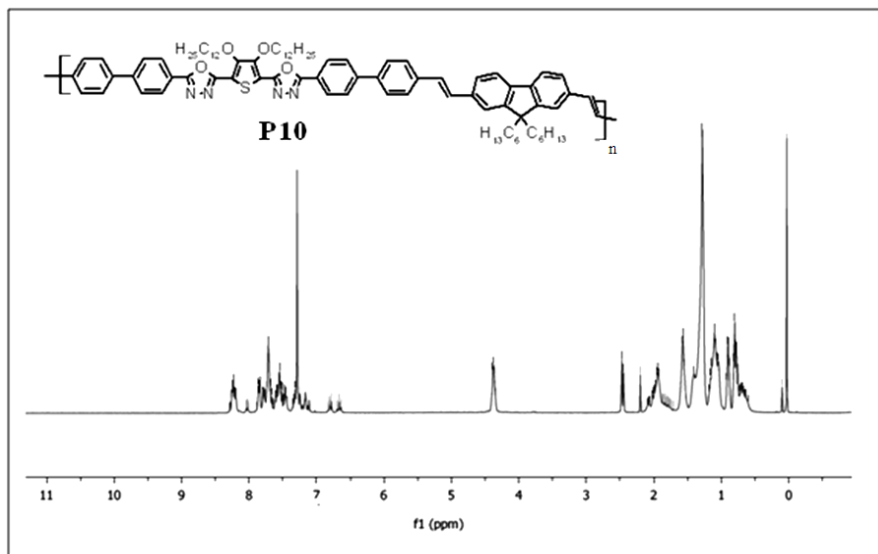


Figure 2.52 1H NMR spectrum of polymer **P10**

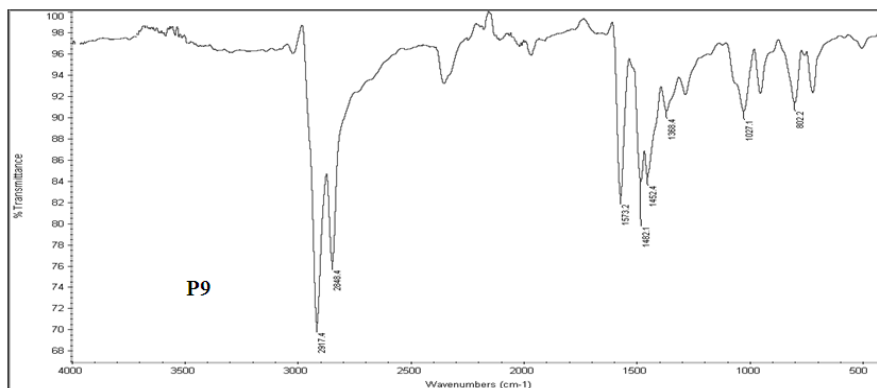


Figure 2.53 FTIR spectrum of polymer **P9**

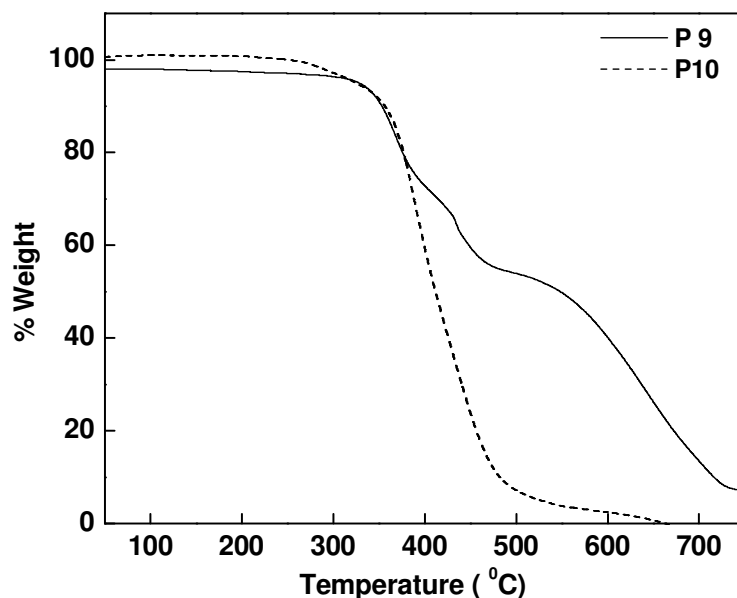


Figure 2.54 Thermogravimetric traces of polymers **P9** and **P10**

The TGA analysis reveals that, both the polymers exhibit good thermal stability. The thermograms of the polymers given in Figure 2.54 show that there is no weight loss up to a temperature of 330 °C and there on the polymers starts decomposing.

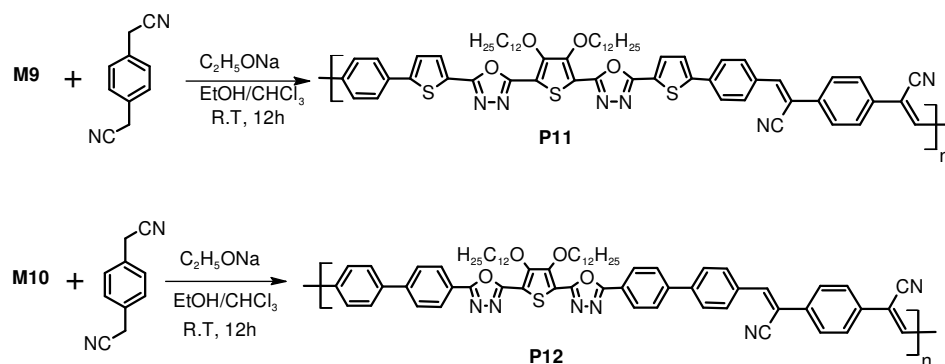
2.4.5 3,4-Didodecyloxythiophene based polymers carrying 1,3,4-oxadiazole and cyanophenylenevinylene segments (**P11** and **P12**)

The D–A conjugated polymers, **P11** and **P12** were synthesized according to the Scheme 2.13. The backbone structure of these polymers is comparable with that of polymers **P9** and **P10**. The dialkylfluorene unit in **P9** and **P10** is replaced with a

cyanophenylenevinylene unit in **P11** and **P12**. The synthetic procedure and the spectral characterization data of these polymers are discussed in the subsequent sections.

2.4.5.1 Synthesis

To prepare D–A conjugated polymers **P11** and **P12**, corresponding dicarbaldehyde monomer (**M9** or **M10**) was condensed with 1,4-phenylene diacetonitrile in presence sodium ethoxide, using Knoevenagel condensation methodology. The polymerization reactions were performed at room temperature under argon atmosphere in ethanol/chloroform solvent system.



Scheme 2.13 Synthesis of polymers **P11** and **P12**

2.4.5.2 Experimental section

Experimental procedure for the synthesis of polymers **P11** and **P12**, and their analytical data are given in the following section.

General procedure for the synthesis of polymers **P11** and **P12**

At room temperature under argon atmosphere, a solution of sodium (20 mg, 0.936 mmol) in 2 ml of anhydrous ethanol was added drop wise to a mixture of monomer **M9** (0.3 g, 0.312 mmol) and 1,4-phenylenediacetonitrile (48 mg, 0.312 mmol) in 5 ml of dry chloroform. The reaction mixture was stirred at ambient temperature for 12 h and was added slowly into 100 ml of methanol. The precipitated yellow solid was washed thoroughly with methanol. The obtained crude polymer **P11** was redissolved in chloroform and precipitated in methanol several times and filtered, and then dried in vacuum oven at 45 °C to obtain polymer as yellow colored powder.

For the synthesis of polymer **P12**, the above procedure is followed starting with monomer **M10**.

Poly[3-(4-(5-(5-(3,4-bis(dodecyloxy)-5-(5-(5-phenylthiophen-2-yl)-1,3,4-oxadiazol-2-yl)thiophen-2-yl)-1,3,4-oxadiazol-2-yl)thiophen-2-yl)phenyl)-2-phenyl acrylonitrile] (P11)

Yield: 70 %. ^1H NMR (400MHz, CDCl_3 , δ): 7.93 – 7.41 (m, 18H, Ar and $-\text{CH}=\text{C}-$), 4.25 (t, 4H, $-\text{OCH}_2-$), 1.83 – 1.17 (m, 40H, $-(\text{CH}_2)_{10}-$), 0.79 (t, 6H, $-\text{CH}_3$). FTIR (cm^{-1}): 2917 and 2848 ($-\text{C}-\text{H}$), 2209 ($-\text{CN}$), 1571 ($-\text{C}=\text{N}-$), 1481, 1452, 1370, 1289, 1023 ($=\text{C}-\text{O}-\text{C}=\text{C}$). Element. anal. calcd. for $\text{C}_{64}\text{H}_{68}\text{N}_6\text{O}_4\text{S}_3$ (%): C 71.08, H 6.34, N 7.78, S 8.88. Found (%): C 71.22, H 6.44, N 7.64, S 8.78. $M_n = 3500$, PD = 1.2.

Poly[3-(4'-(5-(5-(5-(biphenyl-4-yl)-1,3,4-oxadiazol-2-yl)-3,4-is(dodecyloxy) thiophen-2-yl)-1,3,4-oxadiazol-2-yl)biphenyl-4-yl)-2-phenylacrylonitrile] (P12)

Yield: 60 %. ^1H NMR (400MHz, CDCl_3 , δ): 8.29 – 7.63 (m, 22H, Ar and $-\text{CH}=\text{C}-$), 4.37 (t, 4H, $-\text{OCH}_2-$), 1.94 – 1.26 (m, 40H, $-(\text{CH}_2)_{10}-$), 0.89 (t, 6H, $-\text{CH}_3$). FTIR (cm^{-1}): 2918 and 2849 ($-\text{C}-\text{H}$), 2215 ($-\text{CN}$), 1595 ($-\text{C}=\text{N}-$), 1480, 1345, 1370, 1280, 1173, 1044 ($=\text{C}-\text{O}-\text{C}=\text{C}$). Element. anal. calcd. for $\text{C}_{68}\text{H}_{72}\text{N}_6\text{O}_4\text{S}$ (%): C 76.37, H 6.79, N 7.86, S 2.99. Found (%): C 76.48, H 6.72, N 7.78, S 3.04. $M_n = 16300$, PD = 2.8.

2.4.5.3 Structural characterization of polymers **P11** and **P12**

The ^1H NMR and FTIR spectra of both the polymers showed characteristic spectral patterns. The ^1H NMR spectrum of polymer **P12** is shown in Figure 2.55 which displayed aromatic and vinylic protons as a set of multiple peaks in the range δ 8.29 – 7.63. The $-\text{OCH}_2-$ protons of the alkoxy chains of the thiophene ring resonated at δ 4.37 as a triplet. The multiple peaks in the range δ 1.94 – 1.26 were assigned to the protons of alkyl chains attached to thiophene ring. In addition, the absence of absorption peaks due to $>\text{C}=\text{O}$ group in the FTIR spectrum of the polymers further confirms the complete conversion of monomers to the polymers. The FTIR spectrum of polymer **P11** is given in Figure 2.56. Polymer **P11** was partially soluble in THF, whereas polymer **P12** was completely soluble in THF. In case of **P11**, only the molecular weight of the THF soluble fraction was measured. Though these analyses do not give the actual molecular weights of the polymer, the observed molecular

weight confirms the polymeric nature of the obtained product. However, both polymers were completely soluble in organic solvents like DMF, DMSO and chlorobenzene.

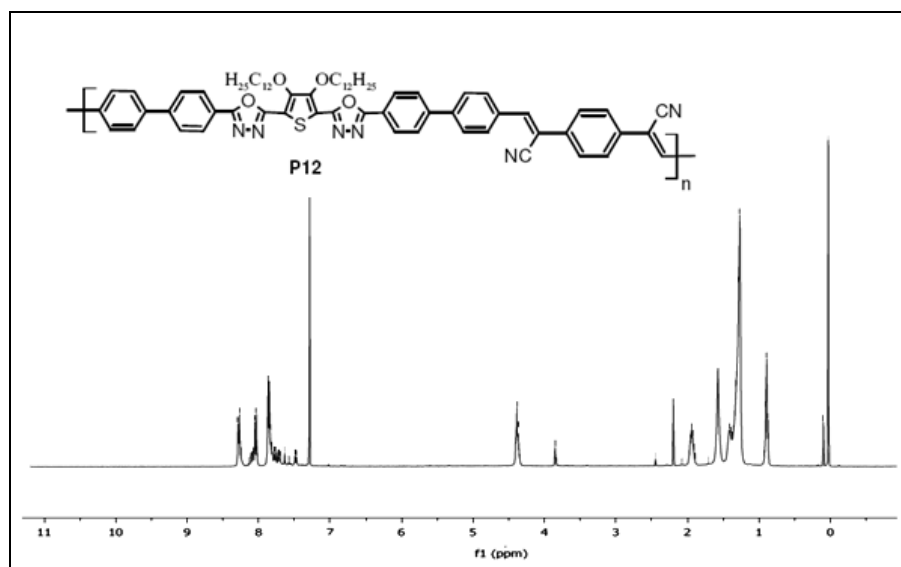


Figure 2.55 ^1H NMR spectrum of polymer **P12**

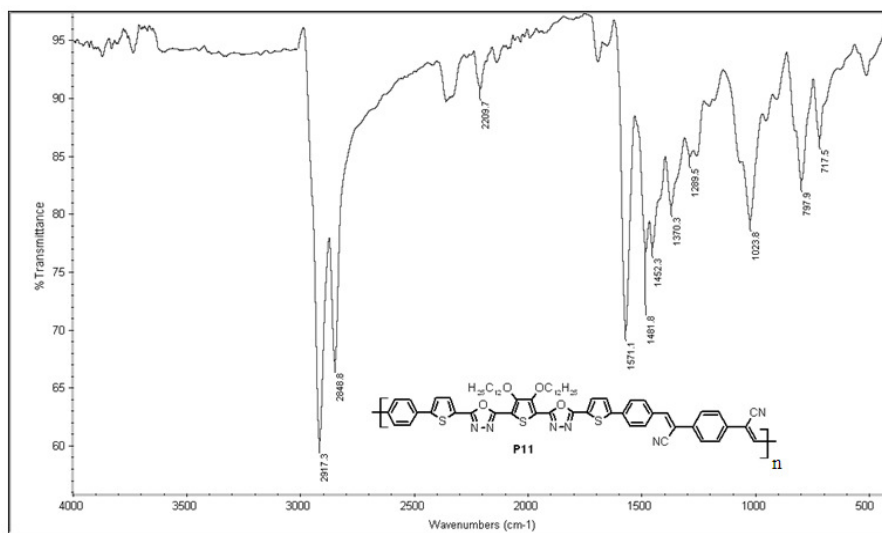


Figure 2.56 FTIR spectrum of polymer **P11**

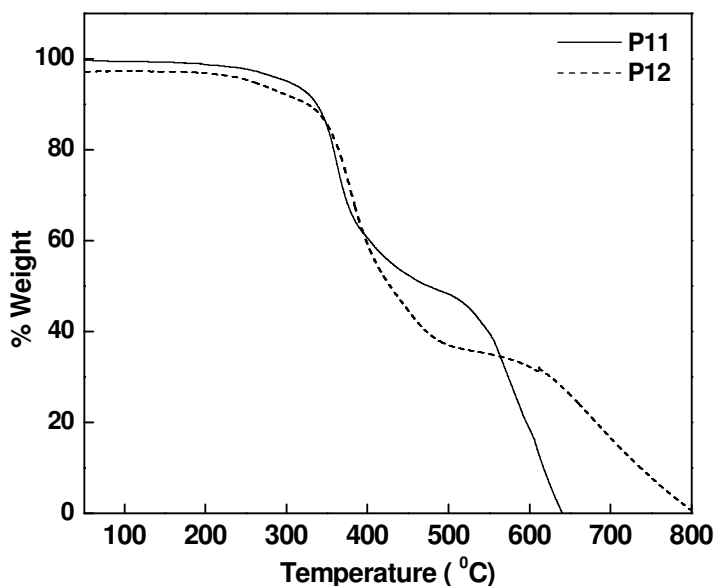


Figure 2.57 Thermogravimetric traces of polymers **P11** and **P12**

The polymers showed good thermal stability under experimental conditions. The thermogravimetric trace of the polymers is shown in Figure 2.57. The onset decomposition temperature of both polymers is approximately 320 °C.

2.5 CONCLUSIONS

In the present work, new 3,4-dialkoxythiophene based monomers viz. 3,4-didodecyloxythiophene-2,5-carboxyhydrazide (**M1**), 3,4-propylenedioxythiophene-2,5-dicarboxylic acid chloride (**M2**), (4,4'-(5,5'-(3,4-bis(dodecyloxy)thiophene-2,5-diyl)bis(1,3,4-oxadiazole-5,2-diyl))bis(4,1-phenylene))bis(methylene)bis(triphenyl phosphonium) bromide (**M4**), 3,4-bis(dodecyloxy)thiophene-2,5-dicarbaldehyde (**M5**), 3,3'-(3,4-bis(dodecyloxy)thiophene-2,5-diyl)bis(2-(thiophen-2-yl)acrylonitrile) (**M6**), 3,3'-(3,4-bis(dodecyloxy)thiophene-2,5-diyl)bis(2-(5-formylthiophen-2-yl)acrylonitrile) (**M7**), 4,4'-(5,5'-(5,5'-(3,4-bis(dodecyloxy)thiophene-2,5-diyl)bis(1,3,4-oxadiazole-5,2-diyl))bis(thiophene-5,2-diyl))dibenzaldehyde (**M9**) and 4',4''-(5,5'-(3,4-bis(dodecyloxy)thiophene-2,5-diyl)bis(1,3,4-oxadiazole-5,2-diyl)) dibiphenyl-4-carbaldehyde (**M10**) were synthesized starting from thiodiglycolic acid with well established synthetic protocol. The diacid chloride monomers **M2** and **M3** were prepared from their respective dicarboxylic acids by refluxing with SOCl_2 . The fluorene Wittig salt monomer **M8** was prepared starting from fluorene. All the

monomers and their intermediate compounds were obtained with good yield. The chemical structure of all the newly synthesized monomers and their intermediate compounds were well characterized with the support of ^1H NMR and FTIR spectroscopic methods and by elemental analyses. Further, the synthesized monomers were used to prepare five new series of D–A conjugated polymers (**P1–P12**) and their synthetic methods were established. The chemical structures and molecular formula of the polymers were evidenced by spectral and elemental analyses techniques, respectively.

To prepare 3,4-didodecyloxythiophene based polymers carrying 1,3,4-oxadiazole and phenyl or 3,4-propylenedioxythiophene segments **P1** and **P2**, polycondensation reaction was employed. The well known Wittig reaction was performed to synthesis 3,4-didodecyloxythiophene based polymers carrying 1,3,4-oxadiazole, phenylenevinylene and thienylenevinylene segments **P3** and **P4**. The 3,4-didodecyloxythiophene based polymer **P5** carrying cyanovinylene moiety was prepared from its monomer **M6** via chemical polymerization method. The 3,4-didodecyloxythiophene based polymer **P7** carrying cyanophenylenevinylene unit in its backbone was synthesized via Knoevenagel polycondensation technique. Other two cyanovinylene based polymers, **P6** which contains fluorenevinylene unit and **P8** which contains 1,3,4-oxadiazole and cyanophenylenevinylene units were prepared using Wittig condensation method. The fluorenevinylene based polymers **P9** and **P10** were synthesized via Wittig condensation method. Polymers **P11** and **P12** carrying cyanophenylenevinylene units along their backbone were prepared using Knoevenagel polycondensation method. All the polymers showed good solubility in common organic solvents due to the presence of long alkoxy pendants at the 3- and 4-positions of the thiophene ring. The gel permeation chromatography was used to estimate the molecular weight of the polymers and the number average molecular weight was found to be in the range of 3500 – 18930. Thermogravimetric analysis revealed that all the polymers are thermally stable up to around 300 °C.

CHAPTER 3

STUDY OF LINEAR OPTICAL AND ELECTROCHEMICAL PROPERTIES OF THE POLYMERS

Abstract

In this chapter, the studies of linear optical and electrochemical properties of the D–A conjugated polymers (P1–P12) have been discussed. To study the linear optical properties of the polymers, UV-Visible absorption and fluorescence emission spectroscopic techniques have been utilized. The electrochemical redox behavior of the polymers was investigated by cyclic voltammetry. Further, the HOMO and the LUMO energy levels of the polymers are determined from their electrochemical data and the results obtained are correlated with the chemical structure of the polymers.

3.1 INTRODUCTION

It is known that in a small molecule containing an isolated double bond, a π -electron can be promoted from the HOMO to the LUMO by the absorption of a photon with energy greater than the band gap, E_g , between two frontier orbitals. In comparison, a similar molecule containing conjugated double bonds will have a higher HOMO energy and a lower LUMO energy. Since the orbital interactions results in a decreased energy gap in such systems, a lower energy photon can promote a π -electron from the HOMO to the LUMO. However, in polymers consisting of similar repeating units that are conjugated each other, the energy band gap, E_g , can be even smaller. Figure 3.1 shows the schematic representation of the interaction between the molecular orbitals in a conjugated polymer which leads to a band structure. The mixing of the HOMOs produces a broadened, electron filled band, analogous to the valence band of a semiconductor. Similarly, mixing of the LUMOs produces a broadened, empty band, analogous to the conduction band of a semiconductor. As a consequence of these orbital interactions, π -conjugated polymers are expected to exhibit semiconducting properties. Further, the electronic structure of the conjugated polymers is not only important in the description of the electrical properties, but it also determines their optical properties. Because the band gap of the conjugated polymers lies between 1 and 3 eV, the materials can therefore absorb light in UV and visible region.

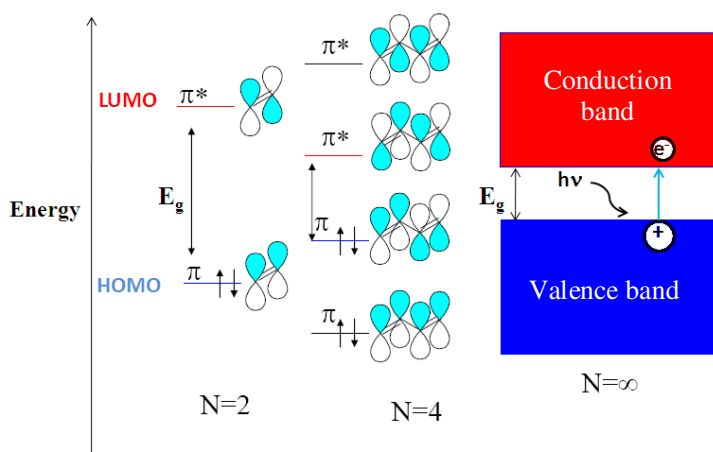


Figure 3.1 Schematic representations of the interaction of HOMO and LUMO energy levels in a conjugated system

In order to absorb light, the energy of the photons must be equal to the band gap energy. Upon absorption of light, the energy of the electronic system increases. This phenomenon can be regarded in a first approximation as the promotion of an electron from an occupied to a higher empty energy state. The transition to the first excited state thus corresponds to the HOMO to the LUMO transition. The resulting hole in HOMO and electron in LUMO represents an electron-hole pair, which is also called exciton. Since the excited electron that is created by the absorption is out of balance with their environment, it returns back or relaxes to its ground state. Relaxation of the electron results in either emitting the energy as radiation or through non-radiative processes. The energy of the emitted light is always lower than the absorbed light energy because some of the energy is lost in vibrational relaxations. In addition, there are many photophysical processes that can occur in electronic excited states, and these can be illustrated in a state energy diagram which is given in Figure 3.2.

The molecule relaxes down from the electronic excited state to the electronic ground state in several steps. First, the molecule relaxes down to the ground state of the electronic excited level via vibration (vibrational relaxation), that is via the dissipation of heat. Second, the molecule relaxes down from the vibrational ground state of the electronic excited level to the electronic ground level through non-radiative or radiative processes.

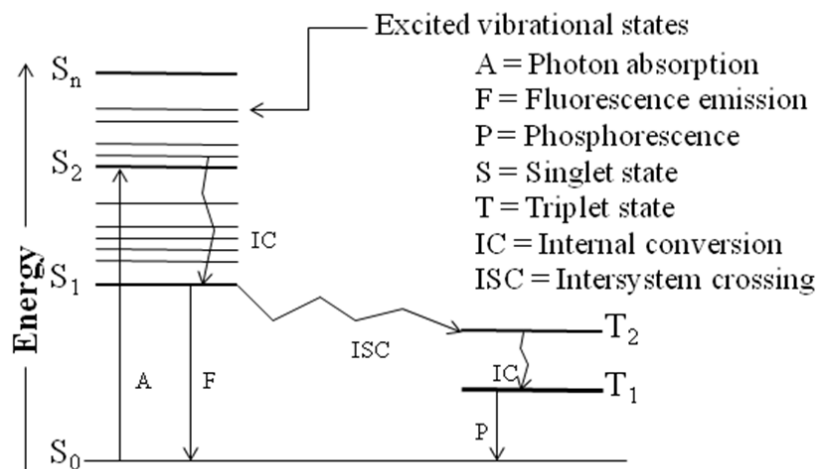


Figure 3.2 State energy diagram of some possible photophysical processes in an organic molecule

The non-radiative process is also known as quenching process, where the molecule relaxes to the ground state by converting the excitation energy into heat (no light emission occur). While in the radiative emission or luminescence the molecule emits light with longer wavelength than the absorbed photons. This luminescence can be classified into two categories, fluorescence and phosphorescence, depending on the spins of the electrons involved in the radiative transition, as illustrated in Figure 3.2.

If the excited electron has the same spin as the corresponding ground state orbital, the emission of light is called fluorescence. Further, phosphorescence involves an electronic transition from triplet excited state (with unpaired electron spins) to a singlet ground state (with paired electron pairs). Since this transition is formally forbidden by quantum-mechanical selection rules, it occurs at a much slower rate than fluorescence, which involves an allowed transition between a singlet excited state to a singlet ground state (Lakowicz 1999).

Luminescence is one of the most useful electronic processes in conjugated polymers. Quantitative analysis of the emission efficiency of the polymer is characterized by its quantum yield of luminescence (Φ_{PL}). The Φ_{PL} is the ratio of the number of photons emitted to the number of photons absorbed, as shown in equation 3.1.

$$\Phi_{PL} = \frac{\text{Photons}_{EM}}{\text{Photons}_{ABS}} \dots\dots\dots (3.1)$$

According to the law of conservation of energy, the maximum Φ_{PL} must be 1. The value of Φ_{PL} is related to the rates of radiative (τ_r) and non-radiative (τ_{nr}) decays, as described in equation 3.2 (Klessinger and Michl 1995, Lakowitz 1999).

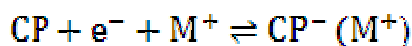
$$\Phi_{PL} = \frac{\tau_r}{\tau_r + \tau_{nr}} \dots\dots\dots (3.2)$$

As τ_{nr} approaches to zero, the quantum yield of luminescence approaches unity. Generally, Φ_{PL} is highest in dilute solutions, where the emitting species are isolated from each other. In most cases, increase in concentration of the polymer in solution decreases the quantum yield of luminescence due to concentration quenching in solid state.

The electrochemical studies of the conjugated polymers are important to understand their basic electronic structures. A unique characteristic of the electrochemical properties of the conjugated polymers is that p-doping/dedoping (oxidation or de-oxidation) reactions takes place at a higher (positive) potential range and the n-doping/dedoping (reduction or de-reduction) reactions occur at a lower (negative) potential range. The conductivity of the polymers increases by ~5 – 10 orders of magnitude upon doping. When p-doping takes place, the conjugated polymer chains are oxidized by removing electrons and counter anions are doped into the oxidized chains to maintain electroneutrality, as depicted below.



Where CP represents the conjugated polymer and $CP^+(A^-)$ represents the oxidized conjugated polymer molecules doped with counter anions of A^- . When the n-doping reaction occurs, the conjugated polymer chains are reduced by injecting electrons to the chains. Counter cations are doped into the reduced polymer to obtain electroneutrality, as depicted below.



Further, the applications of conjugated polymers, such as electrode materials in batteries, modified electrodes, enzyme electrodes, electrochromics, electrocatalysis and electrochemical sensors are based on the electrochemical properties of the polymers. In addition, electrochemical methods are used to convert monomers into the corresponding polymers.

3.2 LINEAR OPTICAL PROPERTIES

The basic electronic structure of the conjugated polymers can be evaluated by investigating their photophysical processes that occur in the electronic excited states. In the present study, UV-Vis absorption and fluorescence emission spectroscopic techniques were used to study the linear optical properties of the polymers. The UV-Vis absorption spectroscopy deals with absorption of sufficiently energetic photon ($h\nu$) in the UV-Vis region by the polymer and measures the electronic transition from ground state to the excited state.

Generally, the observed transitions in absorption spectroscopy of conjugated polymers are attributed to electronic transition from π - π^* states. Whereas, the fluorescence emission spectroscopy deals with the transitions from the excited state to the ground state, as electronic transition from π^* - π states. The measured data in linear optical studies of the polymers are essential and one can evaluate the optical band gap and fluorescence quantum yield of the polymers. These results are very useful in selecting such polymers for device applications such as PLEDs and PSCs.

3.2.1 Materials and instruments

The UV-Vis absorption spectra were measured using a CINTRA-101 (GBC scientific equipment) spectrophotometer. Fluorescence emission spectra were recorded using a JASCO FP-6200 spectrofluorometer. The dilute solutions of the polymers (**P1–P12**) were prepared using chloroform as the solvent. The polymer films were prepared using an ACE-1020 (Dong Ah Trade & Tech. Corp.) spin coating unit. Smooth and optically clear thin solid films on glass substrates were obtained by spin-coating the chloroform solutions of the polymer (1 mg mL^{-1}) at a spin rate of 1500 rpm. The fluorescence quantum yields (ϕ_{fl}) of the polymers in chloroform solution were estimated by comparing with the standard of quinine sulfate as reported

in the literature (Joshi et al. 1999). The structures of the newly synthesized conjugated polymers (P1–P12) are given in Figure 3.3.

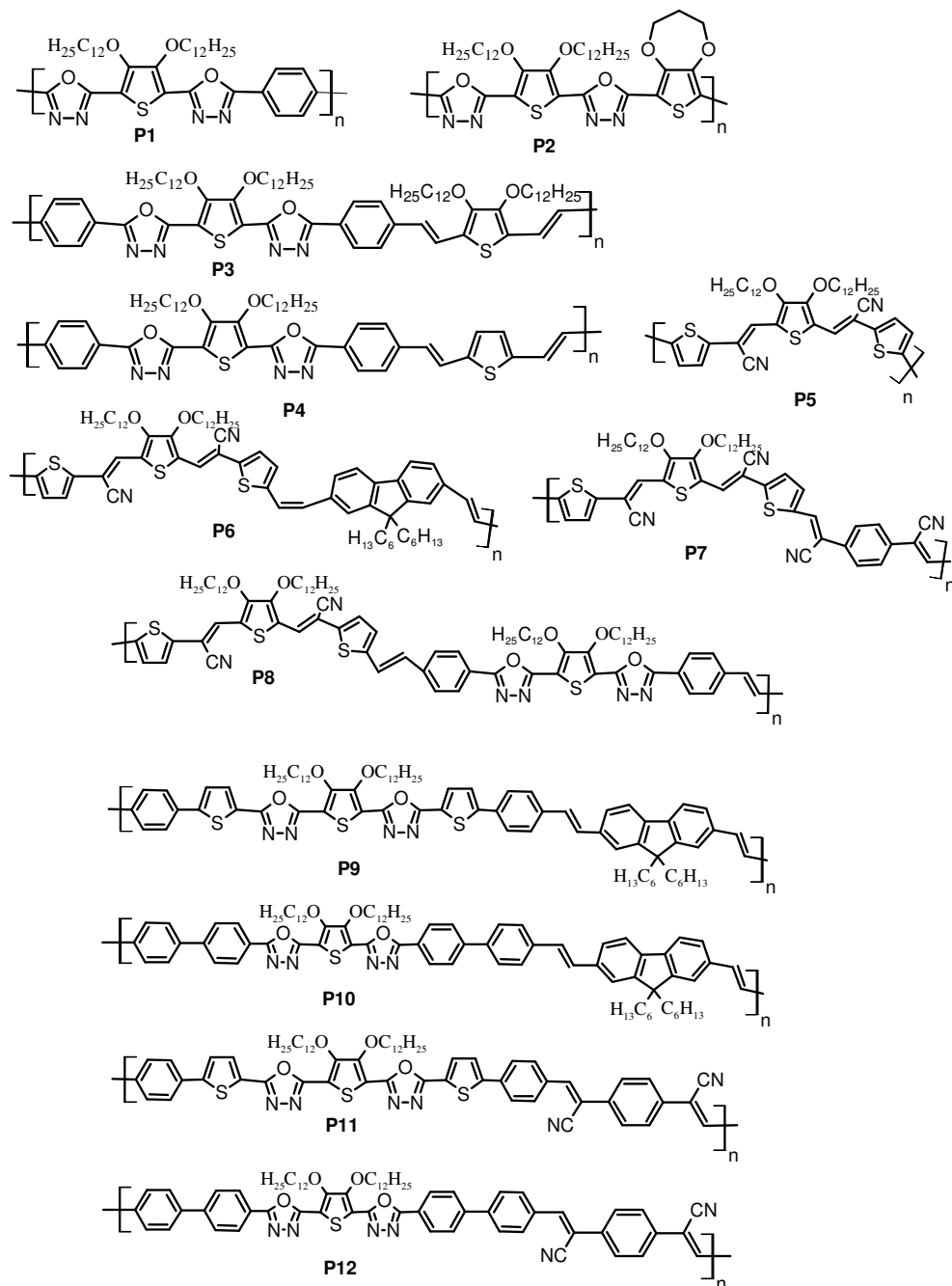


Figure 3.3 Structures of newly synthesized polymers (P1–P12)

In the following section, the UV-Vis absorption and fluorescence emission characteristics of these polymers have been discussed.

3.2.2 Results and discussion

The UV-Vis absorption and the fluorescence emission data of all the polymers are summarized in Table 3.1. The normalized UV-Vis absorption spectra of polymers **P1** and **P2** in dilute chloroform solution (10^{-4} g/ml) and in the film state are given in Figure 3.4. The polymer solutions of **P1** and **P2** showed absorption maxima at 378 and 418 nm respectively, which corresponds to the π - π^* transition in the polymer. The absorption maximum of **P2** in solution state showed a red shift of about 40 nm in comparison with that of **P1**. This red shift can be explained in terms of strong intramolecular charge transfer (ICT) interaction between strong electron donating 3,4-propylenedioxythiophene and electron accepting 1,3,4-oxadiazole units in the polymer chain (Yu et al. 1995, Janekhe et al. 2000 and Campos et al. 2005). The polymer films displayed absorption peaks at 394 and 430 nm respectively for **P1** and **P2**. The absorption spectrum of **P1** in film state was broadened and the absorption maximum is red shifted by about 16 nm as compared to its spectrum in the solution state. A similar red shift in the absorption maximum was observed also for **P2** in the film state. The observed red shift and broadening in the absorption spectra could be attributed to increased extent of the π -stacking in the film state as well as to the increased polarizability of the polymer film (Shang et al. 2007 and Surin et al. 2007). The optical band gaps (E_g^{opt}), defined by the onset absorption (λ_{onset}) of the polymer in the film state are 2.28 eV for **P1** and 2.3 eV for **P2** and it was calculated using the equation $E_g^{\text{opt}} = hc/\lambda_{\text{onset}}$, where h is Planck's constant and c is the velocity of light.

The normalized fluorescence emission spectra of **P1** and **P2** in dilute chloroform solution (10^{-4} g/ml) and in thin film state are given in Figure 3.5. The emission maxima of **P1** and **P2** were observed at 506 and 481 nm, which corresponds to bluish green and blue light respectively. The emission maxima of **P1** and **P2** in the film state exhibited slight red shifts of about 10 and 19 nm respectively in comparison with those of their solutions. This red shift can be attributed to the interchain or/and intrachain mobility of the excitons and excimers generated in the polymer solid state (Harrison et al. 1996). The polymers emitted green (**P1**) and bluish green (**P2**) light in

their film state. Based on the absorption maxima of the polymers, polymer **P2** was expected to show a red shift in the emission maxima as compared to that of polymer **P1**. However a blue shift was observed in the emission maxima of **P2** as compared to that of **P1**. These results suggests that the polymer backbone in the excited state is more planar in **P1** than that in polymer **P2** leading to the bathochromic shift in its emission (Karastatiris et al. 2004). The fluorescence quantum yield (ϕ_f) of the polymers in solution were calculated by comparing with the standard of quinine sulfate (ca. 1×10^{-5} M solution in 0.1 M H_2SO_4 having ϕ_f of 55 %). The quantum yield of **P1** and **P2** were found to be 35 and 32 % respectively.

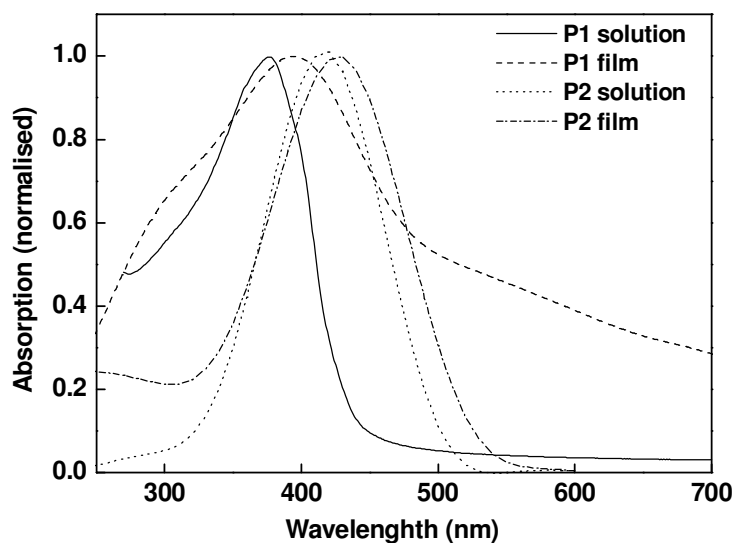


Figure 3.4 UV-Vis absorption spectra of **P1** and **P2**

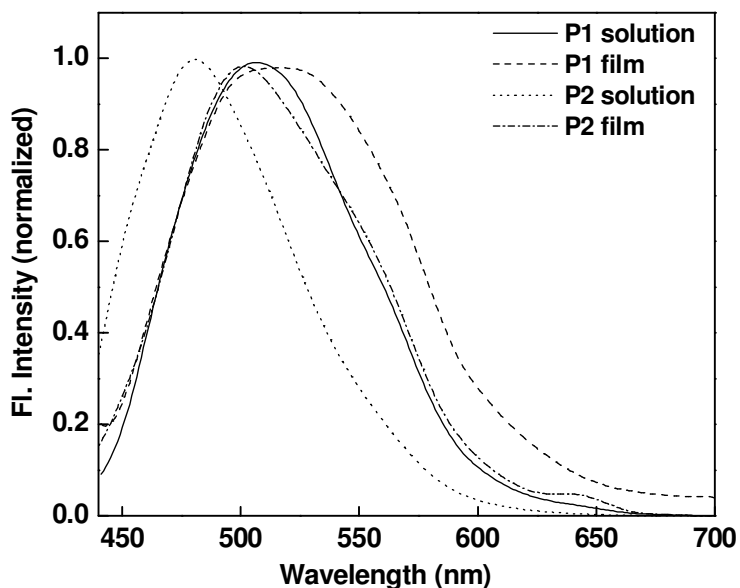


Figure 3.5 Fluorescence emission spectra of **P1** and **P2**

The normalized absorption spectra of polymers **P3** and **P4** in dilute CHCl_3 solution and in thin film state are given in Figure 3.6. Polymer **P3** in solution displayed an absorption maximum at 395 nm, which is due to the π - π^* transition. The polymer film displayed a similar absorption spectrum with no significant shift in the absorption maximum. The observed result could be attributed to the larger interchain distance imposed by the dodecyl chains attached to two thiophene moieties in the polymer backbone which decreases the π -stacking interactions in the solid state (Colladet et al. 2007). The absorption spectrum of **P4** in solution state displayed an optical absorption maximum at 395 nm while in the solid state the π - π^* transitions showed a red shift of about 21 nm with a shoulder in the shorter wavelength region at 368 nm. The red shift in the absorption maximum of **P4** in the film state could be due to the π -stacking effect. Unlike in **P3**, the repeating unit in **P4** contains pendant alkoxy groups only on one of the thiophene rings resulting in lesser interchain distance in **P4** as compared to that in **P3**. Hence π -stacking interactions could be operative in **P4** in the solid state. The optical band gaps of **P3** and **P4** were determined in the film state and were found to be 2.29 and 2.25 eV, respectively. The normalized fluorescence emission spectra of polymers **P3** and **P4** in dilute solution and thin film state are given in Figure 3.7. The emission maxima for **P3** and **P4** in solution were

observed at 547 and 554 nm respectively. In comparison with their solution state, the emission maxima of the polymer thin films showed bathochromic shifts of about 18 and 15 nm respectively for **P3** and **P4**. The polymers emit greenish yellow light in their film state. The fluorescence quantum yields (ϕ_f) of the polymers in chloroform solution are in the range of 40 – 42 %.

Table 3.1 UV-Vis absorption and fluorescence emission spectral data of the polymers

Polymer	λ_{\max}^a (nm)	λ_{\max}^b (nm)	λ_{em}^a (nm)	λ_{em}^b (nm)	E_g^{opt} (eV)	ϕ_f (%)
P1	378	394	506	516	2.28	35
P2	418	430	481	500	2.3	32
P3	395	395	547	565	2.29	40
P4	395	416	554	569	2.25	42
P5	550	550	657	-	1.75	38
P6	548	550	655	-	1.77	42
P7	520	536	590	-	1.70	38
P8	527	540	623	-	1.71	40
P9	427	443	506	513	2.42	40
P10	388	398	457	490	2.63	42
P11	411	458	536	542	2.3	35
P12	360	386	440	514	2.47	38

^a Measured in CHCl₃ solution ^b Cast from CHCl₃ solution on glass substrates

E_g^{opt} Optical band gap calculated from onset absorption edge of the polymer film

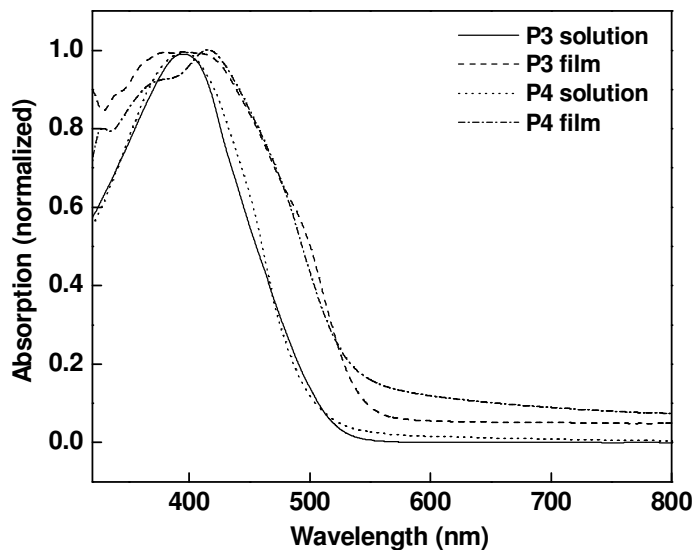


Figure 3.6 UV-Vis absorption spectra of **P3** and **P4**

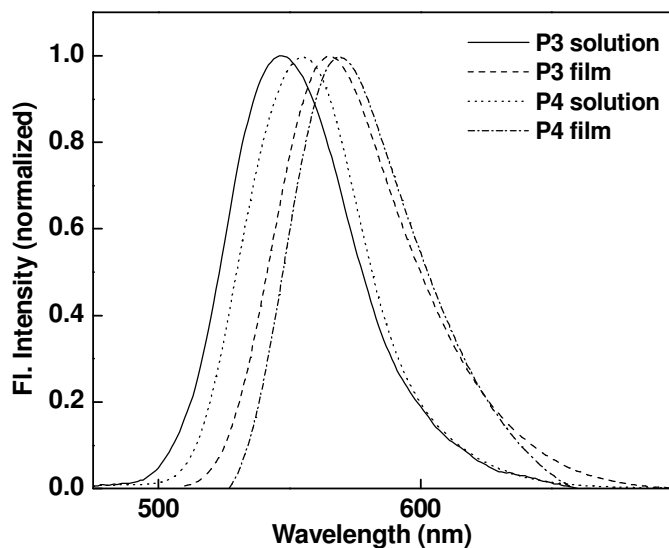


Figure 3.7 Fluorescence emission spectra of **P3** and **P4**

The normalized absorption spectra of polymers **P5–P8** in dilute chloroform solution and in thin film state are given in Figures 3.8 and 3.9 respectively. The absorption maxima of **P5**, **P6**, **P7** and **P8** in solution state were 550, 548, 520 and 527 nm respectively. In addition, the absorption spectrum of **P6** and **P8** showed peaks in the shorter wavelength region at 351 and 361 nm respectively. The observed

absorption maxima of the polymers in the longer wavelength region are due to the effective conjugation length with an efficient ICT through D–A units in the polymers. The incorporation of strong electron donating 3,4-didodecyloxythiophene and electron accepting cyanovinylene units in the polymer backbone resulted in an enhanced ICT between donor and acceptor segments, causing an effective electronic delocalization along the polymer backbone. This further improves the effective conjugation length and leads to an extension of absorption (Wu et al. 2009). Further the presence of strong electron withdrawing cyanovinylene group in these polymers extends the absorption to longer wavelength region. However, the observed variation in the absorption maxima of the polymers **P6–P8** is due to the difference in the chemical structures of the polymer chains. The absorption maximum of **P6** was red shifted in comparison with those of **P7** and **P8**. This can be understood in terms of more planar backbone and the increased conjugation along the polymer backbone by the introduction of electron donating fluorenevinyene unit in **P6**.

Polymer **P5** in the film state showed an absorption maximum at a same wavelength as that of its solution state, but with a red shift of about 68 nm in the onset absorption edge in the film state. In addition, the spectrum of the polymer film showed a peak in the shorter wavelength region at 390 nm and a shoulder at 661 nm. The absorption spectrum of **P6** in thin film state is almost identical to that of its solution state, with no prominent shift in the absorption maximum. The observed behavior could be attributed to the presence of alkyl chains on the fluorene unit which reduces the intermolecular interaction and thus lead to poorer π -stacking in the film state (Rodrigues et al. 2010). The absorption spectra of **P7** and **P8** in the film state displayed a red shift and broadening in the absorption maxima as compared to those of their solutions. The observed red shift for **P7** and **P8** films were about 16 and 13 nm respectively which could be due to the π -stacking effect in the film state. The optical band gaps, defined by the onset absorption of the polymers in the film state were 1.75, 1.77, 1.70 and 1.71 eV, respectively for **P5–P8**. Hence these polymers, with low band gaps as well as broad absorption bands, could be promising candidates for high efficiency polymer solar cells. The polymers, as expected from the donor-acceptor arrangement along the polymers backbone, show narrow band gap energies.

The band gap of the polymers are lower than those of some important conjugated polymers reported in the literature like thiophene based polymers containing 2,1,3-benzothiadiazole segments (Anant et al. 2011), bis(1-cyano-2-thienylvinylene) phenylene based donor-acceptor type polymers (Colladet et al. 2007), fluorene and thiophene based polymer (Lim et al. 2003), PFV (Jin et al. 2002) and some fluorene based conjugated polymers containing oxadiazole pendants (Sung and Lin 2004), which showed improved device efficiencies in PLEDs and PSCs.

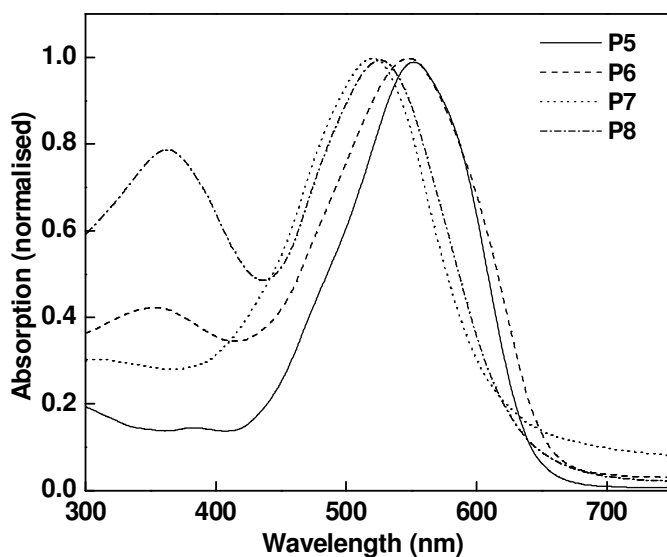


Figure 3.8 UV-Vis absorption spectra of **P5–P8** in solution

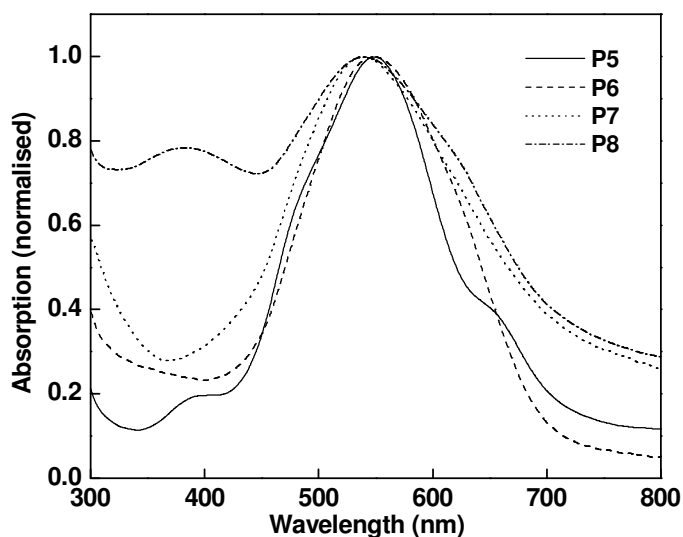


Figure 3.9 UV-Vis absorption spectra of **P5–P8** in thin film

The fluorescence emission spectra of **P5–P8** in dilute solution are given in Figure 3.10. The polymers in solution emit yellowish orange to red light with broad emission spectra. Polymer **P5** showed an emission peak is at 657 nm, whereas polymers **P6–P8** showed emission peaks at 655, 590 and 623 nm respectively. The fluorescence emission spectra of the polymers in the film state were not measured because the wavelengths of the emission maxima were beyond the detection range of our instrument. The fluorescence quantum yields (ϕ_{fl}) of the polymers in chloroform solution were found to be 38 – 42 %. The photophysical data suggest that the polymers have low band gaps with broad absorption bands as well as are highly fluorescent with reasonably good fluorescence quantum yields. Hence these polymers could be promising candidates for the fabrication of polymer based optoelectronic devices such as PLEDs and PSCs.

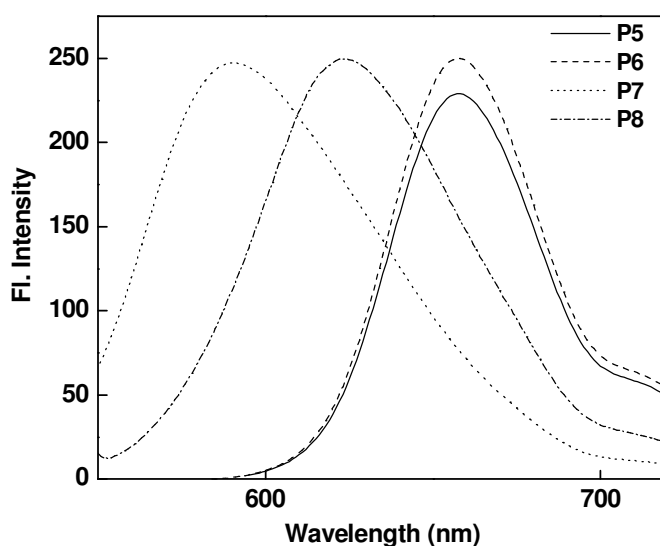


Figure 3.10 Fluorescence emission spectra of **P5–P8** in solution

The normalized UV-Vis absorption spectra of **P9** and **P10** in dilute chloroform solution and in thin film state are given in Figure 3.11. The absorption maxima of polymers in solution state were observed at 427 and 388 nm respectively for **P9** and **P10**, which are attributed to the π - π^* transition in the polymer. The polymers in the film state showed red shifts of about 16 and 10 nm respectively for **P9** and **P10** due to the π -stacking effect in the film state. It was observed that **P9** exhibited red shifts of

about 39 and 45 nm in the absorption maxima in solution and film state respectively as compared to those of **P10**. The observed behavior is a result of the strong electron releasing effect of the conjugative spacer thiophene unit attached to 1,3,4-oxadiazole ring in **P9** (as compared to the spacer phenyl ring in **P10**), which improves the ICT between the donor and the acceptor units. The optical band gaps, defined by the onset absorption in the film state were 2.42 and 2.63 eV, respectively for **P9** and **P10**. The thin films of **P9** and **P10** emit green and bluish green light respectively under the irradiation of UV light. The fluorescence emission maxima of polymer solutions were observed at 506 and 457 nm respectively for **P9** and **P10** (Figure 3.12). In the film state, bathchromic shifts of about 7 and 33 nm were observed for **P9** and **P10**, respectively. The fluorescence quantum yield of the polymers in chloroform solution was in the range 40 – 42 %.

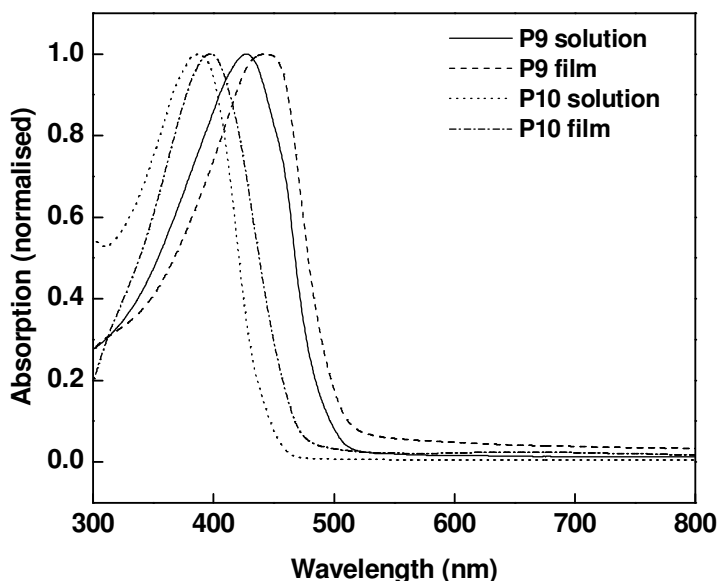


Figure 3.11 UV-Vis absorption spectra of **P9** and **P10**

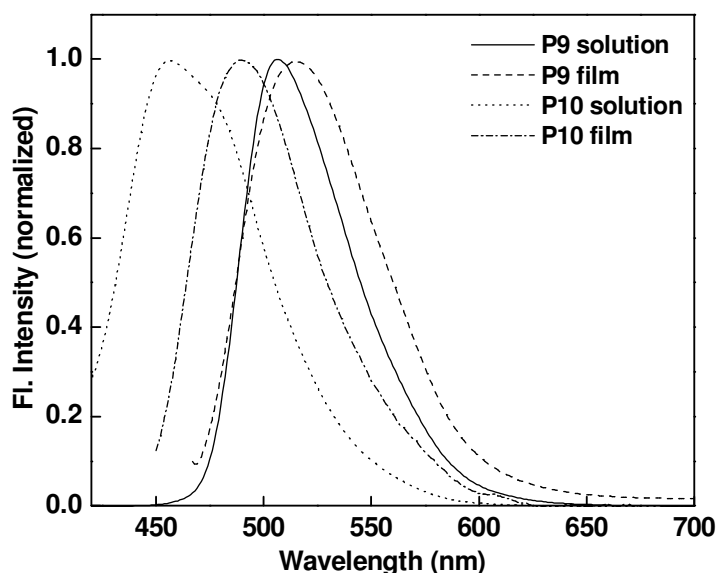


Figure 3.12 Fluorescence emission spectra of **P9** and **P10**

The normalized absorption spectra of **P11** and **P12** are shown in Figure 3.13. The absorption maxima of the polymers in solution were observed at 411 nm for **P11** and at 360 nm for **P12** which are due to π - π^* transition in the polymer. The polymer films showed a red shift in the absorption maximum in comparison with those of their solutions. A red shift of about 47 nm with broad absorption spectrum was observed for **P11** thin film whereas **P12** thin film showed a red shift of about 26 nm, which are attributed to the π -stacking effect in the solid state. However, the absorption maxima of **P11** in solution and film state were red shifted about 51 and 72 nm respectively as compared with those of **P12**. This is due to the electron releasing effect of the thiophene moiety attached to 1,3,4-oxadiazole ring in **P11**, which resulted in the extended conjugation along the polymer backbone. The optical band gaps of the polymers in thin film state were calculated from their onset absorption edge and were found to be 2.3 and 2.47 eV respectively for **P11** and **P12**.

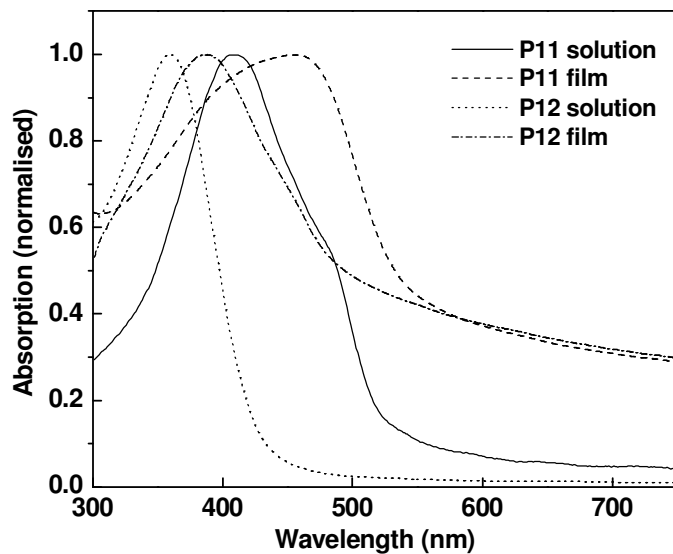


Figure 3.13 UV-Vis absorption spectra of **P11** and **P12**

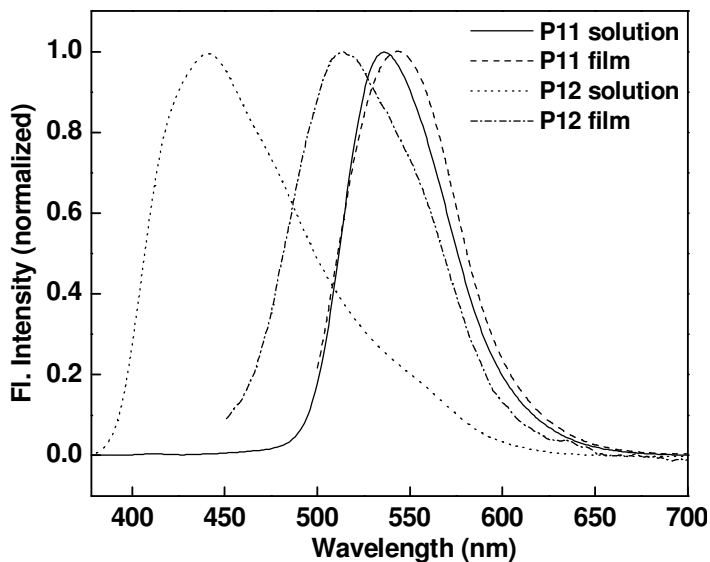


Figure 3.14 Fluorescence emission spectra of **P11** and **P12**

The fluorescence emission spectra of **P11** and **P12** are given in Figure 3.14. The polymers in solution state displayed emission peaks at 536 and 430 nm respectively for **P11** and **P12**. The solid state emission maxima of the polymers were red shifted about 6 and 74 nm respectively for **P11** and **P12**, from the corresponding emission maxima in solution. The polymer films emit green light under the irradiation of UV light. The quantum yield of the polymers in solution is found to be 35 % for **P11** and

38 % for **P12**. Photographs of polymer solutions (**P1–P12**) under day light are given in Figure 3.15.



Figure 3.15 Photographs of polymer solutions (**P1–P12**) under day light

The presence of biphenyl ring along the polymer backbone was found to affect the photophysical properties of the polymers. The 2-phenylthiophene unit in **P9** was replaced by a biphenyl ring in **P10**. A similar structural change was also made between polymers **P11** and **P12**. It is well known that the ground state geometry of the biphenyl molecule has the two phenyl rings bent $\sim 43^\circ$ out of the plane. This lack of planarity causes a significant conjugation break within the backbone of the polymer. So placing biphenyl conjugative spacers within the backbone of polymers **P10** and **P12** causes a drop off in further conjugation enhancement. Lower the conjugation length, higher is the energy required for $\pi\text{-}\pi^*$ transition. As a result, **P10** absorbs light of lower wavelength than that absorbed by **P9**. Similarly, the absorption maximum of **P12** was blue shifted compared to that of **P11**. The nonplanarity caused by the introduction of biphenyl units also affects the band gap energy of the polymers. As a result, **P10** showed higher band gap energy as compared to that of **P9**. A similar trend was also observed between polymers **P11** and **P12**. In addition, the twisted structure of the biphenyl unit not only decreases the effective conjugation length of the polymer, but also limits the interchain interactions, enhancing its fluorescence quantum efficiencies. Because of this effect, **P10** and **P12** showed slightly higher fluorescence quantum yields when compared to those of **P9** and **P11** respectively.

3.3 ELECTROCHEMICAL PROPERTIES

Cyclic voltammetry (CV) is one of important method to determine the electrochemical properties of conjugated polymers. Also CV is the widely used technique to estimate the HOMO and LUMO energy levels of the conjugated polymers, because the onset oxidation and reduction potentials obtained from the cyclic voltammograms correspond to the HOMO and LUMO energy levels, respectively (Li et al. 1999). The typical cyclic voltammetric experimental set up is as shown in Figure 3.16.

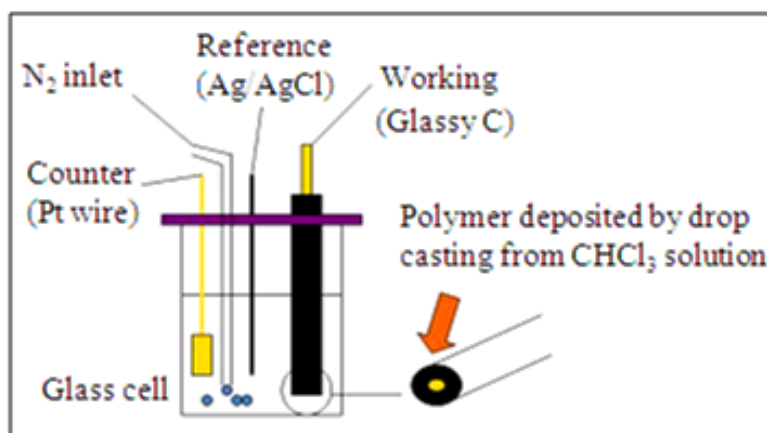


Figure 3.16 Typical cyclic voltammetric experimental set up

As shown in the set up, the electrochemical experiment uses a three-electrode cell consisting of polymer coated on a metal electrode immersed in an electrolyte, a reference electrode and a counter electrode. The three electrodes are connected to a potentiostat, whose function is to supply a current, which is regulated in such a way that the voltage between the working and the reference electrodes remains at a chosen value. Electrons can be exchanged between the polymer and the metal. The exchange proceeds across the polymer-metal interface. In addition, to maintain electroneutrality in the polymer bulk, ions are exchanged between polymer and the electrolyte, across the polymer-electrolyte interface. In case of p-doping, which corresponds to oxidation of the polymer, electrons are transferred from polymer to metal.

In case of n-doping, electrons are transferred from metal to polymer, which is reduction of the polymer. Electron transfer proceeds if the fermi level of the metal is

situated below the level of the polymer valence band (oxidation) or above the conduction band (reduction). The potentiostat enables to shift the electronic levels of the polymer with respect to fermi level of the metal, just by varying the voltage. The current recorded during a linear scan of voltage is the cyclic voltammogram, which gives the information of the redox processes in the polymer. When the polymer is in its insulating state, no current passes between the working and counter electrodes. Additionally, calculation of HOMO and LUMO energy levels are important to predict the charge carrying properties of a conjugated polymer when they are used in optoelectronic devices.

Further, cyclic voltammetric response of a functionalized conjugated polymer is usually very informative. By cyclic voltammetric data, one can get an idea to design a conjugated polymer with desired HOMO and LUMO levels, by the appropriate selection of donor and/or acceptor segments in the polymer structure, for various device applications. In the present study, the redox properties of five new series of thiophene based D–A conjugated polymers **P1–P12** (Figure 3.3) were investigated by cyclic voltammetric studies. The onset oxidation and reduction potentials of the polymers were used to calculate their HOMO and LUMO energy levels and also the electrochemical band gap of the polymers. In the following section the detailed experimental protocols of the electrochemical studies along with results and discussion have been presented.

3.3.1 Materials and instruments

Chloroform and acetonitrile were purchased commercially and they were dried over calcium hydride (CaH_2) and used. Tetrabutylammonium perchlorate (TBAPC) was purchased from Lancaster Company (UK). Polymer thin films were obtained by dissolving the polymer in chloroform and drying it over the glassy carbon disk for electrochemical studies. The electrochemical studies of the polymer were carried out using an AUTOLAB PGSTAT 30 electrochemical analyzer. Cyclic voltammograms were recorded using a three-electrode cell system, with a glassy carbon disk as working electrode, a Pt wire as counter electrode and an Ag/AgCl electrode as the reference electrode. The measurements were carried out at a scan rate of 50 mV/s at room temperature. All measurements were calibrated with the ferrocene/ferrocenium

(Fc/Fc⁺) standard ($E_{\text{FOC}} = 0.53$ vs. Ag/AgCl) according to the literature report (Chen et al. 2002).

The electrochemical measurements were performed in an oxygen and water free environment. Experiments were done in a nitrogen purged glass cell considering the fact that some of the polymers are not stable in the reduced form. Since the cycling over the full potential range resulted in rapid degradation, the oxidation and reduction processes were carried out separately. The redox properties of the polymers were investigated by sweeping them cathodically and anodically in the potential range of 0 – -2 V and 0 – +2 V, respectively. The observed onset oxidation and reduction potentials were used to calculate HOMO and LUMO energy levels and band gap of the polymers.

3.3.2 Results and discussion

In order to study the electrochemical behavior of the polymer, all the polymers were subjected to anodic and cathodic scan cycles using cyclic voltammetric sweep. The cyclic voltammograms of **P1** and **P2** are as shown in Figure 3.17. The polymers showed both n- doping and p- doping processes. On sweeping cathodically, polymer **P1** showed two reduction peaks at -1.1 and -1.8 V. The observed two-step reduction process can be assigned to the n-doping of two different heteroaromatic rings. This is in contrast to PPV and poly(thiophene), where the two-step reduction process has rarely been observed (Moratti et al. 1994). However, in conjugated heteroaromatic alternating polymers, such as poly(furanquinoxaline)s and poly(phenylene-1,3,4-oxadiazole)s, a main peak with a shoulder in the cyclic voltammogram was observed (Janietz et al. 1993 and Kanbara et al. 1995). Polymer **P2** showed a reduction peak in the cathodic scan at -0.92 V. In the anodic sweep, the oxidation peaks were observed at 1.7 and 1.44 V respectively for **P1** and **P2**. The lower oxidation potential of **P2** than that of **P1** could be attributed to the presence of stronger electron releasing 3,4-propylenedioxythiophene unit in **P2**, which makes the oxidation process easier. The onset oxidation and reduction potentials of the polymers are determined and are compiled in Table 3.2. The equations 3.3 and 3.4, reported in the literature (Yang and Jenekhe 1995, Agrawal and Jenekhe 1996, de Leeuw et al. 1997) were used for the determination of the HOMO and the LUMO energy levels of the polymers.

$$E_{\text{HOMO}} = -[E_{(\text{onset})}^{\text{ox}} + 4.8 \text{ eV} - E_{\text{FOC}}] \dots\dots\dots (3.3)$$

$$E_{\text{LUMO}} = -[E_{(\text{onset})}^{\text{red}} + 4.8 \text{ eV} - E_{\text{FOC}}] \dots\dots\dots (3.4)$$

Where, $E_{(\text{onset})}^{\text{ox}}$ and $E_{(\text{onset})}^{\text{red}}$ are the onset potentials for the oxidation and reduction processes of the polymers respectively.

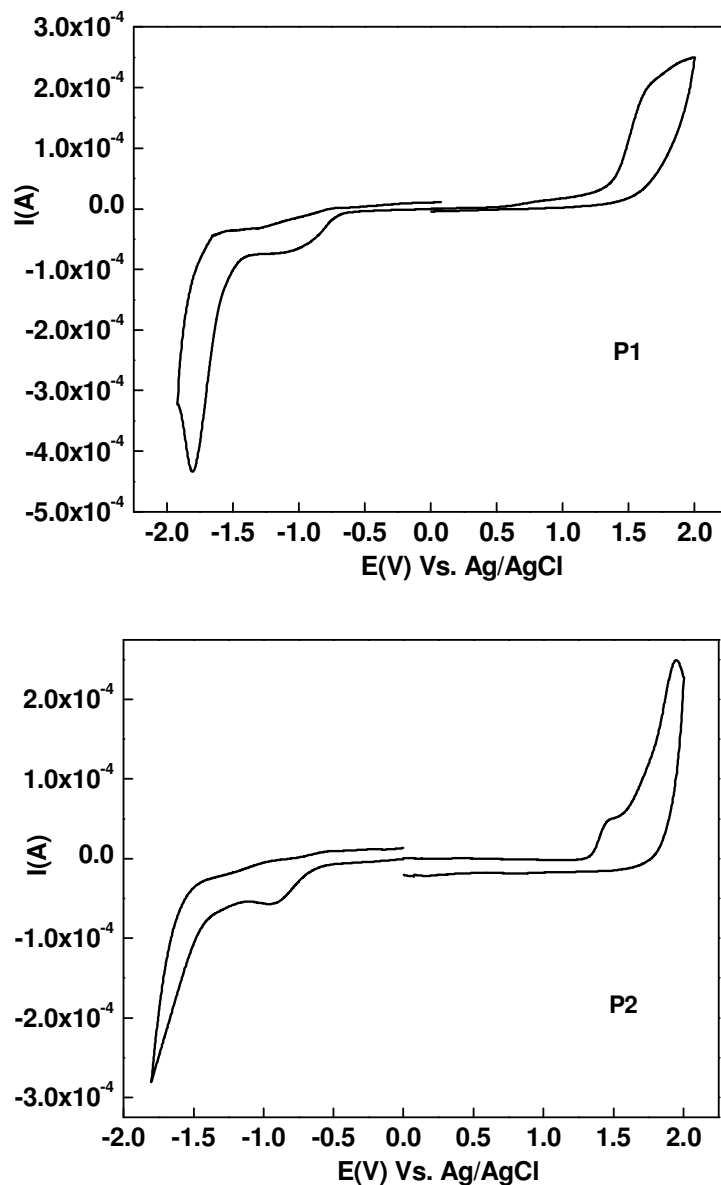


Figure 3.17 Cyclic voltammetric traces of **P1** and **P2**

Accordingly, the HOMO energy levels were estimated to be -5.67 and -5.61 eV and the LUMO energy levels were found to be -3.57 and -3.59 eV respectively for **P1** and **P2**. The HOMO level of **P2** was slightly higher than that of **P1**, which could be due the presence of additional electron releasing PDOT unit in **P2**. But the LUMO levels of **P1** and **P2** are almost the same, as both the polymers contain 1,3,4-oxadiazole ring as the electron acceptor unit.

In general, the HOMO level of conjugated polymers shifts to higher energies (high-lying) by the introduction of strong electron releasing groups whereas the presence of strong electron accepting groups lowers (low-lying) their LUMO levels. In other words, ionization potential of conjugated polymers can be lowered by incorporating strong electron releasing units along the polymer chain and the electron affinity of the polymers can be enhanced by introducing strong electron withdrawing groups. Whereas, the presence of alternating electron donor and electron acceptor units along the polymer chain increases the double bond character between the repeating units, through an effective intramolecular charge transfer, which pulls the HOMO and LUMO energy levels of the polymer to come close to each other. As a result the polymer will have high-lying HOMO level and low-lying LUMO level and, thus shows lower band gap energy. In case of non D–A conjugated polymer containing aromatic rings the introduction of strong electron withdrawing groups also makes the polymer a better hole-blocking material, by lowering its HOMO level.

The electrochemical band gaps of **P1** and **P2** were estimated to be 2.1 and 2.02 eV respectively. The electrochemical band gaps of the polymers are lower than that of their optical band gaps. This difference is due to the creation of free ions in the electrochemical experiment compared with the one measured through UV experiments, which refers to a neutral state. A similar behavior was observed for some conjugated polymers reported in the literature (Hou et al. 2008 and Ma et al. 2008). The electron affinity of the polymers were higher than those of 2-(4-biphenyl)-5-(4-tert-butylphenyl)-1,3,4-oxadiazole (PBD) (Pommerehne et al. 1995), aluminum tris(8-hydroxyquinolate) (Alq_3) (Destruel et al. 1999) and cyano-poly(p-phenylenevinylene) (CN-PPV) (Bradley 1993), which are some of the widely used electron transporting materials. The higher electron affinity can be attributed to the

following reasons: longer conjugation length of the polymers, presence of strong electron accepting 1,3,4-oxadiazole ring in the polymer backbone and the D–A arrangement along the polymers' chain, all contribute to lowering of the LUMO energy levels. From the observed high electron affinity values it can be expected that polymers may show increased electron injection ability when they are used as active materials in PLEDs and hence may improve the efficiency of the devices. The cyclic voltammetry data of all the polymers are compiled in Table 3.2.

The cyclic voltammograms of **P3** and **P4** are given in Figure 3.18. The polymers showed well defined redox peaks. For **P3**, on sweeping cathodically, the onset of the n-doping process occurred at a potential of -0.93 V with a reduction peak at -1.3 V. In the anodic scan, the p-doping onset occurred at 1.07 V with an oxidation peak at 1.2 V. It was expected that **P3** carrying additional alkoxy pendants would show a lower oxidation potential than that of **P4**. But, **P4** showed an oxidation peak at a lower potential (1.1 V) as compared to that of **P3**. The HOMO and LUMO energy levels of **P3** were estimated to be -5.34 and -3.34 eV, respectively and hence the electrochemical band gap is 2 eV. Similarly, the HOMO and LUMO energy levels of **P4** were estimated to be -5.27 and -3.46 eV respectively and the electrochemical band gap was found to be 1.81 eV. The LUMO energy levels of the polymers are lower than those of some reported donor-acceptor poly(aromatic oxadiazole)s (-2.8 to -2.9 eV) (Bradley 1993). The HOMO energy levels of the polymers are almost similar to that of PPV (5.1 eV) indicating that the polymers have similar hole-injection ability when they are used in PLEDs. Further, the high-lying HOMO and low-lying LUMO levels of the polymers are comparable with those of the related D–A polymers containing 1,3,4-oxadiazole units (Udayakumar and Adhikari 2007, Manjunatha et al. 2009).

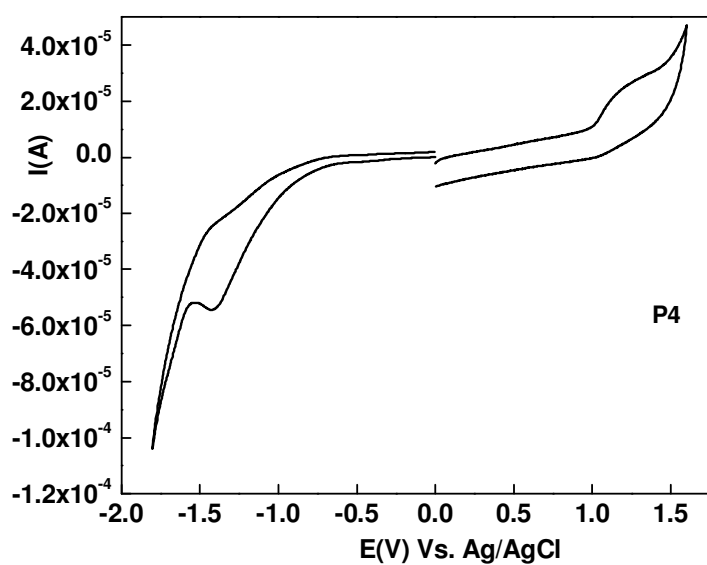
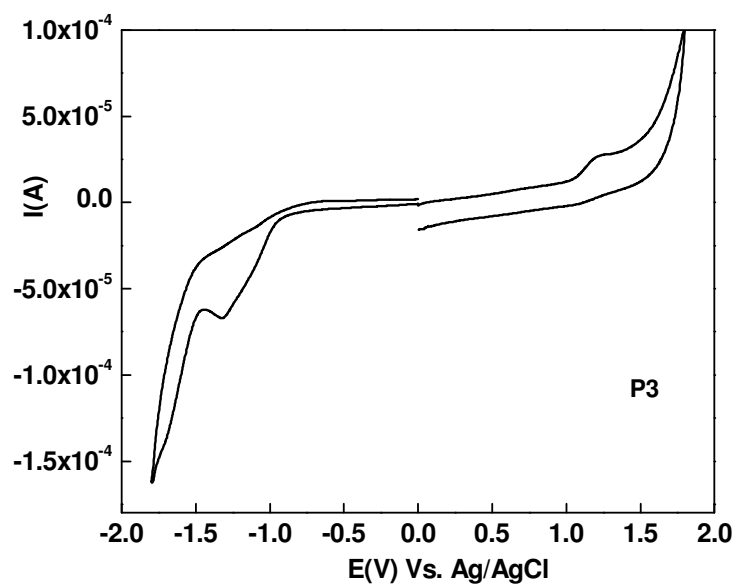


Figure 3.18 Cyclic voltammograms of **P3** and **P4**

Table 3.2 Electrochemical potentials, HOMO and LUMO levels of the polymers

Polymer	$E^{\text{ox}}_{\text{(onset)}}$ (V)	$E^{\text{red}}_{\text{(onset)}}$ (V)	$E(\text{oxd})$ (V)	$E(\text{red})$ (V)	HOMO (eV)	LUMO (eV)	E_{g}^{EC} (eV)
P1	1.4	-0.7	1.7	-1.1/-1.8	-5.67	-3.57	2.1
P2	1.34	-0.68	1.44	-0.92	-5.61	-3.59	2.02
P3	1.07	-0.93	1.2	-1.3	-5.34	-3.34	2.0
P4	1.0	-0.81	1.1	-1.4	-5.27	-3.46	1.81
P5	1.25	-0.75	1.55	-1.06	-5.52	-3.52	2.0
P6	1.21	-0.64	1.65	-0.83	-5.46	-3.63	1.83
P7	1.15	-0.6	1.36/1.79	-0.8	-5.42	-3.67	1.75
P8	1.23	-0.62	1.43/1.74	-0.78	-5.50	-3.65	1.85
P9	1.18	-0.69	1.44	-1.0	-5.45	-3.58	1.87
P10	1.69	-0.9	1.9	-1.2	-5.96	-3.37	2.59
P11	1.51	-0.64	1.81	-0.93	-5.78	-3.63	2.15
P12	1.58	-0.74	1.85	-1.02/- 1.59	-5.85	-3.53	2.32

E_{g}^{Ec} Electrochemical band gap estimated from the difference between E_{HOMO} and E_{LUMO}

Though chemical structure of the polymer chains in **P3** and **P4** is almost the same, except the additional alkoxy groups on one of the thiophene rings in **P3**, the HOMO and LUMO levels of the polymers are not the same. **P4** possess high-lying HOMO level and low-lying LUMO level as compared to those of **P3**. Further, as mentioned earlier, the oxidation potential of **P4** is lower than that of **P3**. These observations indicate that the alkoxy groups on the thiophene ring affect the electrochemical properties of the polymers. A similar trend was also observed in the optical studies of these polymers wherein **P4** showed maximum absorption in the longer wavelength region and slightly lower band gap than those of **P3**, which were attributed to lesser π -

stacking interactions in **P3** due to larger interchain distance imposed by the additional alkoxy groups. The electrochemical results further support this argument.

As shown by the cyclic voltammograms in Figure 3.19, polymers **P5–P8** showed both n-doping and p-doping processes. In the cathodic scan, polymers **P5–P8** showed reduction peaks at -1.06, -0.83, -0.8 and -0.78 V respectively. In the anodic sweep, oxidation peaks were observed at 1.55 and 1.65 V, respectively for **P5** and **P6**. Polymers, **P7** and **P8** showed two step oxidation processes. For **P7**, the main peak at 1.36 V with a small peak at 1.79 V was observed and this could be due to the presence of two different types of aromatic rings in the polymer chain. For **P8**, the main peak was observed at 1.43 V with a small peak at 1.74 V. The two step oxidation process in **P8** could be attributed to the presence of two types of conjugated segments in the polymer backbone (one containing cyanovinylene and thiophene unit and the other containing 1,3,4-oxadiazole and thiophene units). The HOMO energy levels of the polymers were found to be -5.52, -5.46, -5.42 and -5.50 eV respectively for **P5–P8**. The LUMO energy levels of **P5–P8** were estimated to be -3.52, -3.63, -3.67 and -3.65 eV respectively.

Amongst polymers **P5–P8**, polymer **P7** showed the highest (high-lying) HOMO level and the lowest (low-lying) LUMO level, and hence the lowest band gap. This could be attributed to the strong ICT interactions between donor and acceptor units in **P7** (as compared to **P5**, **P6** and **P8**) due to alternate arrangement of donor and acceptor units along the polymer chain. Such a regular arrangement of donor and acceptor units is not present in **P6** and **P8**. Further the repeating unit in **P7** consists more number of strong electron withdrawing cyanovinylene groups than those in other three polymers (**P5**, **P6** and **P8**), which also contributes in lowering the LUMO level of the polymer **P7**. The results obtained in the optical studies of these polymers further supports the presence of stronger ICT interactions in **P7**. That is, the lowest optical band gap was observed for **P7** among these polymers (**P5–P8**).

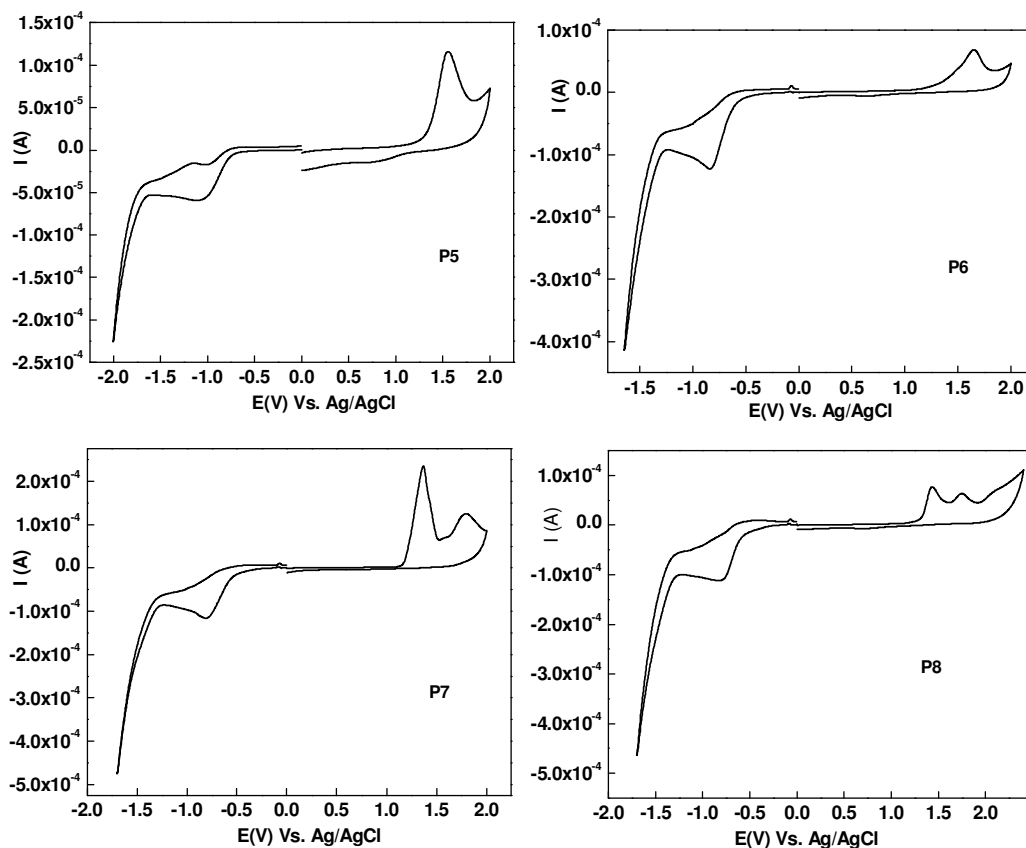


Figure 3.19 Cyclic voltammograms of **P5–P8**

Polymer **P6** possesses lower HOMO level and higher LUMO level and hence higher band gap as compared to that of **P7**. The strong electron accepting cyanophenylenevinylene unit in **P7** was replaced with a substituted fluorene unit to form **P6**. As dialkylfluorene unit is electron rich in nature, the extent of alternate D–A arrangement of the repeating unit in **P6** is lowered as compared to that in **P7**. This decreases the ICT interactions along the polymer chain. As a result the HOMO and the LUMO levels are slightly pulled apart. The HOMO levels of **P5** and **P8** are comparable, but are low-lying compared to those of **P7** and **P6**. The low-lying HOMO level of **P8** could be attributed to decreased ICT interactions in the polymer chain, whereas in **P5** it could be due to shorter conjugation length of the repeating unit. Though the HOMO levels of **P5** and **P8** are almost the same, **P8** possesses low-lying LUMO level than that of **P5**. This is due to the incorporation of additional

electron accepting 1,3,4-oxadiazole rings along with cyanovinylene units in **P8**. For the same reason, the LUMO level of **P8** was slightly lower than that of **P6**. Overall all the polymers **P5–P8** showed low-lying HOMO and LUMO levels due to the incorporation of strong electron withdrawing cyanovinylene units in the polymer chains.

The electron affinity of the polymers is higher than the values reported for some important D–A conjugated polymers like dioxythiophene-benzothiadiazole based polymers (Beaujuge et al. 2010), bis(1-cyano-2-thienylvinylene)phenylene based polymers (Colladet et al. 2007) and fluorene and 4-pyran-4-ylidene(malononitrile) based polymers (Lee et al. 2007) which showed good device properties. Thus, the decrease in LUMO energy level of **P5–P8** is attributed to simultaneous effects of the incorporation of strong electron withdrawing groups like cyanovinylene and/or oxadiazole units and of the D–A structure, along polymers backbone. The electrochemical band gaps of **P5–P8** were estimated to be 2.0, 1.83, 1.75 and 1.85 eV respectively and are almost comparable with the corresponding values obtained for the polymers using UV-Vis absorption studies. The lower band gap achieved in these polymers could be resulted from their unique D–A conjugated structures. Furthermore, introduction of vinylene linkages in the polymer backbone allows the planarization of the polymer chain by eliminating torsional strain, thus extending effective conjugation length, which can lead to a lower band gap.

The cyclic voltammograms of **P9** and **P10** films are given in the Figure 3.20. On sweeping cathodically, the onset of n-doping process occurred at -0.69 and -0.9 V with corresponding reduction peaks at -1.0 and -1.2 V respectively for **P9** and **P10**. In the anodic scan, the p-doping onset was observed at 1.18 and 1.69 V with corresponding oxidation peaks at 1.44 and 1.9 V respectively for **P9** and **P10**. Polymer **P9** carrying strong electron releasing conjugative thiophene unit in the main chain showed lower oxidation potential value when compared with that of **P10**, which contains conjugative phenyl ring instead of thiophene ring. The HOMO energy levels of the polymers were estimated to be -5.45 and -5.96 eV and the LUMO energy levels were determined to be -3.58 and -3.37 eV for **P9** and **P10** respectively. Hence the electrochemical band gap was found to be 1.87 and 2.59 eV respectively for **P9** and

P10. In particular, polymer **P9** showed high-lying HOMO level and low-lying LUMO level due to the presence of electron rich thiophene rings and electron withdrawing 1,3,4-oxadiazole segments in the polymer backbone through a D–A structure.

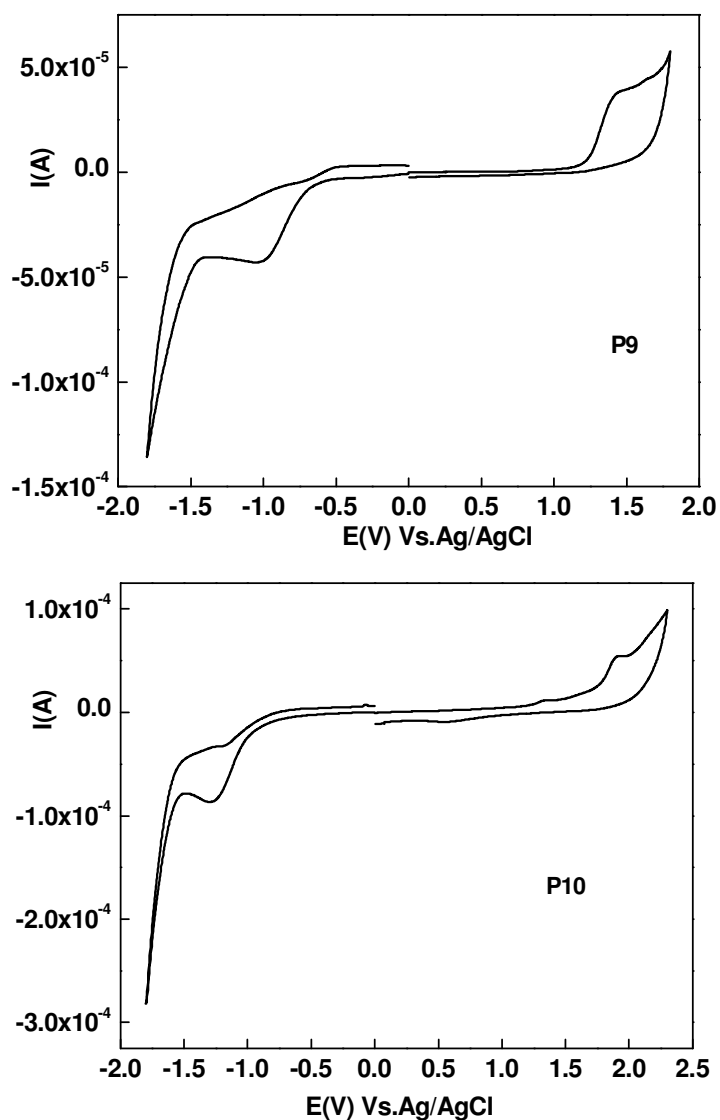


Figure 3.20 Cyclic voltammetric traces of **P9** and **P10**

The HOMO energy level of **P9** is comparable with that of CN-PPV (-5.63 eV) (Li et al. 1999) which was shown to possess good hole blocking properties. In contrast to **P9**, polymer **P10** showed deeply lying HOMO level and high-lying LUMO levels. This could be due to the biphenyl ring present in **P10** which act as conjugation

breaker as the ring is nonplanar. This limits the efficient overlap of p-orbitals throughout the repeating unit. Further, the presence of the biphenyl ring disturbs the ICT interactions between the donor and acceptor units. As a result the HOMO and the LUMO energy levels are pushed apart leading to higher band gap energy. However, the electron affinity of the polymers are lower than those of poly(fluorenevinylenes) (-2.6 eV) (Jin et al. 2003), CN-PPV (-3.02 eV) and some poly(aromatic oxadiazole)s (-2.8 to -2.9 eV) (Bradley 1993). The observed higher electron affinity of the polymers is due to the incorporation of strong electron withdrawing 1,3,4-oxadiazole segment in these polymers. From the high electron affinity value it can be expected that the polymers may show an improved electron transport properties when they are used in PLEDs.

Figure 3.21 shows the cyclic voltammograms of **P11** and **P12**. When swept cathodically, **P11** showed a reduction peak at -0.93 V with an onset of reduction at -0.64 V. In the anodic scan, an oxidation peak was observed at 1.81 V with an onset of oxidation at 1.51 V. For **P12**, an oxidation peak was observed at 1.85 eV with onset oxidation potential at 1.58 V. While sweeping cathodically, **P12** showed two-step reduction processes with two reduction peaks at -1.02 and -1.59 V. The two-step reduction process can be assigned to the n-doping of two different heteroaromatic rings present in the polymer main chain.

The HOMO energy levels of the polymers were estimated to be -5.78 and -5.85 eV and the LUMO energy levels were found to be -3.63 and -3.53 eV respectively for **P11** and **P12**. The electrochemical band gap was estimated to be 2.15 eV for **P11** and 2.32 eV for **P12**. The electrochemical band gaps of the polymers are almost similar to their optical band gaps. The low-lying HOMO level and high-lying LUMO level of **P12** as compared to those of **P11** is due to the presence of biphenyl ring in **P12**. Overall, both polymers possess relatively deeper HOMO levels which can be attributed to the simultaneous presence of two strong electron withdrawing groups (1,3,4-oxadiazole and cyanophenylenevinylene units) in the polymer backbone.

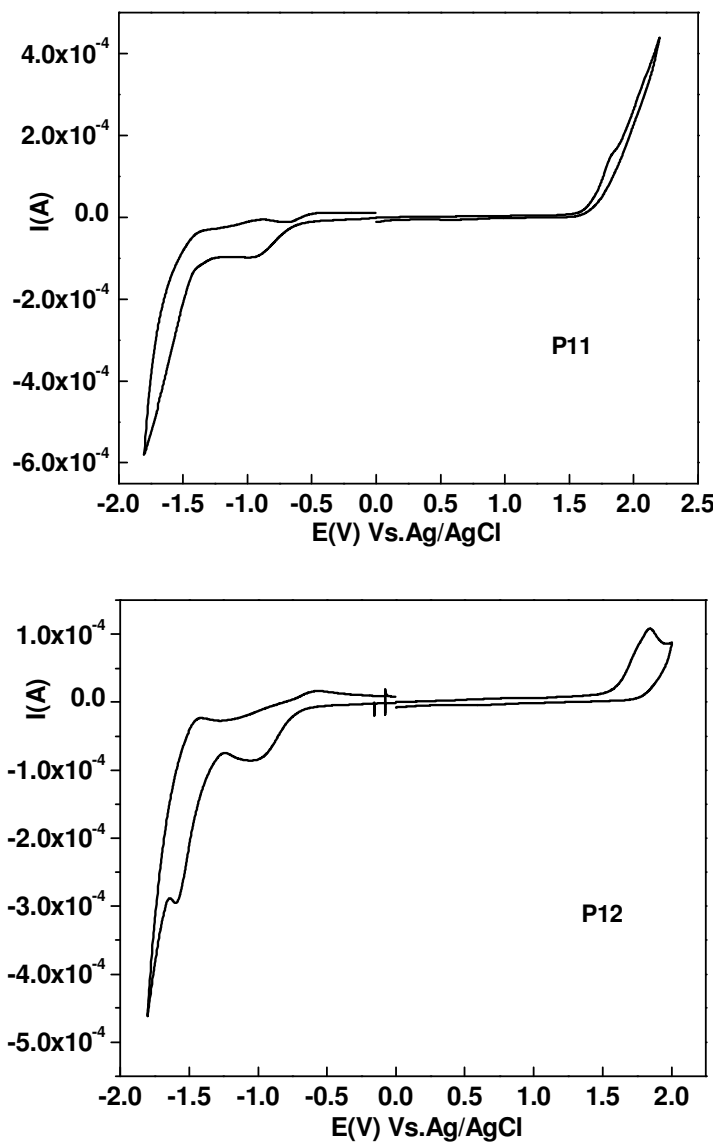


Figure 3.21 Cyclic voltammetric traces of **P11** and **P12**

In addition, the LUMO energy levels of the polymers **P11** and **P12** are lower than those of some related D–A conjugated polymers (Chen and Wu 2001, Cho et al. 2004, Kim et al. 2005 and Hegde et al. 2009) carrying 1,3,4-oxadiazole and/or cyanovinylene units as electron withdrawing segments. These results indicate that the strong electron withdrawing 1,3,4-oxadiazole and cyanovinylene unit is helpful in lowering the LUMO energy level, which is expected to facilitate the electron injection in PLEDs based on these polymers. As evident from Figure 3.3, the dialkylfluorene

units in **P9** and **P10** are replaced by cyanophenylenevinylene units in **P11** and **P12** respectively. Polymer **P11** possesses low-lying HOMO as well as low-lying LUMO levels as compared to those of **P9**. This could be understood on the basis of the electron withdrawing nature of cyanophenylenevinylene unit in **P11**, which lowers both the HOMO and the LUMO energy levels of the polymer. But the similar trend of lowering of energy levels was not observed in case of **P12** with respect to the energy levels of **P10**. That is, **P12** possesses high-lying HOMO level and low-lying LUMO level as compared to those of **P10**. It can be noted that the lowering of the LUMO level was also observed for **P11** when compared with that of **P9**. But, the extent of lowering is more in the case of **P12** than that in **P11**. That is, the value of $E_{\text{LUMO}}(\mathbf{P10}) - E_{\text{LUMO}}(\mathbf{P12})$ is higher (0.16 eV) than the value (0.05 eV) of $E_{\text{LUMO}}(\mathbf{P9}) - E_{\text{LUMO}}(\mathbf{P11})$. These results could be explained by considering extent of conjugation in these polymers. As the presence of biphenyl unit disturbs the conjugation in **P10** and **P12**, the effect of electron withdrawing or electron donating groups becomes more prominent in deciding the energy levels of the polymers. Whereas, in case of **P9** and **P11**, the extent of conjugation as well as the nature of electron withdrawing or electron donating groups determines the energy levels of the polymers. So, the presence of electron withdrawing cyanophenylenevinylene unit in **P12** lowers its LUMO energy level significantly as compared to the LUMO level of **P10**.

The energy level diagram comparing the HOMO and the LUMO energy levels of the newly synthesized polymers (**P1–P12**) with those of PPV and PBD is depicted in Figure 3.22. The HOMO energy levels of **P1–P12** are in the range -5.27 – -5.96 eV and their LUMO energy levels are in the range -3.34 – -3.67 eV. The observed variation in the energy levels of the polymers in comparison with their chemical structures clearly suggest that desired energy levels and hence required band gap in conjugated polymers can be achieved by the incorporation of suitable donor and acceptor segments in the polymer backbone. The electrochemical band gap of the polymers were found to be in the range of 1.75 – 2.59 eV. These results indeed demonstrate that the newly synthesized polymers are promising candidates for the development of efficient devices like PLEDs and PSCs.

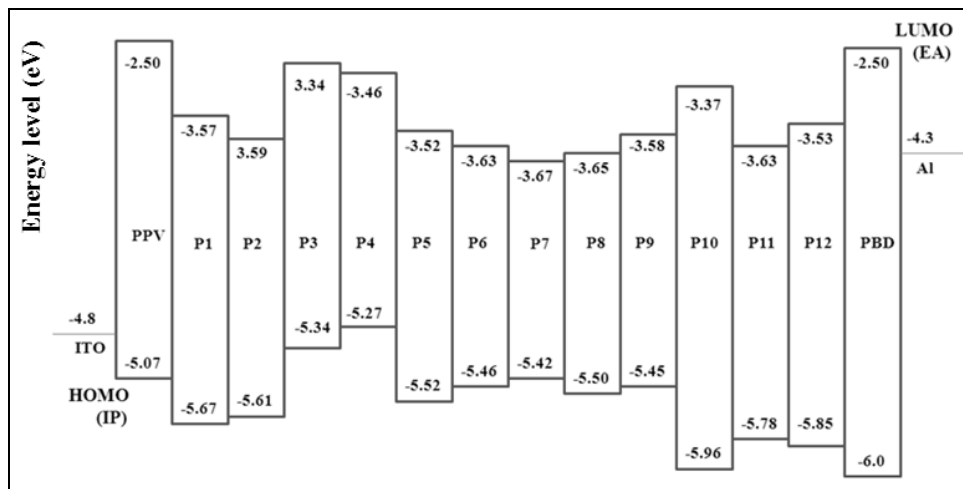


Figure 3.22 HOMO and LUMO levels of new polymers **P1–P12**, PPV and PBD

The energy barriers between the emitting polymers and metal electrodes (anode and cathode) can be estimated by comparing the work functions of electrodes with the HOMO and the LUMO energy levels of emitting polymers. Generally ITO is used as anode and Al is used as cathode in the fabrication of light emitting devices. Then, the hole injection barrier (ΔE_h) is given by equation,

$$\Delta E_h = (E_{\text{HOMO}} - 4.8) \text{ eV} \dots \dots \dots (3.5)$$

The electron injection barrier (ΔE_e) is given by equation,

$$\Delta E_e = (4.3 - E_{\text{LUMO}}) \text{ eV} \dots \dots \dots (3.6)$$

where 4.8 eV is the work function of the ITO anode and 4.3 eV is the work function of aluminum cathode. The difference between ΔE_e and ΔE_h can be employed to estimate the balance of charge injection. Generally the lower ($\Delta E_e - \Delta E_h$) value indicates the balanced injection of electrons and holes from the cathode and anode respectively in PLEDs.

As shown in Table 3.3, all the polymers showed lower electron injection barriers (ΔE_e), which are lower than those of PPV (1.7 eV) one of the commonly used hole transporting polymer. The observed lower electron injection barrier (ΔE_e) is attributed to the presence of strong electron withdrawing units like 1,3,4-oxadiazole and/or

cyanovinylene units in the polymer backbone as well as the D–A structure of the polymers. However, the hole injection barrier (ΔE_h) of the polymers are higher than that of PPV (0.3 eV). This is because of the introduction of electron withdrawing segments attached to the polymer backbone, which lowers the HOMO energy level. However, the hole injection barrier is lower than that of PBD (Bradley 1993, Okumoto and Shirota 2001) and comparable with that of tris(8-hydroxyquinolate)aluminium (Alq₃) (Im et al. 2001), which are widely used electron transporting/hole blocking materials. Further, the barrier energy difference ($\Delta E_e - \Delta E_h$) of the polymers was found to be lower when compared to those of PBD,

Table 3.3 The barrier energies of new polymers for electron/hole injection

Polymer	ΔE_h (eV)	ΔE_e (eV)	$\Delta E_e - \Delta E_h$ (eV)
P1	0.81	0.71	0.10
P2	0.87	0.73	0.14
P3	0.54	0.96	0.42
P4	0.47	0.84	0.37
P5	0.72	0.78	0.06
P6	0.66	0.67	0.01
P7	0.62	0.63	0.01
P8	0.70	0.65	0.05
P9	0.65	0.72	0.07
P10	1.16	0.93	0.23
P11	0.98	0.67	0.31
P12	1.05	0.77	0.28
PPV	0.3	1.70	1.40
PBD	1.2	1.8	0.6
CNPPV	1.3	0.90	0.40

PPV and CN-PPV, which are widely used active materials in PLEDs. Also the barrier energy difference of the new polymers was lower than those of some related D–A conjugated polymers reported in the literature (Chen et al. 2001, Udayakumar and Adhikari 2007, Manjunatha et al. 2009).

These electrochemical results indicate that all the newly synthesized polymers possess fairly balanced injection of electrons and holes from the cathode and anode, respectively. Hence, the newly synthesized polymers are expected to show enhanced charge transporting properties for the development of efficient PLEDs. In addition, the polymers exhibited low-lying HOMO energy levels indicating that they are promising candidates for obtaining high open-circuit voltages when they used in polymer solar cells. Thus the donor–acceptor structure could be a promising molecular design for synthetically tuning HOMO and LUMO energy levels of conjugated polymers.

3.4 CONCLUSIONS

The linear optical properties of the new D–A type conjugated polymers (**P1–P12**) were investigated by UV-Vis absorption and fluorescence emission spectroscopic techniques. Cyclic voltammetry was used to evaluate the electrochemical properties of the polymers. All the polymer films, except films of **P3** and **P5**, showed a red shift in the absorption maxima as compared to those of their solutions, due to the π -stacking effect in polymer films. In **P3** film, the larger interchain distance imposed by the additional dodecyl chains attached to the thiophene ring, whereas the closer proximity of the alkoxy chains in **P5** decreases the π -stacking interactions in the solid state (polymer films). The emission maxima of the polymers in the film state exhibited red shift in comparison with those of their solutions. This red shift can be attributed to the interchain or/and intrachain mobility of the excitons and excimers generated in the polymer solid state.

The polymers emitted blue to red light when irradiated with UV light, depending upon the chemical structure of the polymer backbone. The polymers showed reasonably high fluorescence quantum yields in the range of 32 – 42 %. Among polymers **P1–P12**, polymer **P5–P8** showed low band gap mainly due to the presence of cyanovinylene groups and also because of the D–A structure of the polymer chain.

Polymer **P7** containing cyanovinylene group and a regular D–A arrangement was found to show the lowest band gap. Due to the same reason, **P7** also exhibited the lowest LUMO energy level among these polymers. Thus, introduction of cyanovinylene groups and maintaining a strict alternation of D and A units along the conjugated chain could be a promising molecular design to obtain low band gap polymers with high electron affinity. The results obtained from the optical and electrochemical studies of the polymers were correlated with the chemical structure of the polymers. Further, the presence of biphenyl ring along the polymer backbone was found to affect the photophysical and electrochemical properties of the polymers. The biphenyl ring being nonplanar, limits the π -conjugation along the polymer chain. Hence polymers **P10** and **P12**, both containing a biphenyl ring displayed lowest λ_{\max} values and the highest band gap energy among polymers **P1–P12**.

The HOMO levels of some polymers are comparable with that of good hole transporting materials. Further, the electron affinity of the polymers are higher than that of some widely used electron transporting materials. The low-lying LUMO energy levels of the polymers could be attributed to the strong electron accepting ability of 1,3,4-oxadiazole and/or cyanovinylene segments present in the polymer backbone. The optical and electrochemical studies clearly revealed that by introducing suitable donor and acceptor units in the polymer backbone, one can achieve polymers with desired HOMO and LUMO energy levels. Overall, the newly synthesized polymers are potential candidates for optoelectronic applications. In particular, the polymers which showed narrow band gaps with low HOMO levels are promising candidates for polymer solar cell devices. Further, the low-lying LUMO levels of the polymers suggest that they are good candidates for electron transporting/hole blocking materials in polymer light emitting diodes.

CHAPTER 4

STUDY OF ELECTROLUMINESCENT AND PHOTOVOLTAIC PROPERTIES OF THE POLYMERS

Abstract

This chapter deals with fabrication and characterization of optoelectronic devices based on the new D–A polymers. Polymer light emitting diodes are fabricated using polymers P5, P9, P10 and P12 as the emissive layer and their electroluminescent properties are discussed. Further, the photovoltaic properties of low band gap D–A polymers (P5–P8) are studied by fabricating bulk heterojunction solar cells using polymer as both electron donor and electron acceptor materials.

4.1 INTRODUCTION

In the past decades, there is considerable interest in the development of electronic devices incorporating organic and/or polymer semiconductors owing to their superior properties, simplicity of fabrication, light weight and potentially lower cost when compared to conventional inorganic semiconductors. Further, these materials combine a number of interesting properties which give rise to a broad variety of new applications. Organic polymers typically offer the advantage that they are light weight and flexible materials which can be easily processed by common techniques like spin-coating or simple ink-jet printing. This makes them promising candidates for the production at low cost and for large-area display technologies. Due to these reasons, conjugated polymers have attracted much attention as active materials for organic electronic devices, such as light emitting diodes, field-effect transistors, photovoltaic cells, polymer sensors, components for fuel cells etc. In addition to their attractive material properties, the important advantage of conjugated polymers is the ease of manipulation of their chemical structure. This allows the fabrication of materials with tailor made electronic and/or mechanical properties.

4.2 POLYMER LIGHT EMITTING DIODES

An organic light emitting diode (OLED) consists of an organic semiconductor material layer sandwiched between positive and negative bias electrodes. The positive electrode (anode) is generally a transparent indium tin oxide (ITO) such that the emitted photons can easily escape from the device. The transparent anode has typically a high work function (ϕ) to be able to inject efficiently holes into the valence band of the organic semiconductor (small hole injection barrier, ΔE_h). On the other hand, metal with a low work function (ϕ) such as Ca, Mg-Ag alloy or Al serves as the

cathode. The low work function cathode metals lower the electron injection barrier (ΔE_c) and promote the injection of electrons into the conduction band of the organic semiconductor. Schematic representation of the working principle of a LED based on organic semiconductor is given in Figure 4.1.

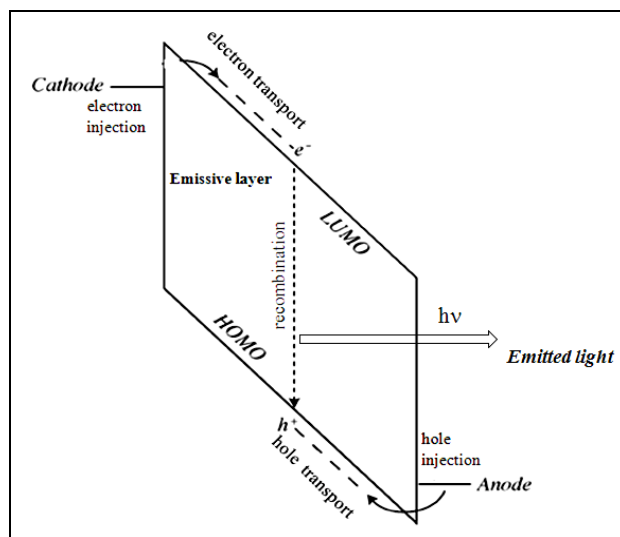


Figure 4.1 Schematic diagram of working principle of LED

A LED works on the principle of double charge injection. There are four processes to be considered during the operation of an OLED: charge injection into the organic layer, charge transport, electron/hole recombination and emissive decay. Initially, an electric field is applied through the electrodes, the electrons from the cathode are injected into the conduction band and holes are injected from the anode into the valence band of the semiconductor. These charge carriers transported through the emissive layer i.e. the semiconductor layer where they undergo recombination to yield excitons. Some of these excitons, usually the singlet excitons undergo radiative decay producing light.

The present interest in the field LEDs is to improve the device properties. In particular, the current challenges in the field of PLEDs are design and synthesis of conjugated polymers with desired optoelectronic properties for applications in flat panel displays. The major concerns in this direction are i) to improve the device properties such as low turn on voltage, high luminescence and high electroluminescence efficiency and ii) to tune the molecular structure of the conjugated polymers to obtain pure red, blue and green emission colors.

In order to address these challenges it is necessary to understand the structure property relationship between the molecular structure of the conjugated polymers and their electroluminescent properties. For efficient charge injection, the HOMO and the LUMO energy levels of the polymer need to match with the work function of the metal electrodes. In this regard, to improve the charge injection/transport, many approaches have been attempted. One strategy is to insert an additional electron injection/transport layer between the emitter and cathode and/or a hole transporting layer between the emitter and the anode (Parker et al. 1994 and Son et al. 1995). However, fabrication of multilayer PLEDs is usually a difficult task. Other approach is that, a low work function metal such as calcium or magnesium can be used as the cathode to lower the energy barrier so as to enhance the injection rate of electrons. Due to the high chemical reactivity to oxygen and moisture of such metals limits their practicality. In this direction, the concept of using donor-acceptor polymers has been found to be a promising approach to obtain efficient devices. Thus one can achieve efficient charge injection by adjusting the HOMO and LUMO energy levels of the organic layer to match with the work functions of stable metal electrodes.

In this context, the D–A conjugated polymers synthesized in the present study are promising candidates for PLEDs. The electrochemical data of the polymers indicate that the LUMO energy level of the polymers is lower than that of some good electron transporting polymers. Further, the HOMO energy level of the polymers is comparable with that of some good hole transporting materials. Therefore it was planned to carryout preliminary studies on electroluminescent behavior of all the synthesized polymers by using them as emissive layers in PLEDs. However, only polymers **P5**, **P9**, **P10** and **P12** were used for PLED fabrication based on their good film forming properties. The PLEDs are fabricated using polymers **P5**, **P9**, **P10** and **P12** as emissive layers, with a configuration of ITO/PEDOT:PSS/**polymer**/Al and their electroluminescent properties were studied. Further, the current density-voltage characteristics were investigated and threshold voltages of the devices were also determined. Figure 4.2 shows the energy band diagram of polymers **P5**, **P9**, **P10** and **P12** in comparison with the energy levels of ITO, PEDOT:PSS and Al.

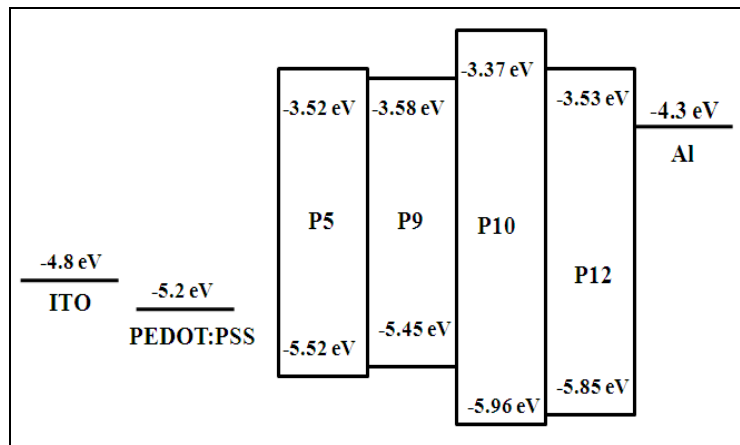


Figure 4.2 Energy level diagram of polymers **P5**, **P9**, **P10** and **P12** in comparison with the energy levels of PEDOT:PSS, ITO and Al

4.2.1 Materials and instruments

Poly(3,4-ethylenedioxythiophene):poly(styrenesulfonate) (PEDOT:PSS) was purchased from Sigma Aldrich Chemical Company. All solvents and other reagents were purchased commercially and used without further purification. Polymers were coated from their solutions using an ACE - 1020 (Dong Ah Trade & Tech. Corp.) spin coating unit. The electroluminescence spectrum was determined using HR 2000 Ocean Optics spectrometer, having a CCD array and a fiber optic probe. The current-voltage characteristic was studied using a Keithley 2400 programmable digital source meter. The thickness of the deposited layer was measured by ellipsometry.

4.2.2 Fabrication of polymer light emitting diodes

In the device fabrication, the simplest sandwich structure was used with PEDOT:PSS coated indium tin oxide glass as the anode, the spin coated polymers (**P5/P9/P10/P12**) as the emissive layer and aluminum as the cathode. To fabricate PLEDs of device configuration ITO/PEDOT:PSS/**polymer**/Al, first the ITO coated glass substrates with a sheet resistance of 20 Ω /square and a thickness of 120 nm (ITO) were cleaned using deionized water, acetone, trichloroethylene and isopropyl alcohol sequentially for about 20 min each using an ultrasonic bath and dried in vacuum oven. Then ITO surface was treated with oxygen plasma for about 5 min to increase its work function. Then, a hole injection layer of PEDOT:PSS was spin coated on the cleaned and patterned ITO substrates at 4000 rpm with about 50-60 nm

in thickness and was dried by baking at 120 °C in vacuum for ~1 h. Then, the emitting layer (**P5/P9/P10/P12**) was spin cast onto the PEDOT:PSS layer at a speed of 2000 rpm from chlorobenzene solution (10 mg/mL) through a 0.45 µm Teflon filter, followed by vacuum annealing at 150 °C for ~2 h in order to remove the organic fraction. Finally, the coated ITO glass plate was transferred to a vacuum deposition chamber, where a layer of Al electrodes was deposited on the polymer layer with about 200 nm in thickness by thermal evaporation at a pressure of 1×10^{-6} torr. For each polymer, four pixels, each of active area of $4 \times 4 \text{ mm}^2$ are defined per substrate, were used to assess the reproducibility of the device performance. The complete fabricated devices were finally annealed at 100 °C in vacuum for 5 min before being characterized. All the characterization of the light emitting diodes was carried out at the room temperature under ambient conditions without any protective encapsulation of the devices. Electroluminescence spectra at different bias voltages were investigated. The current as a function of applied voltage of the device was also studied.

4.2.3 Electroluminescent properties of polymers **P5**, **P9**, **P10** and **P12**

The EL spectra of the device based on **P5** under different driving voltages ranging from 7 to 14 V are as shown in Figure 4.3a. The EL spectra show that with an increase in the applied voltage, the intensity of the emitted light also increases as a function of wavelength. The PLEDs using **P5** as the emissive layer emitted red light with emission peaks originated at 615 and 670 nm. Also, the EL spectrum of the polymer showed stable red emission without any considerable spectral change and/or additional peaks with driven voltage. The EL spectra of the polymer was blue shifted relative to the corresponding photoluminescence spectra which results from different exciton generation processes and heating of the LEDs because of applied voltages during the measurement. This suggests that the local heating in the polymer film at high voltages probably leads to conformational changes of the polymer backbone (Tonzola et al. 2005 and Cao et al. 2006).

The color stability of the device under different voltages for **P5** was also investigated. The Commission Internationale De L'Eclairage (CIE) coordinates of the polymer devices under different voltages of 11 V, 12 V, 13 V and 14 V were (0.64,

0.32), (0.65, 0.32), (0.66, 0.32) and (0.64, 0.32) respectively. The EL peak position and the CIE coordinates of the device were not changed significantly under different driving voltages.

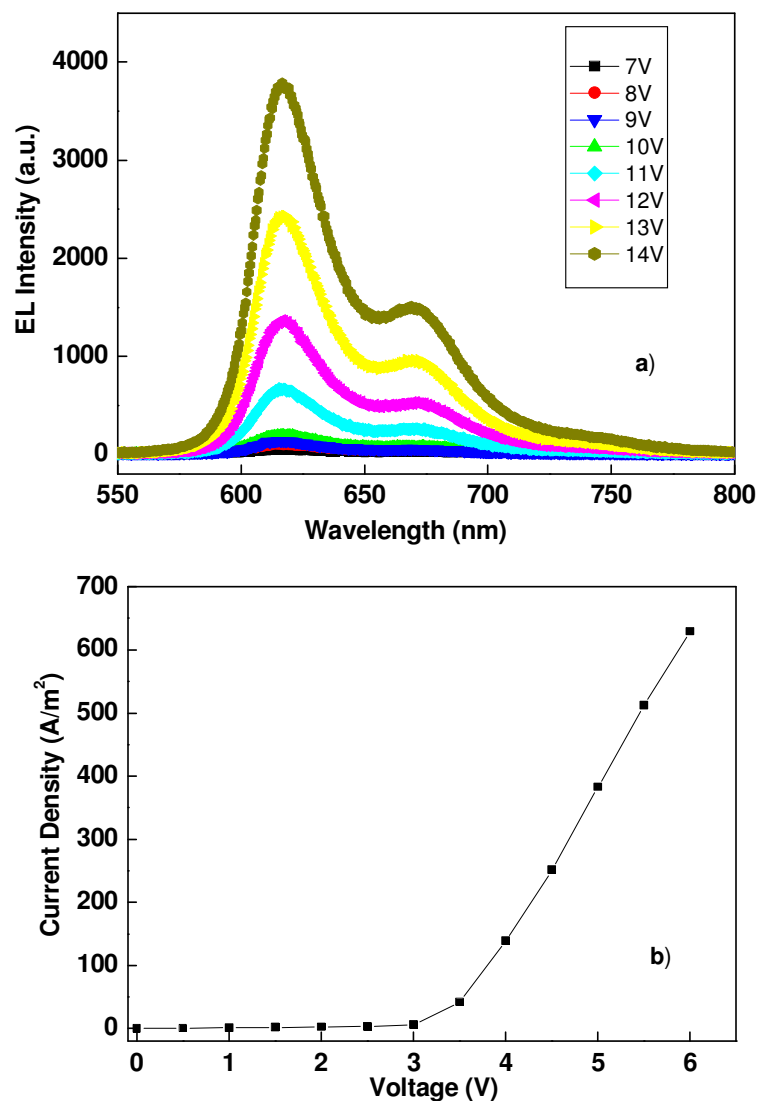


Figure 4.3 a) Electroluminescence spectra of the ITO/PEDOT:PSS/P5/Al device at varying forward applied voltage and b) Current density-voltage characteristics of the device

These results indicate that the polymer shows good color stability under different applied voltages. The color coordinates of the red emitting device is closer to the standard red (0.66, 0.34) demanded by the National Television System Committee (NTSC) indicating that **P5** emits almost pure red color (Gunter and Stiles 1982). The

current density-voltage characteristics of the PLED device (Figure 4.3b) show that the current density of the polymer increases exponentially with the increasing forward bias voltage, which is a typical diode characteristic. The polymer shows low threshold voltage of 3.1 V.

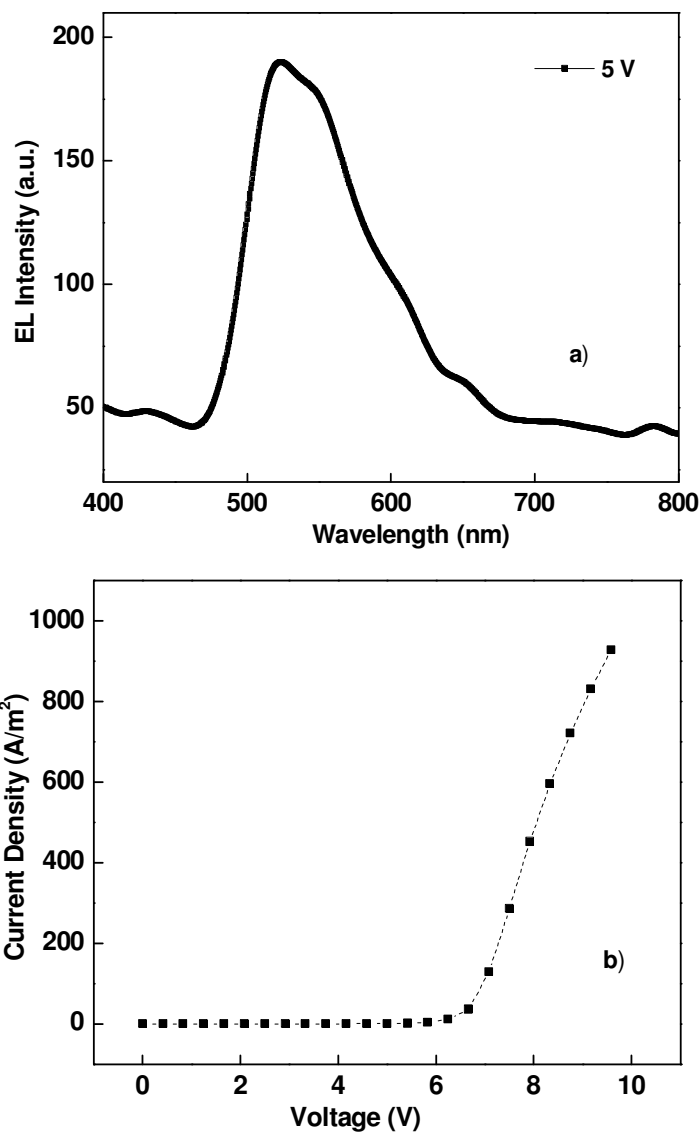


Figure 4.4 a) Electroluminescence spectrum of the ITO/PEDOT:PSS/P9/Al device at a forward applied voltage of 5 V and b) Current density-voltage characteristics of the device

The EL spectrum of polymer **P9** at a driving voltage of 5 V is shown in Figure 4.4a. The EL maximum of the polymer was centered at 524 nm. The PLED based on

P9 emitted green light with CIE coordinates (0.34, 0.47) under a driving voltage of 5 V. The EL spectrum of the polymer was red shifted relative to the corresponding solid state photoluminescence spectrum which probably attributed to the fact that electroluminescent excitons are generally adequately thermalized compared to photoluminescent excitons as a result of different modes of their generation (Zheng et al. 2002). Moreover, the presence of longer alkyl and alkoxy chains attached to thiophene and fluorene ring improve the polymer solubility and film forming capability which leads to a change in the film morphology. The threshold voltage of the polymer (Figure 4.4b) was found to be 6.5 V. Photographs of polymer solutions **P5**, **P9**, **P10** and **P12** under UV light are given in Figure 4.5.

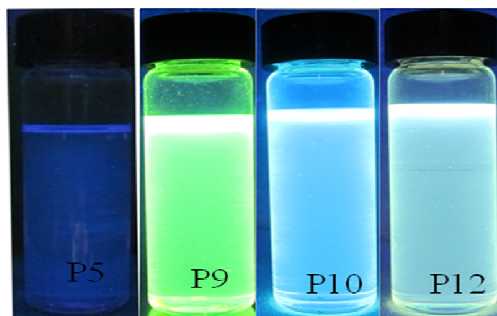


Figure 4.5 Photographs of polymer solutions **P5**, **P9**, **P10** and **P12** under UV light

Figure 4.6 shows the EL spectra of **P10** at various driving voltages and its current density-voltage characteristics. The EL spectra show that with an increase in the applied voltage (10 to 16 V), the intensity of the emitted light also increases as a function of wavelength. The EL maximum of **P10** was centered at 490 nm (Figure 4.6a). The device emitted green light with CIE coordinates of (0.25, 0.39) under a driving voltage of 12 V. No significant change in EL peak position and the CIE coordinates of the device was observed under different driving voltages, indicating good color stability of the device under different applied voltages. The EL spectrum of **P10** was almost identical to the corresponding solid state photoluminescence spectra, indicating that similar excitation may be involved in both the processes. The threshold voltage of the polymer was found to be 7.3 V (Figure 4.6b).

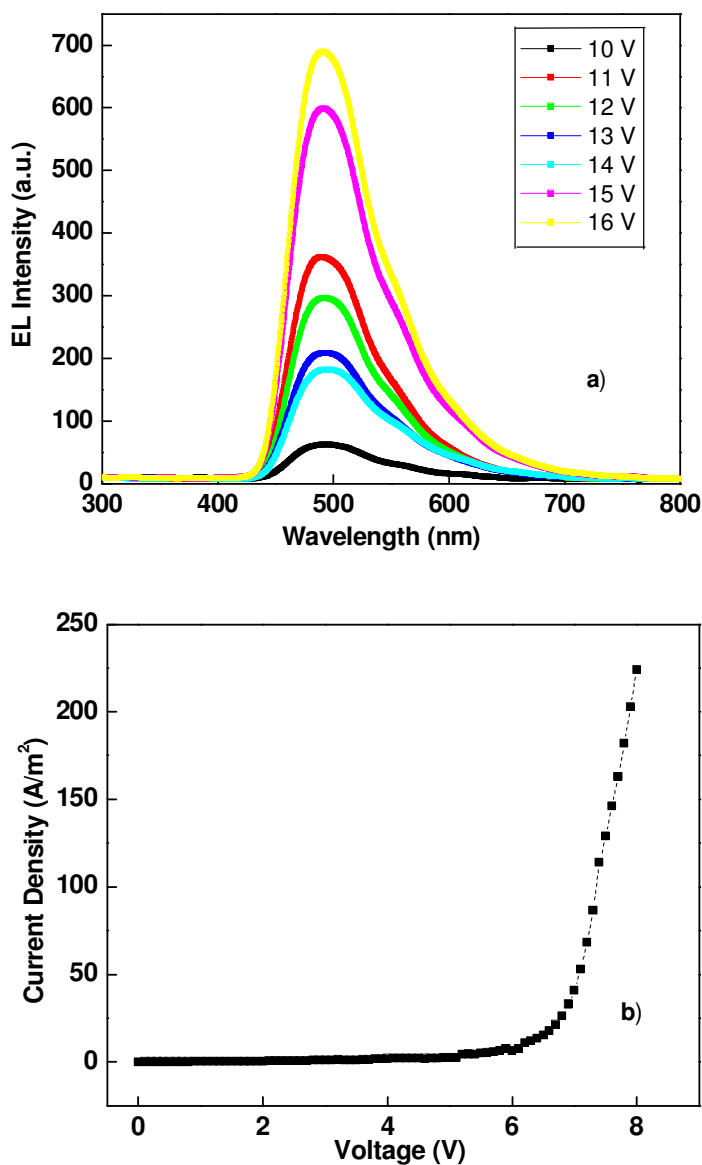


Figure 4.6 a) Electroluminescence spectra of the ITO/PEDOT:PSS/P10/Al device at varying forward applied voltage and b) Current density-voltage characteristics of the device

The EL spectra of **P12** under different driving voltages (13 to 15 V) are as shown in Figure 4.7a. By applying different bias voltages, the intensity of the emitted light was increased as a function of wavelength. The EL maximum of **P12** was observed at 514 nm under a driving voltage of 13 V. No change in the EL maximum was observed under a driving voltage of 14 V. However, a slight red shift of about 6 nm in the EL maximum was observed when the voltage is increased to 15 V. The observed

red shift in the EL spectrum is likely due to more efficient π -stacking and increased order at the internal operating temperatures of the LEDs. The PLEDs based on **P12** emitted white light. The CIE coordinates under a driving voltage of 14 V was (0.32, 0.35) and is close to the standard CIE coordinate for white color (0.33, 0.33). Figure 4.7b shows the current density-voltage characteristics of the PLED devices based on **P12**. The device showed a low threshold voltage of 3.9 V.

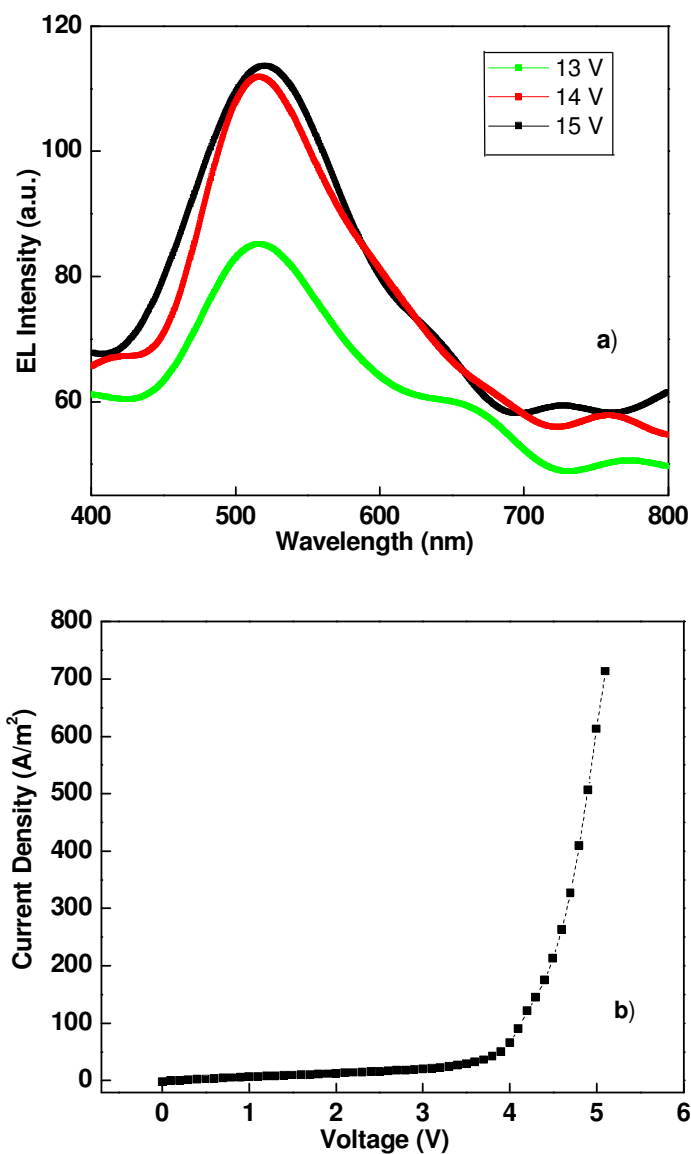


Figure 4.7 a) Electroluminescence spectra of the ITO/PEDOT:PSS/**P12**/Al device at varying forward applied voltages and b) Current density-voltage characteristics of the device

Overall, the observed lower threshold voltages for the polymers can be attributed to the lower energy barrier for electron injection (due to low lying LUMO level of the polymers) from the aluminum electrode. The low threshold voltage value can be comparable with some of the previously reported light emitting polymers which showed good EL performance (Lim et al. 2003 and Egbe et al. 2004). Figure 4.8 shows the CIE 1931 chromaticity coordinates (x,y) of PLEDs based on polymers **P5**, **P9**, **P10** and **P12**. These preliminary EL results suggest that the present polymers are good candidates for light emitting diodes due to their good color stability under different bias voltages and low threshold voltages. However, brightness of the device is very important to evaluate the performance of the PLEDs. Moreover, the performance of the device can be improved by optimizing the device fabrication conditions.

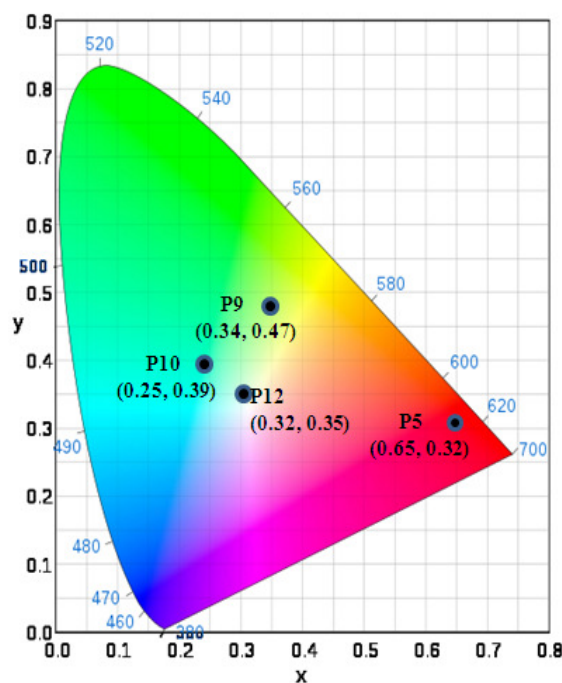


Figure 4.8 CIE 1931 chromaticity coordinates (x,y) of PLEDs based on polymers **P5**, **P9**, **P10** and **P12**

4.3 POLYMER SOLAR CELLS

Figure 4.9 (left) illustrates the mechanism by which light energy is converted into electrical energy in organic solar cells. The energy conversion process has four fundamental steps in the commonly accepted mechanism: 1) Absorption of light and generation of excitons, 2) diffusion of the excitons, 3) dissociation of the excitons with generation of charge and 4) charge transport and charge collection. Initially, the light absorbing material with a band gap in the visible region absorbs photons that excite the electrons from the ground state to the excited state, and bound electron-hole pairs (excitons) are created. The excitons diffuse to the donor–acceptor interface where excitons dissociate into free charge carriers after overcoming the binding energies. The free charge carriers transport to the respective electrodes under the internal electric fields, resulting in the generation of photocurrent. Here the donor material serves to transport the holes whereas the electrons travel within the acceptor material. Figure 4.9 (right) shows a schematic representation of a typical bulk hetero junction (BHJ) solar cell, illustrating the components involved in the mechanistic steps.

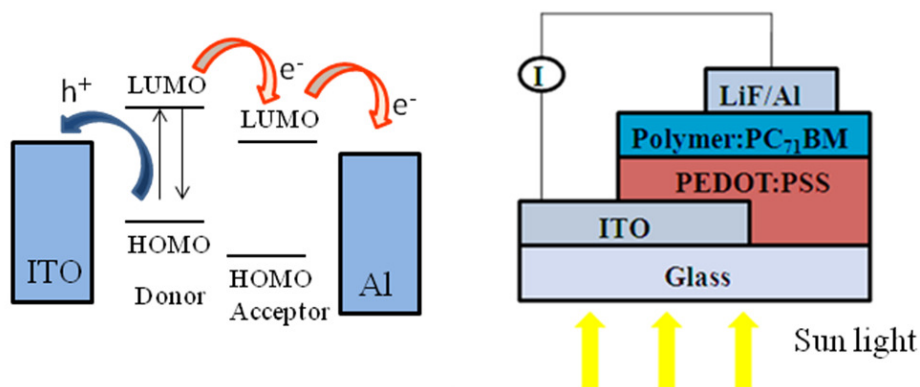


Figure 4.9 Schematic illustration of a photoenergy conversion in solar cells (left). Typical device architecture of a bulk heterojunction polymer solar cell (right)

The solar cells are usually tested under Air Mass (AM) 1.5 G conditions, 100 mW cm^{-2} . These conditions are experienced when the sun is at an angle of about 48° and are considered to best represent the Sun's spectrum on the Earth's surface (Rostalski and Meissner 2000). The typical current–voltage curve defining the primary quantities

which are used to validate the performance of a solar cell is shown in Figure 4.10. In the dark there is almost no current flowing until external voltage larger than the open-circuit voltage is applied. By allowing the device to short circuit under illumination the maximum current, which flow in the device when no voltage is applied, can be read at the intersection with the ordinate and is identified as the short-circuit current (J_{sc}). The maximum voltage the device can produce is called the open-circuit voltage (V_{oc}) which can be read at the intersection with the abscissa under illumination.

The maximum power the device can produce is characterized by the maximum power point (MPP) where the dark area in Figure 4.10 is maximized. The maximum power point (MPP) is determined by using equation:

$$MPP = V_{max} \times J_{max} \dots\dots\dots (4.1)$$

where V_{max} and J_{max} are the voltages and current at the MPP. Further, the fill factor (FF) is the ratio of the MPP to the maximum theoretical power limit of a solar cell and is calculated according to the equation:

$$FF = \frac{MPP}{V_{oc} \times J_{sc}} = \frac{V_{max} \times J_{max}}{V_{oc} \times J_{sc}} \dots\dots\dots (4.2)$$

The efficiency of the device can then be calculated by:

$$\eta = \frac{MPP}{P_{in}} = \frac{V_{oc} \times J_{sc} \times FF}{P_{in}} \dots\dots\dots (4.3)$$

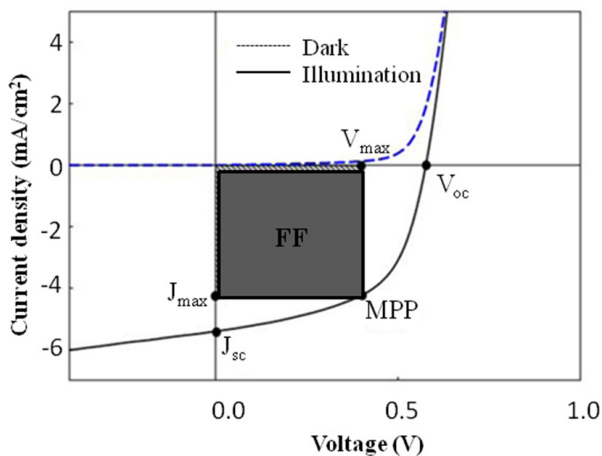


Figure 4.10 Current-voltage (J - V) curves of an organic solar cell in dark and under illumination

The bulk heterojunction device architecture using polymer semiconductor as electron donors and high electron affinity fullerene derivatives such as PC₆₁BM or PC₇₁BM as electron acceptors has proven to be the most successful concept in polymer solar cells (Halls et al. 1995 and Thompson et al. 2006). The main concern of the studies of PSCs is to increase the power conversion efficiency of the devices. However, the performance of polymer solar cells has been significantly improved in the past decade through optimization of device structure, interfacial layer engineering, processing conditions and synthesis of new high performance semiconductors. Recently, the power conversion efficiency of greater than 7 % has been achieved by using various donor-acceptor conjugated polymers and optimizing device processing conditions (Ma et al. 2005, Liang and Yu 2010).

It is noteworthy that, the efficiency of PSCs is still lower than their inorganic materials, such as silicon, CdTe and copper indium gallium selenide (Green et al. 2010), which prevents their practical applications in large scale. There are several factors limiting the performance of the PSCs. It is known that, the PCE is proportional to the open-circuit voltage, short-circuit current and fill factor of the PSCs. In this context, for the conjugated polymer as the electron donor material in the active layer of PSCs, the main issues to be considered in their molecular design are broad absorption spectra to enhance sunlight harvest for higher J_{sc} , appropriate lower HOMO energy levels to maximize the V_{oc} and high hole mobility for higher J_{sc} and FF. Further, the suitable lowest LUMO energy level, matching with those of the fullerenes, is required to provide enough offset for charge separation. In addition, the morphology of the active layer plays a vital role in the performance of the solar cells.

The regio-regular poly(3-hexylthiophene) and PCBM based BHJ-PSCs have showed a significant enhancement in the power conversion efficiency (up to ~6 %) (Liang et al. 2009 and Piliago et al. 2010). However, P3HT based PSCs showed relatively low open-circuit voltage ($V_{oc} \sim 0.6$) as P3HT can utilize only less than 25 % of solar photons. Therefore, conjugated polymers with an optimized molecular geometry and a lower band gap are needed to replace P3HT for improved light harvesting in high performance BHJ-PSCs. Hence, various approaches have been used to synthesize new low band gap conjugated polymers. Among them, donor-acceptor polymers are shown to exhibit lower band gap energy. Further the HOMO

and LUMO energy levels of these polymers could be tuned by the proper choice of the donor and the acceptor units.

However, the bulk heterojunction device architecture using fullerene based electron acceptors have several drawbacks like they have negligible light absorption in the visible-near IR region, relatively poor photochemical and chemical stability requiring extensive encapsulation for the operation of the organic solar cells in air, the available chemistry for the synthesis of fullerene derivatives is limited and the cost of fullerene synthesis and purification is high (Ahmed et al. 2011). It is important to note that, the open-circuit voltage of polymer-fullerene based devices is typically limited to 0.8 V, which leads to the low PCE in the devices. The high open-circuit voltage can be achieved by adjusting smaller offsets of the HOMO and the LUMO levels of both polymer (donor) and acceptor units. This leads to the loss of less energy during the transfer of photoexcited electrons from the polymer donor to the acceptor molecule in PSCs.

In this regard, one can replace commonly used fullerene acceptor with a n-type organic semiconductor having desired HOMO and LUMO levels in PSCs. In this direction, the major challenges are to design and investigate new n-type organic semiconductors, which could potentially replace fullerene acceptors in PSCs. In view of this, various small organic semiconductors (Lloyd et al. 2007 and Anthony 2011) and conjugated polymers have been used as non-fullerene acceptor in the PSCs. Among them, some important n-type organic semiconductors studied are cyano-poly (phenylenevinylene) (Kietzke et al. 2005), cyanopentacenes (Lloyd et al. 2007), vinazene derivatives (Shin et al. 2007 and Woo et al. 2010), polyfluorene (benzothiadiazole) (McNeill et al. 2008), perylene diimides (Rajaram et al. 2009 and Sharma et al. 2010), bifluorenylidene (Brunetti et al. 2010) and diketopyrrolopyrrole derivatives (Sonar et al. 2010). The highest power conversion efficiency of BHJ solar cells using these n-type small molecules varies from 1.87 % PCE in perylene diimides derivatives (Sharma et al. 2010) and 1.4 % PCE in vinazene derivatives (Woo et al. 2010) to 1 % PCE in diketopyrrolopyrrole derivatives (Sonar et al. 2010). The major current challenges in developing more efficient non-fullerene BHJ polymer solar cells are the lack of suitable n-type organic semiconductors that combine solution processability with suitable HOMO/LUMO energy levels, good charge transport and

other properties. Indeed, the factors essential to the design and development of new electron acceptor materials for the realization of more efficient non-fullerene PSCs remain to be elucidated.

Keeping this in view, some of the D–A polymers synthesized in the present study which possess low band gap and appropriate HOMO and LUMO energy levels, may be considered as promising donor/acceptor material for PSCs. In particular, polymers **P5–P8** based on thiophene and cyanovinylene moieties showed low optical band gaps with broad absorption in the wavelength region of 400 – 700 nm. The electrochemical data of the polymers revealed that, they possess low-lying HOMO energy levels and hence expected to show high open-circuit voltage when polymers are used as electron donor materials in the devices. Figure 4.11 shows the energy level diagram of **P5–P8** in comparison with the HOMO/LUMO energy levels of P3HT, a frequently used electron donor material in BHJ solar cells. The LUMO energy levels of the polymers are comparable to the LUMO levels of various fullerene acceptors reported in the literature (Guan et al. 2010).

The HOMO/LUMO energy levels of the acceptor material relative to the HOMO/LUMO of the donor conjugated polymer, should offer sufficient offsets to facilitate photoinduced electron/charge transfer and efficient charge separation while maximizing the photovoltage. In case of donor polymer and acceptor fullerene BHJ solar cells, for efficient charge transfer and charge separation, the desired range of LUMO/LUMO offset (ΔE_{LUMO}) is 0.12 – 0.3 eV or higher (Coakley and McGehee 2004, Thompson and Frechet 2008) and the HOMO/HOMO offset (ΔE_{HOMO}) is in the 0.2 – 0.3 eV or higher (Zhang et al. 2008). By considering this criterion in case of non-fullerene acceptors, it can be concluded that the polymers **P5–P8** are promising candidates as acceptor materials in BHJ solar cells. For instance, if P3HT is considered as the donor material and the polymers as the acceptor material, then ΔE_{LUMO} is ~0.6 eV and ΔE_{HOMO} is ~0.5 eV, which are greater than the target 0.3 eV. Thus, the obtained energy level differences (ΔE_{LUMO} and ΔE_{HOMO}) suggest that these polymers are promising candidates for unrestricted and directed charge transfer when they are used as electron acceptor material in non-fullerene BHJ solar cells.

The photovoltaic properties of the polymers **P5–P8** were investigated by fabricating bulk heterojunction solar cells using polymers as electron donor and PC₇₁BM as the electron acceptor materials under 100 mW/cm² AM1.5 sunlight illumination in air. In the current-voltage characteristics of **P5** and **P8** based devices; it was observed that the devices were short. This may be attributed to the poor quality of polymer films and hence the results from them are not discussed. The non-fullerene bulk heterojunction solar cells were fabricated using the polymers **P6** or **P7** as the acceptor and poly(3-hexylthiophene) as the donor materials.

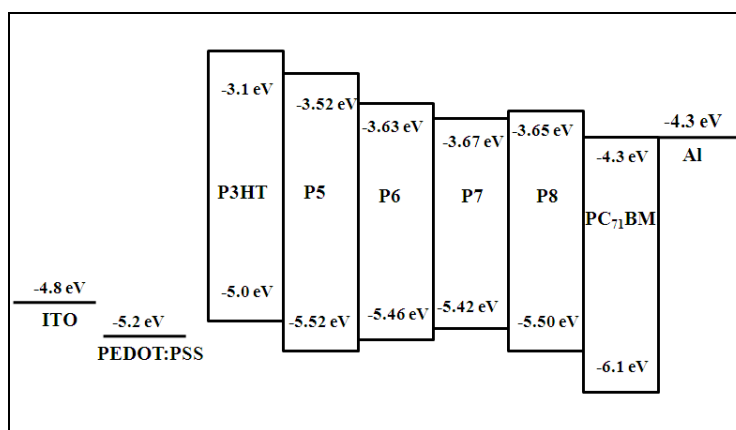


Figure 4.11 Energy level diagram of polymers **P5–P8**, PEDOT:PSS, P3HT and PC₇₁BM

4.3.1 Materials and instruments

Poly(3,4-ethylenedioxythiophene):poly(4-styrenesulfonate) (Clevios™ P VP Al 4083) was purchased from H.C. Starck, Germany. Poly(3-hexylthiophene) was purchased from Sigma Aldrich Chemical Company. [6,6]-Phenyl-C₇₁-butyric acid methyl ester was purchased from American Dye Source Inc. and used as received. ITO - coated glass substrates (10Ω/square) were purchased from Shanghai B. Tree Tech. Consult Co. Ltd, Shanghai, China. All solvents and other reagents were purchased commercially and used without further purification.

The current-voltage characteristics of the devices were measured by using a HP4155A semiconductor parameter analyzer (Yokogawa Hewlett-Packard, Tokyo). The light intensity of 100 mW/cm² AM1.5 sunlight from a filtered Xe lamp was

calibrated by a Si photodiode calibrated at the National Renewable Energy Laboratory (NREL). All the characterization steps were carried out under ambient laboratory air.

4.3.2 Fabrication of polymer solar cells

The photovoltaic properties of polymers **P6** and **P7** were evaluated by fabricating fullerene based bulk heterojunction solar cells of the device architecture ITO/PEDOT:PSS/**polymer:PC₇₁BM**/LiF/Al and by fabricating non-fullerene BHJ solar cells of the structure ITO/PEDOT:PSS/**P3HT:polymer**/LiF/Al. Initially, the ITO coated glass substrate was consecutively cleaned with detergent, then sonicated in acetone, isopropyl alcohol and subsequently dried in an oven overnight at 100 °C. The PEDOT:PSS layer was spin coated at 3500 rpm for 40 sec on top of the ITO coated glass, followed by baking at 150 °C for 10 min under vacuum before being transferred into a glove box. Here PEDOT:PSS layer improves the surface roughness of the substrate and improves and stabilizes the electrical contact between ITO and the active layer. The active layers for fullerene based bulk heterojunction solar cells (**P6:PC₇₁BM** and **P7:PC₇₁BM**) and for non-fullerene bulk heterojunction solar cells (**P3HT:P6** and **P3HT:P7**) were spin coated on top of the PEDOT:PSS layer with a thickness in the range of 60–80 nm. A solution of the donor and acceptor material of the composition 1:1 (wt:wt) was employed for this purpose. For **P6** based solar cell, the active layer was spin coated from 1,2-dichlorobenzene solution at room temperature and for **P7** based solar cell, the active layer was spin coated from the same solvent but at a temperature of 120 °C. Finally, the cathode layer was deposited consisting of a thin hole blocking layer of lithium fluoride (LiF) (1.0 nm) and aluminum layer (Al) (100 nm), by thermal evaporation under vacuum (8×10^{-7} torr). The fabricated solar cell has an active area of 9 mm².

4.3.3 Photovoltaic properties of polymers P6 and P7

The current density-voltage characteristics of the **P6:PC₇₁BM** and **P7:PC₇₁BM** blend solar cells under dark and under 100 mW/cm² AM1.5 solar illumination are shown in Figure 4.12. The measured photovoltaic parameters of **P6:PC₇₁BM** blend solar cells were, an open-circuit voltage of 0.55 V, a short-circuit current density of 3.33 mA/cm², fill factor of 0.3 and the average power conversion efficiency of 0.55 %. When **P7** was used as donor component in **P7:PC₇₁BM**, a higher open-circuit

voltage of 0.87 V was observed with a short-circuit current density of 0.75 mA/cm², fill factor of 0.28 and average power conversion efficiency of 0.18 %.

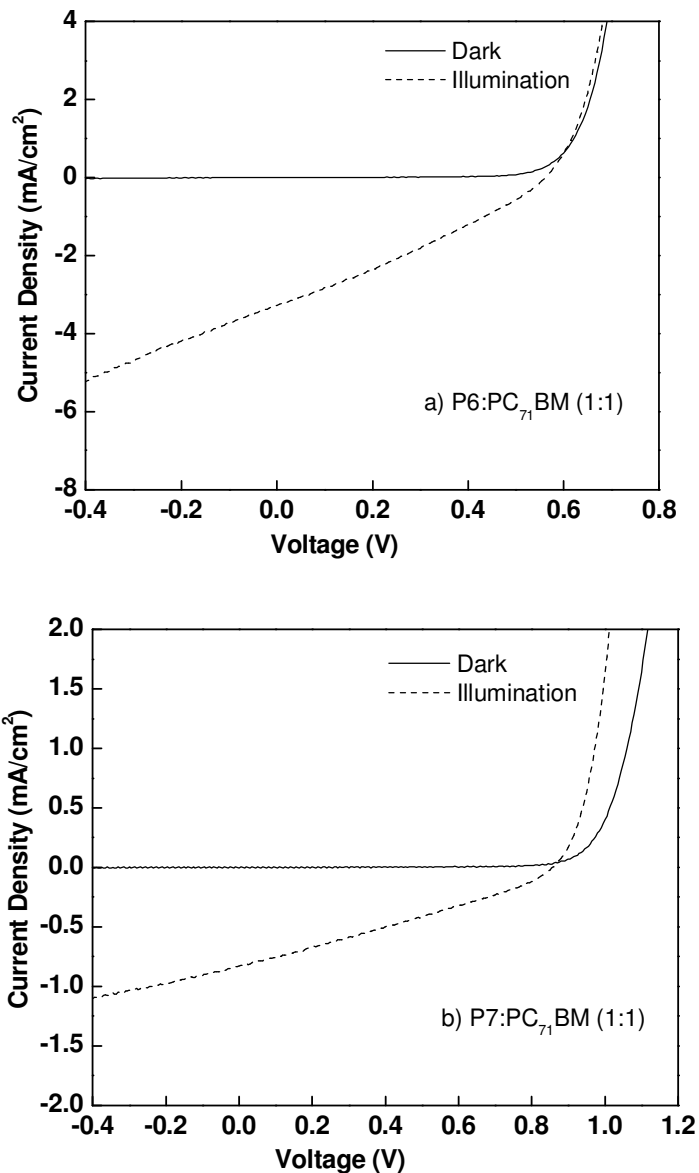


Figure 4.12 Current density-voltage curves of BHJ solar cells based on a) **P6:PC₇₁BM** and b) **P7:PC₇₁BM** in dark and under 100 mW/cm² AM1.5 solar illumination

The open-circuit voltage of solar cells can approximately be predicted by the energy differences between the HOMO of donor and LUMO of acceptor components (Ma et al. 2005). However, it is noteworthy that **P6** based solar cell exhibited lower

V_{oc} (0.55 V) compared to that of **P7** based solar cell, despite its (**P6**) lower HOMO energy level. This difference in V_{oc} cannot be explained only by the differences in the HOMO energy levels of donor and the LUMO levels of the acceptor components. This discrepancy from expectation may arise from a number of factors such as carrier recombination, blend morphology, resistance due to film thickness and the degree of phase separation, which have been reported to affect the open-circuit voltage (Perez et al. 2009 and Brabec et al. 2001). The measured J_{sc} and FF values of both the devices were low which could be because of poor film quality, lower charge separation and insufficient electron transfer in the devices (Yang et al. 2010). Further, it is believed that the device performance can be improved by the modification of the chemical structure of the polymers and device engineering such as optimized thickness, solvent, additive, buffer layer etc.

In non-fullerene bulk heterojunction solar cells, the polymers **P6** and **P7** were used as electron acceptor and P3HT as electron donor components. The current density-voltage characteristics of the **P3HT:P6** and **P3HT:P7** blend solar cell under dark and under 100 mW/cm^2 AM1.5 solar illumination are shown in Figure 4.13. The photovoltaic parameters, including V_{oc} , J_{sc} , FF and the power conversion efficiency are summarized in Table 4.1. Here also the observed variation of the V_{oc} from 0.78 V for **P3HT:P6** and 0.45 V for **P3HT:P7** cannot be fully understood on the basis of the differences in the energy levels of donor and acceptor materials, since the LUMO energy levels of the polymers are almost the same. The polymer solar cells based on polymer **P6** showed moderately high power conversion efficiency of 0.74 % with an open circuit voltage of 0.78 V. Although the photovoltaic performance of the polymers as electron acceptor material is low with relatively high V_{oc} , these results indeed demonstrate that the polymers **P6** and **P7** are potential as new electron acceptor materials in BHJ solar cell applications. Further, factors such as morphology of the polymer film and the light absorption range may also influence the device performance (Thompson et al. 2008 and Peet et al. 2009).

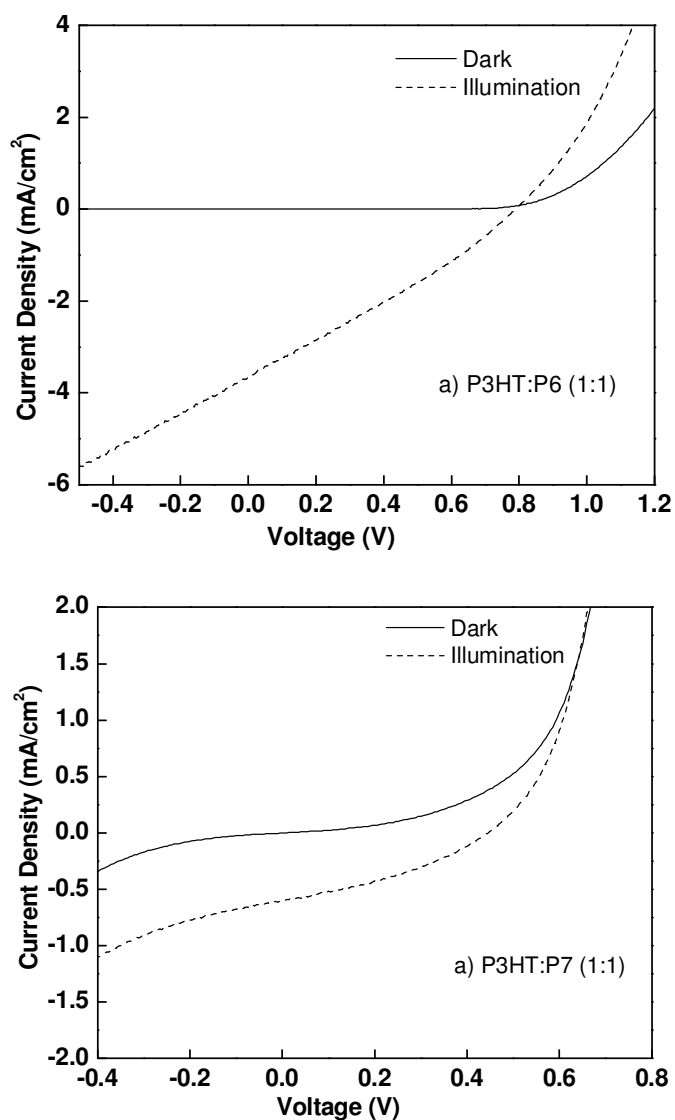


Figure 4.13 Current density-voltage curves of non-fullerene BHJ solar cells based on a) **P3HT:P6** and b) **P3HT:P7** in dark and under 100 mW/cm² AM1.5 solar illumination

Table 4.1 Photovoltaic properties of the BHJ polymer solar cells

Active layer (1:1, w/w)	V_{oc} (V)	J_{sc} (mA/cm ²)	Fill Factor (FF)	PCE %
P6: PC ₇₁ BM	0.55	3.33	0.30	0.55
P7: PC ₇₁ BM	0.87	0.75	0.28	0.18
P3HT: P6	0.78	3.36	0.28	0.74
P3HT: P7	0.45	0.60	0.33	0.08

4.4 CONCLUSIONS

The preliminary studies on electroluminescent and photovoltaic properties of the newly synthesized D–A conjugated polymers were performed by fabricating PLEDs and PSCs. Based on the results obtained in the optical and electrochemical studies as well as based on good film forming properties, some of the polymers among **P1–P12** were selected for the device fabrication. The PLED devices were fabricated with a configuration of ITO/PEDOT:PSS/polymer/Al using the polymers **P5**, **P9**, **P10** and **P12** as emissive layer. The polymer **P5** showed almost pure red emission with a CIE coordinate of (0.65, 0.32), which is very close to the CIE coordinate of standard red color. The PLEDs using **P9** as emissive layer emitted green light with a CIE coordinate of (0.34, 0.47) under a driving voltage of 5 V. The EL spectrum of the **P9** was red shifted relative to its photoluminescence spectra. The emission maximum of the electroluminescence device based on **P10** centered at 490 nm and emitted green light with CIE coordinates value of (0.25, 0.39) at 12 V. The EL device based on **P12** showed white light emission with CIE coordinate value of (0.32, 0.35) at 14 V, which is very close to the value (0.33, 0.33) for standard white light emission. The devices based on **P5** and **P10** showed good color stability under different bias voltages without any protective encapsulation. In addition, the current density of all the polymers increases exponentially with the increasing forward bias voltage, which is typically a diode characteristic. The polymers **P5**, **P9**, **P10** and **P12** showed low threshold voltages of 3.1, 6.5, 7.3 and 3.9 V respectively due to low-lying LUMO levels of the polymers.

The photovoltaic properties of low band gap polymers **P6** and **P7** were evaluated by fabricating BHJ solar cells using polymer as the electron donor material with the device configuration of ITO/PEDOT:PSS/polymer:PC₇₁BM/LiF/Al. The solar cell device based on **P7** exhibited relatively higher open-circuit voltage of 0.87 V. In addition, non-fullerene bulk heterojunction solar cells were fabricated with the configuration of ITO/PEDOT:PSS/P3HT:polymer/LiF/Al using polymer as the electron acceptor material. The solar cell device based on **P6** as electron acceptor demonstrated moderately high power conversion efficiency of 0.74 % with an open-circuit voltage of 0.78 V.

CHAPTER 5

STUDY OF NONLINEAR OPTICAL PROPERTIES OF THE POLYMERS AND POLYMER/TiO₂ NANOCOMPOSITES

Abstract

In this chapter, the nonlinear optical properties of the donor-acceptor conjugated polymers studied using z-scan technique are discussed. The chapter also describes the preparation and characterization of conjugated polymer/TiO₂ nanocomposites and their z-scan studies.

5.1 INTRODUCTION

Conjugated organic molecules and polymers offer exciting opportunities in the area of nonlinear optics due to their possible applications in all-optical devices such as optical limiters, optical switches and optical modulators (Zyss 1994). As a result, in the last three decades, there has been great interest in the synthesis of novel monomers and polymers with the intention of producing materials having large nonlinear optical properties. The study has been focused mainly on finding materials with large nonlinear optical effects, fast responses, good solubility, processability and high durability. In this direction, conjugated polymers are a promising class of third-order nonlinear materials because of their potentially large third-order susceptibilities associated with fast response time in addition to their variety and processability. Further, the strong delocalization of π -electrons in conjugated polymeric backbone determines a very high molecular polarizability and thus remarkable third-order optical nonlinearities (Prasad and David 1991). Moreover, these macromolecules offer good flexibility at both molecular and bulk levels so that structural modifications necessary to optimize them for specific device applications are possible. As the nonlinear response of these systems is determined primarily by their chemical structure, one can design unique molecular structures and synthesize compounds with enhanced nonlinear response by introducing suitable substituent groups. In this regard, a deeper understanding of the structure-property relationship would help in designing new organic conjugated molecules and polymers by the judicious choice of functional substituents, and thus to tune their optical properties for photonic applications.

In this direction, design of D–A conjugated polymers containing proper electron rich and electron deficient moieties along the polymer backbone is emerging as a promising strategy for tuning the linear and nonlinear optical properties of conjugated

polymers (Cassano et al. 2002, Kiran et al. 2006 and Ramos-Ortiz et al. 2010). Here the presence of alternate electron donor and electron acceptor units in the polymer backbone would enhance the NLO properties of the polymer, mainly due to increase in effective π -electron delocalization. Among various π -conjugated materials, thiophene based polymers are currently under intensive investigation as materials for nonlinear optics because of their large third order response, chemical stability, readiness of functionalization and their good film forming characteristics (Nisoli et al. 1993, Kishino et al. 1998 and Hegde et al. 2010). Additionally, the NLO properties in poly(thiophene)s can be synthetically tuned by introducing electron releasing and electron accepting segments in the polymer chain (Gubler et al. 2002, Ronchi et al. 2003 and Ellinger et al. 2011).

Metal and semiconductor nanoparticles exhibit characteristic size and shape dependent electronic structure leading to unique optical and nonlinear optical properties (Gayvoronsky et al. 2005 and Porel et al. 2007). These attributes find application in a wide range of fields including electronics, photonics, plasmonics and sensing. Further, the plasmon absorption of metal nanoparticles such as copper, silver, gold and palladium occur in the UV-Vis region of the spectrum. Multi photon excitations in this energy range and further excited state absorptions can be exploited to elicit NLO responses from these nanomaterials. For instance, a third-order NLO susceptibility ($\chi^{(3)}$) value of 0.8×10^{-12} esu has been observed for yellow Ag colloidal nanoparticles (Chen et al. 2008). A large third-order NLO susceptibility value as high as 2×10^{-5} esu has been observed for nanoporous layers of titanium dioxide (TiO_2) (Gayvoronsky et al. 2005).

From a material point of view, it is advantageous to embed metal/semiconductor nanoparticles in thin polymer films for optical applications. The polymer matrix serves not only as a medium to assemble the nanoparticles and stabilize them against aggregation but also with its characteristic mechanical properties suits for device applications. Nanocomposites wherein materials are mixed on the nanoscale are of particular interest as they combine the properties of two or more different materials with the possibility of observing novel mechanical, electronic or chemical behaviors (Sih and Wolf 2005). Further, nanocomposite structures are also known to enhance optical nonlinearities substantially. According to the local field enhancement under

the surface plasmon resonance condition, larger third-order nonlinearity of composite films has been observed in the presence of metal nanoparticles. These high nonlinear materials have been thought to be good candidates for new optical and electronic devices. As a result, several conjugated polymer-metal/semiconductor nanocomposites have been prepared from a range of different metals, and with different types of conjugated polymers. The effects of this on the optical properties of the nanoparticles, electronic behavior of both the nanoparticles and conjugated materials, and some applications have been investigated.

For instance, a larger third order nonlinearity of polydiacetylene (PDA) composite films has been observed in the presence of metal/semiconductor nanoparticles (Masuhara et al. 2001). In wake of this observation, later on the third-order NLO optical properties of other such metal/semiconductor polymer nanocomposites have been investigated. Chen et al. (2008) reported the synthesis of nanometer-size silver-coated PDA composites. NLO properties of these PDA/Ag nanocomposite vesicles were measured by the z-scan technique. The value of nonlinear refractive index (n_2) for pure PDA vesicles was $1.2 \times 10^{-14} \text{ cm}^2\text{W}^{-1}$ and for PDA/Ag nanocomposite vesicles (on the outer surface) was $7.3 \times 10^{-14} \text{ cm}^2\text{W}^{-1}$. Nearly seven times enhancement of n_2 value was observed as a result of local field enhancement under the surface plasmon resonance of silver nanoparticles at the interface. The two-photon absorption (2PA) of poly(styrene maleic anhydride)/TiO₂ nanocomposites was studied by Wang et al. (2001) by z-scan technique. Based on the 2PA, they have investigated the optical limiting behavior of the nanocomposites. Sezer et al. (2009) reported the synthesis and nonlinear optical properties of poly(aniline) and poly(aniline) silver nanocomposite thin films. Chen et al. (2010) reported the synthesis of poly (substituted diacetylene) (PNADA)/silver nanocomposites. The silver nanoparticles were dispersed in the polymer films. The introduction of silver nanoparticles into the polymer films led to the enhancement of nonlinear optical properties. The value of nonlinear refractive index for PNADA/Ag nanocomposite films was $11.6 \times 10^{-15} \text{ cm}^2 \text{W}^{-1}$.

Thus it is evident that a combination of conjugated polymer and metal/semiconductor nanoparticles in the form of nanocomposites show improved optical and NLO properties in comparison with those of conjugated polymers alone. In this

regard, TiO₂ nanomaterials have attracted much attention and their optical nonlinearities have been extensively investigated. By the incorporation of TiO₂ nanoparticles into conjugated polymers, could improve the mechanical, electrical and optical properties of the nanocomposite. These composite materials have attracted interest in both fundamental studies and applications: inorganic semiconducting nanoparticles for their small size and novel properties, and conjugated polymers for their attributes as easily processed semiconductor materials with potential in optoelectronic applications. However so far, there is no report available in the literature on NLO studies of thiophene based D–A conjugated polymer/TiO₂ nanocomposites.

There are various phenomena responsible for the nonlinear absorption property exhibited by the optical materials. The materials with different nonlinear absorption processes such as saturable absorption, reverse saturable absorption, two-photon absorption and multi-photon absorption are promising in the different applications of science and technology (Sutherland 1996 and He et al. 2007). For example, the saturable absorption (SA) materials (the transmittance increases with the increase of optical intensity) have been used in lasers as Q-switching elements. Two-photon absorption (2PA), three-photon absorption (3PA), multiphoton absorption (MPA) and reverse saturable absorption (RSA) materials (their transmittances reduce with the increase of optical intensity) have been used in two-photon microscopy and optical limiters. Therefore, in case of materials showing nonlinear absorption properties it is necessary to identify their nonlinear absorption effects, and to determine their nonlinear absorption parameters, such as the saturable intensity for saturable absorber, the MPA coefficient for multi-photon absorbing material. The mechanism of number of nonlinear absorption processes can be represented in an energy level diagram as shown in Figure 5.1. The diagram shows the different energy levels of a molecule, the singlet ground state S₀, the excited singlet states S₁ and S₂, as well as the triplet excited states T₁ and T₂. It also displays the different transitions between the energy levels.

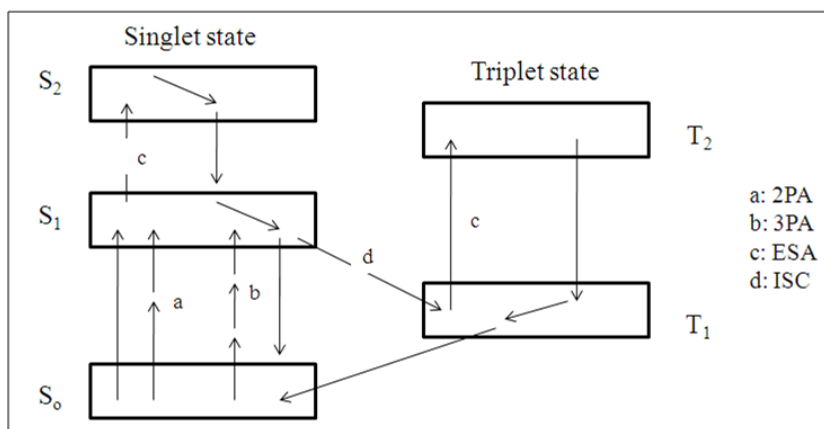


Figure 5.1 Energy level diagram showing 2PA, 3PA, ESA and ISC

When two photons, of the same or different energy are simultaneously absorbed from the ground state to a higher excited state (S_0 to S_1), it is denoted as two-photon absorption. When the excited state absorption (ESA) occurs, molecules are excited from an already excited state to a higher excited state (e.g. S_1 to S_2 and/or T_1 to T_2). For this to happen the population of the excited states (S_1 and/or T_1) needs to be high so that the probability of photon absorption from that state is high. Therefore high intensity light is needed to pump up the molecules to the excited state before a substantial amount of ESA to take place. The ESA could be enhanced if the molecules could undergo intersystem crossing (ISC) to the triplet state. If more absorption occurs from the excited state than from the ground state it is usually called reverse saturable absorption. The triplet excited state absorption may result in RSA if the absorption cross-section of triplet excited state is greater than that of singlet excited state.

5.2 EXPERIMENTAL SECTION

The NLO properties of newly synthesized D–A conjugated polymers (**P1–P12**) in solution state were investigated using z-scan technique. Further, polymers **P1** and **P5** were used to prepare polymer/TiO₂ nanocomposite films. The resulting polymer nanocomposites were characterized by FTIR, UV-Vis absorption spectroscopy, field emission scanning electron microscopy (FESEM) and thermogravimetric analysis. The NLO properties of the nanocomposites were also investigated and were compared with those of the polymers.

5.2.1 Materials and instrumentation

Nano sized TiO_2 powder was purchased from Sigma Aldrich Chemical Co. All solvents and other reagents were purchased commercially and used without further purification. FESEM images were obtained with a CARL ZEISS SUPRA 40 VP (NTS GmbH Germany) field emission scanning electron microscopy.

5.2.2 Z-scan measurements

The “open aperture” z-scan technique has been widely used method (Sheik Bahae et al. 1990) to measure the nonlinear absorption properties of various materials. In this method, a laser beam is used for optically exciting the sample and its propagation direction is considered as the z-axis. The beam is focused using a convex lens and the focal point is taken as $z = 0$. Obviously, the beam will have maximum energy density at the focal point, which will symmetrically reduce towards either side of it, for the positive and negative values of z . The schematic representation of open aperture z-scan experimental set up is given in Figure 5.2. In the experiment, the sample was placed in the beam at different positions with respect to the focus (i.e. at different values of z), and the corresponding optical transmission values were measured. Then a graph was plotted between z and the measured sample transmission (normalized to its linear transmission), which is known as the z-scan curve. The shape of the z-scan curve will provide information on the nature of the nonlinearity viz. reverse saturable, two photon absorption, three photon absorption, saturable absorption etc. By fitting the experimental data to theory, the parameters like nonlinear absorption coefficient (β), saturation intensity (I_s) of the sample can be calculated. The experimental data are very useful in assessing the NLO behavior of the sample under study.

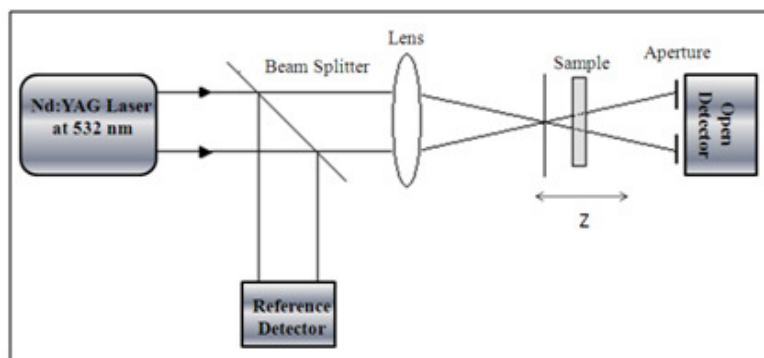


Figure 5.2 The open aperture z-scan setup

In the z-scan experiment a stepper-motor controlled linear translation stage was used to move the sample through the beam in precise steps. Two pyroelectric energy probes (Rj7620, Laser Probe Inc.) were used to measure the transmission of the sample at each point. One energy probe monitors the input energy, while the other monitors the transmitted energy through the sample. The second harmonic output (532 nm) of a Q-switched Nd:YAG laser (Minilite-Continuum, 5 ns full width at half maximum laser pulses) was used for excitation of samples. The experiments were carried out in the “single shot” mode, allowing sufficient time between successive pulses to avoid accumulative thermal effects in the sample. The experiment was automated, controlled by a data acquisition program written in Lab VIEW.

5.3 RESULTS AND DISCUSSION

5.3.1 Nonlinear optical properties of polymers P1–P12

In the z-scan experiment, the linear transmittance of all the samples studied was fixed between 50 and 60 %. The laser pulse energies used to excite the samples were between 75 and 100 μJ . The open aperture z-scan curves of polymers **P1–P4** and **P9–P12** in chloroform solution are given in Figures 5.3 and 5.4 respectively. The samples show a strong optical limiting behavior; i.e., the transmission of the sample gets decreased as the input light intensity increases (intensity is maximum at $z = 0$). In polymer systems under resonant excitation conditions, an optical limiting behavior can be attributed to effects such as excited state absorption (excited singlet and/or triplet absorption), two or three-photon absorption (2PA or 3PA), and self-focusing/defocusing. Of these, 2PA or 3PA and self focusing/defocusing are electronic nonlinearities that require high laser intensities usually available only from pulsed picosecond or femtosecond lasers. Therefore the cause of the observed optical limiting turns out to be excited state absorption. The net effect is then known as “effective” 2PA process. The nonlinear transmission behavior of the present samples can be modeled by defining an effective nonlinear absorption coefficient of the form,

$$\alpha(I) = \frac{\alpha_0}{1 + \left(\frac{I}{I_s}\right)} + \beta I \dots\dots\dots (5.1)$$

where α_0 is the unsaturated linear absorption coefficient at the wavelength of excitation, I is the input laser intensity, I_s is the saturation intensity (intensity at which the linear absorption drops to half of its original value) and β is the effective 2PA coefficient. For calculating the transmitted intensity for a given input intensity, the propagation equation 5.2 was numerically solved.

$$\frac{dI}{dz'} = - \left[\left(\alpha_0 / \left(1 + \frac{I}{I_s} \right) \right) + \beta I \right] I \dots\dots\dots (5.2)$$

Here z' indicates the propagation distance within the sample. By determining the best-fit curves for the experimental data, the nonlinear parameters could be calculated. In the z-scan curves (Figures 5.3 and 5.4), circles are data points while the solid curve is a numerical fit according to equation 5.2.

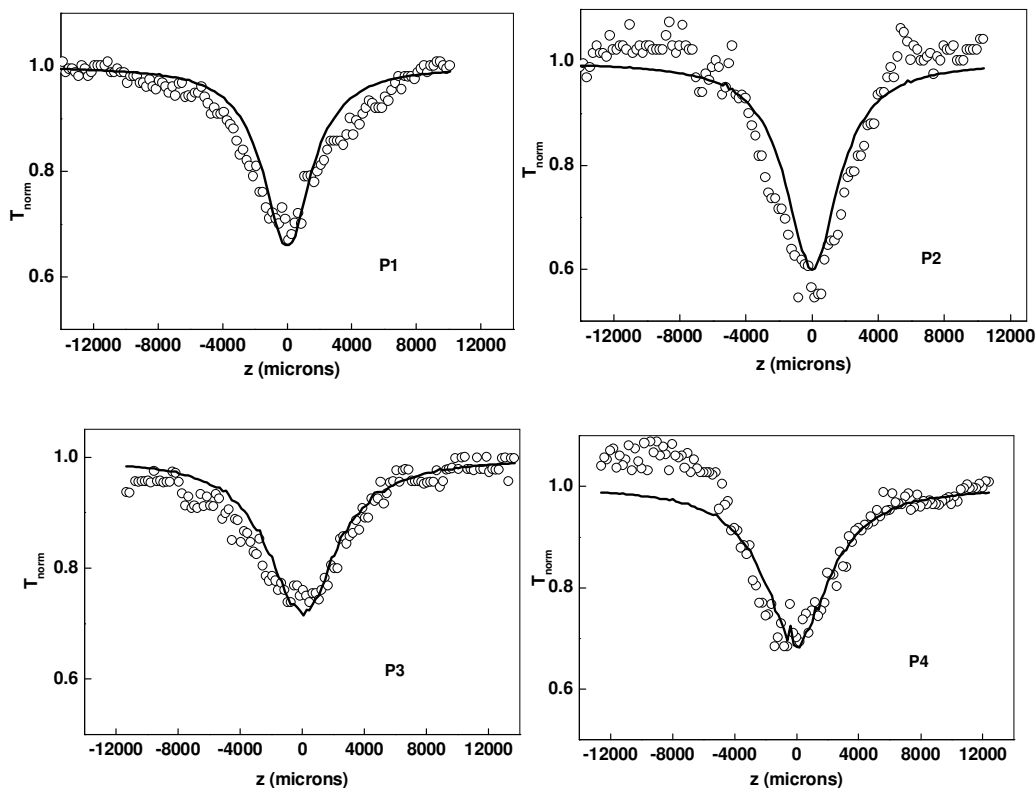


Figure 5.3 Z-scan curves of polymers **P1–P4**

The effective 2PA coefficient (β) of the polymers was found to be of the order of 10^{-10} – 10^{-12} m/W. The estimated β values of the polymers are summarized in Table

5.1. The higher β values observed for these polymers could be attributed to the effective π -electron delocalization along the polymer backbone due to the D–A arrangement. The β values of **P1** and **P2** was found to be of the order 10^{-10} m/W. The chemical structures of the polymers **P1** and **P2** are almost similar and hence no much difference in their β value was observed. The observed improvement in NLO behavior of these polymers could be attributed to the regular (alternating) D–A structure of the polymer chains. For **P3** and **P4**, the β value was found to be of the order 10^{-11} m/W. The β value for **P9** was determined to be 3.5×10^{-10} m/W, where as for **P10** it was found to be 3.3×10^{-12} m/W.

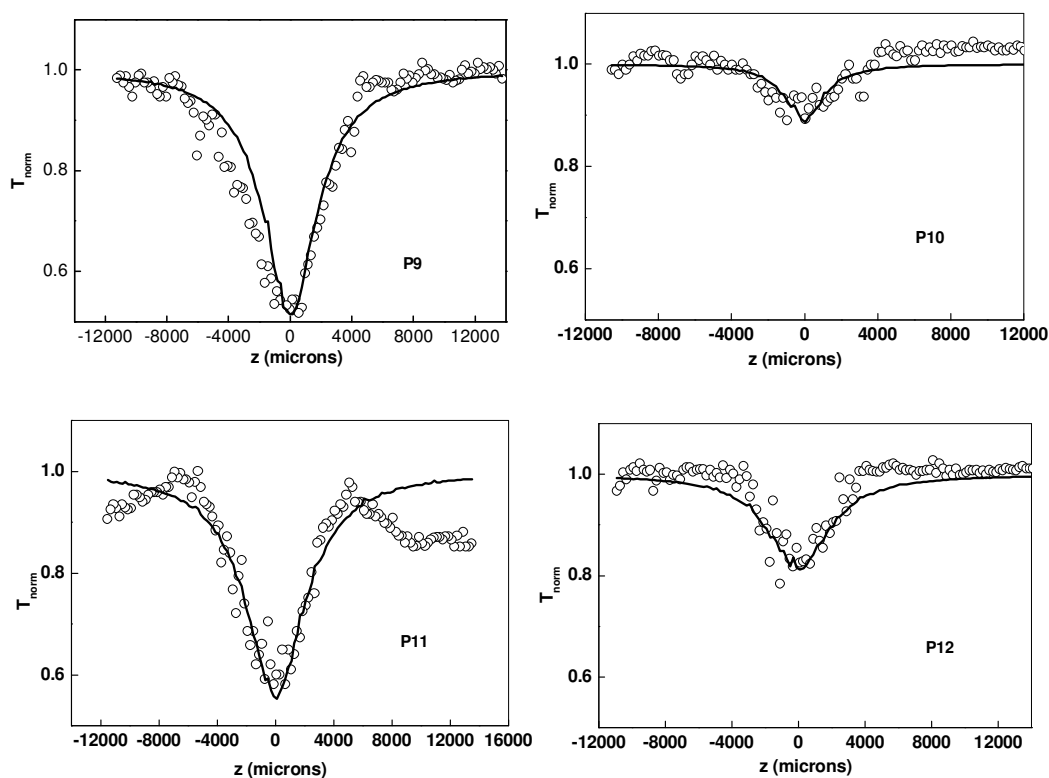


Figure 5.4 Z-scan curves of polymers **P9–P12**

The observed β value of **P9** is almost 100 times higher than that of **P10**. The enhancement of NLO response in **P9** could be due to the presence of strong electron donating fluorenevinylene unit in the polymer backbone which extends the π -electron delocalization in the polymer. Whereas, the presence of nonplanar biphenyl ring attached to the 1,3,4-oxadiazole ring in **P10** limits the π -electron delocalization along

the polymer chain. Polymers **P11** and **P12** showed β values of the order 10^{-11} m/W. The β value of **P11** is slightly higher than that of **P12** which could be attributed to the presence electron rich thiophene unit in **P11**.

Overall, in the present study, polymers **P1**, **P2** and **P9** showed the highest nonlinearity with promising optical limiting behavior. The β value was found to be 4×10^{-10} m/W, 3×10^{-10} m/W and 3.5×10^{-10} m/W respectively for **P1**, **P2** and **P9**.

Table 5.1 Effective 2PA coefficient (β) of the polymers

Polymer	Structure	Effective 2PA coefficient, β (m/W)
P1		4×10^{-10}
P2		3×10^{-10}
P3		4.4×10^{-11}
P4		3.1×10^{-11}
P9		3.5×10^{-10}
P10		3.3×10^{-12}
P11		5.3×10^{-11}
P12		1.0×10^{-11}

For comparison, under similar excitation conditions, the effective 2PA coefficient values of some materials are $10^{-10} - 10^{-12}$ m/W for Cu nanocomposite glasses (Karthikeyan et al. 2008), 3×10^{-11} m/W for functionalized carbon nanotubes (He et al. 2009) and 0.53×10^{-10} m/W for bismuth (Bi) nanorods (Sivaramakrishnan et al. 2007). Further, the obtained β values are comparable with some important D–A conjugated polymers reported in the literature (Hua et al. 2004 and Qian et al. 2009). Overall, the observed results indicate that the present samples exhibit an improved optical nonlinearity and hence expected to be promising candidates for optical limiting applications.

The z-scan profile usually shows a valley with a maximum and a minimum on each side of the focal point. However, the open aperture z-scan profile of polymers **P5–P8** showed a typical peak, symmetric about the focus, which is known to be the signature of saturable absorption phenomenon (Figure 5.5). The peak appears at the focal point where the laser pulse has the strongest fluence. The linear absorption spectra of the **P5–P8** further confirm the observed saturation behavior, where the excitation wavelength of 532 nm is close to their absorption peak, which is a favorable situation for the absorption saturation. Saturable absorption is a property of a material where the absorption of light decreases with the increase of light intensity. At sufficiently high incident light intensity, atoms or molecules in the ground state of a saturable absorber material become excited into upper energy state at such a rate that there is insufficient time for them to decay back to the ground state before the ground state becomes depleted, and the absorption subsequently saturates. One consequence of saturable absorption is optical bistability. Certain nonlinear optical systems can possess more than one output state for a given input state. The term optical bistability refers to the situation in which two different output intensities are possible for a given input intensity. Also, the term optical multistability is used to describe the circumstance in which two or more stable output states are possible. A similar type of saturable absorption behavior in the near-field transmission was observed for inorganic materials (Cassano et al. 2001).

The z-scan curves (Figure 5.5) obtained were fitted with numerically simulated results using equation 5.3 (Boyd 2007)

$$\alpha = \alpha_0 \frac{1}{1 + \left(\frac{I}{I_s}\right)} \dots \dots \dots (5.3)$$

where α_0 is the linear absorption coefficient at the wavelength of excitation, I is the incident intensity and I_s is the saturation intensity (intensity at which the absorption becomes half of the linear absorption).

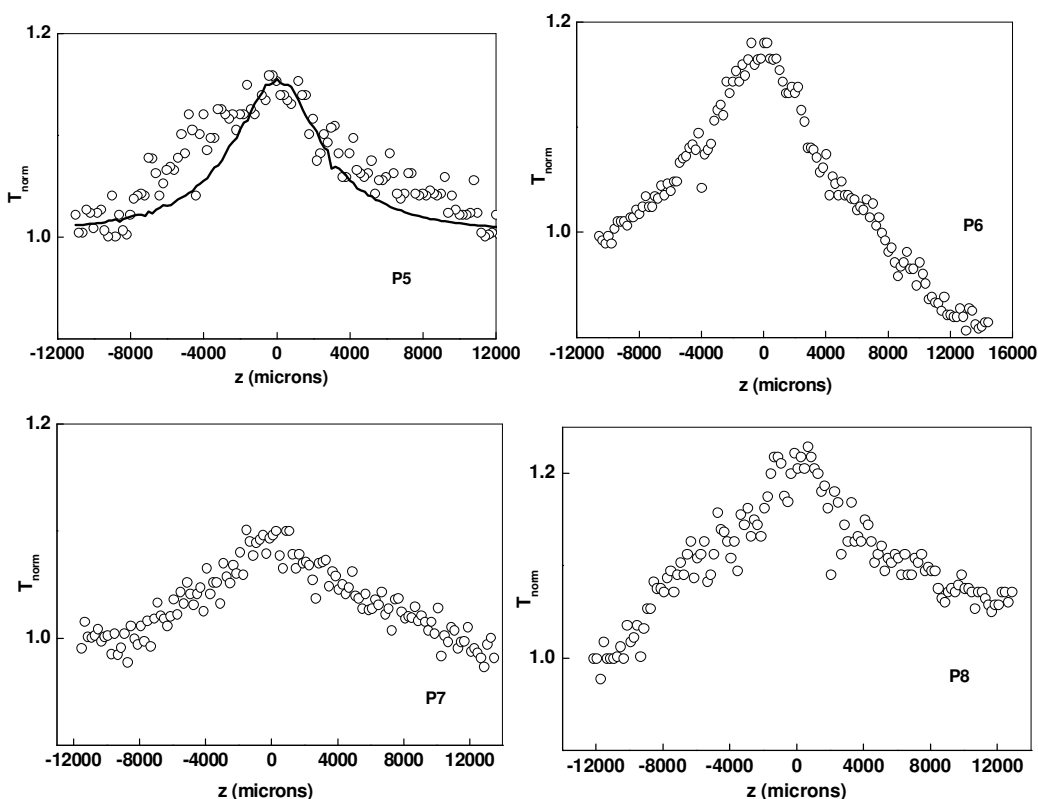


Figure 5.5 Z-scan curves of polymers **P5–P8**

By determining the best-fit curves for the experimental data, the nonlinear parameters could be calculated. In Figure 5.5, circles denote the experimental data points and the solid line is a theoretical fit with equation 5.3. For **P5** solution, saturation intensity (I_s) was found to be $2 \times 10^{12} \text{ W/m}^2$. The experimental data of

P6–P8 do not significantly fit to the theoretical equation 5.3. Hence, their nonlinear optical parameters were not determined.

Generally, reverse saturable absorption and saturable absorption are the two basic excited state absorption processes taking place in organic materials. If the excited state has strong absorption compared to ground state, the transmission can exhibit RSA behavior. These nonlinear absorption processes are highly dependent on the excitation wavelengths, intensities and excited state lifetime of the molecules. The most important application of RSA materials is in optical limiting devices used for the protection of sensitive optical devices. Optical limiting is defined as any process which limits the amount of light that can get through a material at high intensity. Moreover, optical limiters for low power continuous wave (cw) lasers are very important in applications such as optical damage protection of extremely sensitive sensors including human eyes, which are vulnerable to damage even with a few mW of radiation from a laser pointer. Also, they find applications in pulse smoothing, pulse shortening, mode locking, spatial light modulation etc. Further, when the frequency of incident light is near to the absorption resonance of the material, the absorption may saturate as the intensity increases. The saturable absorption materials are mainly useful in the areas of optical communication and optical computing, particularly for Q-switching and mode-locking lasers. Because the lowest loss occurs when the laser modes are locked together into pulses, introduction of a saturable absorber into a laser cavity enables it to passively mode-lock, an important way to generate ultra-short pulses. Saturable absorbers are also useful for nonlinear filtering outside laser resonators, which can clean up pulse shapes. Saturable absorption is particularly strong in semiconductor lasers at wavelengths just above the band edge.

Polymer **P1** which showed strong optical limiting behavior and **P5** which showed interesting saturable absorption behavior along with good film forming properties were used to prepare polymer/TiO₂ nanocomposite films. The prepared nanocomposites were characterized and the z-scan method was employed to study their NLO properties.

5.3.2 Preparation and characterization of polymer/TiO₂ nanocomposites

For the preparation of polymer/TiO₂ nanocomposites, 10 weight % TiO₂ nanoparticles were dispersed in the polymer using chloroform/chlorobenzene solvent system (10:1 volume ratio) and sonicated for 2 h. Smooth and optically clear thin polymer films on glass substrates were obtained by spin-coating the chloroform solutions of the polymer (1 mg mL⁻¹) at a spin rate of 1500 rpm. In a similar way nanocomposite films were also prepared. The polymer and the nanocomposite films were dried under vacuum for 1 h. Figure 5.6 shows the FESEM images of **P1**/TiO₂ and **P5**/TiO₂ nanocomposites. A moderately uniform distribution of TiO₂ nanoparticles was observed with average particle sizes ranging from 25 to 50 nm. The thickness of polymer films and nanocomposite films were determined by SEM cross section and was found to be in the range 0.9 – 1 micrometer.

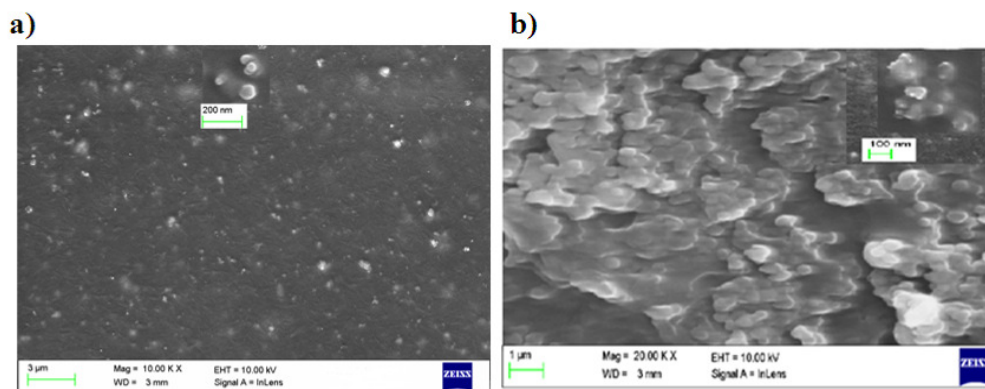


Figure 5.6 FESEM images of a) **P1**/TiO₂ nanocomposite and b) **P5**/TiO₂ nanocomposite film (inset: magnified image, Mag=100 KX)

The FTIR spectra of **P1**, TiO₂ nanoparticles and **P1**/TiO₂ nanocomposite are shown in Figure 5.7 (a). The strong bands at 2919 and 2851 cm⁻¹ in the FTIR spectrum of **P1** are due to (-C-H) stretching vibrations of the alkyl chains. The band at 1572 cm⁻¹ is assigned to the imine >C=N in an oxadiazole ring. The band at 1043 cm⁻¹ is due to the oxadiazole =C-O-C= stretching vibration. The FTIR spectrum of TiO₂ nanoparticles exhibits a band at 3395 cm⁻¹ due to O-H stretching mode of Ti-OH. The characteristic absorption band of Ti-O-Ti was observed at 472 cm⁻¹. All these characteristic bands arising from both **P1** and TiO₂ nanoparticles were observed in the FTIR spectrum of **P1**/TiO₂ nanocomposite, confirming the incorporation of TiO₂

nanoparticles in the nanocomposite. A similar spectral trend was observed also for **P5**/TiO₂ nanocomposite and its FTIR spectrum is given in Figure 5.7 (b).

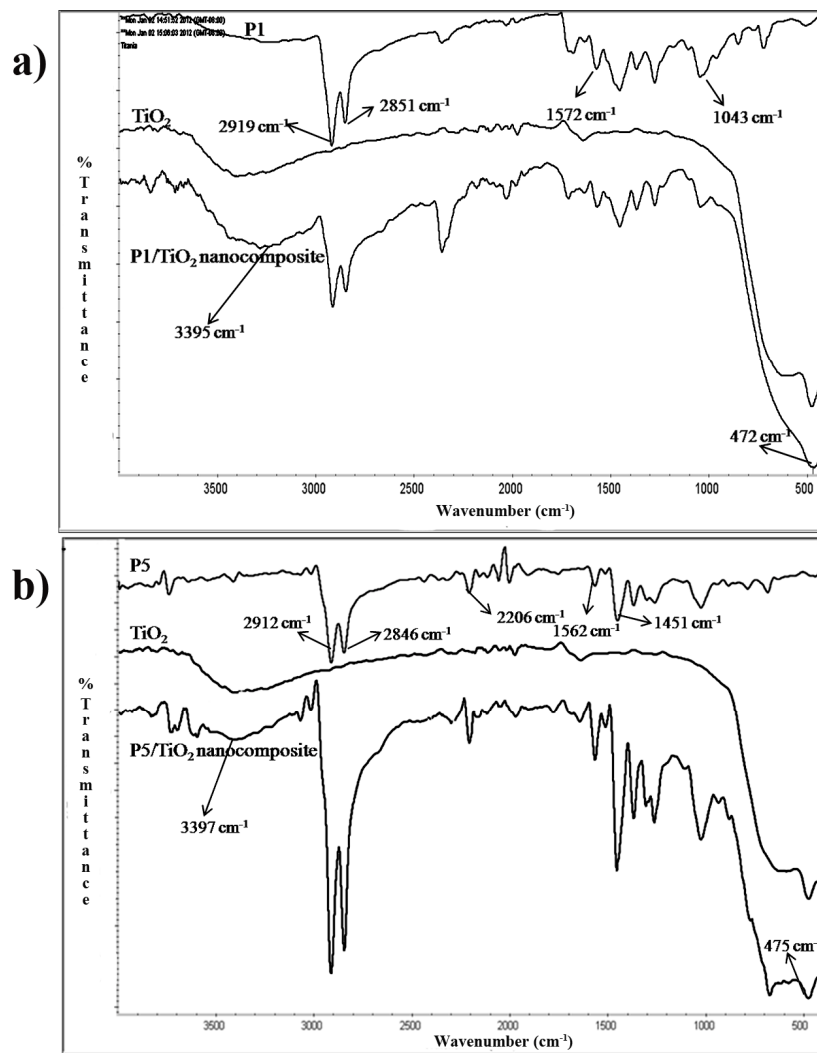


Figure 5.7 FTIR spectra of a) **P1**, pure TiO₂ nanoparticles and **P1**/TiO₂ nanocomposite and b) **P5**, pure TiO₂ nanoparticles and **P5**/TiO₂ nanocomposite

5.3.2.1 Linear optical properties of polymer/TiO₂ nanocomposites

The UV-Vis absorption spectra of polymer **P1** in chloroform solution, polymer thin film and P1/TiO₂ nanocomposite film are shown in Figure 5.8. Polymer **P1** in solution displayed an absorption maximum at 378 nm while its film showed a red shift of 16 nm in the absorption spectrum. The polymer **P1**/TiO₂ nanocomposite film

showed absorption peaks at 412 nm ($\pi \rightarrow \pi^*$ of polymer) and at 310 nm and a shoulder at 250 nm (characteristic absorptions of TiO_2). Incorporation of TiO_2 nanoparticles causes a slight red shift in the absorption maximum. The absorption maximum of the nanocomposite film shifts about 18 nm as compared that of the polymer film.

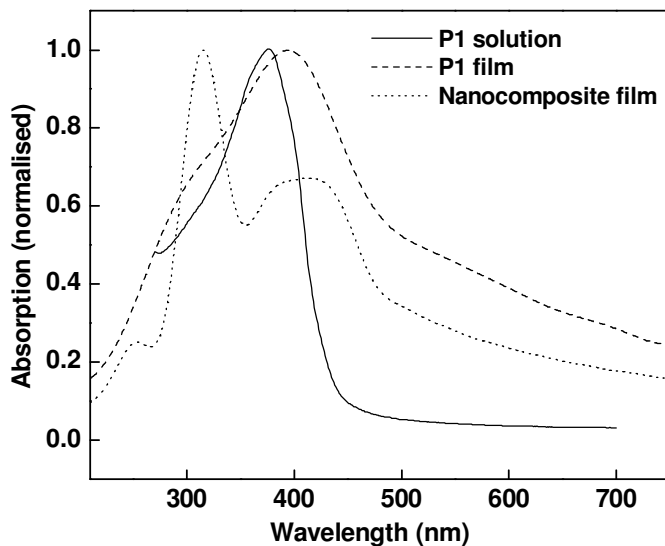


Figure 5.8 UV-Vis absorption spectra of **P1** in chloroform solution, **P1** thin film and **P1/TiO₂** nanocomposite thin film

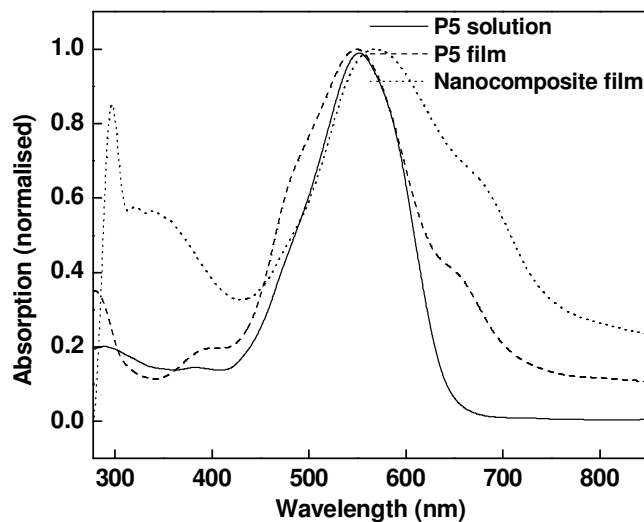


Figure 5.9 UV-Vis absorption spectra of **P5** in chloroform solution, **P5** thin film and **P5/TiO₂** nanocomposite thin film

Similarly a red shift of about 18 nm in the absorption maximum was observed for **P5**/TiO₂ nanocomposite film as compared to that of **P5** film (Figure 5.9). The observed red shifts in the absorption maxima can be understood in terms of effective π -conjugation length in polymer/TiO₂ nanocomposite films which is longer than that in pure polymer films. Similar red shift in the absorption maximum was observed for MEH-PPV/TiO₂ nanocomposite films (Yang et al. 2007). These optical results indicate that some interactions occur between the conjugated polymer chains and TiO₂ nanoparticles in the nanocomposite structure.

5.3.2.2 Thermal stability of polymer nanocomposites

Thermogravimetric analysis of polymers **P1** and **P5** and their nanocomposites were carried out under nitrogen atmosphere at a heating rate of 5 °C/min. As shown in Figure 5.10, polymer **P1** decomposes slowly in the temperature region 180 – 310 °C whereas the onset decomposition temperature of **P1**/TiO₂ nanocomposite was observed at 300 °C, indicating that the nanocomposite is thermally more stable than the polymer. A similar trend in the thermal stability was observed also for **P5**/TiO₂ nanocomposite. It is evident from the TGA traces given in Figure 5.11 that the nanocomposite is thermally stable up to 300 °C. When the temperature was increased beyond 300 °C, there was a sharp weight loss in the temperature range 350 – 650 °C. These results indicate that there is a strong interaction exists at the interface of polymer and TiO₂ nanoparticles in the nanocomposite. A similar trend in the thermal behavior was observed for polymer nanocomposites reported in the literature (Zhu et al. 2008). The improved thermal stability in polymer/TiO₂ nanocomposites could be explained through the reduced mobility of the polymer chains in the nanocomposite. Consequently, the degradation process will be slowed and hence decomposition will take place at higher temperature in the nanocomposite structure.

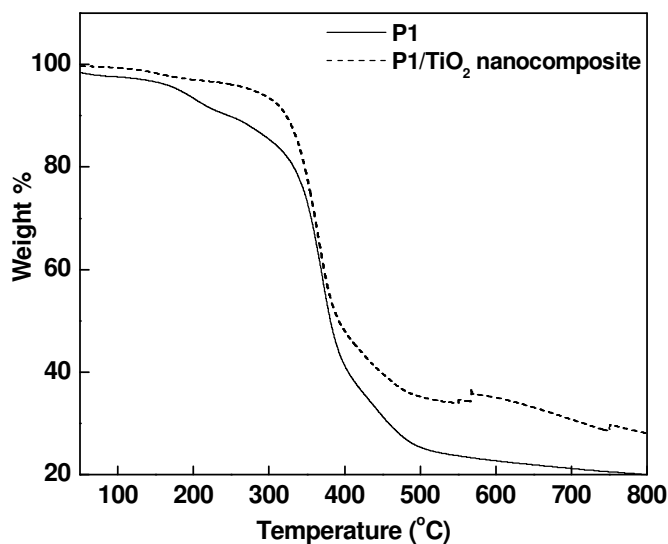


Figure 5.10 TGA curves of **P1** and **P1/TiO₂** nanocomposite

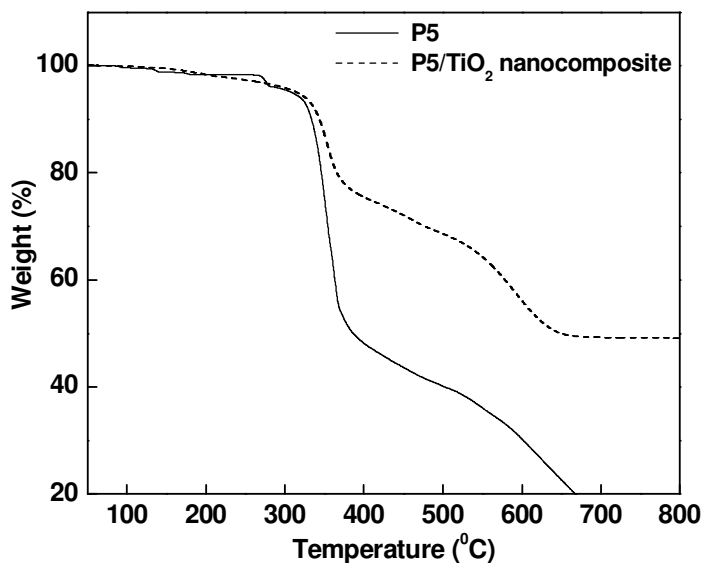


Figure 5.11 TGA curves of **P5** and **P5/TiO₂** nanocomposite

5.3.3 Nonlinear optical properties of polymers **P1** and **P5** films and polymer/TiO₂ nanocomposite films

In the z-scan experiment, the linear transmittances of the film samples studied were between 50 and 60 %. The laser pulse energies used for **P1** and its nanocomposites were between 75 and 100 μJ . The open aperture z-scan curves obtained for **P1** and **P1/TiO₂** films are given in Figure 5.12. Both films show a strong

optical limiting behavior; i.e., the transmission of the sample gets decreased as the input light intensity increases. The effect is quite strong because the normalized transmission gets decreased to values like 0.1. The observed optical limiting behavior under the present experimental conditions can be attributed to effects such as excited state absorption, thermal blooming and induced thermal scattering. However no induced scattering was visually observed during the experiment. Further, the numerical aperture of the detector was large enough to accommodate the transmitted beam fully even if moderate thermal blooming were to happen. Hence the cause of the observed optical limiting turns out to be excited state absorption. The “effective” 2PA coefficient was calculated by fitting the experimental data to the standard nonlinear transmission equation.

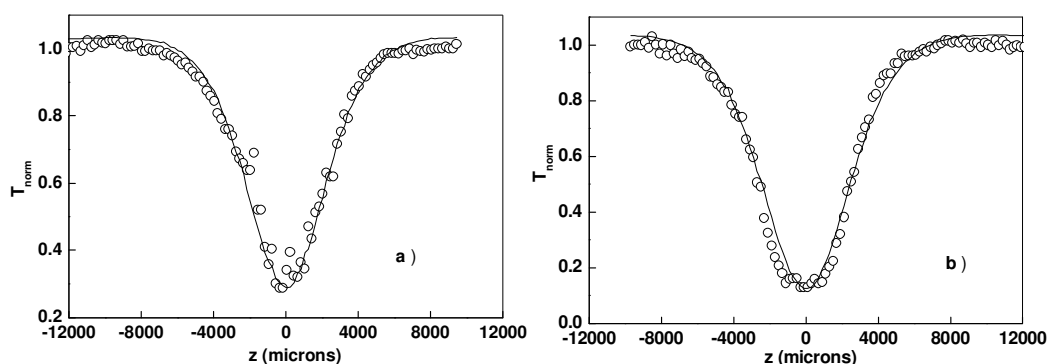


Figure 5.12 Z-scan curves of a) **P1** film and b) **P1/TiO₂** nanocomposite film

The effective nonlinear absorption coefficient was estimated by determining the best-fit curves for the experimental data according to the numerical equation 5.2. For polymer **P1** film effective 2PA coefficient was found to be 1×10^{-7} m/W, and for the **P1/TiO₂** nanocomposite film it was 2×10^{-7} m/W. Obviously there is an enhancement of nonlinearity in **P1/TiO₂** nanocomposite film compared to the pure polymer film. This is not substantial though, the reason being that the polymer films themselves are highly nonlinear in nature. From a device point of view both **P1** and **P1/TiO₂** nanocomposite films are equally useful because the optical limiting efficiency exhibited by them is high.

To put the above β values in perspective, the values obtained in similar systems under similar excitation conditions are, 6.0×10^{-8} m/W in p-(N,N-dimethylamino)-

dibenzylideneacetone in PMMA matrix (Kiran et al. 2008), 10^{-7} to 10^{-9} m/W in Au:Ag-PVA nanocomposite films (Karthikeyan et al. 2006) and 6.8×10^{-7} m/W in a ZnO/PMMA nanocomposite (Sreeja et al. 2010). Obviously, the present films are potentially suited for fabricating optical limiters, which can protect sensitive light detectors and also human/animal eyes from accidental exposure to high levels of optical radiation, while maintaining normal transparency for safe low level inputs.

The open aperture z-scan curves obtained for **P5** film and **P5/TiO₂** nanocomposite film are shown in Figure 5.13. The laser pulse energies used to excite the samples were between 10 and 100 μ J. The z-scan curves obtained were fitted with numerically simulated results using equation 5.3. By determining the best-fit curves for the experimental data, the nonlinear parameters were calculated. For **P5** film, saturation intensity was found to be 6×10^{11} W/m² and for **P5/TiO₂** nanocomposite film it was found to be 9×10^{11} W/m². There is an enhancement of the nonlinearity in **P5/TiO₂** nanocomposite film compared to pure polymer film.

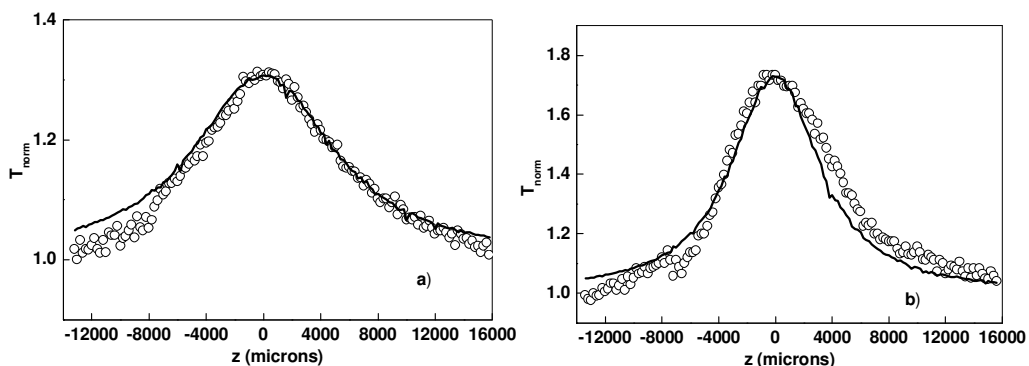


Figure 5.13 Z-scan curves of a) **P5** film and b) **P5/TiO₂** nanocomposite film

For comparison, a similar saturable absorption behavior was observed for some organic materials reported in the literature. The values obtained are $1.5 - 4.5 \times 10^{13}$ W/m² in phthalocyanines (Venkatram et al. 2008), $1 - 4 \times 10^{10}$ W/m² in poly(indenofluorene) (Samoc et al. 1998), $10^{10} - 10^{11}$ W/m² for Rhodamine B (Venkatram et al. 2002) and $1.4 - 6.8 \times 10^{13}$ W/m² for thiophene based conjugated polymers (Hegde et al. 2011). The saturation intensity obtained for **P5** film is almost 100 times lower than the values obtained for thiophene based donor-acceptor polymers (Hegde et al. 2011), indicating a better NLO response in **P5**. This could be

due to the presence of stronger electron withdrawing cyanovinylene group in **P5** in comparison with 1,3,4-oxadiazole groups in the reported polymers. Because of their large saturable absorption, both **P5** and **P5/TiO₂** nanocomposite films are expected to be useful candidates for photonic applications mainly in areas such as Q-switching and mode-locking of lasers, pulse shaping and optical switching.

5.4 CONCLUSIONS

The NLO properties of newly synthesized D–A conjugated polymers **P1–P12** were studied using z-scan technique. The polymer samples showed improved nonlinearity as compared to some important NLO materials reported in the literature. Among these polymers, **P1**, **P2** and **P9** showed the highest optical nonlinearity with promising optical limiting behavior. The regular D–A structure in **P1** and **P2** and the presence electron donating dialkylfluorene unit with extended conjugation in **P9** could be responsible for the observed trend. Interestingly, polymers **P5–P8** showed saturable absorption behavior at the measured wavelength whose linear absorption peak is close to the excitation wavelength of 532 nm.

Polymers **P1** and **P5** were used to prepare polymer/TiO₂ nanocomposites. Incorporation of TiO₂ nanoparticles into the polymer matrix was found to improve the thermal stability of the polymer. The polymer nanocomposite films showed a red shift in the absorption maxima as compared to those of polymer films. These results indicate the presence of some interactions between the polymer and TiO₂ nanoparticles in the nanocomposite structures. The NLO properties of **P1** film and **P1/TiO₂** nanocomposite film were measured by the open aperture z-scan technique. All film samples showed a strong optical limiting behavior and the incorporation of TiO₂ nanoparticles marginally enhances the nonlinear absorption coefficient value of the polymer. These results suggest that **P1** and **P1/TiO₂** nanocomposite films are expected to be potential candidates for fabricating efficient optical limiters. Polymer **P5** and **P5/TiO₂** nanocomposite films exhibited strong saturable absorption behavior and the saturation intensity (I_s) was found to be of the order of 10^{11} W/m². These NLO results signify that **P5** and its nanocomposite films are promising materials for applications in photonic switching devices. Hence donor-acceptor conjugated polymers containing strong electron donating and electron withdrawing units arranged

alternatively along the polymer chain could be a promising class of molecular materials to achieve high NLO responses. Further enhancement in the NLO properties in these systems could be achieved by incorporating TiO₂ nanoparticles in to the polymer matrix, in the form of nanocomposite structures.

CHAPTER 6

SUMMARY, CONCLUSIONS AND FUTURE SCOPE

6.1 SUMMARY

The emergence of conjugated polymers as a new class of electronic materials has attracted considerable attention because the study of these systems has generated entirely new scientific concepts which led to the development of new technologies. In particular these polymers are considered as potential candidates for the development of optoelectronic devices like PLEDs and PSCs. In this regard, various approaches have been used to achieve high EL efficiencies in PLEDs and high PCE in PSCs. Among them, controlling of polymer properties (in particular the optical and the electrochemical properties) through the modification of the chemical structure of the polymer chain is found to be a promising approach. In this direction, donor-acceptor conjugated polymers consisting of alternating electron rich and electron deficient substituents along the polymer backbone are emerging as suitable materials to obtain efficient devices. In these systems, the desired optical and electrochemical properties could be obtained by the proper selection of electron donor and electron acceptor units. Though, various such D–A conjugated polymers are designed and synthesized for optoelectronic applications, thiophene based alternating D–A conjugated polymers have been of particular recent interest because the intramolecular charge transfer interaction between the thiophene donor moieties and electron acceptor units within the D–A system can be readily tailored to modulate their electronic structures (HOMO/LUMO levels) and hence to modify their electronic and optoelectronic properties. However, the design and synthesis of efficient D–A conjugated polymers still remains as a challenging area and attracts many researchers to work out with different combinations of electron donor and electron acceptor units so as to obtain D–A systems with desired optical and electrochemical properties.

In view of this, five new series of thiophene based D–A type conjugated polymers (**P1–P12**) were designed in the present study. The core structure of the polymers consists of 3,4-didodecyloxythiophene as electron donor unit and is attached to various electron withdrawing units, viz. 1,3,4-oxadiazole, cyanovinylene and cyanophenylenevinylene moieties along with conjugative spacers like phenylenevinylene, thienylenevinylene and biphenyl units. The chemical structures of these polymers are designed in such way as to obtain polymers having low band gap,

high thermal stability, good solvent processability and film forming property with desired optical and electrochemical properties for optoelectronic applications. The reason for choosing 3,4-dialkoxythiophene unit as the core donor segment is that poly(3,4-dialkoxythiophene)s show facile dopability and lower band gap due to the electron donating nature of the alkoxy moiety. Further introduction of long alkoxy pendants at 3- and 4- positions of the thiophene ring facilitates the solvent processability of the corresponding polymer.

The possibility of steric interactions between the alkoxy groups of adjacent thiophene rings, which reduces the coplanarity and thus decreases the effective conjugation length of the polymer, is avoided in polymers **P1–P12** by introducing conjugated spacers between any two thiophene rings in the polymer chain. The (1,3,4-oxadiazolyl)benzene unit in **P1** and (1,3,4-oxadiazolyl)-3,4-propylenedioxythiophene unit in **P2** were incorporated between two alkoxy substituted thiophene rings, so as to minimize steric interactions between the alkoxy groups. The chemical structure of the repeating unit in **P4** is almost similar to that in **P3**, except that one of the 3,4-dialkoxythiophene rings in **P3** is replaced by an unsubstituted thiophene ring in **P4**. Such a simple structural modification in the polymer chain allowed studying the effect of alkoxy pendant groups on optical and electrochemical properties of the conjugated polymers. In the case of polymers **P5–P8**, cyanovinylene group was introduced along the polymer chain as cyano containing polymers are expected to show low band gap and extended absorption in the visible region. The conjugation length of repeating units in **P6–P8** was extended as compared to that in **P5**, by introducing an electron donating dialkylfluorene unit in **P6** and an electron withdrawing cyanophenylenevinylene unit in **P7** and a donor-acceptor conjugated system in **P8**. It was expected that, incorporation of these units along the polymer chain would affect the optical and electrochemical properties of the polymers. As compared to **P6–P8**, the number of vinylic linkages in polymer **P9** and **P10** were reduced so as to obtain chemically stable polymers. The chain structure of **P11** and **P12** are comparable with those **P9** and **P10** respectively. The electron donating dialkylfluorene rings in **P9** and **P10** were replaced with a strong electron withdrawing cyanophenylenevinylene unit in **P11** and **P12**. This structural modification was expected to enhance the electron transporting and hole blocking properties of the polymers. Further, it was expected

that such structural modifications would help in understanding the structure-property relationship in D–A conjugated polymers.

To obtain designed thiophene based D–A type conjugated polymers, various monomers (**M1–M10**) and their intermediate compounds were synthesized through multistep reaction sequence. The chemical structures of all the newly synthesized intermediate compounds and monomers were established by ¹H NMR and FTIR spectroscopic methods as well as by elemental analyses. These monomers were used for the synthesis of following five new series of target polymers.

1. 3,4-Didodecyloxythiophene based polymers carrying 1,3,4-oxadiazole and phenyl or 3,4-propylenedioxythiophene segments (**P1** and **P2**) (Scheme 2.9)
2. 3,4-Didodecyloxythiophene based polymers carrying 1,3,4-oxadiazole, phenylenevinylene and thienylenevinylene units (**P3** and **P4**) (Scheme 2.10)
3. 3,4-Didodecyloxythiophene based polymers carrying cyanovinylene moieties (**P5–P8**) (Scheme 2.11)
4. 3,4-Didodecyloxythiophene based polymers carrying 1,3,4-oxadiazole and fluorenevinylene segments (**P9** and **P10**) (Scheme 2.12)
5. 3,4-Didodecyloxythiophene based polymers carrying 1,3,4-oxadiazole and cyanophenylenevinylene units (**P11** and **P12**) (Scheme 2.13)

The newly designed polymers were synthesized using appropriate synthetic routes like polycondensation reaction, Wittig reaction, Knoevenagel polycondensation and chemical oxidative polymerization methods. The synthesized polymers were purified by reprecipitation technique in appropriate solvents. The chemical structure of the polymers was evidenced by ¹H NMR and FTIR spectroscopic methods and their molecular formula was confirmed by elemental analyses data. The thermal stability and molecular weight of the polymers were determined by TGA and GPC techniques respectively.

The linear optical properties of the polymers were studied by UV-Vis absorption and fluorescence emission spectroscopic techniques. The cyclic voltammetric technique was employed to investigate the electrochemical redox behavior of the polymers. Further, the results obtained in linear optical and electrochemical studies of the polymers were correlated with their chemical structure. The preliminary studies on

electroluminescent properties of polymers **P5**, **P9**, **P10** and **P12** were studied by fabricating polymer light emitting diodes using polymers as the emissive layer. Low band gap polymers **P6** and **P7** were used as both electron donor and electron acceptor materials in bulk heterojunction solar cells and their photovoltaic properties were studied. The nonlinear optical properties of the polymers were studied using z-scan technique. Polymer/TiO₂ nanocomposites were prepared using polymers **P1** and **P5** and their NLO properties were studied likewise.

6.2 CONCLUSIONS

- Five new series of thiophene based D–A conjugated polymers (**P1–P12**) were designed and successfully synthesized.
- The successful reaction between the monomers to form the required polymer was evidenced by the structural characterization of the polymer using spectroscopic methods and elemental analyses.
- The synthesized polymers showed good solubility in common organic solvents due to the presence of long alkoxy pendants at 3 and 4-positions of the thiophene ring.
- All the polymers were found to be thermally stable up to 300 °C which suggests that decomposition of the polymer backbone may not takes place during the fabrication and operation of the optoelectronic devices based on these polymers.
- Among the polymers, polymers **P5–P8** showed low band gap due to the presence of cyanovinylene groups and also because of the strong intramolecular charge transfer interaction in the polymer chain.
- Polymer **P7** containing cyanovinylene group and a regular D–A arrangement was found to show the lowest band gap and the lowest LUMO energy level among these polymers.
- This suggest that introduction of cyanovinylene groups and maintaining a strict alternation of D and A units along the conjugated chain could be a promising molecular design to obtain low band gap polymers with high electron affinity.

- Further, the presence of biphenyl ring along the polymer backbone was found to affect the photophysical and electrochemical properties of the polymers. Hence polymers **P10** and **P12** displayed lowest λ_{max} values and the highest band gap energy among polymers **P1–P12** due to the presence of biphenyl rings which limits the π -conjugation along the polymer chain.
- The polymers emitted blue to red light when irradiated with UV light, depending upon the chemical structure of the polymer backbone.
- The new polymers possess low-lying LUMO energy levels due to the presence of strong electron accepting ability of 1,3,4-oxadiazole/cyanovinylene segments present in the polymer backbone.
- The electrochemical results suggest that by introducing suitable donor and acceptor units in the polymer backbone, one can achieve polymers with desired HOMO and LUMO energy levels.
- The polymers which showed narrow band gaps with low HOMO levels are promising candidates for polymer solar cell devices. Further, the low-lying LUMO levels of the polymers suggest that they are potential candidates as electron transporting/hole blocking materials in polymer light emitting diodes.
- The PLEDs based on polymers **P5**, **P9**, **P10** and **P12** emit red, green, green and white light respectively.
- The PLEDs based on **P5** and **P10** showed good color stability under different bias voltages.
- The polymers **P5** and **P10** showed almost pure red and white light emission with CIE coordinate values of (0.65, 0.32) and (0.32, 0.35) respectively.
- The PLEDs based on polymers **P5**, **P9**, **P10** and **P12** exhibit lower threshold voltages due to low-lying LUMO energy levels of these polymers.
- The BHJ solar cells based on narrow band gap polymer **P7** as electron donor material exhibited high open circuit voltage of 0.87 V. The obtained V_{oc} value is the highest for any polymer solar cells based on thiophene and cyanovinylene derivatives reported so far.
- Non-fullerene BHJ solar cells based on polymer **P6** demonstrated moderately high power conversion efficiency of 0.74 % with open circuit voltage of 0.78 V.

- An optical limiting behavior was observed in polymers **P1–P4** and **P9–P12**, when excited at 532 nm excitation wavelength.
- Among the polymers, **P1**, **P2** and **P9** showed a strong optical limiting behavior which is correlated to their unique chemical structures.
- As the linear absorption of polymers **P5–P8** is close to the excitation wavelength of 532 nm, these polymers showed saturable absorption behavior.
- Polymer **P1** and **P1/TiO₂** nanocomposite films showed even stronger optical limiting behavior compared to that of the polymer solution and the incorporation of TiO₂ nanoparticles into the polymer matrix marginally enhanced the nonlinear absorption coefficient value of the polymer. Thus they are expected to be promising materials for fabricating optical limiters.
- Polymer **P5** and **P5/TiO₂** nanocomposite films exhibited stronger saturable absorption behavior than the polymer solution and hence are promising materials for applications in photonic switching devices.

6.3 FUTURE SCOPE

In recent years, conjugated polymers are of growing interest for organic optoelectronic and electronic applications, including photovoltaic cells, light emitting diodes, field effect transistors and optical switching devices due to their possibility of low cost fabrication, light weight, simple process and mechanical flexibility. In this direction, the thiophene based D–A conjugated polymers synthesized in the present study would be promising materials because of the simplicity of synthetic methods and solution processability of the polymers. Further, it is possible to tune and optimize the electronic and optical properties of these polymers as desired by the proper selection of electron donor and electron acceptor units in the polymer chain. The electrochemical redox behavior and preliminary studies of electroluminescent properties of the newly synthesized polymers indicate that these materials are promising candidates as active materials in the development of highly efficient PLEDs. However, the practical applicability of the present polymers requires further studies on luminescence properties as well the efficiency of the devices. Further the device performance and lifetime could be enhanced by optimizing the fabrication conditions and also by modifying the device structure, such as fabrication of

multilayer devices using additional electron transporting/hole blocking materials along with a proper protective encapsulation of the device.

The preliminary photovoltaic studies revealed that the present narrow band gap polymers with broad absorption spectrum are promising active materials in BHJ solar cells. However the solar cell devices fabricated in the present study showed low power conversion efficiencies. The efficiency of the devices could be improved by high hole mobility, blend compositions, optimizing film morphology, annealing conditions and device fabrication conditions. The other recent approach to improve the efficiency of the organic solar cells is to increase the optical absorption and photocurrent generation in the photoactive layer over a broad range of visible wavelength by incorporating plasmonic structures in to the device. The nonlinear optical studies revealed that the synthesized polymers and polymer/TiO₂ nanocomposite show promising optical limiting as well as strong saturable absorption behavior. The practical applicability of these materials could be checked by fabricating optical limiters or photonic switching devices.

Appendix 1

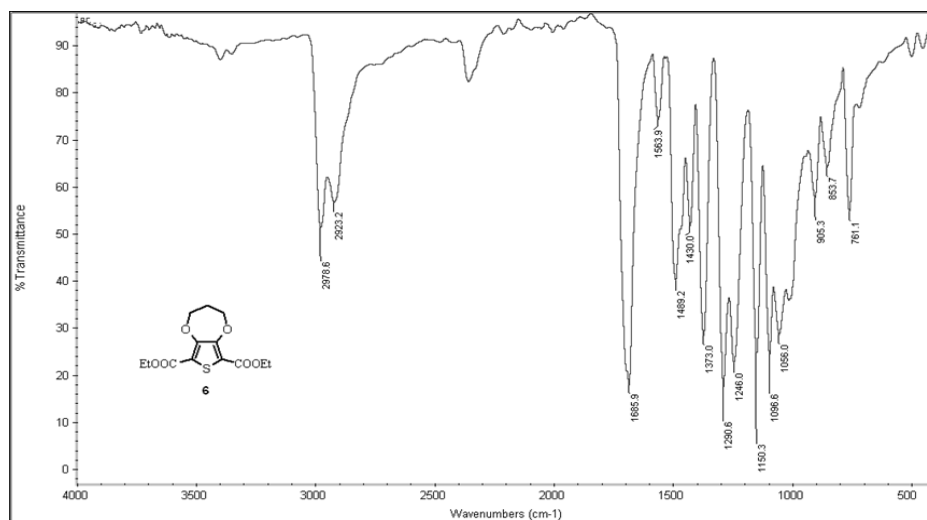


Figure A1. FTIR spectrum of 3,4-propylenedioxythiophene-2,5-dicarboxylate (6)

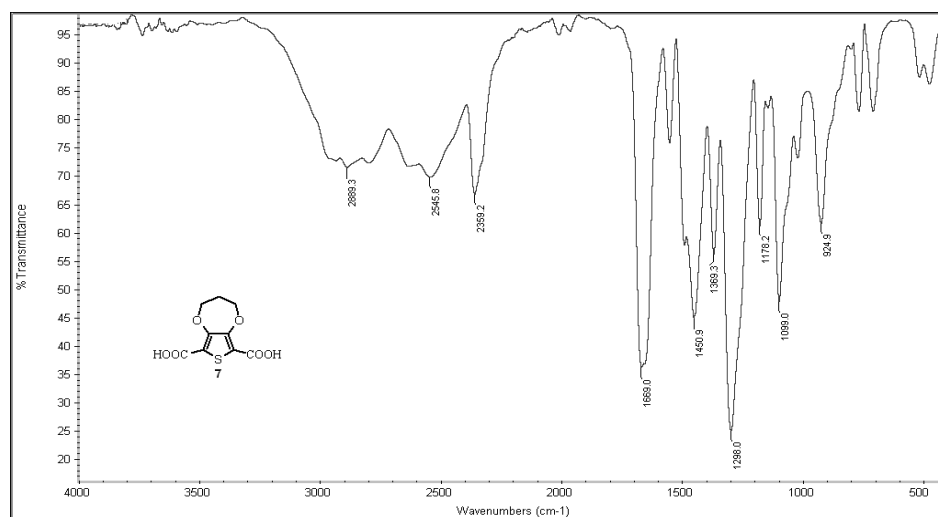


Figure A2. FTIR spectrum of 3,4-propylenedioxythiophene-2,5-dicarboxylic acid (7)

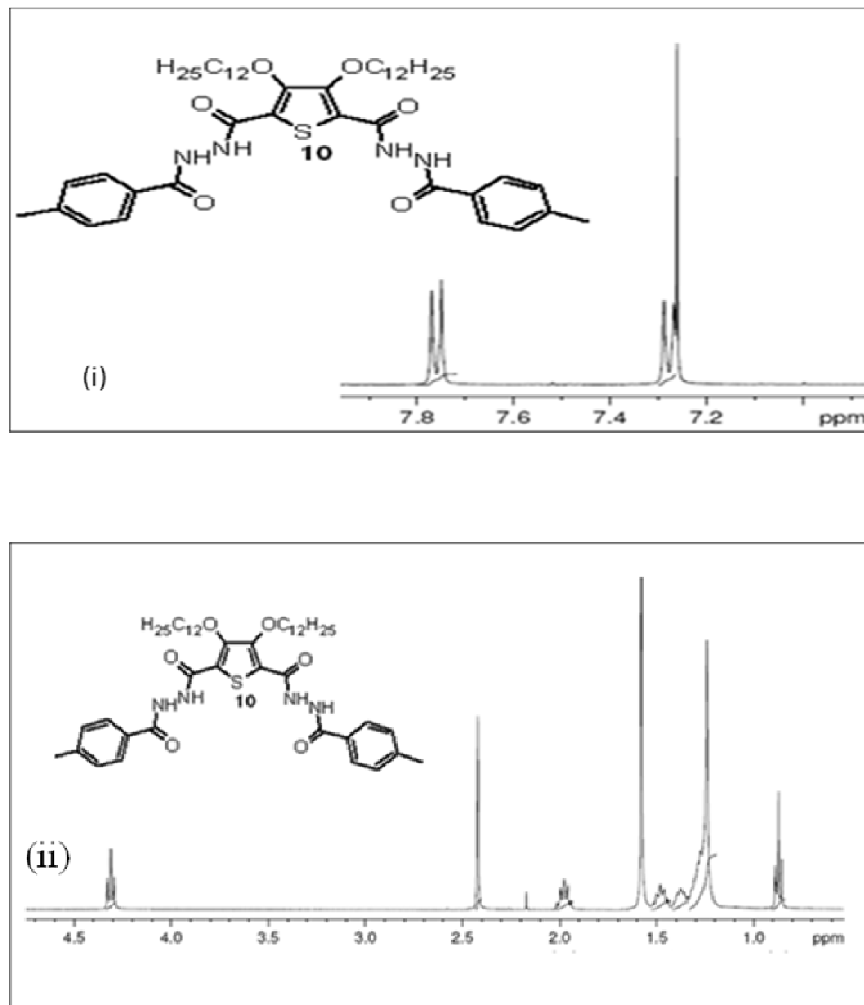


Figure A3. i) Enlarged image of the ^1H NMR spectrum of N^2, N^5 -di-(4-methylbenzoyl)-3,4-bis(dodecyloxy)thiophene-2,5-dicarbohydrazide (**10**) in the aromatic region.

ii) Enlarged image of the ^1H NMR spectrum of N^2, N^5 -di-(4-methylbenzoyl)-3,4-bis(dodecyloxy)thiophene-2,5-dicarbohydrazide (**10**) in the aliphatic region.

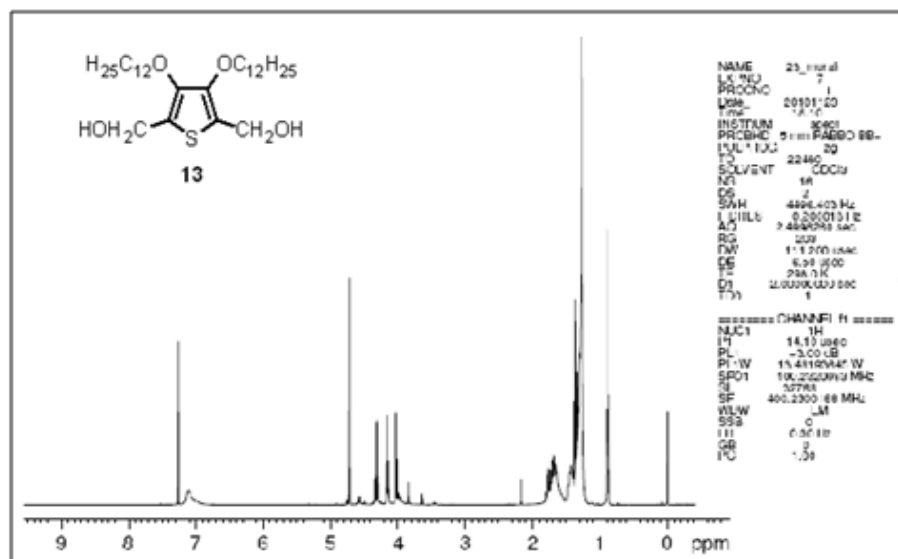


Figure A4. ^1H NMR spectrum of (3,4-bis(dodecyloxy)thiophene-2,5-diyl)dimethanol (**13**)

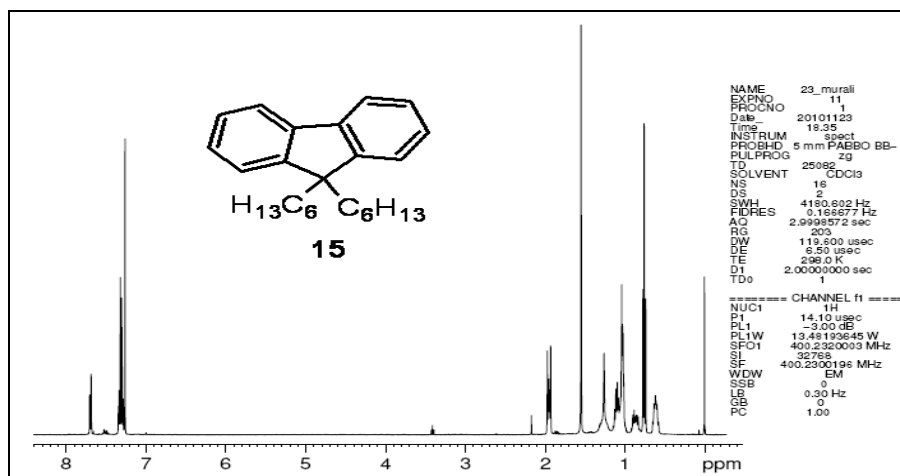
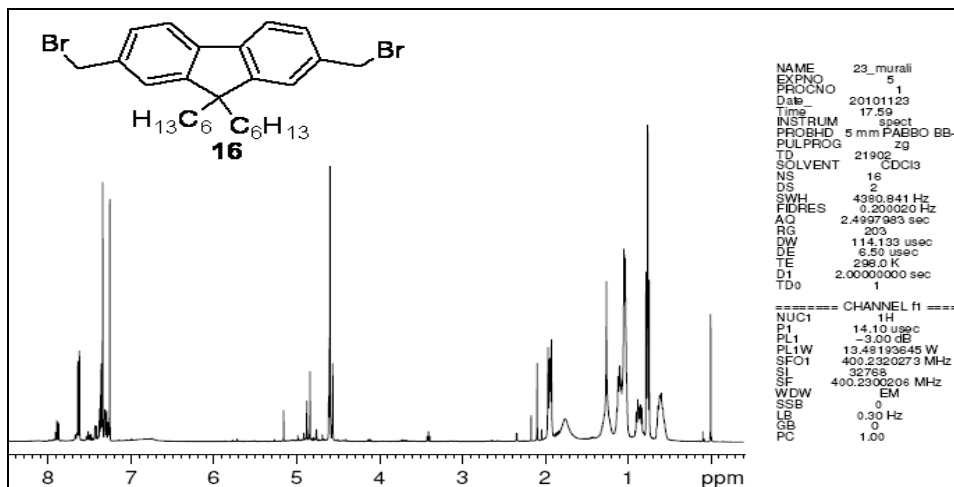
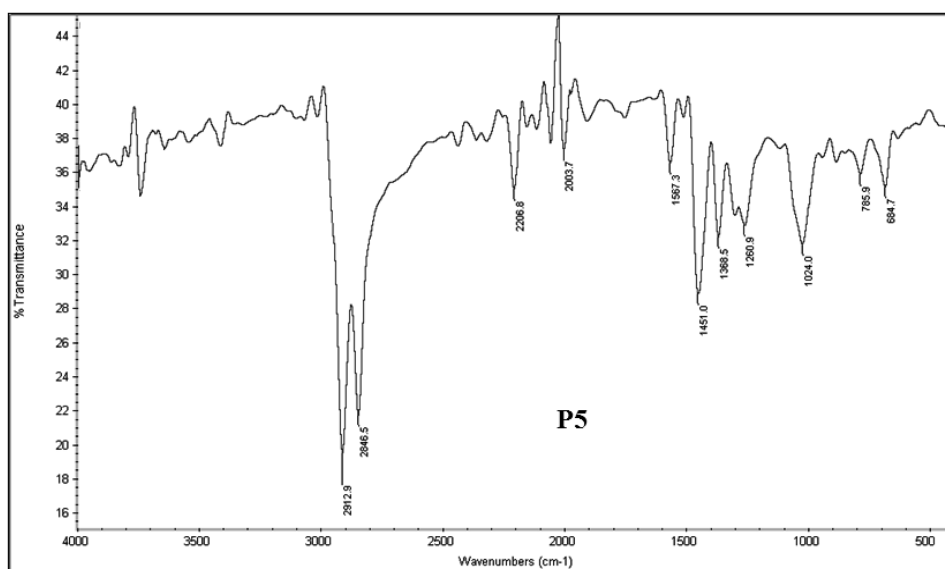


Figure A5. ^1H NMR spectrum of 9,9'-di-*n*-hexylfluorene (**15**)

Figure A6. ^1H NMR spectrum of 2,7-bis(bromomethyl)-9,9'-di-*n*-hexylfluorene (**16**)Figure A7. FTIR spectrum of polymer **P5**

REFERENCES

Agrawal, A.K. and Jenekhe, S.A. (1996). "Electrochemical properties and electronic structures of conjugated polyquinolines and polyanthrazolines." *Chem. Mater.*, 8, 579–589.

Ahmed, E., Ren, G., Kim, F.S., Hollenbeck, E.C. and Jenekhe, S.A. (2011). "Design of new electron acceptor materials for organic photovoltaics: synthesis, electron transport, photophysics, and photovoltaic properties of oligothiophene-functionalized naphthalene diimides." *Chem. Mater.*, 23, 4563–4577.

Ajayaghosh, A. (2003). "Donor-acceptor type low band gap polymers: polysquaraines and related systems." *Chem. Soc. Rev.*, 32, 181–191.

Albota, M., Beljonne, D., Bredas, J.L., Ehrlich, J.E., Fu, J.Y., Heikal, A.A., Hess, S.E., Kogej, T., Levin, M.D., Marder, S.R., McCord-Moughon, D., Perry, J.W., Rockel, H., Rumi, M., Subramaniam, G., Webb, W.W., Wu, X.L. and Xu, C. (1998). "Design of organic molecules with large two-photon absorption cross sections." *Science*, 281, 1653–1656.

Anant, P., Mangold, H., Lucas, N.T., Laquai, F. and Jacob, J. (2011). "Synthesis and characterization of donor-acceptor type 4,4'-bis(2,1,3-benzothiadiazole)-based copolymers." *Polymer*, 52, 4442–4450.

Anthony, J.E. (2011). "Small-molecule, nonfullerene acceptors for polymer bulk heterojunction organic photovoltaics." *Chem. Mater.*, 23, 583–590.

Balan, A., Gunbas, G., Durmus, A. and Toppare, L. (2008). "Donor-acceptor polymer with benzotriazole moiety: enhancing the electrochromic properties of the donor unit." *Chem. Mater.*, 20, 7510–7513.

Beaujuge, P.M., Subbaih, J., Choudhury, K.R., Ellinger, S., Mccareley, T.D., So, F. and Reynolds, J.R. (2010). "Green dioxythiophene-benzothiadiazole donor-acceptor copolymers for photovoltaic device applications." *Chem. Mater.*, 22, 2093–2106.

- Brabec, C.J., Cravino, A., Meissner, D., Sariciftci, N.S., Fromherz, T., Rispen, M.T., Sanchez, L. and Hummelen, J.C. (2001). "Origin of the open circuit voltage of plastic solar cells." *Adv. Funct. Mater.*, 11, 374–380.
- Brabec, C.J., Sariciftci, N.S. and Hummelen, J.C. (2001). "Plastic solar cells." *Adv. Funct. Mater.*, 1, 15–26.
- Bradley, D.D.C. (1993). "Conjugated polymer electroluminescence." *Synth. Met.*, 54, 401–415.
- Braun, D. and Heeger, A.J. (1991). "Visible light emission from semiconducting polymer diodes." *Appl. Phys. Lett.*, 58, 1982–1985.
- Bricaud, Q., Cravino, A., Leriche, P. and Roncali, J. (2009). "Terthiophene-cyanovinylene-conjugated polymers as donor material for organic solar cells." *Synth. Met.*, 159, 2534–2538.
- Brocks, G. and Tol, A. (1996). "Small band gap semiconducting polymers made from dye molecules: polysquaraines." *J. Phy. Chem.*, 100, 1838–1846.
- Brunetti, F.G., Gong, X., Tong, M., Heeger, A.J. and Wudl, F. (2010). "Strain and huckel aromaticity: driving forces for a promising new generation of electron acceptors in organic electronics." *Angew. Chem., Int. Ed.*, 49, 532–536.
- Campos, L.M., Tontcheva, A., Gunes, S., Sonmez, G., Neugebauer, H., Sariciftci, N.S. and Wudl, F. (2005). "Extended photocurrent spectrum of a low band gap polymer in a bulk heterojunction solar cell." *Chem. Mater.*, 17, 4031–4033.
- Cao, D., Liu, Q., Zeng, W., Han, S., Peng, J. and Liu, S. (2006). "Synthesis and characterization of novel red-emitting alternating copolymers based on fluorene and diketopyrrolopyrrole derivatives." *J. Polym. Sci., Part A: Polym. Chem.*, 44, 2395–2405.
- Cassano, T., Tommasi, R., Babudri, F., Cardone, A., Farinola, G.M. and Naso, F. (2002). "High third-order nonlinear optical susceptibility in new fluorinated poly(p-

phenylenevinylene) copolymers measured with the z-scan technique.” *Opt. Lett.*, 27, 2176–2178.

Cassano, T., Tommasi, R., Tassara, M., Babudri, F., Cardone, A., Farinola, G.M. and Naso, F. (2001). “Substituent-dependence of the optical nonlinearities in poly(2,5-dialkoxy-p-phenylenevinylene) polymers investigated by the z-scan technique.” *Chem. Phys.*, 272, 111–118.

Chang, D.W., Ko, S.J., Kim, G.H., Bae, S.Y., Kim, J.Y., Dai, L. and Baek, J.B. (2012). “Molecular engineering of conjugated polymers for solar cells and field-effect transistors: side-chain versus main-chain electron acceptors.” *J. Polym. Sci., Part A: Polym. Chem.*, 50, 271–279.

Chen, H. Y., Hou, J., Zhang, S., Yang, G., Yang, Y., Wu, Y. and Li, G. (2009). “Polymer solar cells with enhanced open-circuit voltage and efficiency.” *Nat. Photonics*, 3, 649–653.

Chen, X., Tao, J., Zou, G., Zhang, Q. and Wang, P. (2010). “Nonlinear optical properties of nanometer-size silver composite azobenzene containing polydiacetylene film.” *Appl. Phys. A*, 100, 223–230.

Chen, X., Zou, G., Deng, Y. and Zhang, Q. (2008). “Synthesis and nonlinear optical properties of nanometer-size silver-coated polydiacetylene composite vesicles.” *Nanotechnology*, 19, 195703–195711.

Chen, Y. and Wu, T.Y. (2001). “Synthesis, optical and electrochemical properties of luminescent copolymers containing N-hexyl-3,8-iminodibenzyl chromophores.” *Polymer*, 42, 9895–9901.

Chen, Y., Huang, Y.Y and Wu, T.Y. (2002). “Synthesis and characterization of luminescent polyethers with 2,5-distyrylthiophene and aromatic oxadiazole chromophores.” *J. Polym. Sci. Part A: Polym. Chem.*, 40, 2927–2936.

Chiang, C.K., Fincher, Jr C.R, Park, Y.W., Heeger, A.J., Shirakawa, H., Louis, E.J., Gau, S.C. and MacDiarmid, A.G. (1977). "Electrical conductivity in doped polyacetylene." *Phys. Rev. Lett.*, 39, 1098–1101.

Cho, N.S., Hwang, D.H., Jung, B.J., Lim, E., Lee, J. and Shim, H.K. (2004). "Synthesis, characterization and electroluminescence of new conjugated polyfluorene derivatives containing various dyes as comonomers." *Macromolecules*, 37, 5265–5273.

Coakley, K.M. and McGehee, M.D. (2004). "Conjugated polymer photovoltaic cells." *Chem. Mater.*, 16, 4533–4542.

Colladet, K., Fourier, S., Cleji, T.J., Lutsen, L., Gelan, J. and Vanderzande, D. (2007). "Low band gap donor-acceptor conjugated polymers toward organic solar cells applications." *Macromolecules*, 40, 65–72.

Daoust, G. and Leclerc, M. (1991). "Structure-property relationship in alkoxy substituted polythiophenes." *Macromolecules*, 24, 455–459.

de Leeuw, D.M., Simenon, M.M.J., Brown, A.B. and Einerhand, R.E.F. (1997). "Stability of n-type doped conducting polymers and consequences for polymeric microelectronic devices." *Synth. Met.* 87, 53–59.

Destruel, P., Jolinat, P., Clergereaux, R. and Farenc, J. (1999). Pressure dependence of electrical and optical characteristics of Alq₃ based organic electroluminescent diodes. *J. Appl. Phys.*, 85, 397–400.

Dietrich, M., Heinze, J., Heywang, G. and Jonas, F. (1994). "Electrochemical and spectroscopic characterization of polyalkylenedioxythiophenes." *J. Electroanal. Chem.*, 369, 87–92.

Duan, C., Hua, X., Chen, K.S., Yip, H.L., Li, W., Huang, F., Jen, A.K.Y. and Cao, Y. (2012). "Fully visible light-harvesting conjugated polymers with pendant donor-p-acceptor chromophores for photovoltaic applications." *Sol. Energy Mater. Sol. Cells.*, 97, 50–58.

Egbe, D.A.M., Kietzke, T., Carbonnier, B., Muhlbacher, D., Horhold, H.H., Neher, D. and Pakula, T. (2004). "Synthesis, characterization and photophysical, electrochemical, electroluminescent and photovoltaic properties of Yne-containing CN-PPVs." *Macromolecules*, 37, 8863–8873.

Ellinger, S., Graham, K.R., Shi, P., Farley, R.T., Steckler, T.T., Brookins, R.N., Taranekar, P., Mei, J., Padilha, L.A., Ensley, T.R., Hu, H., Webster, S., Hagan, D.J., Van Stryland, E.W., Schanze, K.S. and Reynolds, J.R. (2011). "Donor-acceptor-donor-based π -conjugated oligomers for nonlinear optics and near-IR emission." *Chem. Mater.*, 23, 3805–3817.

Gayvoronsky, V., Galas, A., Shepelyavy, E., Dittrich, T., Timoshenko, V.Y., Nepijko, S.A., Brodyn, M.S. and Koch, F. (2005). "Giant nonlinear optical response of nanoporous anatase layers." *Appl. Phys. B.*, 80, 97–100.

Green, M.A., Emery, K., Hishikawa, Y. and Warta, W. (2010). "Solar cell efficiency tables." *Prog. Photovoltaics.*, 18, 144–150.

Guan, Z.-L., Kim, J.B., Wang, H., Jaye, C., Fischer, D.A., Loo, Y.-L. and Kahn, A. (2010). "Direct determination of the electronic structure of the poly(3-hexylthiophene):phenyl-[6,6]-C61 butyric acid methyl ester blend." *Org. Electron*, 11, 1779–1785.

Gubler, U., Concilio, S., Bosshard, C., Biaggio, I., Gunter, P., Martin, R.E., Edelmann, M.J., Wykto, J.A. and Diederich, F. (2002). "Third-order nonlinear optical properties of in-backbone substituted conjugated polymers." *Appl. Phys. Lett.*, 82, 2322–2325.

Gunter, W. and Stiles, W.S. (1982). "Color science: concepts and methods, quantitative data and formulae." 2nd ed.; John Wiley and Sons, New York.

Guo, X., Xin, H., Kim, F.S., Liyanage, A.D.T., Jenekhe, S.A. and Watson, M.D. (2011). "Thieno[3,4-c]pyrrole-4,6-dione-based donor-acceptor conjugated polymers for solar cells." *Macromolecules*, 44, 269–277.

Halls, J.J.M., Walsh, C.A., Greenham, N.C., Marseglia, E.A., Friend, R.H., Moratti, S.C. and Holmes, A.B. (1995). "Efficient photodiodes from interpenetrating polymer networks." *Nature*, 376, 498–500.

Harrison, N.T., Baigent, D.R., Samuel, I.D.W. and Friend, R.H., Grimsdale, A.C., Moratti, S.C. and Holmes, A.B. (1996). "Site-selective fluorescence studies of poly(p-phenylene vinylene) and its derivatives." *Phys. Rev. B*, 53, 15815–15822.

Havinga, E.E., Hoeve, W. and Wynberg, H. (1993). "Alternate donor-acceptor small-band-gap semiconducting polymers; polysquaraines and polycroconaines." *Synth. Met.*, 55, 299–306.

He, G.S., Yong, K.T., Zheng, Q., Sahoo, Y., Baev, A., Rysanyanskiy, A.I. and Prasad, P.N. (2007). "Multi-photon excitation properties of CdSe quantum dots solutions and optical limiting behavior in infrared range." *Opt. Express*, 15, 12818–12833.

He, N., Chen, Y., Bai, J., Wang, J., Blau, W.J. and Zhu, J. (2009). "Preparation and optical limiting properties of multiwalled carbon nanotubes with π -conjugated metal-free phthalocyanine moieties." *J. Phys. Chem. C*, 113, 13029–13035.

Hegde, P.K., Adhikari, A.V., Manjunatha, M.G., Sandeep, C.S.S. and Philip, R. (2010). "Nonlinear optical studies on new conjugated poly{2,2l-(3,4-dialkoxythiophene-2,5-diyl) bis[5-(2-thienyl)-1,3,4-oxadiazole]}s." *J. Appl. Polym. Sci.*, 117, 2641–2650.

Hegde, P.K., Adhikari, A.V., Manjunatha, M.G., Suchand Sandeep, C.S. and Philip, R. (2009). "Synthesis and nonlinear optical characterization of new poly{2,2-(3,4-didodecyloxythiophene-2,5-diyl)bis[5-(2-thienyl)-1,3,4-oxadiazole]}." *Synth. Met.*, 159, 1099–1105.

Hegde, P.K., Adhikari, A.V., Manjunatha, M.G., Suchand Sandeep, C.S. and Philip, R. (2011). "Nonlinear optical characterization of new thiophene-based conjugated polymers for photonic switching applications." *Adv. Polym. Tech.*, 30, 312–321.

- Hou, J., Park, M.H., Zhang, S., Yao, Y., Chen, L.M., Li, J.H. and Yang, Y. (2008). "Band gap and molecular energy level control of conjugated polymer photovoltaic materials based on benzo[1,2-b:4,5-b']dithiophene." *Macromolecules*, 41, 6012–6018.
- Hua, J.L., Li, B., Meng, F.S., Ding, F., Qian, S.X. and Tian, H. (2004). "Two-photon absorption properties of hyperbranched conjugated polymers with triphenylamine as the core." *Polymer*, 45, 7143–7149.
- Huang, C., Sartin, M.M., Cozzuol, M., Siegel, N., Barlow, S., Perry, J.W. and Marder, S.R. (2012). "Photoinduced electron transfer and nonlinear absorption in Poly(carbazole-alt-2,7-fluorene)s bearing perylene diimides as pendant acceptors." *J. Phys. Chem. A*, 116, 4305–4317.
- Im, W-B., Hwang, H-K., Lee, L-G., Han, K. and Kim, Y. (2001). "Bright pure blue emission from multilayer organic electroluminescent device with purified unidentate organometallic complex." *Appl. Phys. Lett.*, 79, 1387–1390.
- Intemann, J.J., Mike, J.F. Cai, M., Bose, S., Xiao, T., Mauldin, T.C., Roggers, R.A., Shinar, J., Shinar, R. and Jeffries-EL, M. (2011). "Synthesis and characterization of poly(9,9-dialkylfluorenevinylene benzobisoxazoles): new solution-processable electron-accepting conjugated polymers." *Macromolecules*, 44, 248–255.
- Invernale, M.A., Acik, M. and Sotzing, G.A. (2009). "Thiophene-based electrochromic materials, Handbook of thiophene-based materials: applications in organic electronics and photonics." John Wiley and Sons, Ltd, Chichester, UK.
- Janietz, S., Schulz, B., Torronen, M. and Sundholm, G. (1993). "Electrochemical investigations on poly(phenylene-1,3,4-oxadiazoles)." *Eur. Polym. J.*, 29, 545–549.
- Jenekhe, S.A. and Yi, S. (2000). "Efficient photovoltaic cells from semiconducting polymer heterojunctions." *Appl. Phys. Lett.*, 77, 2635–2638.
- Ji, W., Elim, H.I., He, J. Fitrilawati, F., Baskar, C., Valiyaveetil, S. and Knoll, W. (2003). "Photophysical and nonlinear-optical properties of a new polymer: hydroxylated pyridyl para-phenylene." *J. Phys. Chem. B*, 107, 11043–11047.

Jin, S.H., Kang, Y.S., Kim, Y.M. and Chan, Y.U. (2003). "Synthesis and electroluminescence properties of poly(9,9'-di-n-octylfluorenyl-2,7-vinylene) derivatives for light-emitting display." *Macromolecules*, 36, 3841–3847.

Jin, S.H., Park, H.J., Kim, J.Y., Lee, K., Lee, S.P., Moon, D.K., Lee, H.J. and Gal, Y.S. (2002). "Poly(fluorenevinylene) derivative by gilch polymerization for light-emitting diode applications." *Macromolecules*, 35, 7532–7534.

Joshi, H.S., Jamshidi, R. and Tor, Y. (1999). "Conjugated 1,10-phenanthrolines as tunable fluorophores." *Angew. Chem., Int. Ed. Engl.*, 38, 2721–2725.

Junkers, T., Vandenberg, J., Adriaensens, P., Lutsen, L. and Vanderzande, D. (2012). "Synthesis of poly(p-phenylene vinylene) materials via the precursor routes." *Polym. Chem.*, 3, 275–285.

Kanbara, T. Miyazaki, Y. and Yamamoto, T. (1995). "New π -conjugated heteroaromatic alternative copolymers with electron-donating thiophene or furan units and electron-withdrawing quinoxaline units: Preparation by palladium-catalyzed polycondensation and characterization of the copolymers." *J. Polym. Sci. Part A: Polym. Chem.*, 33, 999–1003.

Kanimozhi, C., Balraju, P., Sharma, G.D. and Patil, S. (2010). "Synthesis of diketopyrrolopyrrole containing copolymers: a study of their optical and photovoltaic properties." *J. Phys. Chem. B*, 114, 3095–3103.

Karastatiris, P., Mikroyannidis, J.A., Spiliopoulos, I.K., Kulkarni, A.P and Jenekhe, S.A. (2004). "Synthesis, photophysics, and electroluminescence of new quinoxaline-containing poly(p-phenylenevinylene)s." *Macromolecules*, 37, 7867–7878.

Karthikeyan, B., Anija, M. and Philip, R. (2006). "In situ synthesis and nonlinear optical properties of Au:Ag nanocomposite polymer films." *Appl. Phys. Lett.*, 88, 053104–053107.

Karthikeyan, B., Anija, M., Suchand Sandeep, C.S., Muhammad, N.T.M. and Philip, R. (2008). "Optical and nonlinear optical properties of copper nanocomposite glasses annealed near the glass softening temperature." *Opt. Commun.*, 281, 2933–2937.

Kietzke, T., Hoerhold, H.H. and Neher, D. (2005). "Efficient polymer solar cells based on M3EH–PPV." *Chem. Mater.*, 17, 6532–6537.

Kim, Y.H. Shin, D.C. and Kwon, S.K. (2005). "Synthesis and characterization of poly(terphenylenevinylene)derivative with electron withdrawing CN group and an electron donating alkoxy group." *Polymer*, 46, 4647–4653.

Kiran, A.J., Rai, N.S., Udayakumar, D., Chandrasekharan, K., Kalluraya, B., Philip, R., Shashikala, H.D and Adhikari, A.V. (2008). "Nonlinear optical properties of *p*-(*N,N*-dimethylamino)dibenzylideneacetone doped polymer." *Mat. Res. Bull.*, 43, 707–713.

Kiran, A.J., Udayakumar, D., Chandrasekharan, K., Adhikari, A.V. and Shashikala, H.D. (2006). "Z-scan and degenerate four wave mixing studies on newly synthesized copolymers containing alternating substituted thiophene and 1,3,4-oxadiazole units." *J. Phys. B: At. Mol. Opt. Phys.*, 39, 3747.

Kishino, S., Ueno, Y., Ochiai, K., Rikukawa, M., Sanui, K., Kobayashi, T., Kunugita, H. and Ema, K. (1998). "Estimate of the effective conjugation length of polythiophene from its $|\chi(3)(\omega; \omega, \omega, -\omega)|$ spectrum at excitonic resonance." *Phys. Rev. B*, 58, R13430-R13433.

Klessinger, M. and Michl, J. (1995). "Excited states and photochemistry of organic molecules." Marcel Dekker, VCH, New York.

Kraft, A., Burn, P.L., Holmes, A.B., Bradley, D.D.C., Friend, R.H. and Martens, J.H.F. (1993). "Hole-transporting compounds for multi-layer polymer light-emitting diodes." *Synth. Met.*, 57, 4163–4167.

Kraft, A., Grimsdale, A.C. and Holmes, A.B. (1998). "Electroluminescent conjugated polymers-seeing polymers in a new light." *Angew. Chem. Int. Ed.*, 37, 402–428.

Lakowicz, J.R. (1999). "Principles of fluorescence spectroscopy." 2nd ed. Kluwer Academic/Plenum: New York.

Lee, J., Cho, N.S., Lee, J., Lee, S.K. and Shim, H.K. (2005). "Emission color tuning of new fluorene-based alternating copolymers containing low band gap dyes." *Synth. Met.*, 155, 73–79.

Lee, S.K., Jung, B.J., Ahn, T., Jung, Y.K., Lee, J.I., Kang, I.N., Lee, J., Park, J.H. and Shim, H.K. (2007). "White electroluminescence from a single polyfluorene containing bis-DCM units." *J. Polym. Sci. Part A: Polym. Chem.*, 45, 3380–3390.

Levi, M.D., Fisyuk, A.S., Demadrille, R., Markevich, E., Gofer, Y., Aurbacha, D. and Pron, A. (2006). "Unusually high stability of a poly(alkylquaterthiophene-alt-oxadiazole) conjugated copolymer in its n and p-doped states." *Chem. Commun.*, 3299–3301.

Li, Y., Cao, Y., Gao, J., Wang, D., Yu, G., and Heeger, A.J. (1999). "Electrochemical properties of luminescent polymers and polymer light-emitting electrochemical cells." *Synth. Met.*, 99, 243–248.

Liang, Y. and Yu, L. (2010). "A new class of semiconducting polymers for bulk heterojunction solar cells with exceptionally high performance." *Acc. Chem. Res.*, 43, 1227–1236.

Liang, Y., Feng, D., Wu, Y., Tsai, S.-T., Li, G., Ray, C. and Yu, L. (2009). "Highly efficient solar cell polymers developed via fine-tuning of structural and electronic properties." *J. Am. Chem. Soc.*, 131, 7792–7799.

Liang, Y., Xu, Z., Xia, J., Tsai, S.T., Wu, Y., Li, G., Ray, C. and Yu, L. (2010). "For the bright future-bulk heterojunction polymer solar cells with power conversion efficiency of 7.4 %." *Adv. Mater.*, 22, E135–E138.

Lim, B., Jo, J., Khim, D., Jeong, H.G., Yu, B.K., Kim, J. and Kim, D.Y. (2010). "Synthesis of an alternating thienylenevinylene–benzothiadiazole copolymer with high hole mobility for use in organic solar cells." *Org. Electron.*, 11, 1772–1778.

- Lim, E., Jung, B.J. and Shim, H.K. (2003). "Synthesis and characterization of a new light-emitting fluorene–thieno[3,2-b]thiophene based conjugated copolymer." *Macromolecules*, 36, 4288–4293.
- Liu, Y., Wan, X., Yin, B., Zhou, J., Long, G., Yin, S. and Chen, Y. (2010). "Efficient solution processed bulk-heterojunction solar cells based a donor–acceptor oligothiophene." *J. Mater. Chem.*, 20, 2464–2468.
- Lloyd, M.T., Anthony, J.E. and Malliaras, G.G. (2007). "Photovoltaics from soluble small molecules." *Mater. Today*, 10, 34–41.
- Ma, C.Q., Fonrodona, M., Schikora, M.C., Wienk, M.M., Janssen, R.A.J. and Bauerle, P. (2008). "Solution-processed bulk-heterojunction solar cells based on monodisperse dendritic oligothiophenes." *Adv. Funct. Mater.*, 18, 3323–3331.
- Ma, W., Yang, C., Gong, X., Lee, K. and Heeger, A.J. (2005). "Thermally stable, efficient polymer solar cells with nanoscale control of the interpenetrating network morphology." *Adv. Funct. Mater.*, 15, 1617–1622.
- Manjunatha, M.G., Adhikari, A.V. and Hegde, P.K. (2009). "Design and synthesis of new donor–acceptor type conjugated copolymers derived from thiophenes." *Eur. Polym. J.*, 45, 763–771.
- Masuhara, A., Kasai, H. Kato, T. Okada, S., Oikawa, H., Nozue, Y., Tripathy, S.K. and Nakanishi, H. (2001). "Hetero multilayered thin films made up of polydiacetylene microcrystals and metal fine particles." *J. Macromol. Sci. Part A Pure Appl. Chem.*, 38, 1371–1382.
- McCullough, R.D. (1998). "The chemistry of conducting polythiophenes." *Adv. Mater.*, 10, 93–116.
- McNeill, C.R., Halls, J.J.M., Wilson, R., Whiting, G.L. Berkebile, S. Ramsey, M.G., Friend, R.H. and Greenham, N.C. (2008). "Efficient polythiophene/polyfluorene copolymer bulk heterojunction photovoltaic devices: device physics and annealing effects." *Adv. Funct. Mater.*, 18, 2309–2321.

McQuade, D.T., Pullen, A.E. and Swager, T.M. (2000). "Conjugated polymer-based chemical sensors." *Chem. Rev.*, 100, 2537–2574.

Moratti, S.C., Bradley, D.D.C., Cervivi, R., Friend, R.H., Greenham, N.C. and Holmes, A.B. (1994). "Light-emitting polymer LEDs." Advanced photonics materials for information technology, in: S. Etamad, (Ed.), SPIE Proceedings, 2144, 108–114.

Nielsen, C.B., Turbiez, M. and McCulloch, I. (2013). "Recent advances in the development of semiconducting DPP-conducting polymers for transistor applications." *Adv. Mater.*, 25, 1859-1880.

Nisoli, M., Cybo-Ottone, A., De Silvestri, S., Magni, V., Tubino, R. Botta, C. and Musco, A. (1993). "Femtosecond transient absorption saturation in poly(alkylthiophene-vinylene)s." *Phys. Rev. B*, 47, 10881–10884.

Okumoto, K. and Shirota, Y. (2001). "Development of high-performance blue-violet-emitting organic electroluminescent devices." *Appl. Phys. Lett.*, 79, 12301–12303.

Overberger, C.G. and Lal, J. (1951). "The preparation of 3,4-dimethoxy-2,5-dicarbethoxythiophene, dimethoxy thiphenes." *J. Am. Chem. Soc.*, 73, 2956–2957.

Parker, I.D., Pei, Q. and Marrocco, M. (1994). "Efficient blue electroluminescence from a fluorinated polyquinoline." *Appl. Phys. Lett.*, 65, 1272–1275.

Peet, J., Heeger, A.J. and Bazan, G.C. (2009). "Plastic solar cells: self-assembly of bulk heterojunction nanomaterials by spontaneous phase separation." *Acc. Chem. Res.*, 42, 1700–1708.

Peng, Q., Kang, E.T., Neoh, K.G., Xiao, D. and Zou, D. (2006). "Conjugated alternating copolymers of fluorene and 2-pyridine-4-ylidenemalononitrile: synthesis, characterization and electroluminescent properties." *J. Mater. Chem.*, 16, 376–383.

Perez, M.D., Borek, C., Forrest, S.R. and Thompson, M.E. (2009). "Molecular and morphological influences on the open circuit voltages of organic photovoltaic devices." *J. Am. Chem. Soc.*, 131, 9281–9286.

- Piliego, C., Holcombe, T.W., Douglas, J.D., Woo, C.H., Beaujuge, P.M. and Frechet, J.M. (2010). "Synthetic control of structural order in N-Alkylthieno[3,4-c]pyrrole-4,6-dione-based polymers for efficient solar cells." *J. Am. Chem. Soc.*, 132, 7595–7597.
- Pommerehne, J., Vestweber, H., Guss, W., Mahrt, R.F., Bässler, H., Porsch, M. and Daub, J. (1995). "Efficient two layer leds on a polymer blend basis." *Adv. Mater.*, 7, 551–554.
- Poortmans, J. and Arkhipov, V. (2006). "Thin film solar cells; fabrication, characterization and applications." Wiley.
- Porel, S., Venkatram, N., Rao, D.N. and Radhakrishnan, T.P. (2007). "Optical power limiting in the femtosecond regime by silver nanoparticle–embedded polymer film." *J. Appl. Phys.*, 102, 33107–33113.
- Prasad, P.N. and David, J.W. (1991). "Introduction to nonlinear optical effects in molecules and polymers." Wiley-Interscience, New York.
- Qian, Y., Meng, K., Lu, C.G., Lin, B.P., Huang, W. and Cui, Y.P. (2009). "The synthesis, photophysical properties and two-photon absorption of triphenylamine multipolar chromophores." *Dyes Pigm.*, 80, 174–180.
- Qing, F., Sun, Y., Wang, X., Li, N., Li, Y., Li, X. and Wang, H. (2011). "A novel poly(thienylenevinylene) derivative for application in polymer solar cells." *Polym. Chem.*, 2, 2102–2106.
- Rajaram, S., Armstrong, P.B., Kim, B.J. and Frechet, J.M.J. (2009). "Effect of addition of a diblock copolymer on blend morphology and performance of poly(3-hexylthiophene):perylene diimide solar cells." *Chem. Mater.*, 21, 1775–1777.
- Ramos-Ortiz, G., Maldonado, J.L., Hernández, M.C.G., Zolotukhin, M.G., Fomine, S., Fröhlich, Scherf, N., Galbrecht, F., Preis, E., Salmon, M., Cardenas, J. and Chavez, M.I. (2010). "Synthesis, characterization and third-order non-linear optical properties of novel fluorene monomers and their cross-conjugated polymers." *Polymer*, 51, 2351–2359.

- Ranjith, K., Swathi, S.K., Kumar, P. and Ramamurthy, P.C. (2012). "Dithienylcyclopentadienone derivative-co-benzothiadiazole: An alternating copolymer for organic photovoltaics." *Sol. Energy Mater. Sol. Cells*, 98, 448–454.
- Rodrigues, R.F.A., Charas, A., Morgado, J. and Macanita, A. (2010). "Self-organization and excited-state dynamics of a fluorene–bithiophene copolymer (F8T2) in solution." *Macromolecules*, 43, 765–771.
- Roncali, J. (1992). "Conjugated poly(thiophenes): synthesis, functionalization, and applications." *Chem. Rev.*, 92, 711–738.
- Ronchi, A., Cassano, T., Tommasi, R., Babudri, F., Cardone, A., Farinola, G.M. and Naso F. (2003). " $\chi(3)$ measurements in novel poly(2',5'-dioctyloxy-4,4',4''-terphenylenevinylene) using the Z-scan technique." *Synth. Met.*, 139, 831–834.
- Rostalski, J. and Meissner, D. (2000). "Monochromatic versus solar efficiencies of organic solar cells." *Sol. Energy Mater. Sol. Cells.*, 61, 87–95.
- Sahin, O., Osken, I. and Ozturk, T. (2011). "Investigation of electrochromic properties of poly(3,5-bis(4-methoxyphenyl)dithieno[3,2-b;2',3'-d]thiophene)." *Synth. Met.*, 161, 183–187.
- Samoc, M., Samoc, A., Davies, B.L., Reish, H. and Scherf, U. (1998). "Saturable absorption in poly(indenofluorene): a picketfence polymer." *Opt. Lett.*, 23, 1295–1297.
- Sezer, A., Gurudas, U., Collins, B., Mckinlay, A. and Bubb, D.M. (2009). "Nonlinear optical properties of conducting polyaniline and polyaniline–Ag composite thin films." *Chem. Phys. Lett.*, 477, 164–168.
- Shang, Y.L., Wen, Y.Q., Li, S.L., Du, S.X., He, X.B., Cai, L., Li, Y.F., Yang, L.M., Gao, H.J. and Song, Y. (2007). "A triphenylamine-containing donor–acceptor molecule for stable, reversible, ultrahigh density data storage." *J. Am. Chem. Soc.*, 129, 11674–11675.

Sharma, G.D., Suresh, P., Mikroyannidis, J.A. and Stylianakis, M.M. (2010). "Efficient bulk heterojunction devices based on phenylenevinylene small molecule and perylene-pyrene bisimide." *J. Mater. Chem.*, 20, 561–567.

Sheik-Bahae, M., Said, A.A., Wei, T.-H., Hagan, D.J. and Van Stryland, E.W. (1990). "Sensitive measurement of optical nonlinearities using a single beam." *IEEE J. Quantum Electron.*, 26, 760–769.

Shin, R.Y.C., Kietzke, T., Sudhakar, S., Dodabalapur, A., Chen, Z.-K. and Sellinger, A. (2007). "N-type conjugated materials based on 2-vinyl-4,5-dicyanoimidazoles and their use in solar cells." *Chem. Mater.*, 19, 1892–1894.

Sih, B.C. and Wolf, M.O. (2005). "Metal nanoparticle conjugated polymer nanocomposites." *Chem. Commun.*, 3375–3384.

Sivaramakrishnan, S., Muthukumar V.S., Sivasankara, S.S., Venkataramanaiah, K., Reppert, J., Rao, A.M., Anija, M., Philip, R. and Kuthirummal, N. (2007). "Nonlinear optical scattering and absorption in bismuth nanorod suspensions." *Appl. Phys. Lett.*, 91, 093104–093107.

Small, C.E., Chen, S., Subbiah, J., Amb, C.M., Tsang, S.W., Lai, T.H., Reynolds, J.R. and So, F. (2012). "High-efficiency inverted dithienogermole-thienopyrrolodione-based polymer solar cells." *Nat. Photonics*, 6, 115–120.

Son, S., Dodabalapur, A., Lovinger, A.J. and Galvin, M.E. (1995). "Luminescence enhancement by the introduction of disorder into poly(p-phenylene vinylene)." *Science*, 269, 376–378.

Sonar, P., Ng, G.-M., Lin, T.T., Dodabalapur, A. and Chen, Z.-K. (2010). "Solution processable low bandgap diketopyrrolopyrrole (DPP) based derivatives: novel acceptors for organic solar cells." *J. Mater. Chem.*, 20, 3626–3629.

Song, S.Y., Jang, M.S. and Shim, H.K. (1999). "Highly efficient light-emitting polymers composed of both hole and electron affinity units in the conjugated main chain." *Macromolecules*, 32, 1482–1487.

Sreeja, R., John, J., Aneesh, P.M. and Jayaraj, M.K. (2010). "Linear and nonlinear optical properties of luminescent ZnO nanoparticles embedded in PMMA matrix." *Opt. Commun.*, 283, 2908–2913.

Subramaniyan, S., Xin, H., Kim, F.S. and Jenekhe, S.A. (2011). "New thiazolothiazole copolymer semiconductors for highly efficient solar cells." *Macromolecules*, 44, 6245–6248.

Sung, H.H. and Lin, H.C. (2004). "Novel alternating fluorene-based conjugated polymers containing oxadiazole pendants with various terminal groups." *Macromolecules*, 37, 7945–7954.

Surin, M., Sonar, P., Grimsdale, A.C., Mullen, K., De Feyter, S., Habuchi, S., Sarzi, S., Braeken, E., Heyen, A.V., Vander Auweraer, M., De Schryver, F.C., Cavallini, M., Moulin, J.F., Biscarini, F., Femoni, C., Roberto, L. and Leclere, P. (2007). "Solid-state assemblies and optical properties of conjugated oligomers combining fluorene and thiophene units." *J. Mater. Chem.*, 17, 728–735.

Sutherland, R.L. (1996). "Handbook of nonlinear optics." Marcel Dekker, New York.

Skotheim, T.A. and Reynolds, J.R. (2007). "Handbook of conducting polymers." Third edition, CRC press, Taylor and Francis group.

Thompson, B.C. and Frechet, J.M.J. (2008). "Polymer-fullerene composite solar cells." *Angew. Chem. Int. Ed.*, 47, 58–77.

Thompson, B.C., Kim, Y.G., McCarley, T.D. and Reynolds, J.R. (2006). "Soluble narrow band gap and blue propylenedioxythiophene-cyanovinylene polymers as multifunctional materials for photovoltaic and electrochromic applications." *J. Am. Chem. Soc.*, 128, 12714–12725.

Tonzola, C.J., Alam, M.M. and Jenekhe, S.A. (2005). "A new synthetic route to soluble polyquinolines with tunable photophysical, redox and electroluminescent properties." *Macromolecules*, 38, 9539–9547.

Udayakumar, D. and Adhikari, A.V. (2007). "Synthesis and characterization of novel conjugated copolymers containing 3,4-dialkoxythiophene and 1,3,4-oxadiazole units." *Eur. Polym. J.*, 43, 3488–3499.

Udayakumar, D. and Adhikari, A.V. (2007). "Synthesis and characterization of fluorescent poly(oxadiazole)s containing 3,4-dialkoxythiophenes." *Optical Materials*, 29, 1710–1718.

Van Mullekom, H.A.M. (2000). "The chemistry of high and low band gap π -conjugated polymers." Ph.D. Thesis, Technische Universiteit Eindhoven.

Venkatram, N., Naga Srinivas, N.K.M. and Rao, D.N. (2002). "Nonlinear absorption and excited state dynamics in Rhodamine B studied using z-scan and degenerate four wave mixing techniques." *Chem. Phys. Lett.*, 361, 439–445.

Venkatram, N., Rao, D.N., Giribabu, L. and Rao, S.V. (2008). "Femtosecond nonlinear optical properties of alkoxy phthalocyanines at 800 nm studied using z-scan technique." *Chem. Phys. Lett.*, 464, 211–215.

Wang, K.L., Leung, M.K., Hsieh, L.G., Chang, C.C. Lee, K.R., Wud, C.L., Jiang, J.C., Tseng, C.Y. and Wang, H.T. (2011). "Conjugated polymers containing electron-deficient main chains electron-rich pendant groups: Synthesis and application to electroluminescence." *Org. Electron.*, 12, 1048–1062.

Wang, C., Zhao, B., Cao, Z., Shen, P., Tan, Z., Li, X. and Tan, S. (2013). "Enhanced power conversion efficiencies in bulk heterojunction solar cells based on conjugated polymer with isoindigo side chain." *Chem. Comm.*, DOI: 10.1039/c3cc40620b

Wang, S.X., Zhanga, L.D., Sub, H., Zhanga, Z.P., Li, G.H., Menga, G.W., Zhanga, J. Wang, Y.W., Fana, J.C. and Gao, T. (2001). "Two-photon absorption and optical limiting in poly(styrene maleic anhydride)/TiO₂ nanocomposites." *Phy. Lett. A*, 281, 59–63.

Woo, C.H., Holcombe, T.W., Unruh, D.A., Sellinger, A. and Frechet, J.M.J. (2010). "Phenyl vs alkyl polythiophene: a solar cell comparison using a vinazene derivative as acceptor." *Chem. Mater.*, 22, 1673–1679.

Wu, P.T., Bull, T., Kim, F.S., Luscombe, C.K. and Jenekhe, S.A. (2009). "Organometallic donor–acceptor conjugated polymer semiconductors: tunable optical, electrochemical, charge transport, and photovoltaic properties." *Macromolecules*, 42, 671–681.

Wu, P.-T., Kim, F.S., Champion, R.D. and Jenekhe, S.A. (2008). "Conjugated donor–acceptor copolymer semiconductors. Synthesis, optical properties, electrochemistry and field-effect carrier mobility of pyridopyrazine-based copolymers." *Macromolecules*, 41, 7021–7028.

Wu, X., Liu, Y. and Zhu, D. (2001). "Synthesis and characterization of a new conjugated polymer containing cyano substituents for light-emitting diodes." *J. Mater. Chem.*, 11, 1327–1331.

Xiao, S., Stuart, A.C., Liu, S., Zhou, H. and You, W. (2010). "Conjugated polymer based on polycyclic aromatics for bulk heterojunction organic solar cells: a case study of quadrathienonaphthalene polymers with 2 % efficiency." *Adv. Funct. Mater.*, 20, 635–643.

Yang, C.-J. and Jenekhe, S.A. (1995). "Conjugated aromatic polyimines. 2. Synthesis, structure and properties of new aromatic polyazomethines." *Macromolecules*, 28, 1180–1196.

Yang, Q., Jin, H., Xu, Y., Wang, P., Liang, X., Shen, Z., Chen, X. Zou, D., Fan, X. and Zhou, Q. (2009). "Synthesis, photophysics and electroluminescence of mesogen-jacketed 2d conjugated copolymers based on fluorene-thiophene-oxadiazole derivative." *Macromolecules*, 42, 1037–1046.

Yang, S-H., Rendu, P.L., Nguyen, T-P. and Hsu, C-S. (2007). "Fabrication of MEH-PPV/SiO₂ and MEH-PPV/TiO₂ nanocomposites with enhanced luminescent stabilities." *Rev. Adv. Mater. Sci.*, 15, 144–149.

Yang, Y., Zhang, J., Zhou, Y., Zhao, G., He, C., Li, Y., Anderson, M., Inganas, O. and Zhang, F. (2010). "Solution-processable organic molecule with triphenylamine core and two benzothiadiazole-thiophene arms for photovoltaic application." *J. Phys. Chem. C*, 114, 3701–3706.

Yu, G., Gao, J., Hummelen, J.C., Wudl, F. and Heeger, A.J. (1995). "Polymer photovoltaic cells: enhanced efficiencies via a network of internal donor-acceptor heterojunctions." *Science*, 270, 1789–1791.

Zhang, Q.T. and Tour, J.M. (1998). "Alternating donor/acceptor repeat units in polythiophenes. Intramolecular charge transfer for reducing band gaps in fully substituted conjugate polymers." *J. Am. Chem. Soc.*, 120, 5355–5362.

Zhang, Y., Cai, X., Bian, Y., Li, X. and Jiang, J. (2008). "Heteroatom substitution of oligothiophenacenes: from good p-type semiconductors to good ambipolar semiconductors for organic field-effect transistors." *J. Phys. Chem. C*, 112, 5148–5159.

Zhao, B., Liu, D., Peng L., Li H., Shen, P., Xiang, N., Liu, Y. and Tan, S. (2009). "Effect of oxadiazole side chains based on alternating fluorene–thiophene copolymers for photovoltaic cells." *Eur. Polym. J.*, 45, 2079–2086.

Zheng, M., Ding, L., Lin, Z. and Karasz, F.E. (2002). "Synthesis and characterization of fluorenediylvinylene and thiophenediylvinylene-containing terphenylene-based copolymers." *Macromolecules*, 35, 9939–9946.

Zhu, Y., Xu, S., Jiang, L., Pan, K. and Dan, Y. (2008). "Synthesis and characterization of polythiophene/Titanium dioxide composites." *React. Funct. Polym.*, 68, 1492–1498.

Zotti, G., Zecchin, S., Schiavon, G., Berlin, A. and Penso, M. (1999). "Ionochromic and potentiometric properties of the novel polyconjugated polymer from anodic coupling of 5,5'-bis(3,4-(ethylenedioxy)thien-2-yl)-2,2'-bipyridine." *Chem. Mater.*, 11, 3342–3351.

Zyss, J. (1994). "Molecular nonlinear optics materials, physics, and devices." Academic Press, London.

RESEARCH PUBLICATIONS

Research papers published/communicated in international journals

- [1] **Murali, M.G.**, Ramya, M.G., Udayakumar, D., Lakshmi, N.B. and Reji Philip. “Synthesis and third order optical nonlinearity studies of the donor-acceptor conjugated polymer, poly(2-[3,4-didodecyloxy-5-(1,3,4-oxadiazol-2-yl)thiophen-2-yl]-5-phenyl-1,3,4-oxadiazole) and a polymer/TiO₂ nanocomposite.” *Synthetic Metals*, Volume 160, Issue 23–24, December 2010, Pages 2520–2525.
- [2] **Murali, M.G.** and Udayakumar, D. “Synthesis and characterization of a new donor-acceptor conjugated polymer and polymer/Ag nanocomposites.” Optics: Phenomena, Materials Devices and Characterization. *American Institute of Physics Conference Proceedings*, Volume 1391, May 2011, Pages 624–626.
- [3] **Murali, M.G.**, Naveen, P., Udayakumar, D., Vandana Yadav and Ritu Srivastava. “Synthesis and characterization of thiophene and fluorene based donor-acceptor conjugated polymer containing 1,3,4-oxadiazole units for light-emitting diodes.” *Tetrahedron Letters*, Volume 53, Issue 2, January 2012, Pages 157–161.
- [4] **Murali, M.G.**, Udayakumar, D., Vandana Yadav and Ritu Srivastava. “New thiophene based donor-acceptor conjugated polymers carrying fluorene and cyano substituted units: synthesis, characterization and electroluminescent properties.” *Polymer Engineering and Science*, November 2012, DOI: 10.1002/pen.23371.
- [5] **Murali, M.G.**, Udayakumar, D. and Kishore Shridharan. “Synthesis, characterization and nonlinear optical properties of donor-acceptor conjugated polymers and polymer/Ag nanocomposites.” *Journal of Materials Science*, Volume 47, Issue 23, December 2012, Pages 8022–8034.
- [6] **Murali, M.G.**, Udayakumar, D., Vandana Yadav, Ritu Srivastava and Safakath, K. “Thiophene based donor-acceptor conjugated polymer as potential optoelectronic and photonic Material.” *Journal of Chemical Science*, Volume 125, Issue 2, March 2013, Pages 247–257.

- [7] **Murali, M.G.** and Udayakumar, D. “Design and synthesis of new low band gap conjugated polymers based on thiophene and cyanovinylene units for solar cell applications.” *Polymer International*, under revision.

Research papers presented in conferences

- [1] **Murali, M.G.**, Ramya, M.G., Supriya R. Prabhu and Udayakumar, D. “Synthesis and characterization of a fluorescent polyoxadiazole containing 3,4-dialkoxythiophene and 1,4-divinylbenzene units.” Asian polymer association (**APA-2009**), Indian Institute of Technology Delhi, India, 17-20th December 2009.
- [2] **Murali, M.G.** and Udayakumar, D. “Synthesis and characterization of a new conjugated polymer containing 3,4-dialkoxythiophene, 1,3,4-oxadiazole and 2,5-divinylthiophene units.” National conference on recent trends in chemical research (**NCRTCR-2010**), NITK Surathkal, India, 8-10th March 2010.
- [3] **Murali, M.G.** and Udayakumar, D. “Synthesis and characterization of a new donor-acceptor conjugated polymer and polymer/TiO₂ nanocomposites.” International conference on recent trends in materials science and technology (**ICMST-2010**), Indian Institute of Space Science and Technology, Thiruvananthapuram, India, 29-31st October 2010.
- [4] **Murali, M.G.** and Udayakumar, D. “Synthesis and characterization of a new donor-acceptor conjugated polymer and polymer/Ag nanocomposites.” **Optics-11**, NIT Calicut, India, 22-24th May 2011.
- [5] **Murali, M.G.**, Udayakumar, D. and Safakath, K. “Synthesis, characterization and nonlinear optical properties of thiophene and fluorene based donor-acceptor conjugated polymer containing 1,3,4-oxadiazole units.” International conference on synthetic and structural chemistry (**ICSSC-2011**), Mangalore University, India, 8-11th December 2011.

- [6] **Murali, M.G.** and Udayakumar, D. “Study of linear and nonlinear optical properties of a donor-acceptor conjugated polymer”. **International Conference on Physics Science and Technology 2011**, UAE, Dubai, 28-30th December 2011.
- [7] **Murali, M.G.** and Udayakumar, D. “Synthesis and characterization of a new donor-acceptor conjugated polymer and polymer/TiO₂ nanocomposite film for photonic applications.” **ICONSAT-2012**, Hyderabad, India, 20-23rd, January 2012.

Curriculum Vitae

Murali M.G.

E mail: muralinalur@gmail.com

Phone: +91-9741011288

Education

- Ph.D. Thesis title: “Synthesis and characterization of thiophene based conjugated polymers for optoelectronic applications”, submitted to NITK, Surathkal.
Research supervisor: Dr. Udaya Kumar D.
- M.Sc. Industrial Chemistry, Kuvempu University, 78%, 2005-2007, Karnataka, India.
- B.Sc. Chemistry, Kuvempu University, 80%, 2002-2005, Karnataka, India.

Work Experience

Worked as Research associate in the area of Synthetic Organic Chemistry at Syngene International Ltd., (A Biocon Company) Bangalore, India. June 2007– December 2008.

Expertise

Reaction handled

- ❖ Synthesis of organic molecules involving Knoevenagel condensation, Michael addition, Suzuki coupling, Heck coupling, Sonogashira coupling, Wittig reaction, Vilsmeier haack reaction, Swern oxidation and Reductive amination etc.
- ❖ Microwave reactions under various conditions.

Reagents handled

- ❖ Lithium Aluminum Hydride, Sodium hydride, Butyl Lithium, Tert-Butyl Lithium etc.
- ❖ NaCN, KCN, ZnCN, CuCN
- ❖ Grignard reagents
- ❖ Pd/C, Raney nickel etc.

Skills

- Analytical interpretation of organic molecules by ^1H NMR, ^{13}C NMR, FTIR and LCMS.
- Purification of organic compounds using column chromatography technique.
- Fabrication of polymer light emitting diode and polymer solar cell devices.
- Instruments handled:
Radley's parallel synthesizer, Biotage microwave initiator, Pressure reactor, Autoclaves, Spin coater, FTIR, DSC, UV-Visible spectrometer, Fluorescence emission spectrometer, Gas chromatography, Electrochemical work station (cyclic voltammetry).

Research publications

1. **Murali, M.G.**, Ramya, M.G., Udayakumar, D., Lakshmi, N.B. and Reji Philip. "Synthesis and third order optical nonlinearity studies of the donor-acceptor conjugated polymer, poly(2-[3,4-didodecyloxy-5-(1,3,4-oxadiazol-2-yl)thiophen-2-yl]-5-phenyl-1,3,4-oxadiazole) and a polymer/TiO₂ nanocomposite." **Synthetic Metals** 160 (2010) 2520–2525.
2. **Murali, M.G.** and Udayakumar, D. "Synthesis and characterization of a new donor-acceptor conjugated polymer and polymer/Ag nanocomposites." *Optics: Phenomena, Materials Devices and Characterization. American Institute of Physics Conference Proceedings* 1391 (2011) 624–626.
3. **Murali, M.G.**, Naveen, P., Udayakumar, D., Vandana Yadav and Ritu Srivastava. "Synthesis and characterization of thiophene and fluorene based

- donor–acceptor conjugated polymer containing 1,3,4-oxadiazole units for light-emitting diodes.” **Tetrahedron Letters** 53 (2012) 157–161.
4. **Murali, M.G.**, Udayakumar, D. and Kishore Shridharan. “Synthesis, characterization and nonlinear optical properties of donor-acceptor conjugated polymers and polymer/Ag nanocomposites.” **Journal of Materials Science** 47 (2012) 8022–8034.
 5. **Murali, M.G.**, Udayakumar, D., Vandana Yadav and Ritu Srivastava. “New thiophene based donor-acceptor conjugated polymers carrying fluorene and cyano substituted units: synthesis, characterization and electroluminescent properties.” **Polymer Engineering and Science** 2012, DOI: 10.1002/pen.23371
 6. **Murali, M.G.**, Udayakumar, D., Vandana Yadav, Ritu Srivastava and Safakath, K. “Thiophene based donor–acceptor conjugated polymer as potential optoelectronic and photonic Material.” **Journal of Chemical Science** 125 (2013), 247–257.
 7. **Murali, M.G.** and Udayakumar, D. “Design and synthesis of new low band gap conjugated polymers based on thiophene and cyanovinylene units for solar cell applications.” **Polymer International**, under revision.
 8. Udaya Kumar, D., John Kiran, A., **Murali, M.G.** and Adhikari, A.V. “Donor-acceptor conjugated polymers and their nanocomposites for photonic applications.” Book chapter-Nonlinear Optics, Edited by Natalia Kamanina, InTech publisher, ISBN 978-953-51-0131-4, 130–160.

Research papers presented in conferences

1. **Murali, M.G.**, Ramya, M.G., Supritha R. Prabhu and Udayakumar, D. “Synthesis and characterization of a fluorescent polyoxadiazole containing 3,4-dialkoxythiophene and 1,4-divinylbenzene units.” Asian polymer association (**APA-2009**), Indian Institute of Technology Delhi, India, 17-20th December 2009.

2. **Murali, M.G.** and Udayakumar, D. “Synthesis and characterization of a new conjugated polymer containing 3,4-dialkoxythiophene, 1,3,4-oxadiazole and 2,5-divinylthiophene units.” National conference on recent trends in chemical research (**NCRTC-2010**), NITK Surathkal, India, 8-10th March 2010.
3. **Murali, M.G.** and Udayakumar, D. “Synthesis and characterization of a new donor-acceptor conjugated polymer and polymer/TiO₂ nanocomposites.” International conference on recent trends in materials science and technology (**ICMST-2010**), Indian Institute of Space Science and Technology, Thiruvananthapuram, India, 29-31st October 2010.
4. **Murali, M.G.** and Udayakumar, D. “Synthesis and characterization of a new donor-acceptor conjugated polymer and polymer/Ag nanocomposites.” **Optics-11**, NIT Calicut, India, 22-24th May 2011.
5. **Murali, M.G.**, Udayakumar, D. and Safakath, K. “Synthesis, characterization and nonlinear optical properties of thiophene and fluorene based donor-acceptor conjugated polymer containing 1,3,4-oxadiazole units.” International conference on synthetic and structural chemistry (**ICSSC-2011**), Mangalore University, India, 8-11th December 2011.
6. **Murali, M.G.** and Udayakumar, D. “Study of linear and nonlinear optical properties of a donor-acceptor conjugated polymer”. **International Conference on Physics Science and Technology 2011**, UAE, Dubai, 28-30th December 2011.
7. **Murali, M.G.** and Udayakumar, D. “Synthesis and characterization of a new donor-acceptor conjugated polymer and polymer/TiO₂ nanocomposite film for photonic applications.” **ICONSAT-2012**, Hyderabad, India, 20-23rd, January 2012.

Personal details

Father's name: Gopalkrishna M.
Address for the correspondence: Nalur
Nalur, Thirthahalli
Shimoga
Karnataka -577424
India.
Date of birth: 23-02-1985
Sex: Male
Languages known: English, Hindi and Kannada

References

Dr. Udaya Kumar D.

Assistant Professor
Department of Chemistry,
National Institute of Technology Karnataka,
Surathkal, Mangalore,
Karnataka -575 025, India

Prof. A.V. Adhikari

Professor
Department of Chemistry,
National Institute of Technology Karnataka,
Surathkal, Mangalore,
Karnataka -575 025, India

Dr. Anandhan Srinivasan

Assistant Professor
Department of Metallurgical and Materials engineering,
National Institute of Technology Karnataka,
Surathkal, Mangalore,
Karnataka -575 025, India